POLITECNICO DI TORINO

MASTER's Degree in Electronic Engineering

MASTER's Degree Thesis

Development of generalized bandwidth estimation and optimization techniques for load modulated power amplifiers

Relatore

Prof. Vittorio CAMARCHIA

Candidato

Ten. Stefano FIORITONI

Correlatori

Dott.ssa Anna PIACIBELLO

Magg. ing. Daniele FERRANTE

Anno Accademico 2022-2023

Abstract

The aim of this work is to create a method for estimating the bandwidth and performance of power amplifiers based on load modulation. This method is designed to assist during the design process and requires an accurate depiction of complex and highly non-linear systems using equivalent models and linear simulations. This approach facilitates optimizations and multiple iterations, which can be challenging to achieve with non-linear simulations. The proposed technique is based on a numerical code that characterizes passive power combiner networks and models the response of active devices, like transistors, to generate significant performance indicators related to the amplifier. This innovative method considers certain physical limitations that cannot be modeled with CADs. Results have been validated by comparing them with simulations produced by the software ADS and differences have been highlighted.

"Divorare le lagrime in silenzio,
donare sangue e vita.
Questa è la nostra legge e in questa legge
Dio."

Acknowledgements

Al termine di questo importante capitolo della mia vita, il primo ringraziamento va alla grande famiglia dell'Esercito Italiano, nella speranza di essere sempre all'altezza nell'assolvimento dei miei Doveri nei confronti delle Istituzioni.
Un sentito ringraziamento va al Politecnico di Torino il quale, con i suoi esimi Docenti, ha saputo trasmettere stimoli e curiosità nell'ambito di specializzazione scelto.
Un ringraziamento particolare va al Chiar.mo Prof. Vittorio Camarchia e alla Dott.ssa Anna Piacibello, i quali hanno saputo infondermi un profondo interesse nella materia affrontata nella trattazione, trasmettendo la loro stessa passione e dedicando energie nella stesura del seguente studio.
Con grande piacere, ringrazio il Magg. ing. Daniele Ferrante per l'importante contributo che ha dato al presente lavoro, per il supporto profuso nell'arco di questi anni di formazione e per essersi dimostrato sempre disponibile.
Un particolare ringraziamento alle colonne portanti del mio essere, sempre pronte a sostenermi: alla mia famiglia, che mi ha accompagnato nella gioia e nei momenti difficili, dedico questo lavoro, tutte le soddisfazioni raggiunte e tutte quelle che verranno.
Un grazie a tutte le persone non citate che, con le loro azioni, hanno contribuito alla mia persona.

E infine, un ringraziamento a me, a tutte le salite percorse e a quelle vette ancora da scalare, a tutte le difficoltà ancora da superare che contribuiranno a farmi vedere, nella mia, la vita più bella del mondo!

Una Acies!
Stefano Fioritoni

Table of Contents

List of Tables

List of Figures

Chapter 1

Introduction to Radio Systems

In this introductory chapter, the aim is to describe the general architecture of a radio system, providing an overview of the building blocks that are essential for any communication system. The primary challenge of a radio system is to transfer the maximum amount of information in a time unit while ensuring reliable communication and using minimal energy. To understand the issues involved in technological improvements, some crucial points need to be underlined:

- *Scaling*: Moore's Law states that the scaling factor in device fabrication follows an exponential behaviour. However, since the individual components cannot be scaled indefinitely, a "More than Moore" approach is needed to integrate different systems into the same device. In the last century, this approach has been used to advance analog and telecommunication systems. As a result, the technology has evolved from solid-state discrete devices in 1950 to modern and functional radio units integrated circuits;
- *Frequency*: To achieve faster communication and take advantage of more efficient communication protocols, it is necessary to use higher frequencies. However, this poses a significant challenge not only from a technological standpoint but also in terms of design. This is because the behaviour of every building block of a system and electronic device is strongly influenced by frequency, and as the frequency increases, a new set of problems arise that are not present at lower frequencies.

Scaling issues are not faced in this treatment, where the system level is analyzed and discussed for the final aim.

1.1 General overview on a radio system

As a definition, a radio system is an element or a set of elements able to transmit information and data using a communication line working in the electromagnetic domain. In order to communicate, information must be transmitted through an electromagnetic wave that propagates in the air (as shown in Figure 1.1). To achieve this, a spectral content signal must first be up-converted through modulation, and then down-converted for demodulation and recovery.

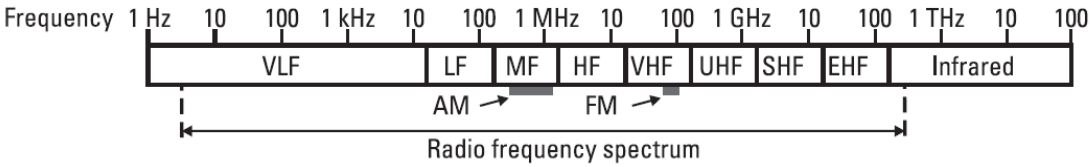

Figure 1.1: Radio frequency spectrum. [1]

For this aim, the basic transfer chain is built as follows (see Figure 1.2):

- *Information source*: to transmit information from a physical domain to an electrical one, it is necessary to convert the information into an electrical signal. This signal is usually provided as a baseband signal and requires efficient processing before being transmitted through the medium;
- *Transmitter* (TX): it is the functional unit that converts the baseband signal provided by the source into a properly modulated signal able to be transmitted in the medium. Because information travels in the environment through electromagnetic wave propagation, baseband signal must be up-converted into the radiofrequency spectrum to be rightly propagated into the environment;
- *Channel*: it is the medium in which modulated signals travel from the transmitter to the receiver. It is a source of interference and noise. For the right modelling of the transmission chain, it needs to be mathematically described for the specific purpose (i.e. AWGN channel model);
- *Receiver* (RX): it is the main block able to receive signals from the electromagnetic domain and recover the information contained in the RF signal. Data recovery is a critical process that involves converting the detected RF signal and processing the data to ensure minimal errors. This is particularly important as the received signal may be affected by noise and interference introduced by the channel and the TX/RX electronics;
- *Information user*: this module retrieves data from the receiver and utilizes it for its intended purpose.

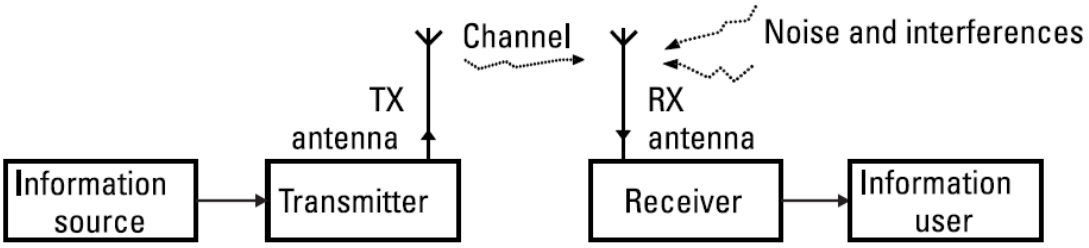

Figure 1.2: Information transfer chain in a radio system. [1]

In radio systems, there are additional elements present in the chain that ensure the reliability and security of the transmission. These elements include the *source encoder/decoder*, *encryptor/decryptor* and *channel encoder/decoder*. However, this overview will only focus on the RX/TX functional parts and their building blocks necessary for data transport between two points. The information source, user, and other types of data manipulation systems are excluded from this discussion. It is common to have the transmitter and receiver in the same device, which can enable either half-duplex or full-duplex transmission. In this case, the device is known as a *transceiver*, and it shares the same antenna or antenna array for both transmitting and receiving. Although the transmitter and receiver building blocks are similar, they are used in different ways to solve distinct tasks. The main differences between them are the practical problems they solve, such as frequency behaviour, noise reliability, and non-linearity that can impact communication. Therefore, each building block must be specifically designed to suit its unique task.

1.2 Basic receiver

A radio receiver is a device that can receive a modulated RF signal picked up by an antenna and extract the information contained in one of the channels. [1] The basic structure of a receiver is illustrated in Figure 1.3 and it must perform the following sequence of functions:

- *Tuning and selectivity* to isolate the wanted portion of the spectrum (channel) from the entire RF signals collected by the antenna;
- *Amplification* to increase the power and the amplitude of the selected signal. In fact, signals collected by antenna usually have very low power (affected by noise, distortion and interference) that needs to be managed by the electronics, which is another important font of distortion and noise;
- *Demodulation* for recovering the information from the RF signal, transforming it in a baseband signal through a down-conversion.

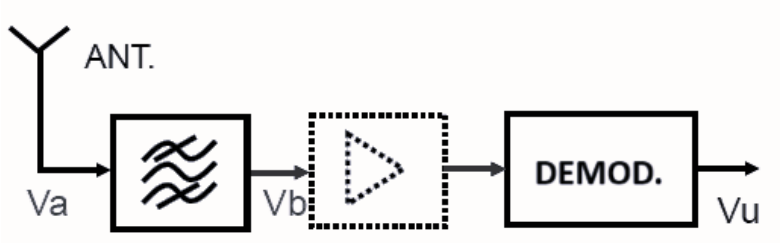

Figure 1.3: Basic structure of a receiver.

The basic structure is the same for every receiver and it is shown in Figure 1.3. The main differences are in the demodulation phase, which depends basically on the kind of modulation used in the communication.

1.2.1 RF Filter

The RF (radio frequency) filter is the first block in the receiver chain, responsible for selectivity. It is a bandpass filter that only allows a specific bandwidth to pass through, which is necessary for the radio system to receive and process information. As the first stage, it is designed to handle two specific purposes:

- Selecting the right bandwidth in the entire spectrum that the radio system must be able to handle, removing noise;
- helping the demodulation step in the image rejection.

A broadband BPF is used as an RF filter to select adjacent channels. This is particularly useful in multichannel systems where working at high frequency can help on relaxing filter specifications in terms of quality factor Q. However, the wider the bandwidth selected by the filter, the more difficult it becomes to reject unwanted channels in the image rejection step. Therefore, a good RF filter should have a flat response within the bandwidth and steep slopes at the bandwidth edge to guarantee the rejection of unwanted channels. It is worth noting that this type of RF filter is not tunable and the narrow-band selection of the single channel is accomplished by other means.

1.2.2 Low noise amplifier

When electromagnetic waves reach the RX antenna, they are often weak and affected by noise and interference from various sources such as transmission path non-idealities and propagation issues. As a result, the output voltage from the antenna is usually in the millivolt or microvolt range, which is comparable to the electronic devices' noise level, such as thermal noise. Therefore, the RF signal

detected must be amplified to a higher voltage level before being processed. However, the first amplifier stage is a critical point. According to Friis' formula of noise for a chain of N devices with individual noise factor F_{k} and an individual gain G_{k}, amplifying the signal can also amplify the noise, making it necessary to carefully balance the amplifier's gain and noise factor:

$$F = \frac{SNR_{\mathrm{in}}}{SNR_{\mathrm{out}}} = F_1 + \sum_{\mathrm{k}=2}^{\mathrm{N}} \frac{F_{\mathrm{k}} - 1}{\prod_1^{\mathrm{k}-1} G_{\mathrm{k}}} = F_1 + \frac{F_2 - 1}{G_1} + \frac{F_3 - 1}{G_1 G_2} + ... \tag{1.1}$$

Friis's formula in (1.1) shows that the main noise contribution is given by the first stage of the chain and, if gains are sufficiently large, the other therm may be neglected. For this reason, the first amplifier stage must introduce a minor quantity of noise and disturb the entire cascade. This aim is not easy because amplifiers are built using non-linear elements that intrinsically introduce non-linearities. The LNA is the first block in the chain that provides a first voltage level restoration such that the RF signal can be managed in the demodulation phase and, considering the previous hints, must be designed to guarantee a sufficient gain and low noise. To achieve this goal, it is necessary to design properly the input matching network of the amplifier and choose the best trade-off between power transfer to the load and noise Figure. Seldom, in an LNA characterization a minimum noise Figure F_{min} is guaranteed and achievable using an optimal matching network, that does not coincide in general with the maximum power transfer condition. Possible LNA topologies are based on Cascode or CE/CS configurations. Cascode gives more advantages in terms of I/O isolation, higher gain and wider bandwidth and allows to design a stage with lower output impedance and higher input impedance.

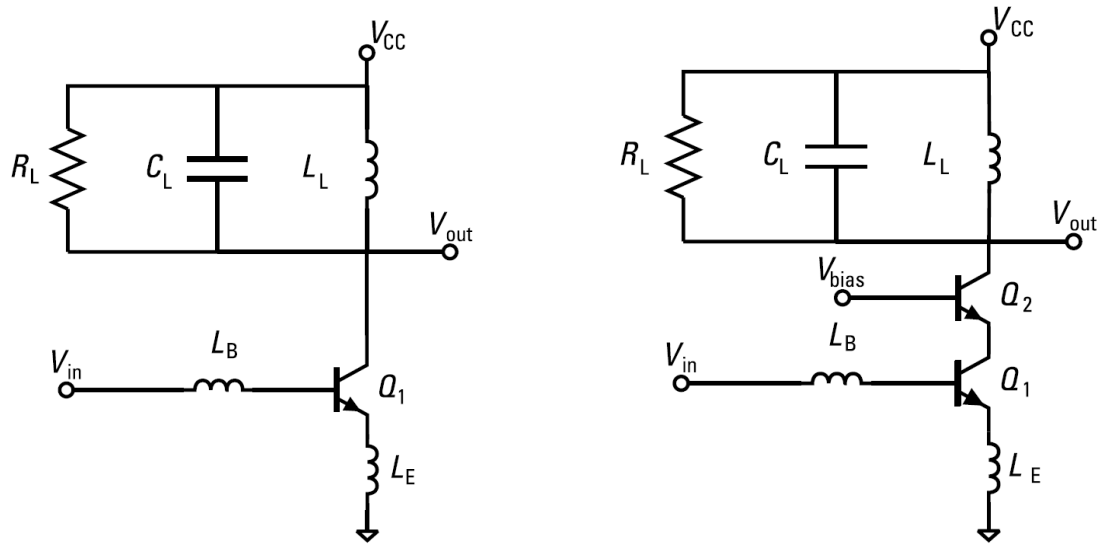

Figure 1.4: Common LNAs with bipolar transistors: (a) C-E configuration, (b) cascode topology. The circuits can be implemented with an identical structure in MOS technology. [1]

1.2.3 Demodulator

It is the core of every receiver. Its task is to recover the original information from the RF-modulated signal arriving from the channel medium. The mathematical principle at the base of demodulation is the fact that the product of two oscillations at different frequencies f_a and f_b is equal to the superposition of the sum beat and the difference beat (*frequency translation*):

$$\begin{aligned} sin(2\pi f_\mathrm{a} t) sin(2\pi f_\mathrm{b} t) &= \frac{1}{2}\left[cos\left(2\pi\left(f_\mathrm{a}+f_\mathrm{b}\right)t\right) + cos\left(2\pi\left(f_\mathrm{a}-f_\mathrm{b}\right)t\right)\right] \\ &= \frac{1}{2}\left[cos\left(2\pi f_\mathrm{S} t\right) + cos\left(2\pi f_\mathrm{D} t\right)\right] \end{aligned} \tag{1.2}$$

In demodulation, a low-pass filter is necessary to select the baseband. *Mixing* two beats in their product is a complex operation from an electronic point of view and the device able to perform this operation is the *mixer*: it receives in input 2 signal and gives in output the product. Mixers are non-linear devices difficult to handle and, for this reason, they introduce non-linear effects that can affect significantly the demodulation. The most common receiver structure is the *heterodyne receiver*, shown in Figure Here, the frequency translation is the key operation for this class of receiver. In this structure, a local oscillator at a given frequency f_LO generates a beat that, mixed with the RF signal at frequency f_RF,

can shift the spectrum to an intermediate frequency $f_{\mathrm{IF}} = f_{\mathrm{RF}} - f_{\mathrm{LO}}$. To select only the difference beat at frequency f_{RF}, it is necessary the action of a BP, able to select only the wanted or a portion of this: the filter with this aim is the *IF filter*. This last one is designed for two aims:

- to remove the translated portion of the spectrum at high frequency, in order to have in the spectrum only IFs;
- to isolate only the wanted channel in the entire spectrum selected by the RF filter.

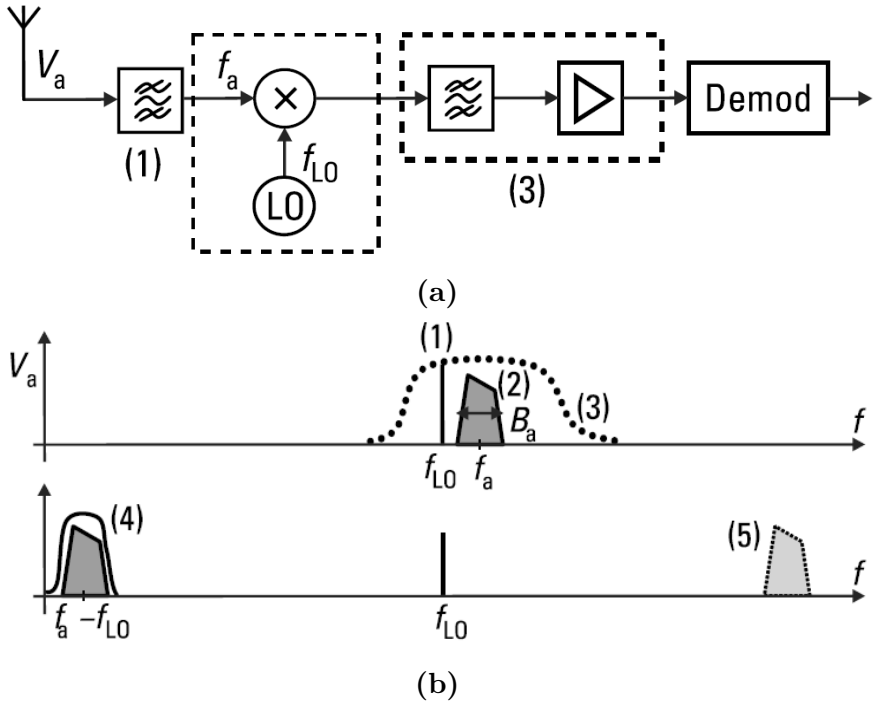

Figure 1.5: Heterodyne receiver. (a) Block diagram: (1) Input BPF, (2) LO and mixer, (3) IF filter and amplifier with narrowband, frequency $f_{\mathrm{IF}} = f_{\mathrm{a}} - f_{\mathrm{LO}}$. (b): Signals in the frequency domain. The input signal, with bandwidth B_{a} is shifted to a frequency $f_{\mathrm{IF}} = f_{\mathrm{a}} - f_{\mathrm{LO}}$. Tuning shifts the frequency f_{LO} of the LO. (1) local oscillator LO, (2) input signal spectrum, (3) input BPF, (4) difference beat IF signal and IF BPF, and (5) sum beat (not used). [1]

In fact, the BW of the IF filter is centred on f_{IF} but the pass-band behaviour is designed to select only one channel from the entire spectrum selected by the RF filter in the front end. This allows the selectivity of the channel. Its selection is handled by

the local oscillator f_{LO}: acting on LO frequency, different portions of the spectrum enter in the IF BW. The main advantage of heterodyne is that frequency tunability is controlled by a local oscillator, rather than passive components which modify filter features. Now, the output of the IF signal needs to be translated into baseband with a further demodulation step. In the classical (and simplest) heterodyne structure, the last step of demodulation is the translation in the baseband of the IF signal, mixing it with another second LO at frequency $f_{\mathrm{LO}_2} = f_{\mathrm{IF}}$ (valid for AM modulation). However, the last demodulation step shown in Figure 1.5a depends on the kind of modulation technique adopted in the transmission for coding the information in a high-frequency signal (transmission). Passing through intermediate frequency relaxes the specification of the following blocks. In general, multiple down-conversion can be used for managing problems related to image rejection. In the case in which the local oscillator is tuned at the frequency $f_{\mathrm{LO}} = f_{\mathrm{RF}}$, the spectrum of the RF signal is directly shifted in the baseband. This technique is called *Zero-IF* (ZIF) and, combined with I/Q modulation, can give advantages in terms of image rejection. Other techniques can be employed to down-shift the spectrum to intermediate frequency:

- *Multiple conversion heterodyne*: At different intermediate frequencies, multiple filtering steps allow for easy removal of images and good channel isolation due to high Q filters at lower frequencies;

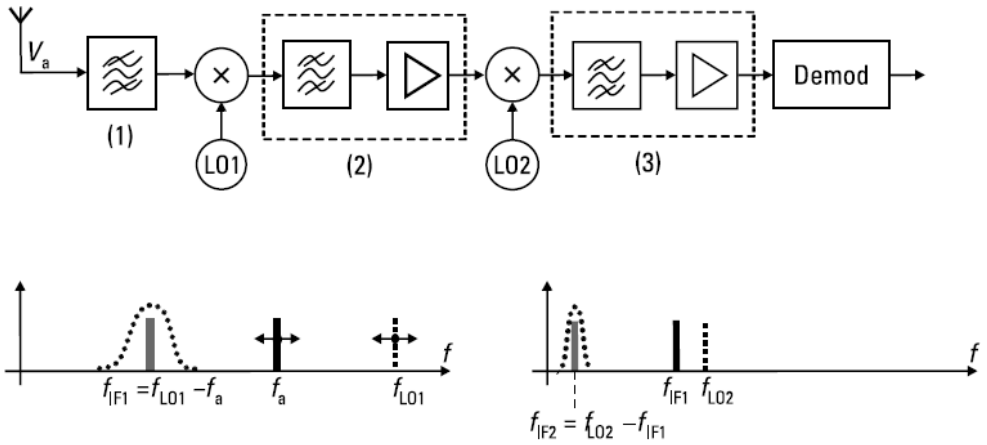

Figure 1.6: Example of multiple conversion heterodyne (double conversion). [1]

- *IQ processing in SSB*: this approach reconstructs the SSB signal by working on its in-phase and quadrature parts, which is useful for saving bandwidth in telecommunications.

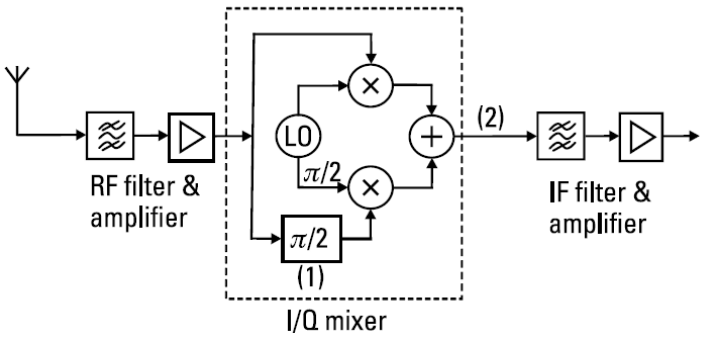

Figure 1.7: Example of SSB receiver. [1]

- *IQ processing for image rejection*: in-phase and quadrature parts can be opportunely combined for solving problems related to image frequency in mixing 1.8

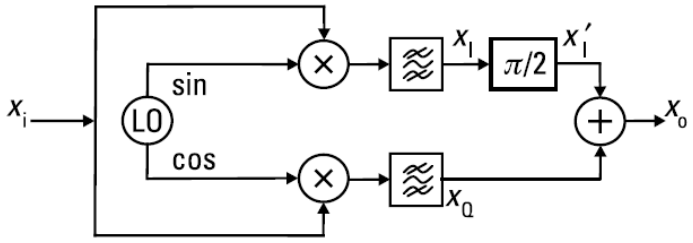

Figure 1.8: Example of IQ processing in image rejection mixing. [1]

In order to solve different problems, the basic structures can be combined and elaborated to obtain more complex architecture. The emphasis in this section is on the demodulator block and how it down-shifts the spectrum. The type of modulation technique adopted determines how the information is recovered. Information can be coded mainly in the amplitude, instant phase, instant frequency, or some combination of these to maximize throughput. There are two different approaches to executing the recovery of information.:

- Non-coherent approach, when information is recovered without knowing the carrier;

- Coherent, when the carrier is recovered from the received signal and used for information recovery.

1.2.4 Analog-to-digital conversion

After receiving a signal, the information is extracted through demodulation. However, before it can be used by the user, it needs to be processed in the digital domain. This requires an Analog Digital Converter (ADC) to be used, which is the final step in the receiver. The transition from the analog domain to the digital domain takes place in two steps:

- *Sampling*: it means to collect samples of the analog signal with a certain sampling frequency f_s. According to Nyquist's theorem, for a baseband signal with maximum frequency f_{max}, the sampling frequency must satisfy the following condition in order to avoid *aliasing*:

$$f_s > 2 \cdot f_{max} \tag{1.3}$$

  This constraint can be generalized for RF signals with bandwidth BW. The sampling frequency must satisfy the following relation:

$$f_s > 2 \cdot BW \tag{1.4}$$

  The circuit capable of performing this operation is known as a sample and hold (S&H). In most cases, the presence of an anti-aliasing filter is necessary;

- *Quantization*: with this operation, continuous voltage levels are converted into a set of discrete and finite levels represented by N bits, allowing for a representation of 2^N discrete levels.

Technological advancements have led to the development of high-performance ADC blocks. Previously, the digital front-end was placed after the demodulation block in the receiver to convert information into the digital domain for processing by other digital systems. This was due to the limited sampling frequency of ADCs. However, with an increase in sampling frequency, it is now possible to substitute some analog blocks with digital processing and place the digital conversion in other points of the receiver. The evolution of this process is shown in Figure 1.9, where the digital front-end is progressively shifted towards higher frequencies and analog blocks are replaced by dedicated hardware that can process information at high frequencies, such as the digital signal processor (DSP). This technological evolution has allowed the development of *software defined radio (SDR)*, where all receiver blocks are implemented via software. The benefit of moving some functions to the digital is the flexibility, due to the possibility to change parameters and working functions only acting on the software.

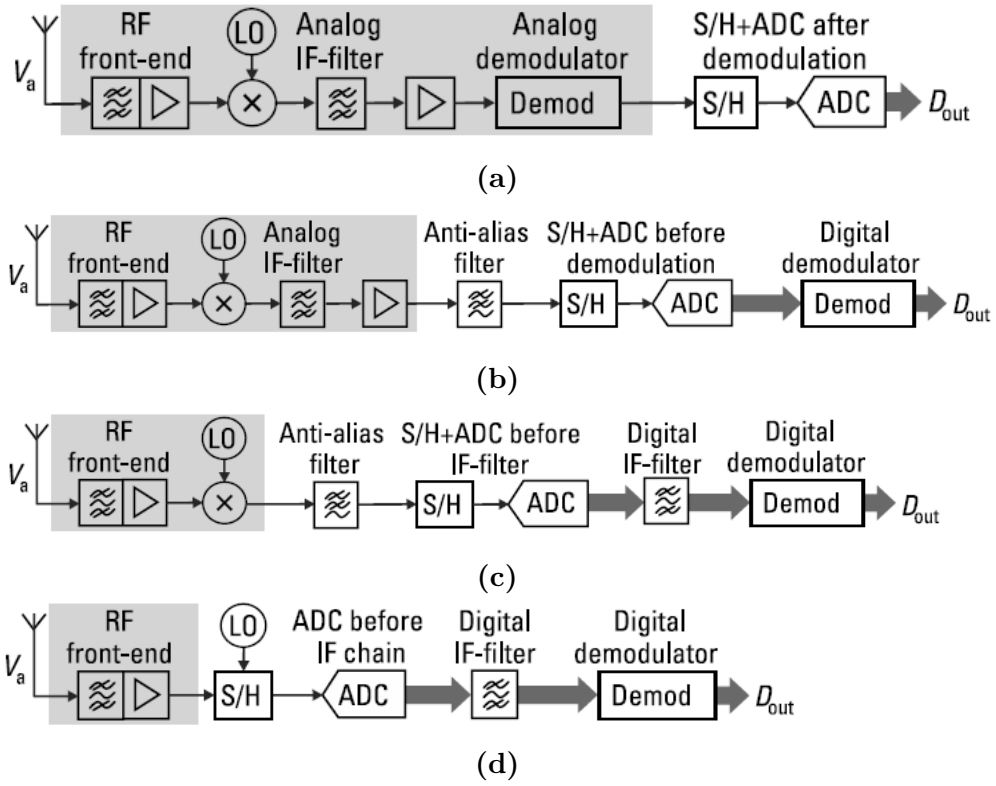

Figure 1.9: Migration of functions from analog to digital. (a) ADC after demodulation, (b) ADC after IF, before demodulation, (c) ADC after the mixer, before the IF chain, and (d) frequency translation merged with sampling. Grey areas indicate analog circuits. [1]

1.3 Basic transmitter

A radio transmitter is a device that can transmit signals through an antenna in the channel medium. It modifies a given baseband signal with a modulating signal to propagate it at a high frequency. This process is called modulation, and it maps the baseband signal into another RF signal. Basic modulation techniques involve varying one or more characteristics of a fixed signal, called a carrier. The combination of the modulating signal with the carrier produces the modulated signal, which is a function of the carrier and the modulating signal. Information can be encoded in different ways to increase the information content and throughput. For example, it can be coded in the amplitude of the carrier (AM), in its instantaneous frequency (FM), in its instantaneous phase, or a combination of them. The basic scheme is presented in Figure 1.10.

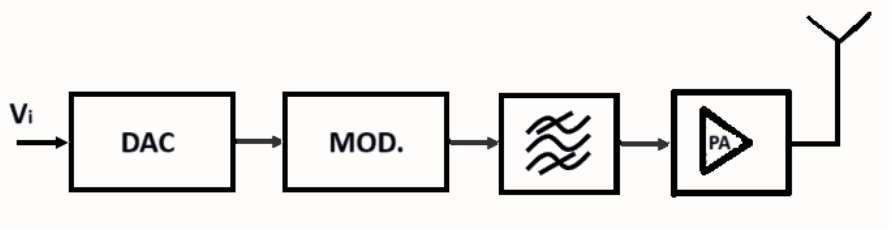

Figure 1.10: Basic radio transmitter.

1.3.1 Digital-to-analog conversion

The information source is often digital and requires D/A conversion for transmission. A DAC (Digital-to-Analog Converter) is a device that converts a digital signal, which is represented by a binary code of N bits, into a set of electrical analog quantities such as current or voltage. However, the number of allowed levels of these electrical quantities remains limited to a discrete set due to the resolution of the DAC. If the DAC works at f_s, the reconstructed signal's spectrum becomes periodic in the frequency domain. Therefore, a reconstruction filter is necessary to filter out the useful portion of the signal. If the system works with a baseband signal, then the reconstruction filter will be a low-pass filter (LPF).

1.3.2 Modulator

This block aims to combine carrier and modulating signals to obtain an RF signal with specific characteristics necessary to be transmitted properly in the electromagnetic spectrum. Modulation allows to code the spectrum of the modulating signal to another one at RF and it consists in up-shifting the original spectrum. In analog telecommunication, the main modulation techniques are the following:

- *Amplitude modulation (AM)*: the modulating signal modifies the envelope of the carrier. It can be implemented by mixing carrier and modulating waves;

$$v_m(t) \mapsto A v_m(t) sin(2\pi f t) \tag{1.5}$$

- *Frequency modulation (FM)*: instantaneous carrier frequency is a function of the modulating wave, so information is coded in the frequency. The frequency of the carrier can be modified with the modulating wave using a VCO(Voltage controlled oscillator);

$$v_m(t) \mapsto A sin\left[2\pi f\left(v_m\left(t\right)\right) t\right] \tag{1.6}$$

- *Phase modulation (PM)*: the message is coded in the instantaneous phase of the carrier.

$$v_{\mathrm{m}}(t) \mapsto A sin\left[2\pi f t + \phi\left(v_{\mathrm{m}}\left(t\right)\right)\right] \tag{1.7}$$

Advanced modulation techniques are allowed and obtained with the right combination of the previous ones to save the band and increase throughput. However, instead of modulating directly at RF, it is suggested to perform a step in IF and then up-shift the spectrum.

1.3.3 Filtering and power amplifiers

In a communication device, the front end consists of a TX antenna, an output filter, and a power amplifier. The output filter helps select the appropriate band for transmission, while the power amplifier ensures that the antenna receives sufficient power to transmit the electromagnetic wave. This is crucial for transforming electrical power into electromagnetic energy. In this work, power amplifiers are a key area of focus.

1.4 Topology considerations and transceiver

From the previous section, it is evident that between TX and RX there are some analogies because one device should exploit the dual function of the other one. In particular:

- when designing a telecommunication system, it is important to take into account the modulation technique used and design the modulator and demodulator accordingly. Demodulation at the receiver end poses a challenge of frequency imaging, which requires multiple conversions to be taken into consideration. Additionally, if Single Sideband (SSB) techniques are used during transmission, the same dual scheme must be adopted during reconstruction;

- both devices use amplifiers, but with different aims and characteristics.

In this chapter, radio transmitters and receivers have been discussed as separate devices. However, in modern technology, they are often combined into a single circuit that enables half-duplex or full-duplex communication, sharing the same antenna. This device is known as a transceiver, and you can see an example of it in Figure 1.11. The transceiver's antenna serves the dual purpose of transmitting RF signals into the environment and receiving EM waves. To manage the antenna, TDM or FDM techniques are frequently used.

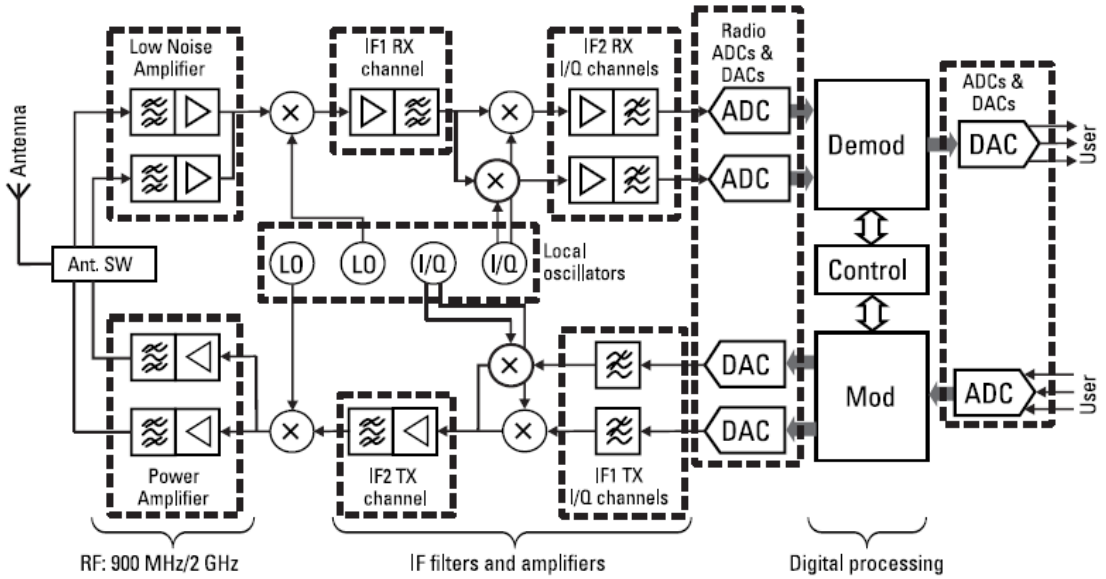

Figure 1.11: Example of a transceiver. [1]

Chapter 2

Power amplifiers

This chapter discusses PAs for RF transmitters. At the end of the transmission chain, a TX antenna is used to convert electrical power to electromagnetic energy. To allow the wave to reach the RX with sufficient power density, the antenna must be supplied with adequate energy. However, part of this energy will be lost due to parasitic phenomena from the antenna and its coupling with the electronic front end. The remaining energy will be converted into electromagnetic energy and propagate in the channel according to the Friis transmission model and described by (2.1):

$$P_{\mathrm{RX}} = P_{\mathrm{TX}} G_{\mathrm{TX}} G_{\mathrm{RX}} \frac{\lambda^2}{16\pi^2 d^2} \tag{2.1}$$

where d is the distance between TX and RX, λ is the wavelength in the channel medium, and $P_{\mathrm{TX/RX}}$ and $G_{\mathrm{TX/RX}}$ are the TX/RX powers and gains, as described in Figure 2.1. Note that ideal antennas are considered in this model.

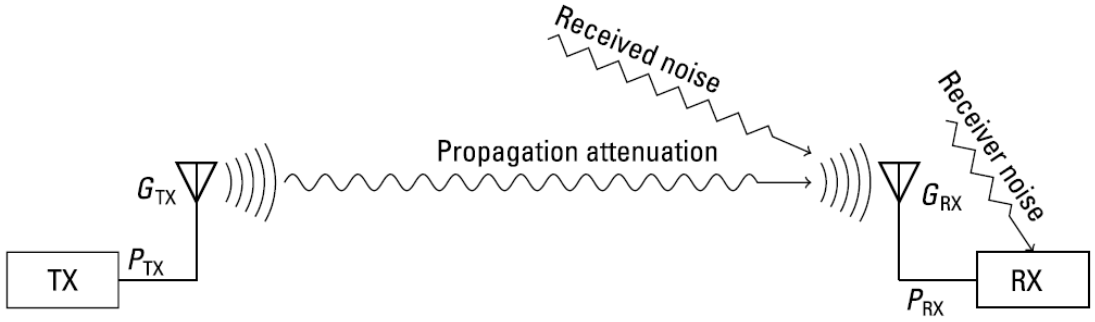

Figure 2.1: Link model of a radio transmission. [1]

To transmit a strong signal, the antenna in TX requires a significant amount of energy. However, most electronic components are designed for low to medium

power usage and are unable to handle high-power requirements. This is where PAs come in, as they are responsible for converting low-power signals into higher power levels required for transmission.

2.1 Introduction to power amplifiers

A PA is a specialized type of amplifier designed to amplify a signal and increase its power. It is commonly used as the final building block in a radio transmitter and is responsible for driving the TX antenna with the necessary power level to ensure signal transmission. Because delivering high energy at RF frequency with reasonable efficiency and power consumption and large bandwidth is challenging, the PA is a critical component in a radio transmitter. The general model is shown in Figure 2.2. The signal source with its impedance models all previous stages of a radio transmitter. It is worth noting that 50Ω is a standard value used as a reference for the real part of the I/O stage impedance due to historical reasons. The key of a PA is the active element (or a set of active elements) that transforms a low-power signal into a high-power one. According to the basics of thermodynamics, an external energy source is necessary to allow the input signal to grow in power. The DC power supply is the energy source that adds energy to the input signal to transform it into the output signal. An active element is needed to perform the power transformation from DC to RF. As a real thermodynamic system is affected by parasitic effects (like the Joule effect), part of the energy is wasted and transformed into heat, and a certain amount of power P_{diss} is dissipated to the environment. According to the principle of energy conservation, the powers involved in the PA are the DC power provided by the supply P_{DC}, the input power coming from the stimulus P_{I} and the output power P_{O} delivered to the load. These quantities are related as follows:

$$P_{\text{DC}} + P_{\text{I}} = P_{\text{O}} + P_{\text{diss}} \tag{2.2}$$

It is important to note that a real amplifier is not a linear device, meaning it does not produce an output signal that is a perfect copy of the input signal. Non-linearity introduces unwanted harmonic content into the output signal, which overlaps with the useful signal. Therefore, the output power represented by P_{O} in (2.2) can be expressed as follows:

$$P_{\text{DC}} + P_{\text{I}}(f_0) = P_{\text{O}}(f_0) + \sum_{\text{n=2,3,4...}} P_{\text{O}}(nf_0) + P_{\text{diss}} \tag{2.3}$$

P_{diss} is the main issue with PAs as they generate waste energy that must be dissipated properly to avoid overheating and system damage.

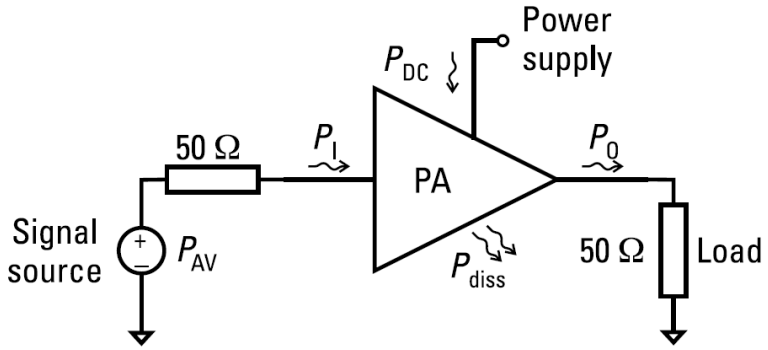

Figure 2.2: Generic PA with main quantities involved. [1]

2.1.1 Figures of merit

PAs are quantitatively characterized by a number of figures of merit that depend on the electrical quantities involved (input/output powers, voltages, etc.). Among these, a very important one is the power gain, which is defined as the ratio of output and input active power at the excitation frequency, which is denoted by $G_{\mathrm{P}}(f_0)$ and expressed as a function of a single frequency tone f_0 in the frequency domain.

$$G_{\mathrm{P}}(f_0) = \frac{P_{\mathrm{O}}(f_0)}{P_{\mathrm{I}}(f_0)} \tag{2.4}$$

In the frequency domain, power is represented by a complex number in the form of a phasor. The *active power* is expressed by the real part of the phasor. It is important to note that quantities are referred to their maximum values, which is why the presence of $\frac{1}{2}$ coefficient is justified.

$$P_{\mathrm{O}}(f_0) = \frac{1}{2}\Re\left\{V_{\mathrm{O}}(f_0)I_{\mathrm{O}}^*(f_0)\right\} \tag{2.5}$$

$$P_{\mathrm{I}}(f_0) = \frac{1}{2}\Re\left\{V_{\mathrm{I}}(f_0)I_{\mathrm{I}}^*(f_0)\right\} \tag{2.6}$$

The power gain of a PA, defined in (2.4), is known as the *operating gain*. It is a characteristic of the amplifier that indicates its ability to convert power *delivered* to its input port into power delivered from its output port. This gain depends solely on the amplifier's design and is not affected by external factors. Its measurement is based on the quantities measured from the I/O ports. However, the PA's capability is related to the power it can transmit to the load relative to the power provided by the RF source. To quantify this capability, the *transducer gain* is defined as the ratio of power *delivered* to the load from the output port to the power *available* from the RF source.

$$G_{\mathrm{T}}(f_0) = \frac{P_{\mathrm{O}}(f_0)}{P_{\mathrm{AV}}(f_0)} \tag{2.7}$$

where $P_{\mathrm{AV}}(f_0)$ is the power available from the RF source defined as follows:

$$P_{\mathrm{AV}}(f_0) = \frac{1}{2}\Re\left\{V_{\mathrm{S}}(f_0)I_{\mathrm{S}}^{*}(f_0)\right\} \tag{2.8}$$

If the input impedance of the PA stage is matched with the output impedance of the signal source, then the power gain of the PA stage G_{P} is equal to the power gain of the total system G_{T} and the power delivered to the PA stage $P_{\mathrm{AV}}(f_0)$ is equal to the input power $P_{\mathrm{I}}(f_0)$. As a definition, the *efficiency* (μ) is defined as the ratio between the output power delivered to the load at a certain frequency and the DC power delivered from the DC supply:

$$\mu(f_0) = \frac{P_{\mathrm{O}}(f_0)}{P_{\mathrm{DC}}} \tag{2.9}$$

Efficiency only considers useful output power compared to input power. *Power-added efficiency (PAE)* also considers input power.

$$PAE(f_0) = \frac{P_{\mathrm{O}}(f_0) - P_{\mathrm{I}}(f_0)}{P_{\mathrm{DC}}} = \mu(f_0)\left[1 - \frac{1}{G_{\mathrm{P}}(f_0)}\right] \tag{2.10}$$

In cases of high gain, *PAE* and μ can be treated as equivalent. However, in most RF applications, gains are relatively low, and the two values can differ significantly. *PAE* provides insight into how the PA distributes power input during bursts. In addition, the active elements used for PA features are highly non-linear and when working with large signals at RF, the gain is heavily dependent on the input power signal. Consequently, the output power is a non-linear function, which is also dependent on the input power. By analyzing the graph in Figure 2.3, which shows the dependence of the figures of merit described on P_{I}, it is possible to conclude that certain considerations need to be taken into account:

- When dealing with small signals, power gain can be expected to increase linearly. However, as the input power increases, the difference between the ideal behaviour and the actual behaviour increases as well, until a certain point is reached. This point is known as the *saturation point*. At saturation, the DC supply and active devices can no longer provide additional power to the output signal. Even if the input power continues to increase, the output power remains constant and clipped due to the breakdown effect, which can damage the entire device if the input power exceeds the saturation point. The maximum power that the power amplifier (PA) can provide at its output port is represented by $P_{\mathrm{O,sat}}$, and the minimum input power required to achieve saturation is represented by $P_{\mathrm{I,sat}}$.

- Efficiency and PAE are quantities that depend on the input. These quantities indicate how well a PA can convert power from a DC source into output power without wasting energy. To operate, active components in a PA require a certain amount of power from the DC source to be polarized to a specific working point. This power is only used for the device to function and does not affect power conversion. In small-signal conditions, the output power is lower than the maximum output power that the PA can support. As a result, DC power dominates the ratio between efficiency and PAE. However, as the input power increases, the output power increases, and the numerator becomes dominant in the ratio. Therefore, high efficiency is achieved when the PA operates near its maximum capability to convert power. Otherwise, the wasted energy becomes more dominant than the useful energy.

- The difference between the ideal gain characteristic and the real one is called *compression level*. As the input power increases bringing the PA near saturation, the operative gain begins to decrease in a monotonic way. Typically, large-signal parameters are defined at a specific compression level, which is selected to ensure good linearity before that point. For example, in Figure 2.3, a 1dB compression level indicates the point in the gain characteristic where the gain is reduced by 1dB. From that point, it is possible to identify on the I/O curve the input power $P_{\mathrm{I,1dB}}$ that corresponds to the desired 1dB compression, as well as the resulting $P_{\mathrm{O,1dB}}$ provided by the output port at that point. The same principle can be extended to μ_{1dB} and PAE_{1dB} by using different compression levels. The lower the compression, the better the linearity will be within the range considered, but it also means a decrease in the I/O dynamic.

After careful consideration, it is clear that a trade-off between efficiency and linearity must be made when selecting a PA. While small signals achieve the best linearity, the primary task of a PA is power amplification, which requires large signals and high power output. Typically, higher efficiency is achieved near the saturation point, which is also where linearity decreases. In high-frequency applications, PAs are designed to operate at maximum performance near the saturation point, sacrificing linearity. However, a PA's performance depends on the input signal and its envelope, and it can function in other points. When an amplifier operates far from the saturation point, it is in the **back-off** region, and the input and output back-off represents the distance between the input or output power and the saturation point (usually expressed in dB).

$$OBO|_{\mathrm{dB}} = 10log_{10}\frac{P_{\mathrm{O,sat}}}{P_{\mathrm{O}}} \tag{2.11}$$

$$IBO|_{\mathrm{dB}} = 10log_{10}\frac{P_{\mathrm{I,sat}}}{P_{\mathrm{I}}} \tag{2.12}$$

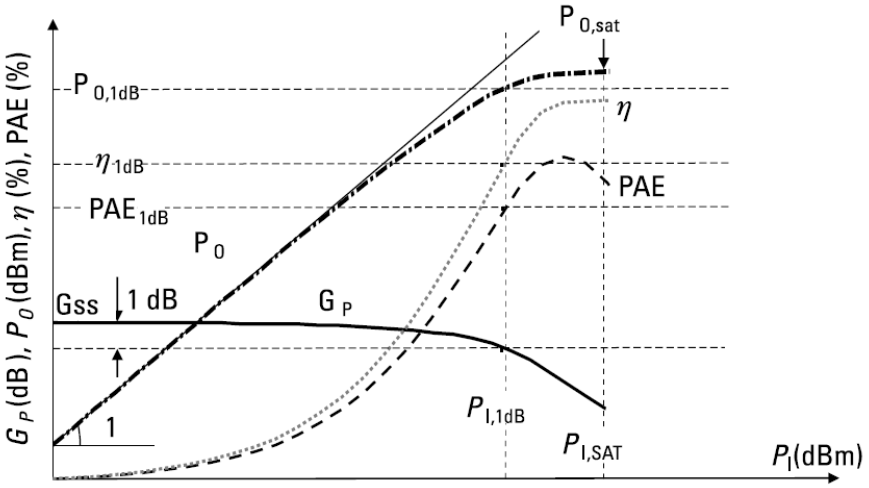

Figure 2.3: Main FOMs as a function of P_{I}. [1]

The efficiency, gain, and PAE of amplifiers can be expressed as functions of the back-off. Although linearity is not a primary concern in PAs, nonlinear effects should be considered to accurately measure output distortion, as linearity is strongly affected by gain compression and saturation. It is also important to note that all of these figures of merit are highly dependent on f_0. The characteristics shown in Figure 2.3 are for a single tone, but in the frequency domain, the overall effects are evaluated by superimposing each frequency contribution. To accurately characterize distortion, it is recommended to test the PA using both single-tone and two-tone excitation. These tests help to determine two significant parameters: the *intercept point of order n-th* (IP_{n}), the *intermodulation distortion* (IMD), and the *carrier-to-intermodulation ratio* ($CIMR$). The *Intercept point of order n-th* (IP_{n}) is determined by evaluating a single-tone test. Non-linear theory of active devices states that non-linearity introduces new harmonic contents in the output signal. Normally, an amplifier receives a signal with a certain bandwidth BW centered at frequency f_0. In an ideal (linear) situation, the frequency content of the output signal should be the same as the input signal with the right amplification. However, with real active devices, the output signal has a different spectral content because every frequency Fourier domain contributes to generating other harmonics. Therefore, if the input signal of the block is a single-tone f_0 evaluated in *continuous wave* (CW) condition, the output signal will have the same tone f_0 with its harmonics. The amplitude of these harmonics depends on the power of the input tone. Figure 2.4a illustrates this. Figure 2.4b shows that IP_{n} is the point on the I/O power plane where the tangent to SS I/O power curve of the fundamental cross the tangent to SS I/O power curve related to the $n-th$ harmonic. The coordinates

of IP_{n} are represented by the *input intercept point of order* $n-th$ (IIP_{n}) and the *output intercept point of order* $n-th$ (OIP_{n}). In electronics, IP_3 is considered as a figure of merit.

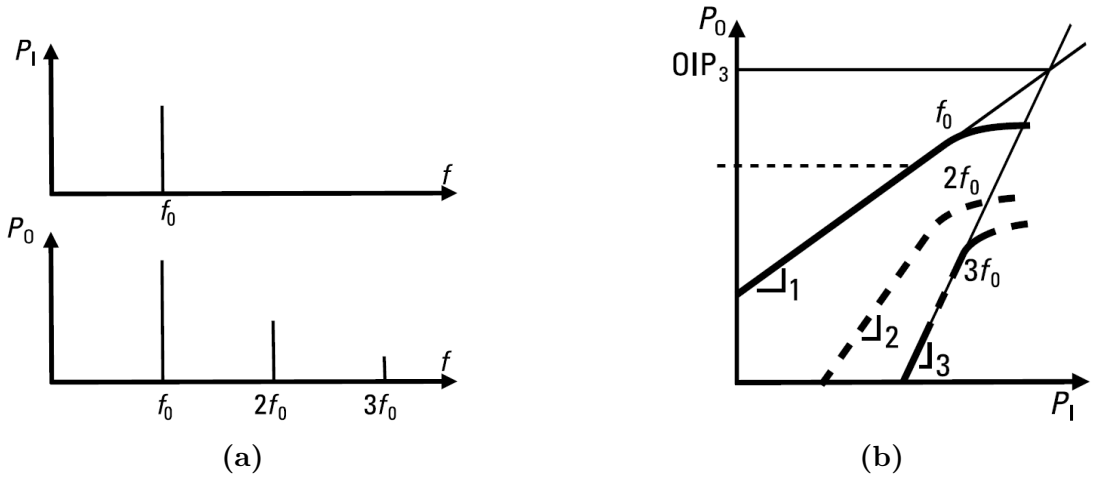

Figure 2.4: Example of a single-tone response.(a): frequency content, (b): IIP_3 definition. [1]

In a two-tone CW test, the same approach can be followed. In this test, the input signal is a combination of two sinusoidal signals with different frequencies (f_1 and f_2) but the same amplitude. The non-linear effects in the system produce an output signal containing the desired two tones and every intermodulation product at frequency $mf_1 \pm nf_2$ where n and m are natural numbers. Figure 2.5a illustrates this phenomenon. $CIMR_{\mathrm{n}}$ is the ratio of the power associated with the two tones used as a test and the $n-th$ intermodulation product in dB. This value depends on the input power. It has been demonstrated that the 3^{rd} order intermodulation products at frequencies $2f_1 - f_2$ and $2f_2 - f_1$ with the same amplitude have the most significant effect on the spectrum.

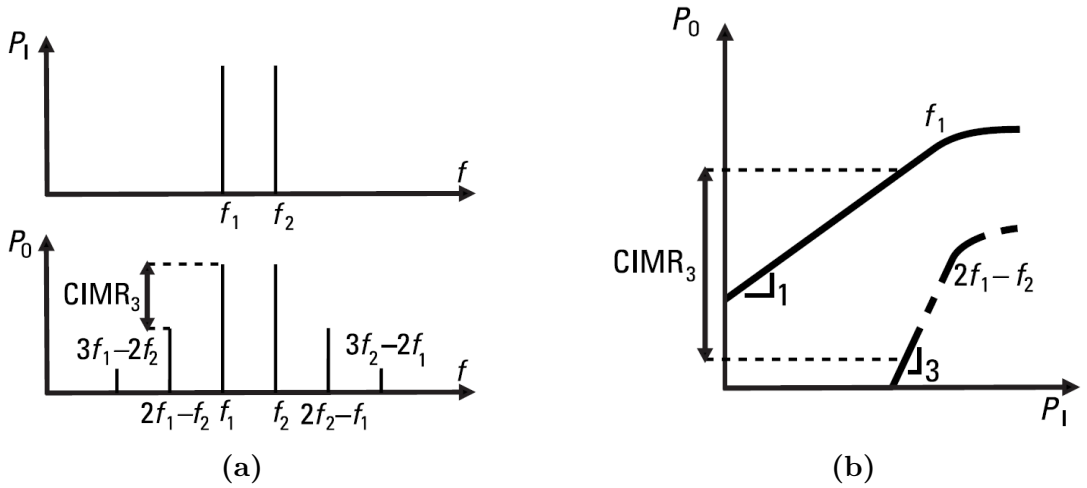

Figure 2.5: Example of the two-tone response in a PA. (a): frequency content and intermodulation products, (b): I/O power plane. [1]

2.1.2 Linear RF amplifier theory

At RF, signal propagation cannot be ignored and the whole amplifier system must be analyzed, taking into account the effects related to transmission lines, to evaluate both gain and stability. Prior to analyzing an amplifier, it is necessary to introduce scattering parameters. These parameters, commonly referred to as S-parameters, are mainly used to characterize the behaviour of a multi-port network at high frequencies, in terms of incident and reflected waves. Unlike Z, Y, and hybrid formalism, S-parameters enable a multi-port system description that considers the reflected wave at its terminals as a function of the incident wave.

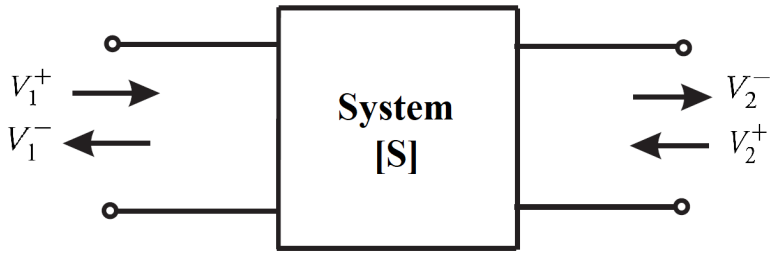

Figure 2.6: Generic 2-port device, incident and transmitted waves are highlighted.

For a generic 2-port device, the scattering matrix is a 2x2 matrix containing scattering parameters that describe the system linearly.

$$\begin{pmatrix} V_1^- \\ V_2^- \end{pmatrix} = \begin{pmatrix} S_{11} & S_{12} \\ S_{21} & S_{22} \end{pmatrix} \begin{pmatrix} V_1^+ \\ V_2^+ \end{pmatrix} = S \begin{pmatrix} V_1^+ \\ V_2^+ \end{pmatrix} \Longleftrightarrow \begin{cases} V_1^- = S_{11}V_1^+ + S_{12}V_2^+ \\ V_2^- = S_{21}V_1^+ + S_{22}V_2^+ \end{cases} \tag{2.13}$$

The scattering formalism was originally created to explain the reflection and transmission of electromagnetic fields along a certain path. This concept can also be applied to other physical quantities such as direct *power intensity* and *reflected power intensity*. In a transmission line, the relationship between these quantities and the incident and reflected waves is directly related to the voltage. However, this is only true if the characteristic impedance is the same for all the ports. S-parameters can be measured in the following way:

- S_{11} is the ratio between reflected and transmitted waves at port 1 when port 2 is adapted with a load equal to its characteristic impedance. In this way there is no reflected wave from the port 2 load, thus there is not any incident wave on port 2. In this condition, it corresponds with port 1 reflection coefficient.

$$S_{11} = \left.\frac{V_1^-}{V_1^+}\right|_{V_2^+=0} = \Gamma_{\mathrm{i}} \tag{2.14}$$

- S_{21} is estimated in the same condition as the previous one and it is the ratio between the reflected wave at port 2 and an incident wave at port 1. For this reason, it corresponds with the voltage gain (transmission rate) of the system.

$$S_{21} = \left.\frac{V_2^-}{V_1^+}\right|_{V_2^+=0} = G_{\mathrm{v},21} \tag{2.15}$$

- S_{22} is the dual of S_{11}. It is measured with a load on port 1 adapted with the characteristic impedance of the line and represents the reflection coefficient at port 2.

$$S_{22} = \left.\frac{V_2^-}{V_2^+}\right|_{V_1^+=0} = \Gamma_{\mathrm{out}} \tag{2.16}$$

- S_{12} is the dual of S_{21}. It is measured in the same load adaptive condition as the previous and represents the reverse voltage gain (reverse transmission rate) from the incident wave in port 2 to the reflected wave from port 1.

$$S_{12} = \left.\frac{V_1^-}{V_2^+}\right|_{V_1^+=0} = G_{\mathrm{v},12} \tag{2.17}$$

A system with N ports can be described by an N x N matrix. Each element of the matrix is obtained by supplying one port at a time with other ports adapted in impedance.

$$\begin{pmatrix} V_1^- \\ V_2^- \\ \vdots \\ V_N^- \end{pmatrix} = \begin{pmatrix} S_{11} & S_{12} & \dots & S_{1N} \\ S_{21} & S_{22} & \dots & S_{2N} \\ \vdots & \vdots & \ddots & \vdots \\ S_{N1} & S_{N2} & \dots & S_{NN} \end{pmatrix} \begin{pmatrix} V_1^+ \\ V_2^+ \\ \vdots \\ V_N^+ \end{pmatrix} \tag{2.18}$$

By analyzing the characteristics of the S-matrix, many features of the system can be understood. For any generic S-matrix, the following statement holds true:

- $S = S^T \iff$ reciprocal network;
- $SS^H = I \iff$ lossless network;
- $I - SS^H$ positive-defined $\iff$ network with loss;
- $S^{-1} = S^T \iff$ reciprocal and lossless network.

The system shown in Figure 2.6 is being considered. In this system, port 1 is connected to an RF source generator with its parasitic impedance Z_S, instead of port 2 which is connected to a real impedance Z_L and is considered as the output. You can see this connection scheme in Figure 2.7. This setup is used to derive the characterization of a generic 2-port device, such as an amplifier.

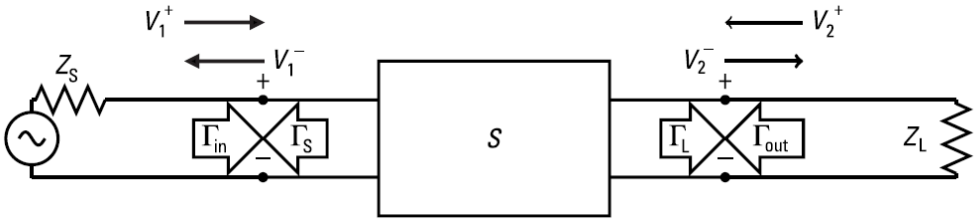

Figure 2.7: 2-port device with input connected to a real RF source and output connected to a generic load. [1]

The relationship between the incident and reflected wave of a system described with S-parameters is affected by external components and depends on the coupling between ports and connected devices. Using scattering formalism, it is possible to estimate a new I/O reflection coefficient by considering that $\Gamma_S = \frac{Z_S - Z_0}{Z_S + Z_0}$ and $\Gamma_L = \frac{Z_L - Z_0}{Z_L + Z_0}$.

$$S'_{11} = \Gamma_i = S_{11} + \frac{S_{12}S_{21}\Gamma_L}{1 - S_{22}\Gamma_L} \tag{2.19}$$

$$S'_{22} = \Gamma_{out} = S_{22} + \frac{S_{12}S_{21}\Gamma_S}{1 - S_{11}\Gamma_S} \tag{2.20}$$

For a generic system, *unconditional stability* is ensured when the following conditions are ensured for each frequency:

$$\begin{cases} |\Gamma_{\mathrm{L}}| < 1 \\ |\Gamma_{\mathrm{S}}| < 1 \\ |\Gamma_{\mathrm{i}}(\Gamma_{\mathrm{L}})| < 1 \\ |\Gamma_{\mathrm{out}}(\Gamma_{\mathrm{S}})| < 1 \end{cases} \tag{2.21}$$

If these conditions are satisfied only in a certain frequency domain, the system is *conditionally stable*. Passive networks are always stable, and in the case studied in this example, the conditions for Γ_{S} and Γ_{L} are guaranteed to be met. However, when dealing with an active device, instability could occur. Stability regions are defined as geometrical loci of points that satisfy the first stability conditions of Γ_{out} and Γ_{i} on the Gauss plane representing Γ_{S} and Γ_{L}. If both stability regions are entirely inside the unit circle, the system is unconditionally stable. Moreover, stability is ensured for Γ_{S} and Γ_{L} inside the unit circle due to the last two stability conditions in (2.21). An important parameter, useful for two-port network stability consideration, is the *Rollet's stability coefficient*:

$$k = \frac{1 + |det(S)|^2 - |S_{11}|^2 - |S_{22}|^2}{|S_{12}||S_{21}|} \tag{2.22}$$

$K > 1$ is a *necessary but not sufficient* condition for unconditional stability. It can be demonstrated that, for a two-port system, the following statement is valid:

$$k > 1 \wedge |det(S)| < 1 \iff \text{the system is unconditionally stable} \tag{2.23}$$

With scattering formalism, it is possible to rewrite the expression of transducer gain in (2.7) as follows:

$$G_{\mathrm{T}} = \frac{P_{\mathrm{O}}}{P_{\mathrm{AV}}} = \frac{1 - |S_{11}|^2}{|1 - S_{11}\Gamma_{\mathrm{S}}|^2} |S_{21}|^2 \frac{1 - |\Gamma_{\mathrm{L}}|^2}{|1 - \Gamma_{\mathrm{out}}\Gamma_{\mathrm{L}}|^2} \tag{2.24}$$

If the system is an amplifier, the following conditions should be met:

1. the system should be unilateral, which means signals can travel only from input to output. In an ideal amplifier, this condition is satisfied with $S_{12} = 0$. In real situations, this is not possible because of parasitic effects but unilateral approximation can be ensured if $|S_{21}| >> |S_{12}|$;

2. the maximum power transfer from source to the system and from system to load happen in *conjugate matching conditions*, that are:

$$\begin{aligned} \Gamma_{\mathrm{S}} &= \Gamma_{\mathrm{S,opt}} = \Gamma_{\mathrm{i}}^* \\ \Gamma_{\mathrm{L}} &= \Gamma_{\mathrm{L,opt}} = \Gamma_{\mathrm{out}}^* \end{aligned} \tag{2.25}$$

Solving these conditions is not a simple problem but it is possible to demonstrate that for conjugate matching in input and output the maximum transducer gain available can be expressed as follows:

$$\begin{cases} G_{\mathrm{MAG}} = \frac{|S_{21}|}{|S_{12}|}(k - \sqrt{k^2 - 1}) \text{ in unconditional stability} \\ G_{\mathrm{MSG}} = \frac{|S_{21}|}{|S_{12}|} \text{ otherwise} \end{cases} \tag{2.26}$$

Matching conditions are achieved by tuning Γ_{S} and Γ_{L} with opportune *matching networks*, as shown in Figure 2.8.

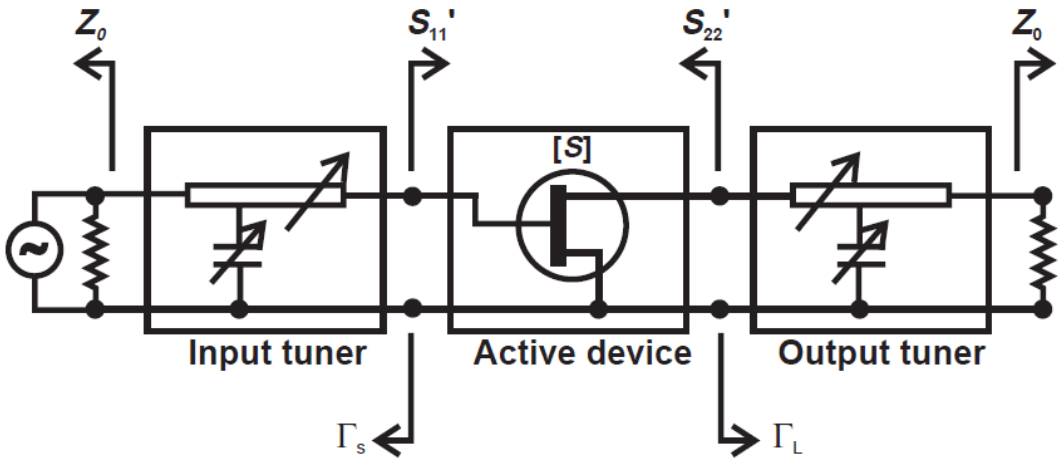

Figure 2.8: 2-port amplifier with I/O matching networks. [2]

2.1.3 ABCD parameters

In the field of electrical engineering, S-formalism is used to describe the relationship between the reflected wave (dependent variable) and the incident wave (independent variable). While this is helpful in characterizing a device, it may not be the best approach in designing and analyzing a system since it fails to establish a relationship between electrical quantities at one port and those on the others in terms of input/output. This makes it difficult to assess how multiple building blocks interact with each other when connected. To address this, a mathematical instrument is required to put quantities related to one port in relation with those of the others. This allows for easy evaluation of the output from one port as a function of what happens to the others, considered as an input. S-parameters provide an adequate system description, but do not facilitate evaluation of *transmission throughput* from one or more ports.

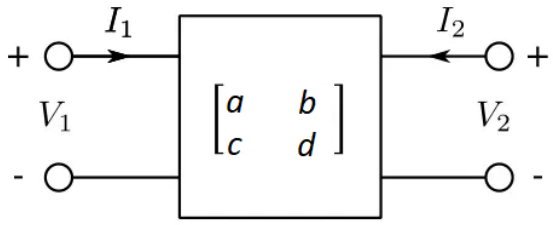

Figure 2.9: A general two-port network with voltage and currents defined [3].

Starting from Figure 2.9, ABCD parameters are defined as follow[3]:

$$\begin{cases} V_1 = aV_2 - bI_2 \\ I_1 = cV_2 - dI_2 \end{cases} \iff \begin{pmatrix} V_1 \\ I_1 \end{pmatrix} = \begin{pmatrix} a & b \\ c & d \end{pmatrix} \begin{pmatrix} V_2 \\ -I_2 \end{pmatrix} = T \begin{pmatrix} V_2 \\ -I_2 \end{pmatrix} \tag{2.27}$$

The ABCD parameters relate electrical quantities at the input port to those exhibited at the output section. This makes it easy to describe a system constructed by a sequence of elementary blocks, with each block described by its ABCD matrix. It is important to note that matrix multiplication is not commutative. Hence, a cascade of blocks described by their ABCD matrices is equivalent to a single block that is described by the product of all individual matrices, from the input section to the output one.

$$\begin{pmatrix} V_1 \\ I_1 \end{pmatrix} = \left(\prod_{\mathrm{i}=1}^{n} T_{\mathrm{i}} \right) \begin{pmatrix} V_2 \\ -I_2 \end{pmatrix} \tag{2.28}$$

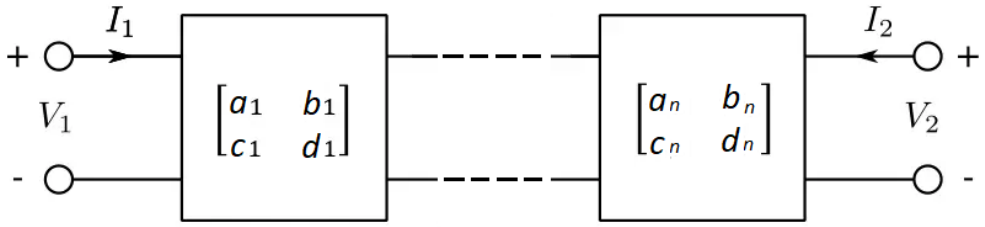

Figure 2.10: Series block connection between devices described by ABCD parameters.

Here, ABCD parameters for main elements are reported[4]:

Series Impedance Z	Shunt admittance Y	Series TL Z,θ
$\begin{pmatrix} 1 & Z \\ 0 & 1 \end{pmatrix}$	$\begin{pmatrix} 1 & 0 \\ Y & 1 \end{pmatrix}$	$\begin{pmatrix} cos(\theta) & jZsin(\theta) \\ j\frac{1}{Z}sin(\theta) & cos(\theta) \end{pmatrix}$

Table 2.1: ABCD parameters for the main passive elements.

2.2 PA Classes and efficiency enhancement

The main way to categorize active devices is based on their DC polarization. This means that the performance of a PA is largely determined by its bias point, as explained in section 2.1.1. When a DC supply is provided to the PA, it delivers energy to the load through the active device [1]. To optimize the conversion of power from DC to RF, the bias point must be chosen carefully. This has a significant impact on the efficiency, output swing, and overall performance of the PA, which must be maximized. The DC supply voltage (V_{DD}) is selected to ensure that the maximum dynamic range is exploited while avoiding breakdown phenomena.

$$V_{\mathrm{DD}} = \frac{V_{\mathrm{DS,br}} - V_{\mathrm{DS,k}}}{2} \tag{2.29}$$

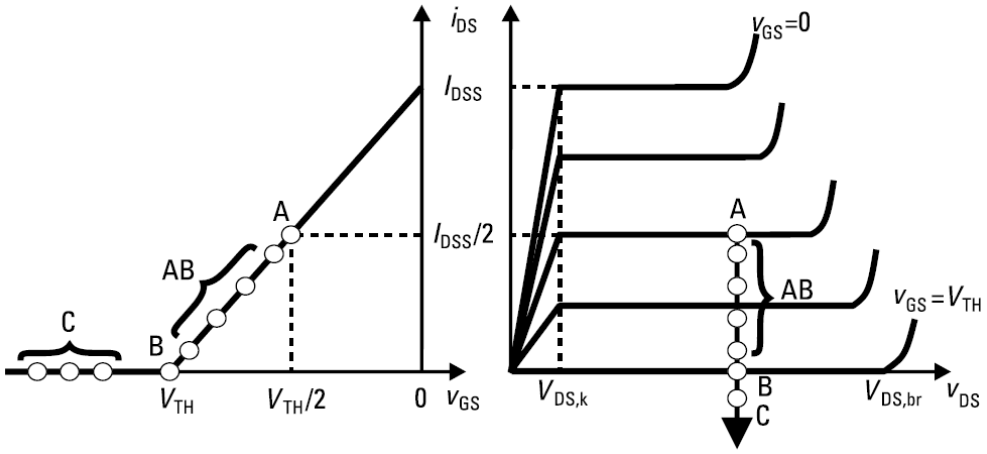

Figure 2.11: Different bias points for different PA classes shown on transcharacteristics and output characteristics of an ideal FETs. [1]

To ensure polarization at the right bias point $Q\,(V_{\mathrm{DS,DC}}; I_{\mathrm{D,DC}})$, bias networks are used. These networks couple and decouple the DC component with the signal, and are placed at both the input and output. At RF, bias-T networks are used instead, as shown in Figure 2.12. Designing a bias-T network is a complex task and is not the focus of this chapter. However, it enables a load voltage on the load that can reach up to $2V_{\mathrm{DD}}$, which is not possible with a normal bias network. Additionally, the load is tuned with a resonant circuit that acts as a bandpass filter to eliminate unwanted harmonics. Only a narrow band centred around the fundamental frequency can be delivered to the load.

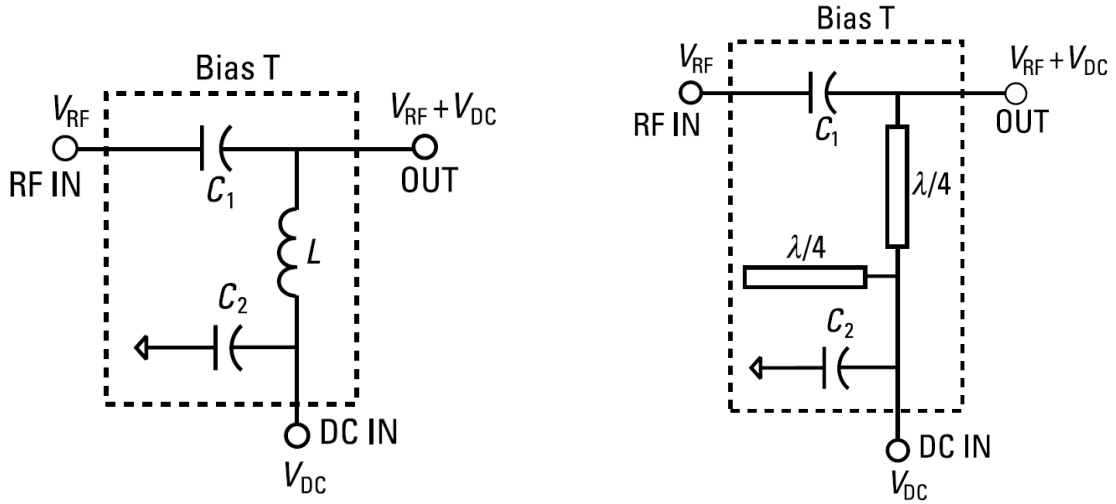

Figure 2.12: Example of bias-T network for biasing active devices. (a): network with lumped elements, (b): network with a transmission line. [1]

2.2.1 Class A, B, AB and C

When the bias point is placed in the middle of the load-line characteristic, as shown in Figure 2.13a, the PA operates in class A. The optimal bias point is located at:

$$Q_A \begin{cases} I_{\mathrm{D,DC}} = \frac{I_{\mathrm{DSS}}}{2} = I_{\mathrm{DD}} \\ V_{\mathrm{DS,DC}} = \frac{V_{\mathrm{DS,br}} - V_{\mathrm{DS,k}}}{2} = V_{\mathrm{DD}} \approx \frac{V_{\mathrm{DS,br}}}{2} \end{cases} \tag{2.30}$$

The active device remains ON constantly, allowing AC components to oscillate around the bias point with their maximum excursion ranging from $v_{\mathrm{ds,min}} = V_{\mathrm{DS,k}}$ to $v_{\mathrm{ds,MAX}} = V_{\mathrm{DS,br}}$. The *conduction angle* ϕ refers to the portion of the input signal domain that causes the active device to conduct and can be expressed as follows in relation to Q:

$$\phi = 2arccos\left(\frac{I_{\mathrm{DD}}}{I_{\mathrm{DD}} - I_{\mathrm{DSS}}}\right) = 2arccos\left(\frac{\frac{I_{\mathrm{DD}}}{I_{\mathrm{DDS}}}}{\frac{I_{\mathrm{DD}}}{I_{\mathrm{DDS}}} - 1}\right) \tag{2.31}$$

For a class A PA, $\phi = 360°$ As a consequence, Q represents the average values for v_{ds} and i_{ds}, while AC voltage and current peak amplitudes are:

$$\begin{cases} i_{\mathrm{D,peak}} = \frac{I_{\mathrm{DSS}}}{2} = I_{\mathrm{DD}} \\ v_{\mathrm{DS,peak}} = \frac{V_{\mathrm{DS,br}} - V_{\mathrm{DS,k}}}{2} = V_{\mathrm{DD}} \approx \frac{V_{\mathrm{DS,br}}}{2} \end{cases} \tag{2.32}$$

Assuming that the load is resistive at the working frequency, the optimal value for maximum power transfer is the one that maximizes both voltage and current, and for a class A amplifier, this value is:

$$R_{\mathrm{L,opt}} = R_{\mathrm{opt}} = \frac{V_{\mathrm{DS,br}} - V_{\mathrm{DS,k}}}{I_{\mathrm{DSS}}} \tag{2.33}$$

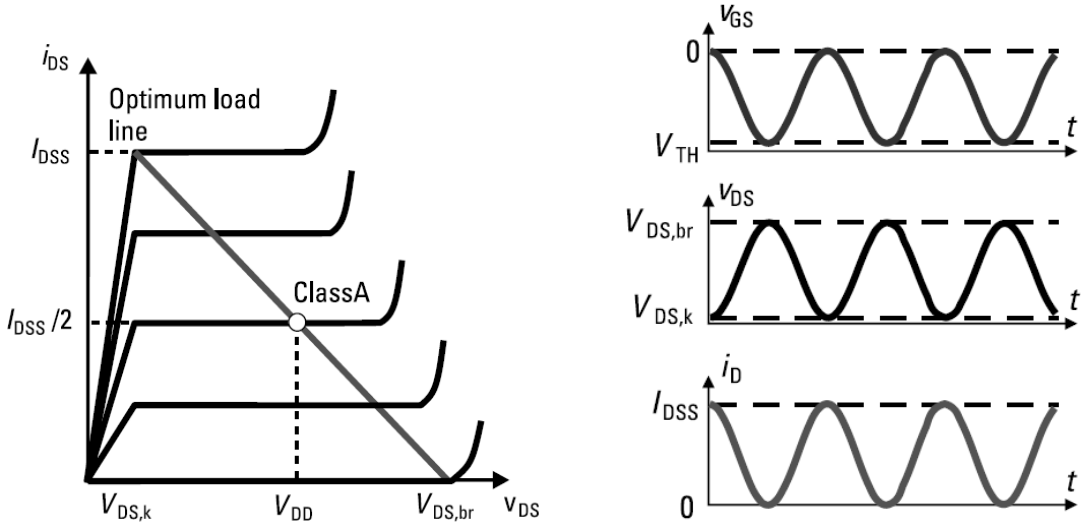

Figure 2.13: PA in class A. (a): quiescent point Q, (b): output characteristics in the time domain. [1]

To measure efficiency for energy usage, it is important to evaluate output power P_{O} and DC power from the supply P_{DC}. In optimal load conditions, P_{O} depends on the input signal's amplitude. If there is no input signal, no power is delivered to the load. However, at maximum output excursion, P_{O} reaches its maximum value $P_{\mathrm{O,max}}$:

$$P_{\mathrm{O,max}} = \left.\frac{V_{\mathrm{DD}} I_{\mathrm{DD}}}{2}\right|_{R_{\mathrm{L}}=R_{\mathrm{opt}}} = \frac{1}{2}\frac{V_{\mathrm{DS,br}} - V_{\mathrm{DS,k}}}{2}\frac{I_{\mathrm{DSS}}}{2} \tag{2.34}$$

while the maximum DC absorbed from the power supply is given by the bias point Q:

$$P_{\mathrm{DC,max}} = V_{\mathrm{DD}} I_{\mathrm{DD}} = \frac{V_{\mathrm{DS,br}} - V_{\mathrm{DS,k}}}{2}\frac{I_{\mathrm{DSS}}}{2} \tag{2.35}$$

As a consequence, the efficiency of a PA in class A can be evaluated:

$$\mu_{\mathrm{max}} = \left.\frac{P_{\mathrm{O,max}}}{P_{\mathrm{DC,max}}}\right|_{\text{class A}} = 50\% \tag{2.36}$$

To sum up, Class A configuration provides excellent linearity, but its efficiency is poor due to the active device being always ON. This results in a higher amount of energy getting dissipated. Keeping the device biased requires an unuseful quantity of power coming from the supply. Furthermore, the efficiency reduces linearly with the back-off. Without an input signal, all DC power is dissipated by the active component. Reducing the back-off can deliver some of the DC power to the load. However, with maximum input drive, only 50% of the power delivered is transferred to the load and the other half is dissipated by the active component. To improve efficiency, it is necessary to reduce DC power consumption. In Class B amplifiers, the bias point is set to the threshold voltage so that the active device conducts only during one-half of the input signal. This means that $\phi = 180°$ and the active device is only ON for a half period. As shown in Figure 2.14b, the voltage across v_{DS} is the same as in Class A amplifiers, but the main difference is in the current i_{D}, which flows in the active device only during the positive half of the input signal. Only the fundamental frequency is delivered to the tuned load. Hence, the new bias point is as follows:

$$Q_{\mathrm{B}} \begin{cases} I_{\mathrm{D,DC}} = 0 \\ V_{\mathrm{DS,DC}} = \frac{V_{\mathrm{DS,br}} - V_{\mathrm{DS,k}}}{2} = V_{\mathrm{DD}} \approx \frac{V_{\mathrm{DS,br}}}{2} \end{cases} \tag{2.37}$$

AC analysis is more complex and, to understand dynamic behaviour, it is necessary to look at the Fourier series of the drain current:

$$\begin{aligned} i_{\mathrm{DS}}(\theta) = \frac{I_{\mathrm{DSS}}}{\pi} + \frac{I_{\mathrm{DSS}}}{2} sin(\theta) - \frac{2I_{\mathrm{DSS}}}{3\pi} cos(2\theta) - \frac{2I_{\mathrm{DSS}}}{15\pi} cos(4\theta) + ... \\ - \frac{2I_{\mathrm{DSS}}}{(n+1)(n-1)\pi} cos(n\theta) + ... \text{ with } n \in 2; 4; 6; ... \end{aligned} \tag{2.38}$$

Considering that only the fundamental is delivered to the load, from the series above is possible to observe that the current delivered to the load is the same for class A and, for this reason, the optimum load can be considered the same as before and also $P_{\mathrm{O,max}}$ is the same of (2.34). On the contrary, $P_{\mathrm{DC,max}}$ is estimate as follows:

$$P_{\mathrm{DC,max}} = \frac{V_{\mathrm{DS,br}} - V_{\mathrm{DS,k}}}{2} \frac{I_{\mathrm{DSS}}}{\pi} \tag{2.39}$$

As a consequence of turning OFF the amplifier for 50% of the period, there is a reduction of DC power supplied and the efficiency increases to:

$$\mu_{\max} = \frac{P_{\mathrm{O,max}}}{P_{\mathrm{DC,max}}}\Big|_{\text{class B}} = \frac{\pi}{4} \sim 78\% \tag{2.40}$$

.

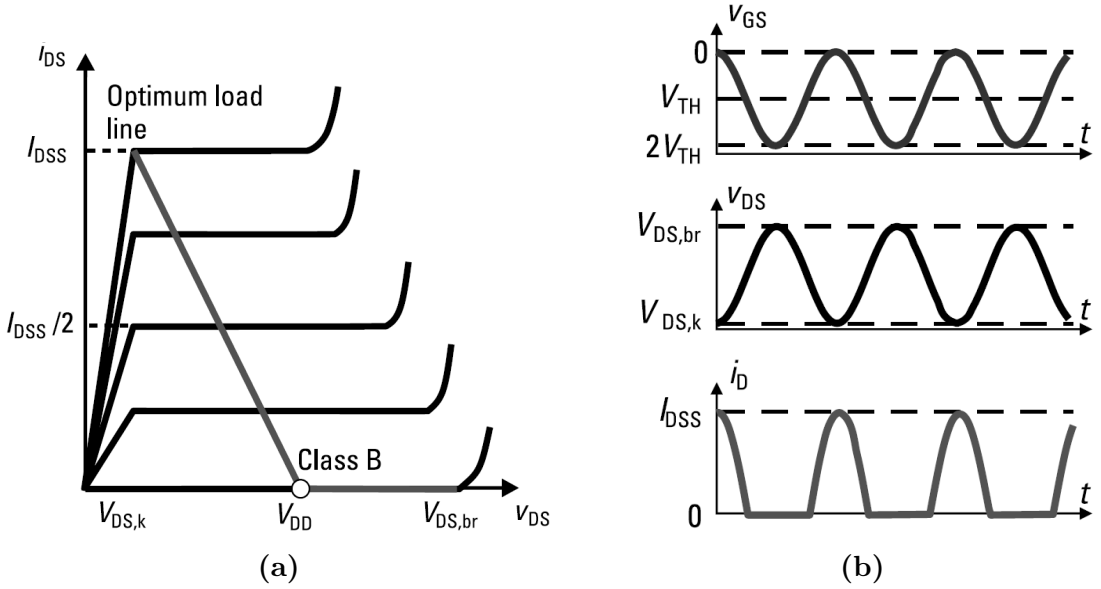

Figure 2.14: PA in class B. (a): quiescent point Q, (b): output characteristics in the time domain. [1]

Class B amplifiers offer a higher maximum achievable efficiency compared to class A amplifiers, with an increase from 50% to 78%. However, linearity is compromised as the entire dynamic range is utilized only for half a period and some energy is wasted in harmonics. To address the linearity issue, techniques like the push-pull PA can be employed. This involves two complementary active devices working on two different half-periods, which helps to avoid information wastage. Additionally, there are other classes of amplifiers available as well:

1. In class AB, the bias point is placed between A and B to find a trade-off between linearity and efficiency. This allows for a conduction angle in the range of $180° < \phi < 360°$ and an efficiency between 50% and 78%;

2. If the amplifier's bias point is below the threshold voltage, it can be classified as a class C amplifier. In this mode, the active device is ON for a period less than half a cycle and has a conduction angle ϕ that is less than 180°. Though class C amplifiers are more efficient than class B amplifiers, their linearity is comparatively worse.

2.2.2 Switching-mode amplifiers: class D and E

In class D, the active element functions as a switch in the ON/OFF condition. A pair of active elements in push-pull configuration is biased in class B, with

each transistor being driven by a square wave of opposite phases. Before driving the configuration, the input signal can be modulated with *pulse-width modulation* (PWM) or *Pulse Duration Modulation* (PDM) techniques. Phase inversion is achieved through *electromagnetic field coupling* (EMF) with the transformers, as shown in Figure 2.15. A resonant circuit is used to deliver only fundamental to the load.

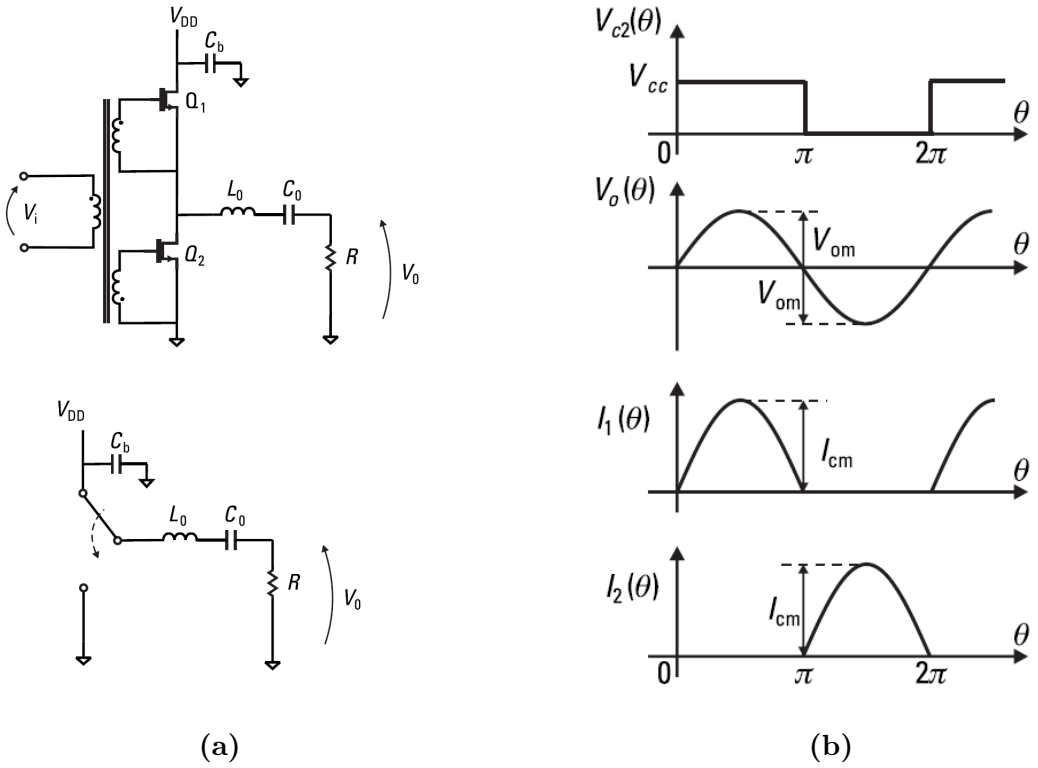

(a) **(b)**

Figure 2.15: PA in class D. (a): scheme and equivalent circuit, (b): waves in time domain. [1]

When a PA is in switching mode, it can operate with an efficiency of up to 100%. However, this theoretical value is influenced by parasitic effects in active elements, which cause dissipation. Specifically, a small voltage drop occurs between the drain and source in the ON state, and a small current flows through the open switch in the OFF state. In Class E amplifiers, only one active element is used instead of a couple of transistors, but the working principle remains the same.

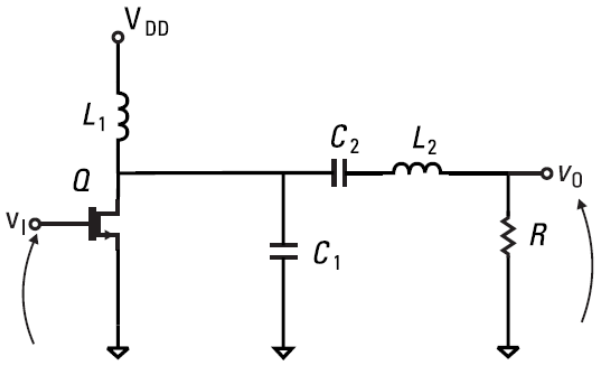

Figure 2.16: Class E, basic scheme. [1]

2.2.3 Harmonic-tuned amplifiers in class F

Up until now, the harmonics caused by non-linear effects have been filtered out by either a tunable load or a filtering system placed on the output port of the amplifier. However, the idea behind the class F amplifier is to shape the power produced by the harmonics in such a way that it enhances the useful signal. This is achieved by using a network that recovers power from the term $\sum_{n=2,3,4...} P_O(nf_0)$ and converts it constructively with $P_O(f_0)$, as described in (2.3). Although this strategy is complex, it leads to achieving efficiency higher than class AB/B.

2.2.4 Back-off efficiency enhancements

The main issue with PAs, as described earlier, is that as the back-off level increases, the amplifier's efficiency decreases. Maximum efficiency is achieved when the input signal is at its maximum power. However, as the input signal weakens, efficiency is significantly reduced due to the behaviour of P_{DC}. To save energy, the aim is to minimize DC power dissipation in back-off. There are two main approaches to achieve this:

1. *Load-modulation* PA: the optimal load in back-off can be achieved by modulating the load itself. The most famous technique able to exploit the load-modulation is the *Doherty PA*;

2. *Envelope tracking* (ET): It is not a power amplifier architecture, but rather a system-level modification in which the bias point dynamically changes according to the input signal's envelope. In this way, the DC power supply is modulated and reduced when not needed.

The Doherty PA will be largely discussed in the following chapters and its analysis is part of this work.

Chapter 3

The Doherty Power Amplifier

In any discussions about RF power amplifier techniques for modern applications, the central goal of maintaining efficiency over a wide signal dynamic range must surely remain paramount[5]. This chapter aims to introduce and explain in detail this common efficiency enhancement technique suitable for RF application when the modulated signal has a high peak-to-average power ratio. All analyzed amplifier classes exhibit maximum efficiency when the input signal is driven to its maximum excursion, resulting in the maximum delivered power to the load. However, as the amplifier operates in back-off, the efficiency decreases in a manner that varies depending on the specific class. This implies that the maximum efficiency is only achievable for constant-envelope modulations such as FM, but this condition can only be met when the input drive is at its maximum. The *Doherty Power Amplifier* (DPA) is a particular configuration that was developed in 1936 to solve efficiency problems in back-off.

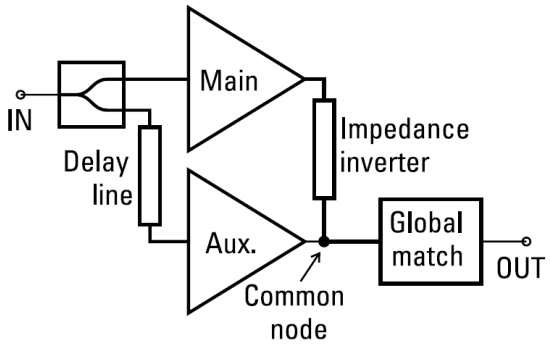

Figure 3.1: Basic DPA.

It was initially based on high-power tube amplifiers. The basic idea is to dynamically adapt the load to its optimal value by using load modulation techniques, to ensure the maximum excursion of the output voltage swing. The concept is based on modifying the RF load by applying current from a second, phase-coherent source [2]. The technique of load modulation is accomplished by using two amplifiers in parallel - the *Main* PA and the *Auxiliary* PA. These amplifiers work by delivering power to a common node and using an impedance inverter to modulate the load. When the input power is low, only the Main amplifier delivers power to the load and the Auxiliary one is off. This condition is maintained until the input power reaches a certain threshold, which corresponds to the saturation point of the Main PA. As the input power increases beyond this threshold, the Auxiliary PA begins to deliver power to the load. The benefits of using a DPA are most apparent in the region between the two saturation points, where both the Main and Auxiliary amplifiers work together to deliver power to the load. Usually, Auxiliary is turned off when OBO is higher than -6dB, which means when the output power is a quarter of the maximum combined one. So, for higher back-off, only the Main works as a normal PA while efficiency enhancement is exploited for $-6\text{dB} < \text{OBO} < 0\text{dB}$. To manage this threshold, the Main PA is usually in class B while the Auxiliary one is in class C.

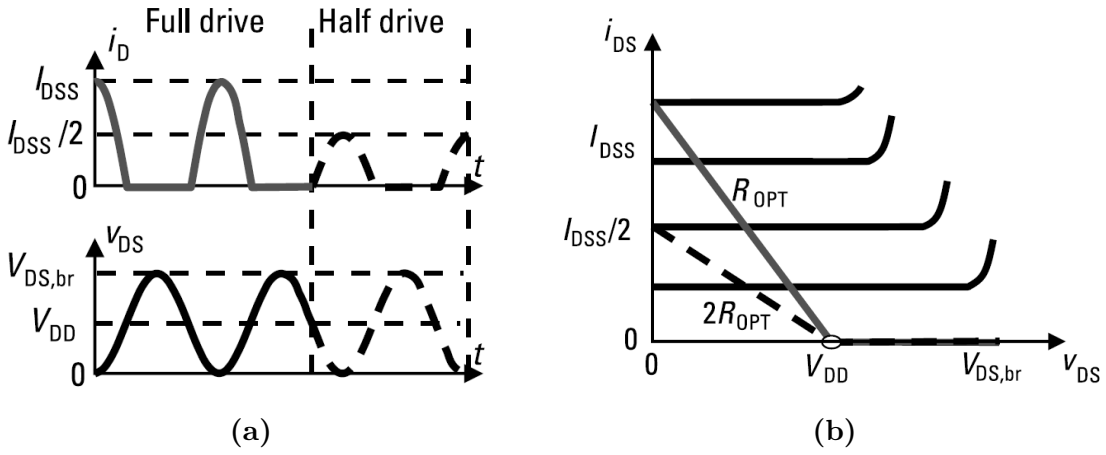

Figure 3.2: Basic DPA. (a): waves in time domain, (b): load lines. [1].

3.1 Working principle

In order to understand how the DPA works, the concept of load modulation first needs to be introduced using the circuit shown in Figure 3.3. The impedance that the output terminals of the first current generator experience must be also considered. When both I_1 from the first generator (as the Main) and I_2 from the

second generator (as an Auxiliary) flow through the load R, the impedance Z_1 seen by the first generator can be calculated as follows [2]:

$$Z_1 = \frac{V_1}{I_1} = \frac{R\,(I_1 + I_2)}{I_1} = R\left(1 + \frac{I_2}{I_1}\right) \tag{3.1}$$

From (3.1), three situation can be distinguished:

1. If $I_2 = 0$, the impedance seen by the Main is trivially the value of the resistance;

2. If $I_2 \neq 0$, the load seen by the Main is different from the original one and can be increased or decreased according to the relative phase between I_2 and I_1.

This fact implies that the impedance that the generator's output presents to the external world, known as the *Main* PA, can be adjusted based on the operation of a second source, known as the *Auxiliary* PA, within the system. This simple principle can be employed in power amplifiers to optimize the load presented to the Main amplifier and simultaneously offer an additional energy source to power the load.

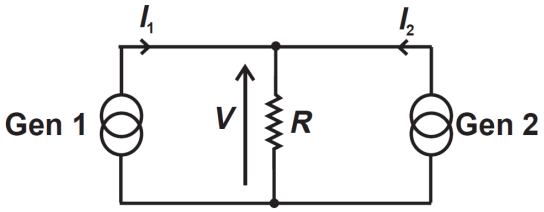

Figure 3.3: Active load-pull with two signal generators. [2]

The basic scheme shown in Figure 3.3 can be modified to create the dynamic circuit of a generic DPA, which is depicted in Figure 3.4a. In this new Figure, only the output stage is highlighted, with generators representing the output stage of each active device. These generators are driven by the input signal, according to the dynamic model of transistors. One key difference between 3.3 and 3.4a is the presence of a quarter-wave transformer, which is crucial for achieving the intended aim. For the analysis, the following hypothesis is assumed:

- Active elements are identical between them and, in terms of current, they have the same maximum current $I_{\max}$;

- It is assumed that Main PA is biased in class B and for this reason fundamental current amplitude is $I_{\max}/2$;

- When the OBO is minor than -6dB, only the Main amplifier is active, operating as a typical class B amplifier. However, when the OBO is between -6dB and 0dB, the Auxiliary power amplifier also delivers current to the load. This control of conduction, which depends on the input signal, can be achieved by adjusting the threshold voltage for each bias. For example, a combination of Main and Auxiliary amplifiers operating in class B and C can be used, or input levels can be controlled;
- The optimal load R_{OPT} is assumed for the class B, neglecting knee-voltages:

$$R_{\mathrm{OPT}} \simeq 2\frac{V_{\mathrm{DD}}}{I_{\mathrm{max}}} \tag{3.2}$$

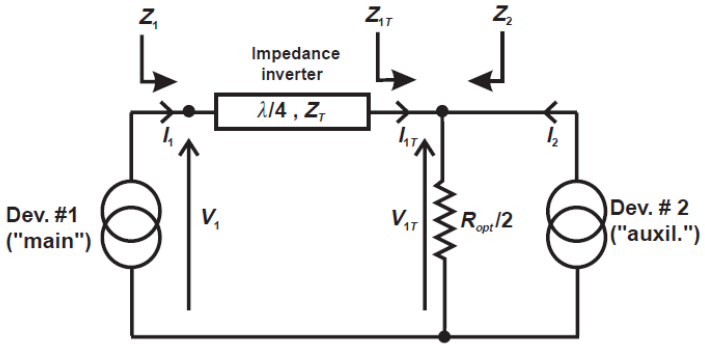

(a)

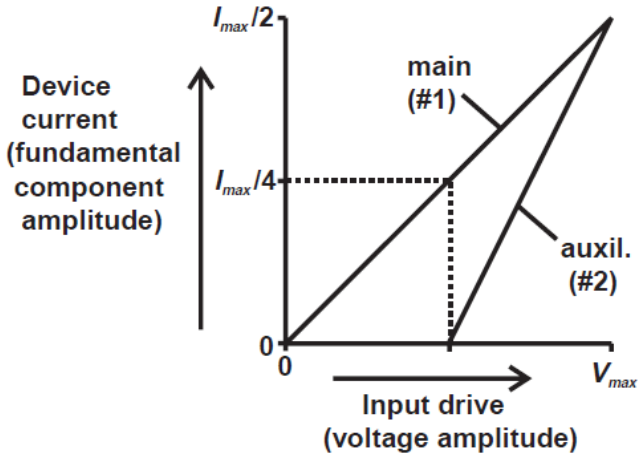

(b)

Figure 3.4: Doherty power amplifier: dynamic behaviour. (a): dynamic DPA scheme, (b): dynamic RF transcharacteristics. [2]

Before beginning, it is necessary to recall the ABCD matrix of the quarter-wave with characteristic impedance Z_{T}, as shown in Figure 3.4a:

$$\begin{bmatrix} V_1 \\ I_1 \end{bmatrix} = \begin{bmatrix} 0 & jZ_{\mathrm{T}} \\ \frac{j}{Z_{\mathrm{T}}} & 0 \end{bmatrix} \begin{bmatrix} V_{1\mathrm{T}} \\ I_{1\mathrm{T}} \end{bmatrix} \Longleftrightarrow \begin{cases} V_1 = jZ_0 I_2 \\ I_1 = \frac{j}{Z_0} V_2 \end{cases} \Longleftrightarrow \begin{cases} V_{1\mathrm{T}} = \frac{Z_{\mathrm{T}}}{j} I_1 \\ I_{1\mathrm{T}} = \frac{V_1}{jZ_{\mathrm{T}}} = -j\frac{V_1}{Z_{\mathrm{T}}} \end{cases} \tag{3.3}$$

Z_{T} is a well-known characteristic of the transmission line in design. By observing the ABCD characterization, it is possible to notice that:

1. When the current enters the common node to the load, the transmission line results in a 90° delay. To ensure constructive power recombination, the current from the second device should also be delayed by 90°. Therefore, an input delay line is used. In conventional Doherty power amplifiers, a $\lambda/4$ transmission line is required at the Auxiliary input. This provides a 90° phase shift to the input signal, allowing for a phase-correct combination at the output[6];

2. The transmission line decouples electrical quantities related to the different sides. In fact, V_1 is related to the current on the other side, $I_{1\mathrm{T}}$, only by the effect of Z_{T} and does not depend on the output voltage and the load.

By combining equations in system shown in (3.3), following results can be obtained:

$$\begin{aligned} V_{1\mathrm{T}} I_{1\mathrm{T}} &= -V_1 I_1 \\ Z_{\mathrm{T}}^2 &= \frac{V_1}{I_1} \cdot \frac{V_{1\mathrm{T}}}{I_{1\mathrm{T}}} = Z_1 Z_{1\mathrm{T}} \end{aligned} \tag{3.4}$$

Starting from now, a mathematical model that describes the behaviour of the DPA in back-off is derived. When the OBO is lower than -6dB, the Auxiliary is OFF, and the DPA operates as a normal class B power amplifier. When the OBO is in the 3dB range, both devices supply currents directly proportional to the input drive voltage. By exploiting the linear I-V relations shown in Figure 3.4b, the currents delivered dynamically by each active element can be expressed as a function of a new dimensionless quantity, ξ, which is used to fix the back-off level. The purpose of this factor is to normalize the dynamic range of the DPA from the back-off threshold at -6dB to the saturation and to decouple the input voltage, which is not taken into account in this demonstration, from the input drive. The value of ξ is between 0 and 1, which corresponds to -6dB back-off and maximum power condition, respectively, according to the following definition:

$$\xi = \xi(V_{\mathrm{in}}) = 2\frac{V_{\mathrm{in}} - V_{\mathrm{in,MAX}}/2}{V_{\mathrm{in,MAX}}} \quad \text{for} \quad \frac{V_{\mathrm{in,MAX}}}{2} \leq V_{\mathrm{in}} \leq V_{\mathrm{in,MAX}} \tag{3.5}$$

In 6dB back-off region, the current profile shown in Figure 3.4b becomes:

$$\begin{aligned} I_1 &= \frac{I_{\max}}{4}(1+\xi) \\ I_2 &= -j\frac{I_{\max}}{2}\xi \end{aligned} \tag{3.6}$$

The Auxiliary input delay at central frequency indicates an imaginary I_2. Referring to 3.4a and recalling (3.1), the pulling effect can be expressed as:

$$\begin{aligned} Z_{1\mathrm{T}} &= \frac{R_{\mathrm{OPT}}}{2}\left(1+\frac{I_2}{I_{1\mathrm{T}}}\right) = \frac{R_{\mathrm{OPT}}}{2}\left(1+j\frac{I_2 Z_{\mathrm{T}}}{V_1}\right) \\ Z_2 &= \frac{R_{\mathrm{OPT}}}{2}\left(1+\frac{I_{1\mathrm{T}}}{I_2}\right) = \frac{R_{\mathrm{OPT}}}{2}\left(1-j\frac{V_1}{I_2 Z_{\mathrm{T}}}\right) \end{aligned} \tag{3.7}$$

It is possible to observe from the last equation that $I_{1\mathrm{T}}$ is still unknown. However, for 0dB back-off ($\xi = 1$), $I_{1\mathrm{T}}$ equals $I_2 = I_{\max}/2$. In this scenario, the pulling effect is exploited at its maximum capability, resulting in $Z_{1\mathrm{T}} = Z_2 = R_{\mathrm{OPT}}$, which is a significant increase from its initial value of $R_{\mathrm{OPT}}/2$. It is also interesting to note the change in impedance seen by the Main. By combining (3.4) with the expression of $Z_{1\mathrm{T}}$, the impedance seen by the output of the Main, Z_1, can be calculated.

$$Z_1 = \frac{Z_T^2}{Z_{1\mathrm{T}}} = \frac{2Z_{\mathrm{T}}^2}{R_{\mathrm{OPT}}\left(1+j\frac{I_2 Z_{\mathrm{T}}}{V_1}\right)} = \frac{2Z_{\mathrm{T}}^2}{R_{\mathrm{OPT}}\left(1+\frac{I_{\max} Z_{\mathrm{T}}}{2V_1}\xi\right)} \tag{3.8}$$

Comparing these last results, it is possible to understand the action of the inverter: as I_2 increases, $Z_{1\mathrm{T}}$ is up-modulated and the impedance inverter reduces the impedance seen by the Main output Z_1, showing an *inverted* behaviour. This is the key point of the Doherty PA. Furthermore, at central frequency, Z_1 assumes real value thanks to the phase compensation introduced by the input delay. After some manipulation, the following results are highlighted:

$$V_1 = \frac{Z_{\mathrm{T}}}{R_{\mathrm{OPT}}}\frac{I_{\mathrm{MAX}}}{2}\left[Z_{\mathrm{T}} + \xi\left(Z_{\mathrm{T}} - R_{\mathrm{OPT}}\right)\right] \tag{3.9}$$

The last equation is crucial to understand the key of Doherty: imposing that the characteristic impedance Z_{T} of the transmission line is equal to the optimal load R_{OPT}, the voltage at the Main output is simplified as follows:

$$V_1 = \frac{Z_{\mathrm{T}}}{R_{\mathrm{OPT}}}\frac{I_{\mathrm{MAX}}}{2}\left[Z_{\mathrm{T}} + \xi\left(Z_{\mathrm{T}} - R_{\mathrm{OPT}}\right)\right]\Big|_{Z_{\mathrm{T}}=R_{\mathrm{OPT}}} = \frac{I_{\max}}{2}R_{\mathrm{OPT}} \tag{3.10}$$

This result is very important because tells that the Main voltage, under the coupling condition $Z_{\mathrm{T}} = R_{\mathrm{OPT}}$, is constant and does not depend on ξ. That means

that V_1 is constant at the maximum dynamic voltage swing in the region with $-6\text{dB} < OBO < 0\text{dB}$. So, thanks to the transmission line working as an impedance inverter, in the -6dB back-off the double effect of inverted load-pulling and the increasing of the Auxiliary current allows to maintain a constant voltage across the Main output stage. It is interesting to use these results to estimate the voltage across the resistive load $V_{1\text{T}}$, which is connected to V_1 through transmission line depicted in (3.4). After some rearrangement, the voltage across can be written as follows:

$$V_{1\text{T}} = I_1 Z_\text{T} = \frac{I_\text{max}}{4}(1+\xi)Z_\text{T}\Big|_{Z_\text{T}=R_\text{OPT}} = \frac{I_\text{max}}{4}(1+\xi)R_\text{OPT} \tag{3.11}$$

In the -6dB back-off region, the voltage across the load follows the entire dynamic range of I_1 available from the Main amplifier. This demonstrates that the Main amplifier is working at its maximum efficiency, as V_1 remains constant at its maximum value throughout the entire range. The power of this topology consists of the double effect of the transmission line that, acting as an inverter, allows that:

- as the impedance on the right side is modulated by the Auxiliary, the inverting effect is exploited with a decrease of the impedance seen by the left side;

- voltage on one side is blocked and does not impact on the other side. In this way, the inversion network decouples sides one from the other and while the Main has saturated the Auxiliary can work with the proper voltage level according to the load modulation principle.

The following statements, referring to -6dB back-off region, resume all concepts that have been demonstrated:

1. The quarter-wave transmission line, working as an impedance inverter, makes the load-modulation effect act in the load-pulling effect;

2. Current coming from the Auxiliary has the double effect of reducing load seen by the Main and giving current to the load. The overall effect under the condition $Z_\text{T} = R_\text{OPT}$ is that the Main voltage V_1 remain constant in the entire range at its maximum value;

3. Working at its maximum swing, the Main PA maintains maximum efficiency;

4. In order to compensate for the 90° delay introduced by the impedance inverter and combine current at the common node with the same phase (so, in a constructive way), an input delay on the Auxiliary is needed.

3.2 Power and efficiency

In terms of efficiency, a DPA configuration offers a significant improvement over the classic PA configuration. This is because, when working in a certain back-off region, the Main amplifier works in saturation while the Auxiliary manages the signal on the load. As discussed in chapter 2, operating at saturation allows the PA stage to achieve maximum efficiency. However, while the Main PA operates at maximum efficiency, the Auxiliary does not work under the same conditions and therefore, the overall DPA efficiency is reduced. Assuming that both PAs work in class B, a model can be derived analytically. For back-off levels lower than -6dB, only the Main amplifier conducts, and the efficiency is the same as that of a classical class B PA.

$$\mu_{\text{tot}} = \frac{\pi}{4} \cdot \frac{2v_{\text{in}}}{V_{\text{max}}} \tag{3.12}$$

In the -6dB back-off region, where both PAs conduce current, the power delivered to the load can be derived easily from (3.11):

$$\begin{aligned} P_{\text{L,tot}} &= \frac{V_{1\text{T}}^2}{2R_{\text{L}}} = \frac{I_1^2 R_{\text{OPT}}^2}{2} \cdot \frac{2}{R_{\text{OPT}}} = \\ &= I_1^2 \cdot R_{\text{OPT}}\Big|_{R_{\text{OPT}} \simeq 2\frac{V_{\text{DD}}}{I_{\text{max}}}} \simeq \frac{I_{\text{max}}}{2} \frac{v_{\text{in}}}{V_{\text{MAX}}} V_{\text{DD}} \end{aligned} \tag{3.13}$$

The DC power absorbed by the Main and Auxiliary is in this example the same for a class B:

$$\begin{aligned} P_{\text{DC,Main}} &= \frac{v_{\text{in}}}{V_{\text{max}}} \frac{I_{\text{max}}}{\pi} V_{\text{DD}} \\ P_{\text{DC,aux}} &= 2\left(\frac{v_{\text{in}}}{V_{\text{max}}} - 0.5\right) \frac{I_{\text{max}}}{\pi} V_{\text{DD}} \end{aligned} \tag{3.14}$$

The overall DC power absorbed from the Main and Auxiliary is the sum of both contributions:

$$P_{\text{DC}} = P_{\text{DC.Main}} + P_{\text{DC,aux}} = \left(\frac{I_{\text{max}}}{\pi}\right) \left[3\left(\frac{v_{\text{in}}}{V_{\text{max}}}\right) - 0.5\right] V_{\text{DD}} \tag{3.15}$$

At the end, the efficiency is a function of the input level and the final result is the following:

$$\mu_{\text{tot}} = \frac{\pi}{2} \cdot \frac{\left(\frac{v_{\text{in}}}{V_{\text{max}}}\right)^2}{3 \cdot \left(\frac{v_{\text{in}}}{V_{\text{max}}}\right) - 1} \tag{3.16}$$

The efficiency of a DPA is determined by two different back-off scenarios, as described in (3.17). When the back-off is lower than -6db, the DPA behaves like a classical class B PA, whereas in the -6dB back-off regime, it shows an improvement in terms of efficiency. Figure 3.5 shows the efficiency described as a function of OBO. The efficiency ripple is due to the DC power absorption of the Auxiliary that does not work in saturation, with a negative impact on efficiency. However, as the Auxiliary output voltage increases, the efficiency improves. Although the general efficiency trend of a DPA is similar to that shown in Figure 3.5, it heavily depends on the class of each PA and their IV characteristics.

$$\mu_{\text{tot}} = \begin{cases} \frac{\pi}{4} \cdot \frac{2v_{\text{in}}}{V_{\text{max}}}, & \text{for OBO<-6dB} \\ \\ \frac{\pi}{2} \cdot \frac{\left(\frac{v_{\text{in}}}{V_{\text{max}}}\right)^2}{3 \cdot \left(\frac{v_{\text{in}}}{V_{\text{max}}}\right) - 1}, & \text{for -6dB<OBO<0dB} \end{cases} \tag{3.17}$$

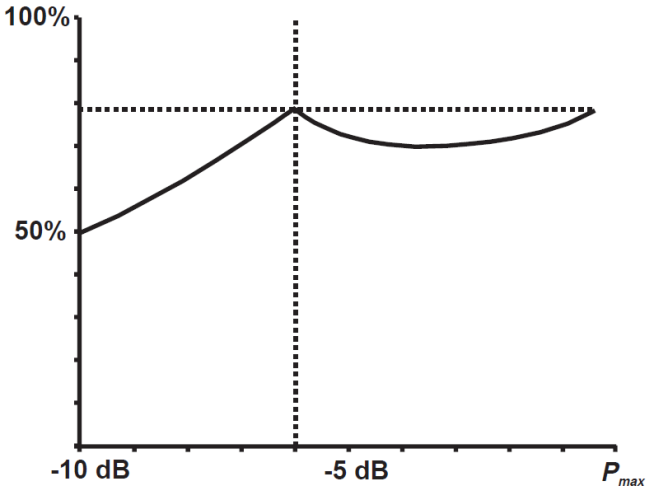

Figure 3.5: Class B/B DPA, efficiency. [2]

3.3 Implementations

It is important to note that the actual performance of a typical DPA may differ from the theoretical analysis discussed in section 3.1, due to various non-ideal operating conditions. The efficiency of the amplifier can be significantly affected by factors:

- In order to ensure equal distribution of input power between Main and Auxiliary branches, a balanced power splitter is typically used. However, this type of

splitter is strongly non-linear and can cause unwanted phase shifts between the Main and Auxiliary signals. Alternatively, an unbalanced power splitter may be used, but this still poses a challenge in terms of managing power division in the design. Despite this, other solutions are available. For example, rather than using a simple power splitter with a quarter-wave transmission line on the Auxiliary branch, the input transmission line can be replaced with lumped elements or the power divider at the DPA input stage can be replaced with a quadrature 3dB splitter [7].

- Main and Auxiliary are two PAs that should utilize the ideal input/output transcharacteristic shown in Figure 3.4b. In the initial Doherty implementation, each amplifier was realized with tubes, and due to specific characteristics of these old components, the I-V curve could be easily controlled in terms of transconductance g_{m} and maximum current I_{max}. However, in modern solutions, tubes have been replaced by active elements such as transistors (especially FETs), which do not offer the same flexibility. The transcharacteristic cannot be managed but strongly depends on the physical characteristics of the transistor (doping levels, material, dimension, and scaling) and the bias. Therefore, the Main and the Auxiliary active elements are not equal but are scaled in a suitable way. Additionally, the class in which every amplifier works is important for the design, and especially for the Auxiliary, it represents a possible way to switch on/off the active element according to the working principle of a DPA.

In the first transistor-based implementation, both the Main and Auxiliary were biased in class B. This configuration is known as a class B-B DPA. The main issue with this configuration is that the Auxiliary needs to be turned on only when the input signal's envelope reaches a certain level, due to the properties of class B. While the Main component is on in every envelope condition, the Auxiliary component starts conducting only when the back-off is higher than -6dB. This solution does not pose any problems for the Main component, but using a class B on the Auxiliary component means conduction in every envelope condition, and this problem needs to be addressed. The issue can be resolved by controlling the Auxiliary bias with a suitable circuit capable of sensing the input envelope and driving a switching circuit to turn on the Auxiliary component only when the input signal is greater than a certain level. The basic scheme of a B-B DPA working with this principle is shown in Figure 3.6. Another solution with *adaptive bias* can be implemented, which improves linearity.

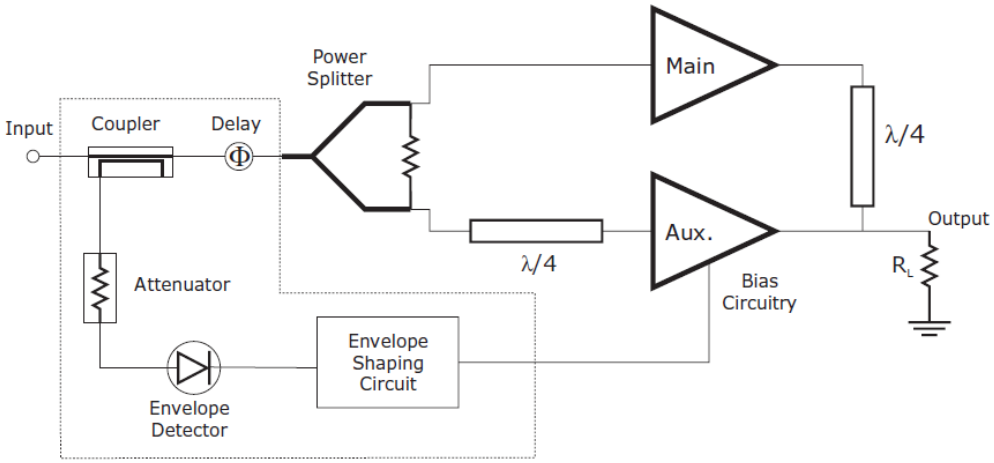

Figure 3.6: Class B-B DPA with switching circuit. [8]

In order to activate the Auxiliary only when the signal reaches a certain threshold, an effective approach is to use a class C PA for the Auxiliary of a class B-C DPA. The bias point is selected to turn on the Auxiliary PA only when the input signal envelope is above the threshold. In this way, the Main amplifier is always on, but the Auxiliary starts to conduct only in the -6dB back-off region. It is recommended to use an unbalanced splitter to ensure proper load modulation. However, using a class C increases the risk of breakdown. Another configuration is the class AB-C DPA, which improves linearity and reduces crossover distortion at the expense of efficiency. Advanced solutions involve using different bias voltages for the Main and Auxiliary or adopting a class F configuration for the Main amplifier.

It has been assumed so far that the load R_{L} is purely resistive and equal to $R_{\mathrm{opt}}/2$. However, this assumption can be too narrow because the effective load that a generic PA needs to supply can be different from the optimal one, which depends on the amplifier's structure. To match the load with the optimal characteristic of a PA, a matching network is used to replace the pure resistive load R_{L}. At working frequency, this matching network appears as a pure resistive optimal load for the purpose. In most cases, a matching network is realized with another transmission line in series between the common node and the effective load that needs to be supplied, with the characteristic impedance chosen as:

$$Z_2^{load} = \sqrt{\frac{1}{2} R_{\mathrm{opt}} R_{\mathrm{L}}} \tag{3.18}$$

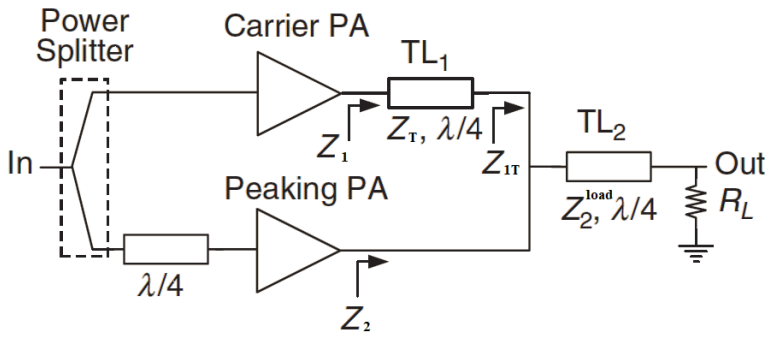

Figure 3.7: Basic DPA architecture with matching network on load.

3.4 Bandwidth and linearity

Assuming that all elements act linearly in the useful band, the Doherty configuration ensures good linearity due to load modulation and the superposition of powers coming from the Main and Auxiliary ones. As seen in Figure 3.8, when only the Main is on, the output power at the common node follows the power characteristic of the Main, and the Auxiliary is off. However, when the Auxiliary starts to conduct, the load-modulation effect is exploited, and the Main output voltage remains constant while the power characteristic behaves as a square root curve. On the other hand, the Auxiliary amplifier experiences an upward load-pull effect, generating an output power proportional to the cube of the increasing input voltage amplitude, giving a "three-halves" power transfer characteristic. The superposition of these two characteristics gives a composite linear power response [2].

It is important to consider non-idealities in the design process of DPA, as it is achieved through strongly non-linear elements, such as transistors. The behaviour of these elements during the realization of Main and Auxiliary PAs can have a significant impact on the design due to their non-linear characteristics. This impact can be attributed to various reasons, which are described below:

- The Auxiliary PA should be turned off below a certain threshold to prevent unwanted current modulation of the Main load;
- In the high-power range, the Main voltage remains close to the maximum level and the I-V curve has a monotonic slope, without being clipped by a saturation point.

Studying the linearity of a DPA is generally more complex than that of a normal Class AB amplifier. From a broad perspective, it is possible to demonstrate that at low power levels, when only the Main amplifier is active, the linearity behaves

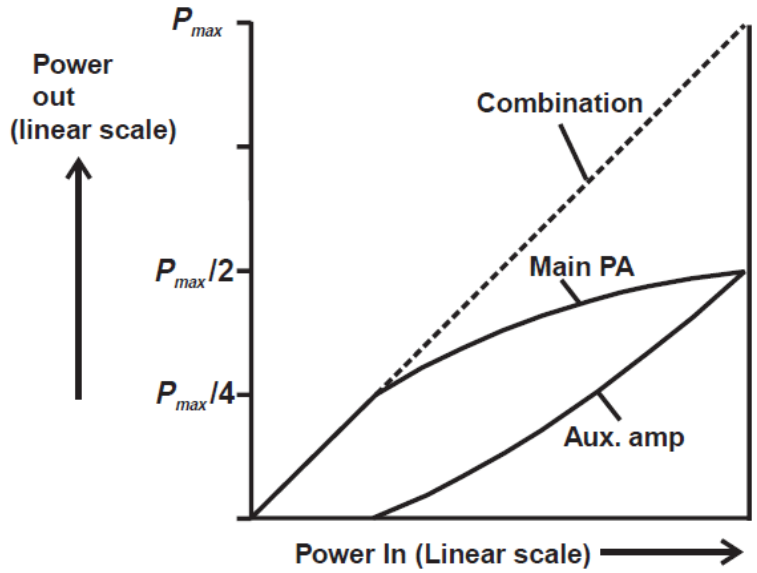

Figure 3.8: "Three-halves" DPA power characteristic. [2]

similarly to the Main amplifier. However, as the Auxiliary amplifier begins to work at high power levels, the gain tends to equalize, and linearity can be improved with harmonic cancellation if both PAs are correctly biased [9].
There are two factors that can negatively affect linearity: the power splitter in input and the Main and Auxiliary bias that generate unwanted harmonics. To improve linearity, some solutions can be adopted such as using an AB class for the Main or adaptive bias control. For more detailed information about linearity, a mathematical discussion about an AB-C DPA can be found in [8]. An important characteristic of an amplifier that needs to be analyzed is the band in which it can operate. With the increasing demand for wide-band 5G applications dealing with mm-wave, bandwidth extension has become a crucial consideration in modern DPA designs. However, there is no technique yet for broadband DPA design, as several factors in the DPA architecture contribute to bandwidth limitation. Recent research has shown that bandwidth extension has received increasing attention, especially for wide-band 5G applications. [10]. TL1 and TL2 are carefully chosen to ensure that both amplifiers can see the optimal load for the task. However, due to the intrinsic characteristics of the transmission line, they only work properly at the single λ designed, making them beneficial only in a narrow-band. TL2 aims to transform the load impedance R_{L} into $R_{\mathrm{opt}}/2$, while the characteristic impedance of TL1 is chosen to match the optimal load resistance at peak power. At -6dB back-off, the Auxiliary is off and the impedance presented to the Main is equal to $2R_{\mathrm{opt}}$, as shown in (3.8). It is important to remember that $Z_{\mathrm{T}} = R_{\mathrm{opt}}$. At

maximum power, both amplifiers are on, and the load seen by each amplifier is equal to R_{opt}. The parameter that defines the ratio of impedance transformation is called the *impedance transformation ratio (k)*:

$$k = \frac{Z_{\text{T}}}{Z_1} \tag{3.19}$$

In this case, at peaking power k is equal to 1 while for -6dB back-off regime k takes the value of 0.5. According to the fundamental theory of transmission lines, assuming load-matching, the following relationships can be demonstrated:

$$Z_1(f) = Z_{\text{c}}(f) = R_{\text{opt}} \frac{k + j \tan\left(\frac{\pi}{2}\frac{f}{f_0}\right)}{1 + jk \tan\left(\frac{\pi}{2}\frac{f}{f_0}\right)} \tag{3.20}$$

Plotting the real part of $Z_1(f)$ normalized to R_{opt} (Figure 3.9), it is evident a narrow-band behaviour in back-off.

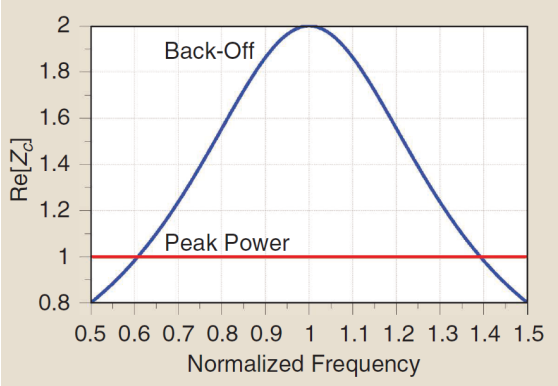

Figure 3.9: $Z_1(f)$ in optimal load condition, normalized to f_0) and R_{opt}. [10]

As previously explained, the transmission line TL2 serves as a matching network to convert R_{L} to $R_{\text{opt}}/2$. However, if the ratio $2R_{\text{L}}/R_{\text{opt}}$ is too high, it can limit the bandwidth. You can determine $Z_1(f)$ by considering the frequency behaviour of TL2, which can be expressed with the following equation:

$$Z_1(f) = Z_{\text{c}}(f) = R_{\text{opt}} \frac{k_{\text{c}} + j \tan\left(\frac{\pi}{2}\frac{f}{f_0}\right)}{1 + jk_{\text{c}} \tan\left(\frac{\pi}{2}\frac{f}{f_0}\right)} \tag{3.21}$$

where k_{c} is a new parameter defined as follows:

$$k_{\text{c}} = k \frac{\frac{1}{m} + j \tan\left(\frac{\pi}{2}\frac{f}{f_0}\right)}{m + j \tan\left(\frac{\pi}{2}\frac{f}{f_0}\right)} \text{ with } m = \sqrt{\frac{R_{\text{opt}}}{2R_{\text{L}}}} \tag{3.22}$$

When $m = 1$, the behaviour of Figure 3.10 is the same as that of Figure 3.9. When $m < 1$, the bandwidth decreases, but when $m > 1$, a higher bandwidth is achieved at the expense of some peak. Therefore, it is preferable to use a configuration and active element that can allow for a higher R_{opt}. However, TL2 can be replaced with higher-order matching networks to improve the bandwidth, but the same cannot be done for TL1, which acts as an impedance inverter.

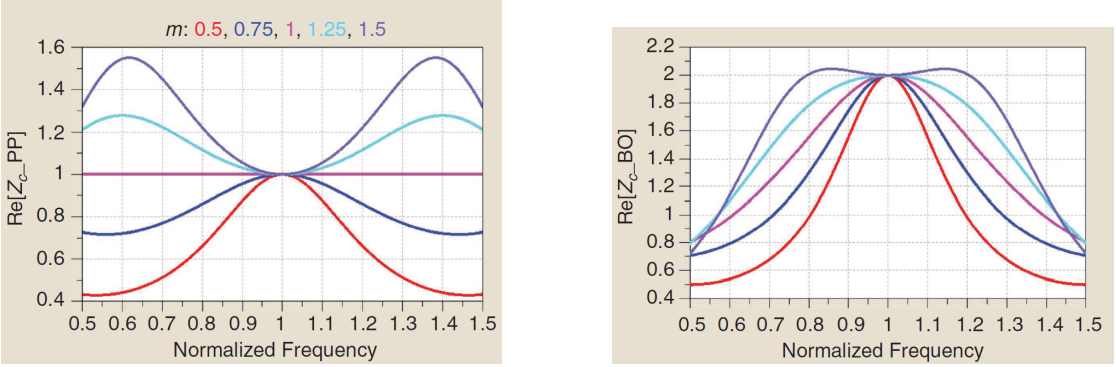

(a) **(b)**

Figure 3.10: $Z_1(f)$ considering the effect of TL2, normalized to f_0 and R_{opt}. (a): maximum power condition, (b): -6db back-off conditions. [10]

Parasitic capacitances can limit the bandwidth. To overcome this, it is possible to either nullify their effect by using other transmission lines or manipulating the ones already present or use a lumped elements solution. The input network of a transmission line, which consists of a power splitter and a phase-shift TL, can also limit its frequency behaviour. To achieve a narrow band, it is possible to combine the delay and splitting into a single component, such as a quadrature splitter. However, bandwidth problems can be solved by adopting certain solutions that act on the coming network at the common node. Two slightly different definitions can be used to start defining the bandwidth for DPA performance estimation [11].

- f_{P} is the frequency range on which the saturated power $P_{\text{OUT,sat}}$ is higher than a threshold $P_{\text{OUT,target}}$;

- f_{L} is defined as the frequency range where the gain compression id Doherty region is lower than a target.

From these definitions, the bandwidth of a generic DPA can be considered as the intersection of these two frequency intervals $f_{\text{P}} \cap f_{\text{L}}$. The gain compression/expansion can be estimated as the difference between IBO and OBO.

3.5 Multi-way and multi-stage configurations

A classical DPA can enhance efficiency within the Doherty region, where the back-off is between 0 and -6dB. The efficiency depends on the back-off, and its behaviour is shown in Figure 3.5. However, when the back-off is lower than -6dB, the efficiency of the DPA degrades depending on the class and the bias chosen for the Main amplifier. In most modern communication systems, *the peak-to-average power ratio* (PAPR) exceeds this value, requiring an extension of the high-efficiency range. To extend the efficiency enhancement for higher back-off levels, the Doherty region can be expanded for back-off lower than -6dB. This can be achieved by adopting designs with more than one Auxiliary, which improves load-modulation. Two viable solutions to increase the high-efficiency back-off region are multi-way and multi-stage DPAs [12].

- The *Multi-way (N-way)* DPA is designed with one Main amplifier and $N-1$ Auxiliary PAs working in parallel and turning ON/OFF simultaneously, at the same back-off level;
- The *Multi-stage (N-stage)* DPA is a more complex architecture made by 1 Main and $N-1$ Auxiliary, as the previous, but here every Auxiliary is turned ON/OFF at different back-off levels.

In an N-way Doherty amplifier, the basic scheme is illustrated in Figure 3.11a. The aim is to combine N-1 Auxiliary amplifiers to create one larger Auxiliary device that operates like a classical DPA. In this configuration, each Auxiliary device is switched on/off at the same back-off level as in the basic configuration. The goal is to deliver currents from each Auxiliary device at the common node with the same phase and at the same time to improve the overall Auxiliary device's ability to modulate the load. This provides a maximum current N-1 times higher than the one supplied by the Main device. Consequently, the efficiency is improved, and the Doherty region is extended to back-off levels lower than -6dB. However, as N increases, the efficiency curve in the Doherty region drops significantly, as shown in Figure 3.11b. To overcome the problem, the N-stage DPA approach is used. This approach is different from the N-way approach because the Auxiliary PAs are not working in parallel but in a cascade configuration. Although there are always N-1 Auxiliary devices, each Auxiliary PA is turned on only when a specific back-off threshold is achieved. Every threshold is different for each Auxiliary PA, resulting in multiple Doherty regions appearing in the efficiency curves. To make it work, every Auxiliary requires a proper control circuit that makes it conduct only when a certain envelope threshold is achieved. Power cannot be delivered simply by a common node, but an opportune combiner network is required to exploit properly the load modulation for each stage in the cascade. Initially, the Main and the

first Auxiliary work as a normal DPA. Increasing the input power causes both the Main and first Auxiliary to saturate, and the third Auxiliary begins to conduce modulating the load of the first Doherty active couple. When the second Auxiliary reaches saturation, the third intervenes, and so on for the other branches.

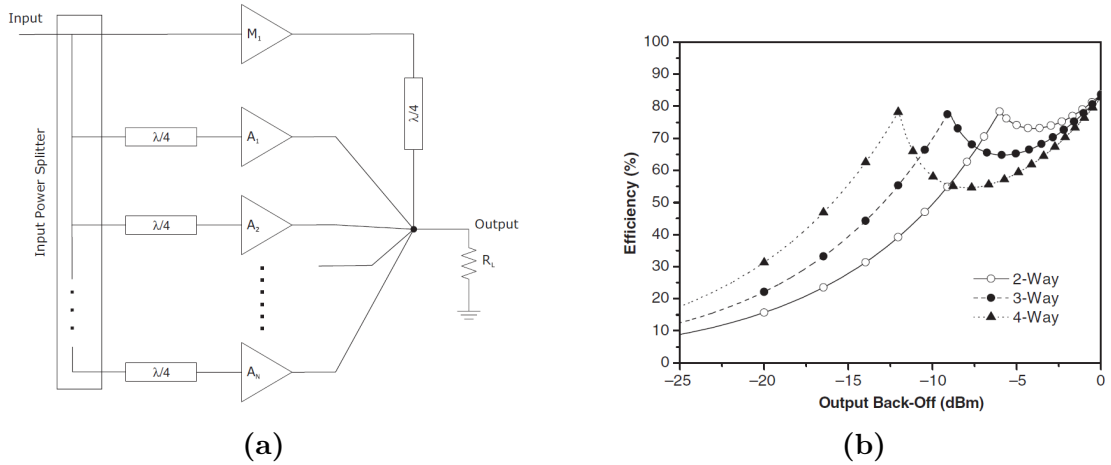

(a) **(b)**

Figure 3.11: N-way DPA. (a): basic scheme, (b): theoretical efficiency. [8]

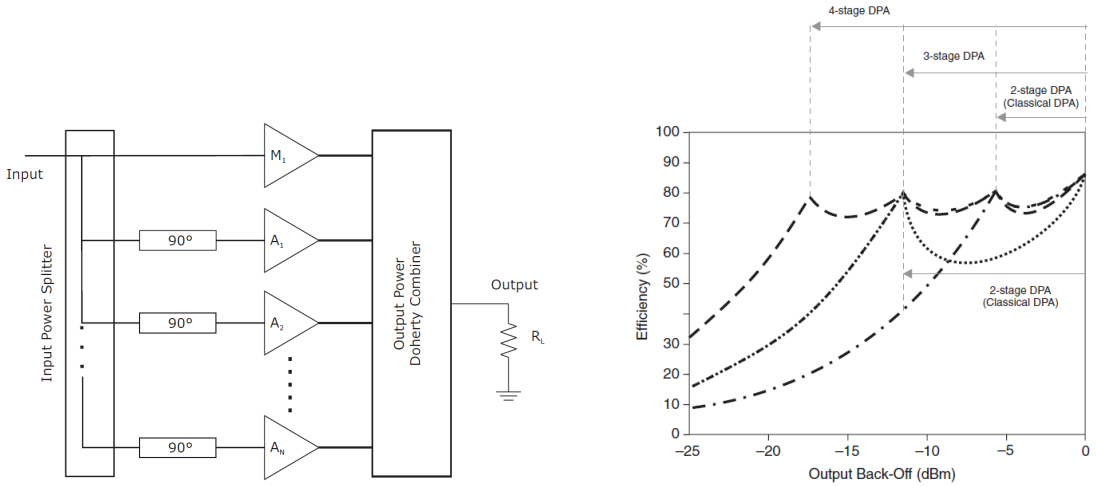

(a) **(b)**

Figure 3.12: N-stage DPA. (a): basic scheme, (b): theoretical efficiency. [8]

The use of an N-stage solution improves efficiency in back-off, as compared to the N-way solution where only one Doherty region is extended and drops in the middle. Implementing more Doherty regions in the N-stage solution leads to a

more complex structure, which requires specific conditions to be met for optimal performance:

- Each Auxiliary PA requires a different switching circuit or bias control to turn on/off at the correct threshold;
- A complex combiner network is required to sum power from each PA in a constructive way and input at each Auxiliary should be delayed properly, according to the combiner topology.

In [8], a possible topology is proposed for an N-stage, as shown in Figure 3.13. This structure requires each output stage to be connected to the following one with a quarter-wave transmission line. Each transmission line is characterized by a characteristic impedance of $Z_{0,\mathrm{i}}$, where i represents the stage identifier. To restore the phase, a 90° delay in input is applied at each Auxiliary. Assuming that each Auxiliary is turned on/off on a different back-off threshold OBO_{i}, each transmission line can be designed using the following relations, where $i = 1,2,...N$ (in this case, the number of Auxiliary devices is represented by N), and $k = 1$ for odd i or $k = 2$ for even i.

$$\begin{aligned} Z_{0,\mathrm{i}} &= R_{\mathrm{L}} \cdot \prod_{j=1}^{i} \frac{1}{\alpha_{\mathrm{j}}} \\ \prod_{j=k}^{\frac{i+k}{2}} \alpha_{\mathrm{2j\text{-}k}} &= 10^{-\frac{OBO_{\mathrm{i}}}{20}} \\ R_{\mathrm{L}} &= (1-\alpha_1)\, R_{\mathrm{opt,AuxN}} \end{aligned} \tag{3.23}$$

It is important to optimize the output transmission line and bias point of each active device to achieve the optimum efficiency curve in real implementations. While the previous topology presented is an example, it does have some drawbacks in terms of linearity due to unwanted modulation-load effects that happen when the saturation point of each Auxiliary is reached. It has been demonstrated that the maximum theoretical efficiency cannot be achieved with this topology. However, other combiner topologies can be used [13]. In this topology, input delay is only required every two stages to adjust the phase to the load. Note that the principle can be used to increase the number of branches in a multi-Doherty structure, but creating a power splitter with a large number of output lines is not feasible. As a result, the number of branches is usually limited to a maximum of three or four, including the Main branch. Additionally, N-way and N-branch are often used interchangeably, but they refer to different things.

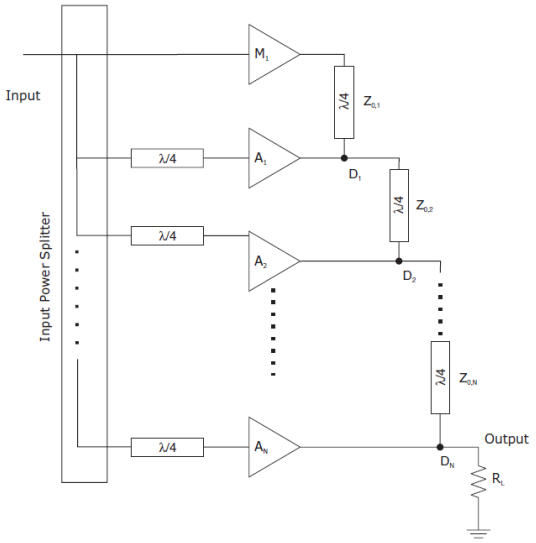

Figure 3.13: Example of an N-way DPA with the proposed combiner topology as example. [8]

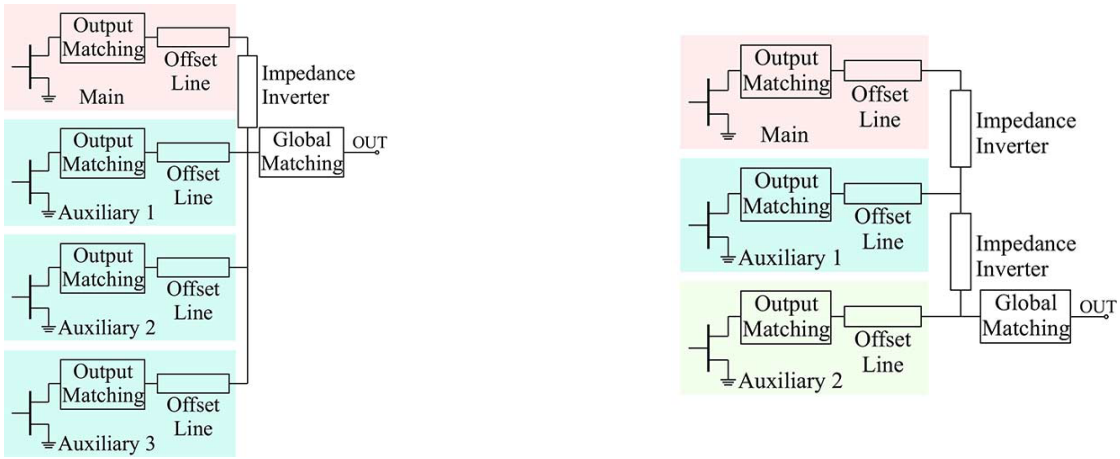

Figure 3.14: Comparison between N-way and two different N-stage topologies. (a): 4-way DPA (input stage is neglected) [12], (b): 3-stage DPA with the example combiner topology analyzed (input stage is neglected) [12]

Chapter 4

Development of a linear method analysis for 3-stage DPAs simulation

The core of this work is presented in the following chapter. It introduces a novel linear model that can simulate the behaviour of a 3-stage DPA assuming linearity for each device for initial bandwidth estimation. The mathematical model proposed here is developed for the analysis of the output stage of a Doherty configuration with a generic combiner. This approach offers a simplified method for 3-stage design and analysis, requiring only linear simulation. Moreover, it is customized and optimized for the architecture suggested in this chapter. After describing the system, its mathematical model has been implemented with MATLAB to develop a simulation tool for the design and analysis of a generic 3-stage DPA. The development of a specific simulation tool was necessary to create a simple model that could bypass the computational complexity caused by non-linear simulations, and overcome some limitations in CAD for simplified modeling. One such limitation is the active device voltage clipping due to saturation limits imposed by the power supply. As the chapter will demonstrate, the initial approach only considers the output stage of each active device in a simplified method that does not rigorously account for the real physics of the transistor and its polarization class. Nevertheless, certain effects that are not negligible must be taken into account, such as clipping, which can limit the dynamic of the entire system. Generally, an amplifier is designed to work in a certain frequency band, and the design goal is to ensure a quasi-constant behaviour in the entire bandwidth. This is a design problem because active and passive elements are strongly frequency-dependent, and some kind of compensation can be achieved with particular networks. However, in general, each component is designed to work properly at a certain central frequency. The design is typically performed

for a central frequency, where the system works according to the specifications, after which the entire network imposes the band behaviour.

In order to transport the concept in a DPA, the combiner network should be designed to ensure impedance inversion and signal recombination at a given frequency to achieve maximum efficiency. However, the impedance levels and behaviour of the entire system depend on the frequency behaviour of the network and should be studied, designed, and optimized properly. This phenomenon must be studied, prevented, and controlled to manage the frequency behaviour of the DPA.

There are various software programs available for RF simulation in commerce, and one of the most efficient options is *ADS-Advanced Design System*. It is an electronic automatic design environment that is recommended for RF design and wireless networks. ADS has a simple graphical interface which makes linear simulation relatively easy. However, modelling only the output stage in a simplified model overlooks all the phenomena that are crucial to the working principle of a typical active device, including saturation. As a result, the outcomes obtained may not be reliable in certain frequency conditions. A major challenge in simulation tools is to perform linear and simplified simulations without neglecting important physical aspects. To address this issue, this work presents a simulation tool that aims to overcome this problem. In [1], a similar approach was developed and described for a classical Doherty configuration with two stages. While mathematical formalism is well developed for two-port networks providing conversion table between different set of parameters[3], dealing with three-port systems can require a major complexity. Some theories based on parameters conversion ideal for three-port systems have been developed based on mathematical relations between different characterization describing the same object [14]. However, parameter conversion implies the acknowledgement of almost one set of parameters that, in most cases, are obtained through measurements to describe the system. In RF, this kind of measurement usually deals with S-parameters characterization techniques [15] The approach followed in this chapter is based on the mathematical manipulation of each subsystem to extract the Z-matrix of the combiner, described as a three-port device.

4.1 Basic idea

The concept of modeling a 3-stage DPA using a linear approximation while considering the physics of the device is based on a model originally developed for a classical DPA configuration at PoliTO, which was described in [11]. This idea has been generalized and applied to analyze a 3-stage DPA with a specific combiner topology in a linear fashion. The 3-stage DPA configuration shown in Figure 4.1 analyzes the relation between electrical quantities in the output stage, neglecting input power splitting.

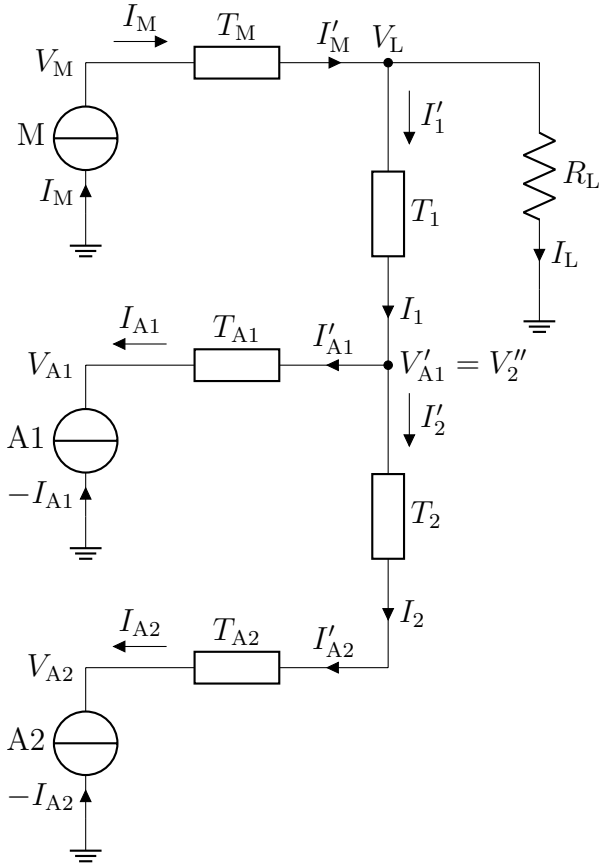

Figure 4.1: Output section of DPA with the generic combiner topology adopted.

The direction of each current has been chosen to simplify the mathematical model developed in the following section. According to this topology, each combiner branch is described with a black box with its ABCD formalism:

$$\begin{pmatrix} V_i \\ I_i \end{pmatrix} = T_x \begin{pmatrix} V_o \\ I_o \end{pmatrix} = \begin{pmatrix} a_x & b_x \\ c_x & d_x \end{pmatrix} \begin{pmatrix} V_o \\ I_o \end{pmatrix} \tag{4.1}$$

At the moment it does not matter how each block is made inside, however, it will be constituted by a cascade of several passive elements taking part in the combiner. Considering real active devices, output stages have non-negligible parasitic elements that affect the frequency behaviour of the entire system. In this work, parasitic quantities are considered and included in the combiner topology: parasitic elements will be modelled as lumped components and they will be included in their relative output branches T_{M}, T_{A1} and T_{A2}. With this assumption, output stages M, $A1$ and $A2$ of each transistor in Figure 4.1 are represented by an ideal current generator driven by the input stage (not considered in this discussion) while their parasitic elements are included in their relative output branches. This choice to split the physic of the output section of each transistor could appear trivial but it allows to consider parasitic elements as a part of the combiner, simplifying the design of each branch. As a consequence, I_{M}, $-I_{\mathrm{A1}}$ and $-I_{\mathrm{A2}}$ are not the current exiting from each device but the one outgoing from the so-called *internal section* of the transistor, before output parasitic lumped elements. It is important to note that the current generators - M, $A1$, and $A2$ - are dependent on the input power splitting and follow a generic transistor model. Even if the input stage for each active is not taken into account, the stimulus of the system is modelled as I_{M}, $-I_{\mathrm{A1}}$, and $-I_{\mathrm{A2}}$ which are complex quantities taking into account the effects of the input power splitter. The combiner topology can be considered as a three-port network where each port is connected to the output stage of each active device. With this assumption, the system can be described with its Z-parameters in the following way (the conventional sign of current entering each port is respected):

$$\begin{pmatrix} V_{\mathrm{M}} \\ V_{\mathrm{A1}} \\ V_{\mathrm{A2}} \end{pmatrix} = Z \begin{pmatrix} I_{\mathrm{M}} \\ -I_{\mathrm{A1}} \\ -I_{\mathrm{A2}} \end{pmatrix} = \begin{pmatrix} Z_{\mathrm{MM}} & Z_{\mathrm{MA1}} & Z_{\mathrm{MA2}} \\ Z_{\mathrm{A1M}} & Z_{\mathrm{A1A1}} & Z_{\mathrm{A1A2}} \\ Z_{\mathrm{A2M}} & Z_{\mathrm{A2A1}} & Z_{\mathrm{A2A2}} \end{pmatrix} \begin{pmatrix} I_{\mathrm{M}} \\ -I_{\mathrm{A1}} \\ -I_{\mathrm{A2}} \end{pmatrix} \tag{4.2}$$

A consideration that needs to be highlighted is that the impedance matrix describes in a linear way only the combiner topology (parasitic effects included), while the DPA working principle will be coded into each stimulus, set in amplitude and phase according to the input splitting method adopted. Once the combiner Z-matrix has been found, $(I_{\mathrm{M}}; -I_{\mathrm{A1}}; -I_{\mathrm{A2}})^T$ is applied according to (4.2). However, this linear mathematical relation does not consider the system's physical limitations due to the power supply limit and for this reason V_{M}, V_{A1} and V_{A2} can overcome their maximum voltage achievable in saturation. Calling $V_{\mathrm{MAX,sub}}$, where *sub* corresponds to M, A1 and A2, the maximum voltage achievable from each active device, physic limitation imposes that:

$$V_{\mathrm{sub}} \leq V_{\mathrm{MAX,sub}} \tag{4.3}$$

Where this relation is not satisfied, it means that:

- the saturation has been achieved and the output voltage has been clipped to $V_{\text{sub}} \leq V_{\text{MAX,sub}}$;
- $(I_{\text{M}}; -I_{\text{A1}}; -I_{\text{A2}})^T$ used in (4.2) is not feasible because too high for the physics of the device, and needs to be reduced for a correct estimation.

For these reasons, a clipping factor c_{sub} is introduced and defined as follows:

$$c_{\text{sub}} = \begin{cases} \frac{V_{\text{MAX,sub}}}{|V_{\text{sub}}|}, \ |V_{sub}| > V_{MAX,sub} \\ 1, \ |V_{sub}| \leq V_{MAX,sub} \end{cases} \tag{4.4}$$

M, A1 and A2 are not independent because of the input power splitting, so the effective clipping factor is given by

$$c = min\{c_{\text{M}}; c_{\text{A1}}; c_{\text{A2}}\} \tag{4.5}$$

and clipped current can be estimated as:

$$I_{\text{sub,clip}} = cI_{\text{sub}} \tag{4.6}$$

Now, it is possible to correct the calculation by taking into account that:

$$\begin{pmatrix} V_{\text{M,clip}} \\ V_{\text{A1,clip}} \\ V_{\text{A2,clip}} \end{pmatrix} = Z \begin{pmatrix} I_{\text{M,clip}} \\ -I_{\text{A1,clip}} \\ -I_{\text{A2,clip}} \end{pmatrix} \tag{4.7}$$

The clipping model will be analyzed in section 4.4 more in detail. $V_{\text{MAX,sub}}$ achievable by each active depends on the supply voltage, the knee voltage $V_{\text{k,sub}}$ and the amplifier class. For an active bias in class B, the maximum voltage achievable by its output stage is given by:

$$V_{\text{MAX,sub}} = V_{\text{DD,sub}} - V_{\text{k,sub}} \tag{4.8}$$

4.2 Mathematical model for combiner description

As mentioned earlier, Figure 4.1 depicts a combiner that needs to be described as a three-port network, stimulated by three current generators. Therefore, Z-parameters are suitable for this purpose. To better understand some useful considerations, it is helpful to analyze the combiner in the representation shown in Figure 4.2.

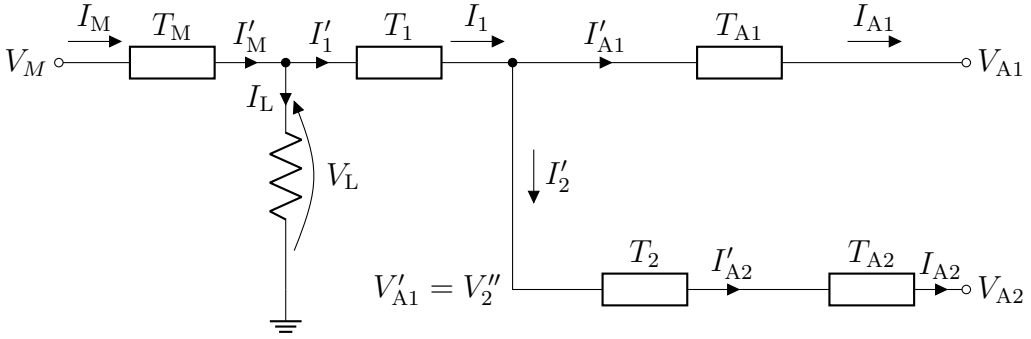

Figure 4.2: Combiner topology under analysis.

It is possible to observe that electrical quantities are being "transmitted" from the Main circuit to the Auxiliary circuits, given the current direction that has been adopted for I_{A1} and I_{A2}. For this reason, the combiner analysis has been divided into two steps:

1. derive a relation, using ABCD-parameters, able to describe the system in the form
$$\begin{pmatrix} V_{\mathrm{M}} \\ I_{\mathrm{M}} \end{pmatrix} = f\left[\begin{pmatrix} V_{\mathrm{A1}} \\ I_{\mathrm{A1}} \end{pmatrix}, \begin{pmatrix} V_{\mathrm{A2}} \\ I_{\mathrm{A2}} \end{pmatrix}\right] \tag{4.9}$$
2. manipulate (4.9) to obtain
$$\begin{pmatrix} V_{\mathrm{M}} \\ V_{\mathrm{A1}} \\ V_{\mathrm{A2}} \end{pmatrix} = Z \begin{pmatrix} I_{\mathrm{M}} \\ -I_{\mathrm{A1}} \\ -I_{\mathrm{A2}} \end{pmatrix} \tag{4.10}$$

For the second step, it is immediate to understand that moving from 2x2 system to a 3x3 one needs a further equation.

4.2.1 Step 1

Figure 4.2 helps in finding the relation between the Main quantity and Auxiliary ones. In fact, exploiting ABCD formalism with KCL and using linearity, it is possible to write the following relation:

$$\begin{pmatrix} V_{\mathrm{M}} \\ I_{\mathrm{M}} \end{pmatrix} = T_{\mathrm{M}} T_{\mathrm{L}} T_1 \cdot \begin{pmatrix} V'_{\mathrm{A1}} \\ I_1 \end{pmatrix}\Big|_{I_1 = I'_{\mathrm{A1}} + I'_2} = T_{\mathrm{M}} T_{\mathrm{L}} T_1 \cdot \left[\begin{pmatrix} V'_{\mathrm{A1}} \\ I'_{\mathrm{A1}} \end{pmatrix} + \begin{pmatrix} 0 \\ I'_2 \end{pmatrix}\right] \tag{4.11}$$

Internal add can also be written as:

$$\begin{pmatrix} V'_{\mathrm{A1}} \\ I'_{\mathrm{A1}} \end{pmatrix} = T_{\mathrm{A1}} \cdot \begin{pmatrix} V_{\mathrm{A1}} \\ I_{\mathrm{A1}} \end{pmatrix} \tag{4.12}$$

$$\begin{pmatrix} 0 \\ I_2' \end{pmatrix} = T_2 T_{\mathrm{A2}} \begin{pmatrix} V_{\mathrm{A2}} \\ I_{\mathrm{A2}} \end{pmatrix} - \begin{pmatrix} V_2' \\ 0 \end{pmatrix} \tag{4.13}$$

Substituting these last two terms in (4.11), the following relation is obtained:

$$\begin{pmatrix} V_{\mathrm{M}} \\ I_{\mathrm{M}} \end{pmatrix} = T_{\mathrm{M}} T_{\mathrm{L}} T_1 \cdot \left[T_{\mathrm{A1}} \cdot \begin{pmatrix} V_{\mathrm{A1}} \\ I_{\mathrm{A1}} \end{pmatrix} + T_2 T_{\mathrm{A2}} \begin{pmatrix} V_{\mathrm{A2}} \\ I_{\mathrm{A2}} \end{pmatrix} - \begin{pmatrix} V_2' \\ 0 \end{pmatrix} \right] \tag{4.14}$$

Now, the same consideration is done for $(V_2'; 0)^T$, obtaining the final relation:

$$\begin{pmatrix} V_{\mathrm{M}} \\ I_{\mathrm{M}} \end{pmatrix} = T_{\mathrm{M}} T_{\mathrm{L}} T_1 \cdot \left[T_2 T_{\mathrm{A2}} \begin{pmatrix} V_{\mathrm{A2}} \\ I_{\mathrm{A2}} \end{pmatrix} + \begin{pmatrix} 0 \\ I_{\mathrm{A1}}' \end{pmatrix} \right] \tag{4.15}$$

The last step is to introduce the following parameters, useful from a calculation point of view:

$$A_{\mathrm{M}} = T_{\mathrm{M}} T_{\mathrm{L}} T_1 \tag{4.16}$$

$$T_{2\mathrm{TOT}} = T_2 T_{\mathrm{A2}} \tag{4.17}$$

$$A_2 = A_{\mathrm{M}} T_{2\mathrm{TOT}} = T_{\mathrm{M}} T_{\mathrm{L}} T_1 T_2 T_{\mathrm{A2}} \tag{4.18}$$

With these parameters, the relation between Main and Auxiliaries quantities become the follows:

$$\begin{pmatrix} V_{\mathrm{M}} \\ I_{\mathrm{M}} \end{pmatrix} = A_2 \begin{pmatrix} V_{\mathrm{A2}} \\ I_{\mathrm{A2}} \end{pmatrix} + A_{\mathrm{M}} \begin{pmatrix} 0 \\ I_{\mathrm{A1}}' \end{pmatrix} = A_2 \begin{pmatrix} V_{\mathrm{A2}} \\ I_{\mathrm{A2}} \end{pmatrix} + A_{\mathrm{M}} \begin{pmatrix} 0 & 0 \\ 0 & 1 \end{pmatrix} T_{\mathrm{A1}} \begin{pmatrix} V_{\mathrm{A1}} \\ I_{\mathrm{A1}} \end{pmatrix} \tag{4.19}$$

4.2.2 Step 2

To write the system in (4.19) in the form $\mathbf{V} = \mathbf{ZI}$, a third equation is needed. It can be found by the following relation, easily verifiable by observing Figure 4.2:

$$V_{\mathrm{A1}}' = V_2'' = T_{2\mathrm{TOT},11} V_{\mathrm{A2}} + T_{2\mathrm{TOT},12} I_{\mathrm{A2}} \tag{4.20}$$

But at the same time, it is valid for the following reasons:

$$\begin{pmatrix} V_{\mathrm{A1}}' \\ I_{\mathrm{A1}}' \end{pmatrix} = T_{\mathrm{A1}} \cdot \begin{pmatrix} V_{\mathrm{A1}} \\ I_{\mathrm{A1}} \end{pmatrix} \Longleftrightarrow \begin{cases} V_{\mathrm{A1}}' = T_{\mathrm{A1},11} V_{\mathrm{A1}} + T_{\mathrm{A1},12} I_{\mathrm{A1}} = V_2'' \\ I_{\mathrm{A1}}' = T_{\mathrm{A1},21} V_{\mathrm{A1}} + T_{\mathrm{A1},22} I_{\mathrm{A1}} \end{cases} \tag{4.21}$$

So, the third equation can become:

$$T_{2\mathrm{TOT},11} V_{\mathrm{A2}} + T_{2\mathrm{TOT},12} I_{\mathrm{A2}} = T_{\mathrm{A1},11} V_{\mathrm{A1}} + T_{\mathrm{A1},12} I_{\mathrm{A1}} \tag{4.22}$$

And the 3x3 system becomes the follows:

$$\begin{cases} V_{\mathrm{M}} = A_{2,11}V_{\mathrm{A2}} + A_{2,12}I_{\mathrm{A2}} + A_{\mathrm{M},12}\left(T_{\mathrm{A1},21}V_{\mathrm{A1}} + T_{\mathrm{A1},22}I_{\mathrm{A1}}\right) \\ I_{\mathrm{M}} = A_{2,21}V_{\mathrm{A2}} + A_{2,22}I_{\mathrm{A2}} + A_{\mathrm{M},22}\left(T_{\mathrm{A1},21}V_{\mathrm{A1}} + T_{\mathrm{A1},22}I_{\mathrm{A1}}\right) \\ T_{2\mathrm{TOT},11}V_{\mathrm{A2}} + T_{2\mathrm{TOT},12}I_{\mathrm{A2}} = T_{\mathrm{A1},11}V_{\mathrm{A1}} + T_{\mathrm{A1},12}I_{\mathrm{A1}} \end{cases} \tag{4.23}$$

At this point, the linear system can be algebraically manipulated to separate current terms from voltage ones. Furthermore, for a correct Z representation, is convenient to consider the current entering in each port. So, because the natural direction of current from A1 and A2 has been set to enter in each transistor for simplifying previous steps, now it is necessary to consider the reverse direction in accordance with Z formalism. The result, referred to Figure 4.2 is the follows:

$$\begin{pmatrix} 1 & -A_{\mathrm{M},12}T_{\mathrm{A1},21} & -A_{2,11} \\ 0 & -A_{\mathrm{M},22}T_{\mathrm{A1},21} & -A_{2,21} \\ 0 & T_{\mathrm{A1},11} & -T_{2\mathrm{TOT},11} \end{pmatrix} \begin{pmatrix} V_{\mathrm{M}} \\ V_{\mathrm{A1}} \\ V_{\mathrm{A2}} \end{pmatrix} = \begin{pmatrix} 0 & -A_{\mathrm{M},12}T_{\mathrm{A1},22} & -A_{2,12} \\ -1 & -A_{\mathrm{M},22}T_{\mathrm{A1},22} & -A_{2,22} \\ 0 & T_{\mathrm{A1},12} & -T_{2\mathrm{TOT},12} \end{pmatrix} \begin{pmatrix} I_{\mathrm{M}} \\ -I_{\mathrm{A1}} \\ -I_{\mathrm{A2}} \end{pmatrix} \tag{4.24}$$

At this point, inverting the relation to find $\mathbf{V}$ is simple. Calling:

$$\Omega = \begin{pmatrix} 1 & -A_{\mathrm{M},12}T_{\mathrm{A1},21} & -A_{2,11} \\ 0 & -A_{\mathrm{M},22}T_{\mathrm{A1},21} & -A_{2,21} \\ 0 & T_{\mathrm{A1},11} & -T_{2\mathrm{TOT},11} \end{pmatrix}, S = \begin{pmatrix} 0 & -A_{\mathrm{M},12}T_{\mathrm{A1},22} & -A_{2,12} \\ -1 & -A_{\mathrm{M},22}T_{\mathrm{A1},22} & -A_{2,22} \\ 0 & T_{\mathrm{A1},12} & -T_{2\mathrm{TOT},12} \end{pmatrix} \tag{4.25}$$

It is immediate to find the final relation:

$$\begin{pmatrix} V_{\mathrm{M}} \\ V_{\mathrm{A1}} \\ V_{\mathrm{A2}} \end{pmatrix} = \Omega^{-1}S \begin{pmatrix} I_{\mathrm{M}} \\ -I_{\mathrm{A1}} \\ -I_{\mathrm{A2}} \end{pmatrix} = Z \begin{pmatrix} I_{\mathrm{M}} \\ -I_{\mathrm{A1}} \\ -I_{\mathrm{A2}} \end{pmatrix} \tag{4.26}$$

(4.26) represents the description of a three-port system stimulated by current in input from each port and considered as independent current, while the voltage vector represents the response of the system. Here, voltages are a linear combination of each current and for this reason, it confirmed the fact that Z contains impedance parameters according to Z-formalism:

$$Z = Z(f) = \Omega(f)^{-1}S(f) = \begin{pmatrix} Z_{\mathrm{MM}}(f) & Z_{\mathrm{MA1}}(f) & Z_{\mathrm{MA2}}(f) \\ Z_{\mathrm{A1M}}(f) & Z_{\mathrm{A1A1}}(f) & Z_{\mathrm{A1A2}}(f) \\ Z_{\mathrm{A2M}}(f) & Z_{\mathrm{A2A1}}(f) & Z_{\mathrm{A2A2}}(f) \end{pmatrix} \tag{4.27}$$

Note that Z parameters are frequency-dependent, so they have to be estimated in the entire frequency range under analysis. At this point, two fundamental concepts need to be underlined:

1. Z-matrix characterizes *only* the combiner, modelled as a three-port network, and it does not describe the entire DPA;

2. DPA description depends on how output current are delivered on load and on how each active device is activated as a function of OBO. Neglecting the input stage, the DPA working principle is coded into each internal current, which should be managed correctly according to DPA principles.

In conclusion, the overall behaviour of a three-stage DPA depends on how the combiner is realized and how active output stages deliver each current, in magnitude and phase, as it will be explained.

4.3 Transmission model and building blocks

Once the mathematical model has been developed according to the current direction assumed in Figure 4.1, it is convenient to rewrite the current exiting from each PA as positive, considering I_{M}, I_{A1} and I_{A2} exiting for each active device.

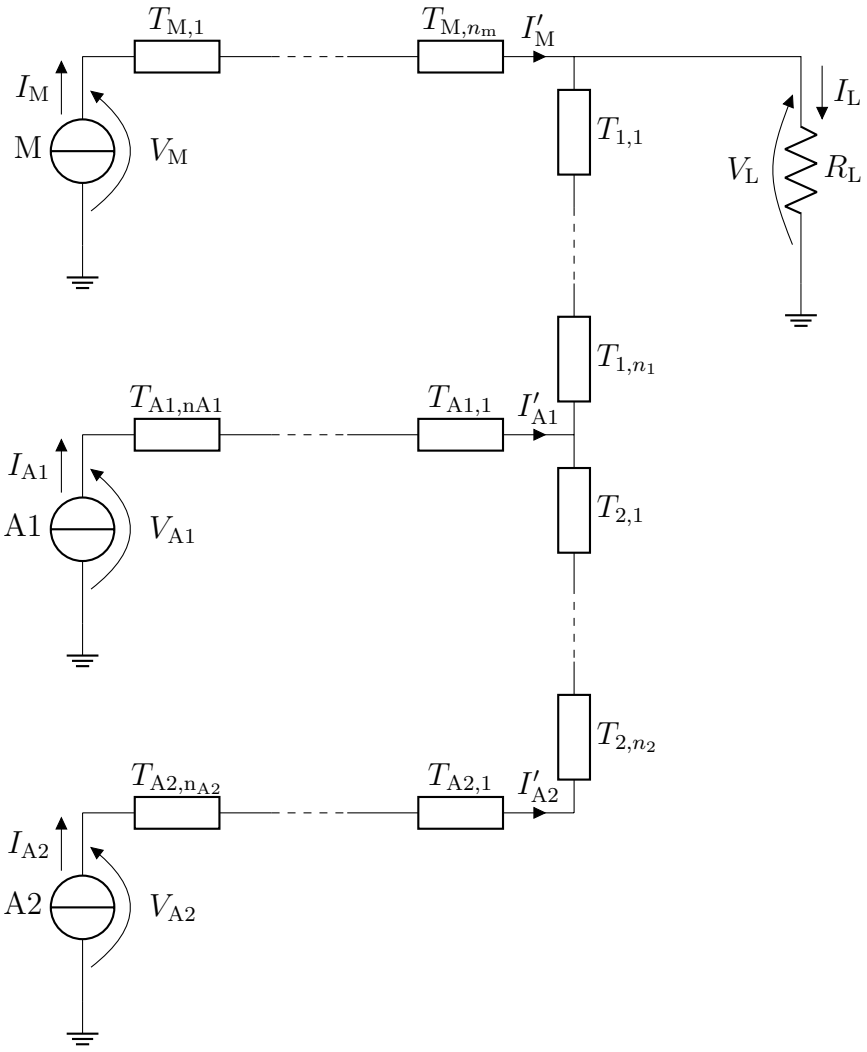

Figure 4.3: Output section of DPA with the generic combiner topology adopted.

From this point onward, each electrical quantity will be referred to in Figure 4.3. Please note that while $\Omega(f)$, $S(f)$, and $Z(f)$ mentioned in section 4.2 remain valid, it is needed to pay more attention to how the T_{x} matrix is defined. As mentioned earlier, a general T_{x} represents the equivalent ABCD matrix of an entire branch made up of a cascade of more elementary blocks or lumped elements. Therefore, the

equivalent matrix for each branch can be estimated by multiplying each elementary ABCD matrix in the correct order based on the "transmission direction" assumed in the mathematical formalism used. In particular, step 1 assumed an electrical transmission direction that propagates from M to A1 and A2. As a result, the notation in Figure 4.3 will be use:

$$T_x = \prod_{\mathrm{n}=1}^{n_x} T_{\mathrm{x,n}} \tag{4.28}$$

In accordance with this convention, the estimation of T_{m} involves a cascade of ABCD-matrices from left to right, $T_{\mathrm{A1,2}}$ from right to left, and $T_{1,2}$ from top to bottom. To achieve this, a generic $T_{\mathrm{x,n}}$ element represents the ABCD matrix of a lumped element that is either put in series in its branch or used as a shunt. Some of the elements used in this work include:

- generic shunt admittance;
- generic series impedance;
- series transmission line;
- open stub transmission line.

Going into detail of each branch, it is possible to affirm that:

- T_{sub} includes inside parasitic element inside the model of each active device and combiner element related to the relative branch like TLs, lumped inversion networks and compensation networks;
- $T_{1,2}$ is made by combiner topology elements.

4.4 DPA analysis with the new approach

After describing the combiner system with its Z-matrix, it becomes possible to simulate the behaviour of the entire system. Assuming active devices biased in a generic class, the maximum output current delivered by the PA is represented by $I_{\mathrm{Max,sub}}$ while the maximum value of the fundamental component achievable by the configuration is represented by $I_{\mathrm{fund,sub}}$. In this work, the following statements have been assumed:

- all devices are biased in class B;
- non-linearities have not been accounted for;
- the combiner is lossless.

This assumption is sufficiently accurate for the aim, considering (2.38). The relation between $I_{\text{Max,sub}}$ and $I_{\text{fund,sub}}$ is:

$$I_{\text{Max,sub}} = 2 \cdot I_{\text{fund,sub}} \tag{4.29}$$

Furthermore, for class B assumption, optimal load $R_{\text{opt,sub}}$ for each device is:

$$R_{\text{opt,sub}} = 2 \cdot \frac{V_{\text{MAX,sub}}}{I_{\text{Max,sub}}} \tag{4.30}$$

As previously discussed, the performance of a DPA is influenced by its electrical characteristics throughout the dynamic range of the entire amplifier. The combiner topology analyzed in this case has a current profile that is generally represented by a normalized dynamic range $x \in [0; 1]$, as shown in Figure 4.4a. It is challenging to realize this type of profile in real devices, as it depends on various factors such as class, bias, linearity, and polarization circuit for each active device. Nonetheless, once this profile has been established, the combiner facilitates the voltage profile shown in Figure 4.4b. Assuming simplified ideal behaviour under the working hypothesis, three operational regions can be identified [13]:

1. *low-power region* $0 \leq x < x_1$: only the Main is conducting with a fixed load while A1 and A2 are OFF, assumed as open circuits;

2. *OBO1 region* $x_1 \leq x < x_2$: M achieves its maximum voltage swing while A1 starts to conduce current, modulating the load seen from the Main thanks to the combiner network;

3. *OBO2 region* $x_2 \leq x \leq 1$: A1 archives its maximum swing and A1 starts to conduce, modulating impedance seen by M and A1 thanks to the combiner network. $x = 1$ corresponds to the saturation condition.

It is important to note that these profiles only refer to the maximum values of each electrical quantity, even if sometimes phasors are referred to as the *root mean square* (RMS) in most conventions. The phase of each current stimulus depends on the input stage, specifically the input power splitter combined with some delay line. Even though the input stage is not being considered, its effect is crucial for DPA characterization, and here its effect is encoded in the phase of each current, denoted by ϕ_{sub}. An ideal input stage for a DPA should ensure a constant current phase at each PA, independent of frequency. However, this does not happen because the input stage is made up of frequency-dependent elements such as a power splitter and transmission lines.

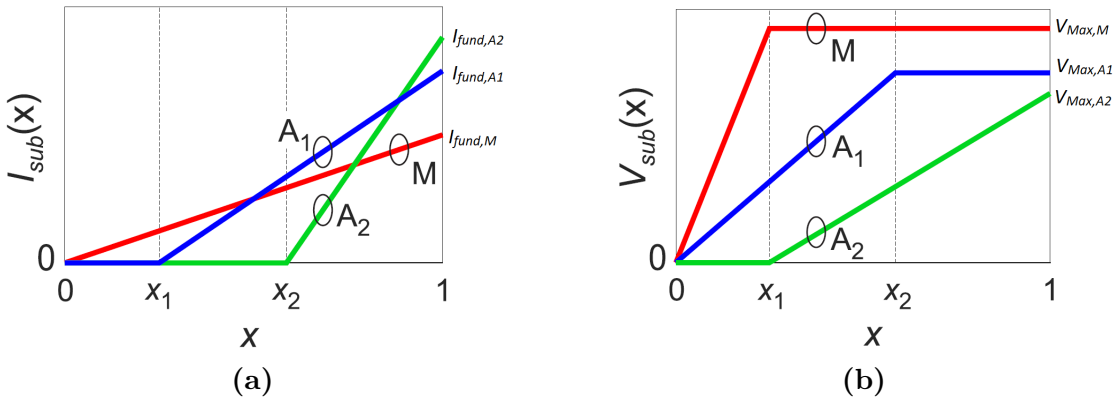

Figure 4.4: Generic electrical quantities profile for a 3-stage DPA (only magnitude is represented). (a): generic current profile, (b): generic voltage profile.

Figure 4.4 shows the typical profile for DPAs realization, which has been historically used and is still the most common. This profile ensures the best efficiency with the combiner topology used in this work. Recent studies have focused on different combiner structures [16], which require different I and V profiles to achieve suitable efficiency. Before starting with calculations, two important parameters related to back-off regions need to be dedicated:

$$\begin{aligned} \alpha_1^2 &= \frac{P_{\mathrm{DPA}}(x_1)}{P_{\mathrm{DPA}}(x=1)} \\ \alpha_1^2 &= \frac{P_{\mathrm{DPA}}(x_2)}{P_{\mathrm{DPA}}(x=1)} \end{aligned} \tag{4.31}$$

According with the definition of $OBO = -10\log_{10}\frac{P_{\mathrm{DPA}}(x)}{P_{\mathrm{DPA}}(x=1)}$, following result are hilighted:

$$\begin{aligned} \alpha_1 &= 10^{-\frac{OBO_1}{20}} = x_1 \\ \alpha_2 &= 10^{-\frac{OBO_2}{20}} = x_2 \end{aligned} \tag{4.32}$$

These relations are very important because relate the back-off with the normalized dynamic range and, as a consequence, with profile different regions. Now, the current stimulus $[I_{\mathrm{M}}(f,x); I_{\mathrm{A1}}(f,x); I_{\mathrm{A2}}(f,x)]^T$ can be defined according to the profile selected:

$$
\begin{aligned}
I_{\mathrm{M}}(f,x) &= x \cdot I_{\mathrm{fund,M}} \cdot e^{j\phi_{\mathrm{M}}(f)} \\
I_{\mathrm{A1}}(f,x) &= \begin{cases} 0 \quad \text{for} \quad x < \alpha_1 \\ \frac{I_{\mathrm{fund,A1}}}{1-\alpha_1} \cdot (x-\alpha_1) \cdot e^{j\phi_{\mathrm{A1}}(f)} \quad \text{for} \quad x \geq \alpha_1 \end{cases} \\
I_{\mathrm{A2}}(f,x) &= \begin{cases} 0 \quad \text{for} \quad x < \alpha_2 \\ \frac{I_{\mathrm{fund,A2}}}{1-\alpha_2} (x-\alpha_2) e^{j\phi_{\mathrm{A2}}(f)} \quad \text{for} \quad x \geq \alpha_2 \end{cases}
\end{aligned} \tag{4.33}
$$

It is important to note that the characterization of a profile has an impact on the DPA characterization. Acting on the position of the dynamic range where each Auxiliary turns on means to establish if the configuration works as a 3-way or a 3-stage and then declare the OBO region. By working with the profile shown in Figure 4.4 and described analytically in (4.33), a 3-stage is dealt. Currently, $\mathbf{I}(f,x)$ is the only stimulus for the combiner network, and physical limits on output current have not been taken into account yet. Furthermore, it depends on frequency only for the phase shift introduced by input power splitting. The next step is to apply the theoretical input to the combiner to find the voltage.

$$
\mathbf{V}(f,x) = \begin{bmatrix} V_{\mathrm{M}}(f,x) \\ V_{\mathrm{A1}}(f,x) \\ V_{\mathrm{A2}}(f,x) \end{bmatrix} = Z(f,x) \begin{bmatrix} I_{\mathrm{M}}(f,x) \\ I_{\mathrm{A1}}(f,x) \\ I_{\mathrm{A2}}(f,x) \end{bmatrix} \tag{4.34}
$$

Numerical estimation corresponds to physical quantities only if results are physically meaningful, which in this case means to affirm that:

$$
V_{\mathrm{sub}}(f,x) \leq V_{\mathrm{Max,sub}} \quad \forall \quad (f,x) \tag{4.35}
$$

So, after having estimated $\mathbf{V}(f,x)$, a check on magnitude for each $V_{\mathrm{sub}}(f,x)$ needs to be done: if there are some $(f_{\mathrm{i}}, x_{\mathrm{j}})$ in the domain where $V_{\mathrm{sub}}(f_{\mathrm{i}}, x_{\mathrm{j}}) > V_{\mathrm{Max,sub}}$, then it means that:

- $V_{\mathrm{sub}}(f_{\mathrm{i}}, x_{\mathrm{j}})$ has no physical meaning and, for $(f_{\mathrm{i}}, x_{\mathrm{j}})$ the active device in question has achieved saturation point and the real voltage is *clipped* on the maximum value $V_{\mathrm{Max,sub}}$;
- having achieved saturation, the entire normalized dynamic range should be re-dimensioned to maintain the original theoretical profile wanted. This means that for a given frequency f_{i}, all $I_{\mathrm{sub}}(f_{\mathrm{i}})$ should be scaled for each $x \in [0;1]$. In this way, $I_{\mathrm{fund,sub}}$ is scaled and the same clipping factor is used for the entire dynamic to maintain linearity in the range.
- because active devices are dependent on them due to input power splitting, current scaling involves every current. In fact, a given $V_{\mathrm{sub}}(f_{\mathrm{i}}, x_{\mathrm{j}})$ is a linear

combination of current coming from each amplifier and the entire $\mathbf{I}(f_\mathrm{i})$ needs to be clipped.

From now on, it is supposed that:

- the system is analyzed in the frequency range between f_min and f_max and discretized in m samples;
- the normalized dynamic range between 0 and 1 is discretized in n samples.

The clipping model developed in this study operates on the assumption that when estimated voltages exceed the saturation limit, it must occur in the saturation region, which corresponds to the highest point of the normalized dynamic range ($x = 1$). Initially, the entire current profile is scaled using a clipping factor estimated for $x = 1$, which might seem sufficient from an intuitive standpoint. However, previous studies have neither confirmed nor denied the possibility of output voltage saturation due to combiner frequency behaviour during load-modulation in back-off. Therefore, to make the script more robust, the check is performed not only at maximum power but also during subsequent scaling in back-off. To consider clipping due to saturation limits, after the first numerical estimation of $\mathbf{V}(f, x)$, the *clipping factor* is estimated for $x = x_\mathrm{n} = 1$:

$$\forall f_\mathrm{i}, \quad c_\mathrm{sub}(f_\mathrm{i}, x_\mathrm{n}) = \begin{cases} \frac{V_\mathrm{MAX,sub}}{|V_\mathrm{sub}(f_\mathrm{i}, x_\mathrm{n})|} & \text{if} \quad |V_\mathrm{sub}(f_\mathrm{i}, x_\mathrm{n})| > V_\mathrm{MAX,sub} \\ 1 & \text{if} \quad |V_\mathrm{sub}(f_\mathrm{i}, x_\mathrm{n})| \leq V_\mathrm{MAX,sub} \end{cases} \tag{4.36}$$

Due to active device dependence, the clipping factor for a given frequency and back-off is associated with the lowest coefficient estimated between devices:

$$c(f_\mathrm{i}, x_\mathrm{n}) = min\{c_\mathrm{M}(f_\mathrm{i}, x_\mathrm{n}); c_\mathrm{A1}(f_\mathrm{i}, x_\mathrm{n}); c_\mathrm{A2}(f_\mathrm{i}, x_\mathrm{n})\} \quad \forall f_\mathrm{i} \tag{4.37}$$

At this point, all current profiles are scaled according to $c(f_\mathrm{i}, x_\mathrm{n})$:

$$I^{(1)}_\mathrm{sub}(f_\mathrm{i}, x_\mathrm{j}) = I_\mathrm{sub}(f_\mathrm{i}, x_\mathrm{j}) \cdot c(f_\mathrm{i}, x_\mathrm{n}) \quad \forall f_\mathrm{i}, j < n \tag{4.38}$$

So, the clipped voltage can be estimated as:

$$V^{(1)}_\mathrm{sub}(f_\mathrm{i}, x_\mathrm{j}) = Z(f_\mathrm{i}) I^{(1)}_\mathrm{sub}(f_\mathrm{i}, x_\mathrm{j}) \quad \forall f_\mathrm{i}, j < n \tag{4.39}$$

After the initial correction, it is recommended to check the limits in back-off by iterating the previous estimation for each back-off level in a loop.

$$
\begin{aligned}
&\forall i,k = \{1,...,n-1\} \\
&\quad c_{\text{sub}}(f_{\text{i}},x_{\text{n-k}}) = \begin{cases} \frac{V_{\text{MAX,sub}}}{|V_{\text{sub}}(f_{\text{i}},x_{\text{n-k}})|} & \text{if} \quad |V_{\text{sub}}(f_{\text{i}},x_{\text{n-k}})| > V_{\text{MAX,sub}} \\ 1 & \text{if} \quad |V_{\text{sub}}(f_{\text{i}},x_{\text{n-k}})| \leq V_{\text{MAX,sub}} \end{cases} \\
&\quad c(f_{\text{i}},x_{\text{n-k}}) = min\{c_{\text{M}}(f_{\text{i}},x_{\text{n-k}}); c_{\text{A1}}(f_{\text{i}},x_{\text{n-k}}); c_{\text{A2}}(f_{\text{i}},x_{\text{n-k}})\} \\
&\quad I_{\text{sub}}^{(1+k)}(f_{\text{i}},x_{\text{n-k}}) = \begin{cases} I_{\text{sub}}^{k}(f_{\text{i}},x_{\text{j}}) \cdot c(f_{\text{i}},x_{\text{n-k}}) & \text{if} \quad j \leq n-k \\ I_{\text{sub}}^{k}(f_{\text{i}},x_{\text{j}}) & \text{if} \quad j > n-k \end{cases} \\
&\quad V_{\text{sub}}^{(1+k)}(f_i,x_{\text{n-k}}) = Z(f_{\text{i}}) I_{\text{sub}}^{(1+k)}(f_{\text{i}},x_{\text{n-k}})
\end{aligned}
\tag{4.40}
$$

The overall clipping process can be resumed in the following step:

1. at first, $x = x_{\text{n}} = 1$ is considered;
2. voltage control is performed in order to determine frequency where saturation law is overcome;
3. the clipping factor is estimated;
4. electrical quantities are scaled according to this factor for the lower dynamic range;
5. a lower x is considered;
6. the loop restarts from 2 until $x = x_1 = 0$.

During the iteration from $x_{\text{n}} = 1$ to $x_1 = 0$, the overall dynamic range is corrected. The clipped electrical quantities at this point are:

$$
\begin{pmatrix} V_{\text{M,clip}} \\ V_{\text{A1,clip}} \\ V_{\text{A2,clip}} \end{pmatrix} = \begin{pmatrix} V_{\text{M}}^{n} \\ V_{\text{A1}}^{n} \\ V_{\text{A2}}^{n} \end{pmatrix}, \quad \begin{pmatrix} I_{\text{M,clip}} \\ I_{\text{A1,clip}} \\ I_{\text{A2,clip}} \end{pmatrix} = \begin{pmatrix} I_{\text{M}}^{n} \\ I_{\text{A1}}^{n} \\ I_{\text{A2}}^{n} \end{pmatrix} \tag{4.41}
$$

When analyzing voltage and current levels, it is important to shift the k index from 1 to $n-1$, which means starting from the maximum dynamic range ($x = 1$) to zero output power ($x = 0$). By doing this, current and voltage correction can be performed from higher to lower x values. It is worth noting that if a correction is needed, it is only propagated towards low power. This is a collateral effect that may occur if clipping at $x = 1$ is not sufficient, causing the current profile to change from a linear relationship to a polyline. Although this approach may require a large number of iterations depending on the number of frequency and dynamic range samples, it eventually returns the desired correction on electrical quantities, giving them a physical meaning according to the device. It is important to observe

that the clipping factor $c(f_{\mathrm{i}}, x_{\mathrm{j}})$ takes into account any correction performed only after the other ones involved from $x_{\mathrm{j+1}}$ to x_{n}. From this point, the clipping matrix C can be defined.

$$C = \begin{bmatrix} c(f_1,x_1)c(f_1,x_2)...c(f_1,x_{\mathrm{n}}) & ... & c(f_1,x_{\mathrm{n\text{-}1}})c(f_1,x_n) & c(f_1,x_{\mathrm{n}}) \\ c(f_2,x_1)c(f_2,x_2)...c(f_2,x_{\mathrm{n}}) & ... & c(f_2,x_{\mathrm{n\text{-}1}})c(f_2,x_{\mathrm{n}}) & c(f_2,x_{\mathrm{n}}) \\ \vdots & \ddots & \vdots & \\ c(f_{\mathrm{m}},x_1)c(f_{\mathrm{m}},x_2)...c(f_{\mathrm{m}},x_{\mathrm{n}}) & ... & c(f_{\mathrm{m}},x_{\mathrm{n\text{-}1}})c(f_{\mathrm{m}},x_{\mathrm{n}}) & c(f_{\mathrm{m}},x_{\mathrm{n}}) \end{bmatrix} \tag{4.42}$$

The construction of this matrix can be useful for understanding the relation between the first current estimation to the one obtained at the end of the clipping loop. In fact, it is easy to demonstrate that the relation between initial quantities and the corrected ones is:

$$\begin{aligned} \mathbf{I}_{\mathrm{clip}}(f_{\mathrm{i}},x_{\mathrm{j}}) &= \begin{pmatrix} I_{\mathrm{M,clip}}(f_{\mathrm{i}},x_{\mathrm{j}}) \\ I_{\mathrm{A1,clip}}(f_{\mathrm{i}},x_{\mathrm{j}}) \\ I_{\mathrm{A2,clip}}(f_{\mathrm{i}},x_{\mathrm{j}}) \end{pmatrix} = C(f_{\mathrm{i}},x_{\mathrm{j}}) \begin{pmatrix} I_{\mathrm{M}}(f_{\mathrm{i}},x_{\mathrm{j}}) \\ I_{\mathrm{A1}}(f_{\mathrm{i}},x_{\mathrm{j}}) \\ I_{\mathrm{A2}}(f_{\mathrm{i}},x_{\mathrm{j}}) \end{pmatrix} \\ \mathbf{V}_{\mathrm{clip}}(f_{\mathrm{i}},x_{\mathrm{j}}) &= \mathbf{I}_{\mathrm{clip}}(f_{\mathrm{i}},x_{\mathrm{j}}) = Z(f_{\mathrm{i}})C(f_{\mathrm{i}},x_{\mathrm{j}}) \begin{pmatrix} I_{\mathrm{M}}(f_{\mathrm{i}},x_{\mathrm{j}}) \\ I_{\mathrm{A1}}(f_{\mathrm{i}},x_{\mathrm{j}}) \\ I_{\mathrm{A2}}(f_{\mathrm{i}},x_{\mathrm{j}}) \end{pmatrix} \end{aligned} \tag{4.43}$$

Once $\mathbf{V}_{\mathrm{clip}}(f,x)$ and $\mathbf{I}_{\mathrm{clip}}(f,x)$ have been estimated correctly, it is possible to calculate some quantities useful for the characterization of the system. The following quantities are estimated under a simplified hypothesis:

- As said before, all devices are in class B;
- all circuit elements are assumed lossless;

For a class B device, DC can be estimated as:

$$I_{0,\mathrm{sub(f,x)}} = 2\frac{|I_{\mathrm{sub,clip}}(f,x)|}{\pi} \tag{4.44}$$

With this information, power considerations can be made:

$$\begin{aligned} P_{\mathrm{DC,sub}}(f,x) &= V_{\mathrm{DD}} I_{0,\mathrm{sub}}(f,x) \\ P_{\mathrm{DC}}(f,x) &= \sum_{\mathrm{sub}} P_{\mathrm{DC,sub}}(f,x) \\ P_{\mathrm{sub}}(f,x) &= \frac{1}{2}\Re\left\{V_{\mathrm{sub,clip}}(f,x)\cdot I_{\mathrm{sub,clip}}(f,x)^*\right\} \end{aligned} \tag{4.45}$$

When using a lossless combiner, the output power of the entire DPA is the sum of power delivered by each DPA, since the power from each DPA is constructively dissipated by the load.:

$$P_{\mathrm{DPA}}(f,x) = \sum_{\mathrm{sub}} P_{\mathrm{sub}}(f,x) \tag{4.46}$$

Now it is possible to estimate the efficiency as:

$$\eta(f,x) = \frac{P_{\mathrm{DPA}}(f,x)}{P_{\mathrm{DC}}(f,x)} \tag{4.47}$$

Impedance levels seen from the internal section of each active device and the reflection coefficient are both represented as complex quantities:

$$\begin{aligned} Z_{\mathrm{sub}}(f,x) &= \frac{V_{\mathrm{sub,clip}}}{I_{\mathrm{sub,clip}}} \\ \Gamma_{\mathrm{sub}}(f,x) &= \frac{Z_{\mathrm{sub}}(f,x) - R_{\mathrm{opt,sub}}/x}{Z_{\mathrm{sub}}(f,x) + R_{\mathrm{opt,sub}}/x} \\ \Gamma_{\mathrm{OPT,sub}}(f,x) &= \frac{Z_{\mathrm{sub}}(f,x) - 50\Omega}{Z_{\mathrm{sub}}(f,x) + 50\Omega} \end{aligned} \tag{4.48}$$

4.5 Code development and implementation

The mathematical concepts described in sections 4.2 and 4.4 can be easily translated into software using a MATLAB script capable of performing AC simulations on a 3-stage DPA based on the linear model developed. The main code is divided into four sections:

1. *Dataset definition*: the user can set parameters related to the combiner topology, initialize quantities for DPA characterization, passive elements in the combiner, adopt models for each active element, consider load, power supply, and analyze bandwidth;

2. *Initialization*: The simulation's primary physical quantities are stored in memory and initialized appropriately.

3. *Simulation*: it is the core of the software. Here Z-parameters are estimated and, after applying the current stimulus to the three-port system, electrical quantities are estimated following the mathematical model developed in this chapter, taking into account clipping phenomena;

4. *Data plots at central frequency*: The simulation results are presented graphically, displaying electrical quantities and power considerations as they vary with back-off for the central frequency. Additionally, data plots are shown for various frequencies within the considered band, highlighting performance in saturation, OBO2 and OBO1 conditions.

Simulation flux follows the flowchart shown in Figure 4.5. In this section, each section will be examined in greater detail. In order to make it easier for users to perform simulations, additional scripts and functions have been developed to improve the structure of the main tools. Since there is no graphical interface available, modifying the initial characteristics of the simulated device requires adjusting certain code parameters and functions.

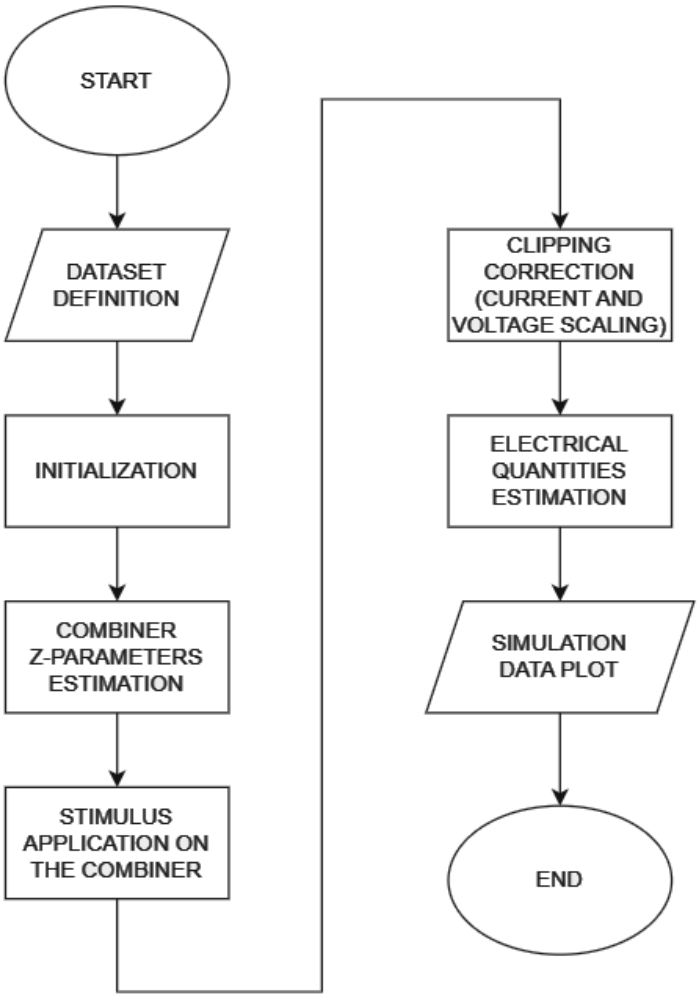

Figure 4.5: Simulation flux.

4.5.1 Dataset definition and initialization

To begin the simulation, the user must first set the parameters and physical quantities for each circuital element involved, based on the topology used. A script called **dataset_*combinername*.m** is available to assist users in selecting the desired dataset for the simulation. The script allows users to adjust the central frequency f_0, as well as the frequency range ($f_{\min}$ to $f_{\max}$) and the frequency resolution f_{res}. The specific combiner type used is identified by the *combinername* variable in the script name. About DPA characterization, the following aspect can be set by modifying the respective variables declared in this scope:

- Transistor parasitic model, described within a lumped model as a shunt resistor $C_{\text{O,sub}}$ and a series impedance $L_{\text{O,sub}}$;
- Supply and OBO levels;
- Parameters related to an eventual compensation network for parasitic;
- Maximum fundamental current $I_{\text{fund,sub}}$ for each device and, as a consequence depending on PA class, the maximum current $I_{\text{max,sub}}$. About the current definition, here the model of the input stage is exploited and coded into the output current phase-shift ϕ_{sub} for each transistor. The phase with which every current flows from the transistor depends on the phase shift introduced by the input stage. From a theoretical point of view, the ideal power splitting should happen with $\phi_{\text{sub}}(f) = \phi_{\text{sub},0}$ but, since power splitters are frequency dependent, modelling $\phi_{\text{sub}}(f)$ with a constant value is not realistic. Some power splitter could be modelled with a linear dependency like $\phi_{\text{sub}}(f) = \frac{\phi_{\text{sub},0}}{f_0} f$.
- Impedance definition for load R_{L} and transmission lines present in the combiner, in terms of characteristic impedance Z_{ch} and phase-shift θ introduced by a delay line (remembering that a quarter-wave TL is characterized by $\theta = \frac{\pi}{2}$ at f_0).

In order to allow users to simulate some default configurations, three datasets have been already created according to three different combiner typologies:

1. *dataset_noparastitic*: active devices are assumed ideal and all parasitic quantities are null;
2. *dataset_Cparastitic*: output stage of each transistor is modelled as a parasitic shunt capacitor, compensated by a shunt inductor in resonance;
3. *dataset_LCparastitic*: the most complete model, where output stages are modelled as a shunt parasitic capacitor in cascade with a series inductor, all compensated by shunt inductors properly sized in the combiner branches.

In the code, the second part involves initializing and allocating memory space to store simulation results. An array or matrix is created with the appropriate size based on the frequency and normalized dynamic range resolution. To declare all simulation variables, a script named *simulation_init.m* is used.

4.5.2 Simulation

It is the core of the entire software and allows the simulation of DPA according to the novel method developed in this chapter. The simulation section can be further divided into three main parts. To estimate Z-parameters for each frequency sample f_{i} in the range between f_{min} and f_{max}, with a resolution of f_{res}, the script employs a function called ***combinername*_combiner.m**. This function is specifically developed for a given *combinername* topology. It receives the frequency samplef_{i} for characterizing the combiner and returns $Z(f_{\mathrm{i}})$. The *combinername_combiner.m* function takes the following parameters as input:

- central frequency f_0;
- frequency sample f_{i};
- parasitic elements quantities for each output stage (like $C_{\mathrm{O,sub}}$ and $L_{\mathrm{O,sub}}$);
- compensation network quantities;
- passive elements quantities related to components present in the combiner topology;
- $Z_{\mathrm{ch,j}}$ and θ_{j} related to eventual j-TL present in the combiner topology.

The function follows the two steps described in section 4.2 to derive Z-parameters:

1. for every branch, the ABCD matrix is calculated as the cascade of all ABCD matrix relating to all passive elements making up the branch itself, remembering that transmission direction in the mathematical model has been assumed from the Main to the other element in the cascade;
2. ABCD-parameters are used to find Z-parameters according to (4.26).

In combiner construction according to simulation rules, the ABCD matrix for each sub-system in each branch can be set using functions associated with some single lumped elements:

- *ABCD_SeriesImpedance(Z)* returns ABCD parameters for a generic impedance Z connected in series in the branch;

- *ABCD_ShuntAdmittance(Y)* returns ABCD parameters for a generic admittance Y shunted in the branch;
- *ABCD_ShuntInductor(L,w)* returns ABCD parameters for a shunt inductor L in the branch;
- *ABCD_ShuntCapacitor(C,w)* returns ABCD parameters for a shunt capacitor C in the branch;
- *ABCD_SeriesInductor(L,w)* returns ABCD parameters for an inductor L connected in series in the branch;
- *ABCD_SeriesCapacitor(C,w)* returns ABCD parameters for an capacitor C connected in series in the branch;
- *ABCD_SeriesTxLine(w0,w,Zch,theta)* returns ABCD parameters for TL connected in series in the branch;

In order to allow users to simulate default configurations described during initialization, three functions have been implemented based on different combiner typologies.

1. *NoParasiticCombiner.m*;
2. *CCompensationCombiner.m*;
3. *LCompensationCombiner.m*.

The combiner used in the software must be the same as the one initialized before, otherwise it may not run or produce incorrect simulations.

The second part of the analysis involves creating a theoretical current profile based on (4.33). This theoretical profile is applied to each frequency and does not take into account physical limitations. The resulting current profile is then applied to the system, and the script **clipping.m** is used to check for electrical incompatibility and correct current and voltage profiles according to saturation limits. The clipping script acts on electrical quantities to detect points $(f_{\mathrm{i}}, x_{\mathrm{j}})$ where the estimated voltage exceeds the saturation limit, estimates the clipping factor, corrects the current profile, and recalculates voltages according to the loop described in section 4.4. The original profiles are overwritten by the clipped ones during implementation, but the clipping matrix C is saved to keep track of the clipping path involved in the loop. In the last part, other electrical quantities are elaborated and derived from $I(f,x)$ and $V(f,x)$. Once that power $P(f,x)$ has been calculated, it is possible to relate normalized dynamic range x with OBO for a better characterization of the DPA.

4.5.3 Data plots at central frequency

It is the first data plot section aimed to show simulation results at the design frequency f_0 with a graphical interface. In this environment, the following curves can be analyzed:

- $I(f_0, x)$ and $V(f_0, x)$ profile at a central frequency as a function of the dynamic range;
- DC power consumption at f_0 for each active device and the total one as a function of the dynamic range;
- AC power consumption at f_0 for each active device and the total one as a function of the dynamic range;
- efficiency curve at a central frequency as a function of dynamic range and OBO both, compared with efficiency curves derived at other different frequency samples in the band.

Graphical plotting functions for this code section have been coded in the script **f0_plots.m**.

4.5.4 Data plots in band

This code section aims to highlight some important results in the entire band considered to observe the frequency behaviour of the system from a different point of view. Results are highlighted for saturation, OBO2 and OBO1 levels. In this environment, the following curves can be analyzed as a function of the frequency:

- effect of clipping and clipping factor analysis in the band;
- output power and efficiency;
- back-off levels;
- Z-parameters;
- input impedance seen by the internal section of each active device Z_{sub};
- reflection coefficient in the Smith chart;

Graphical plotting functions for this code section have been coded in the script **frequency_range_plots.m**.

Chapter 5

Simulations with the novel method and comparison with ADS

This chapter presents the simulation results obtained from MATLAB scripts and compares them with those obtained from ADS. After selecting the combiner topology described in the previous chapter, simulations have been performed using three different types of models that describe active devices. Initially, each active device was assumed to be ideal, without any parasitic elements that could limit the AC dynamic of the system. Frequency limits are associated only with combiner elements and their frequency-dependent behaviour.
Next, simulation has been performed considering for each active device a parasitic capacitance shunted in the output stage. This model resumes all parasitic capacitances that affect the frequency behaviour and should be taken into account in design. A compensation strategy consists of putting in the combiner structure a shunt inductor in parallel to the output stage able to go in resonance with the parasitic capacitance at the central frequency. However, this model is not enough at high frequency.
At RF, the output stage of each active can be described by a more complete model that consists of a cascade of a shunt capacitor and a series inductor. This model has a significant impact on the frequency behaviour of the system. In this scenario, parasitic effects can be partially compensated in the combiner topology by using some design strategies discussed in this chapter, such as using a shunt inductor to neutralize the effect of the parasitic reactance at the central frequency.
In this chapter, each model is treated from a theoretical point of view and simulation results will be discussed to highlight differences between the tool developed and one of the most indicated CAD for RF simulation.

5.1 Simulation environment and setting

In the following sections, some configurations are simulated with the novel method developed in this work and results are compared to ADS simulations in order to verify if the script works correctly and, at the same time, is able to overcome ADS limits. Both simulation environments share the same setting for each simulation session in order to make every result comparable and consistent with the one obtained with the parallel software. Even if some differences are expected in results from a physics meaning, some comparison terms need to be used in order to understand if the MATLAB script works right. In particular, ADS impedance estimation is used as a reference. In fact, impedances depend only on the combiner, which is made only by passive elements. For this reason, it will respond in the same way whether he is stimulated by a feasible signal with a physical meaning according to the device or with a generic mathematical stimulus with, unfeasible for the DPA behaviour. If the script works properly, it will be expected that impedance results simulated by the two different ways will be the same while the differences will be highlighted on power consideration and electric quantities profiles. The DPA structure adopted is the one shown in figure 5.1, where a theoretical design strategy has been already developed[13].

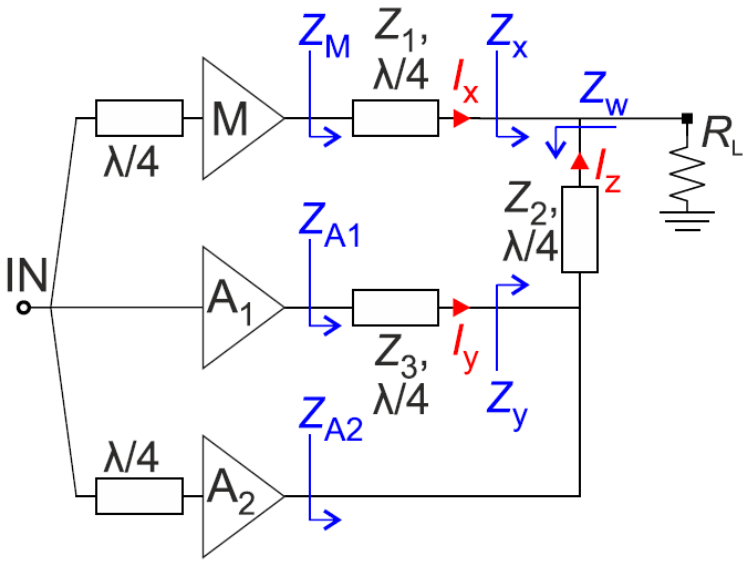

Figure 5.1: DPA under simulation. [13]

While the working principle of this specific combiner topology is not the focus of this work, it is important to note that the signal coming from each branch arrives at the load with a phase of 180° at f_0, thanks to transmission lines. The simulation

is targeted towards the system designed for 5G application, which operates around $f_0 = 28\text{GHz}$. The simulation is conducted within the following frequency range:

$$\begin{aligned} f_{\min} &= 0.85 f_0 = 23.8\text{GHz} \\ f_{\max} &= 1.85 f_0 = 32.2\text{GHz} \end{aligned} \tag{5.1}$$

Frequency resolution is set to $f_{\text{res}} = 0.005 f_0 = 140\text{MHz}$. This setting is the same for both simulation environments. Considering only the output stage without taking into account single PA gains means neglecting relations with the input signal in terms of magnitude. However, input phase inversion cannot be ignored and the effect of the power splitter with a transmission line in M and A2 input has been coded in the phase of each output current. At central frequency, each transmission line introduces a 90° delay. So it is easy to verify that each transmission line TL1, TL2 and TL3 provides a restore with an overall phase of 180° at f_0. However, TLs provide the designed phase-shift only at f_0 and this should be taken into account while in the input stage, the total phase-distortion depends on contributions of both input splitter and input-TLs.The ideal goal for a designer is to guarantee a constant phase shift in all the bands but this is a challenge in input splitting and combiner designs. Because the aim of this work is based on the combiner behaviour analysis, it is assumed that input phases are constant in the overall bandwidth considered (ideal splitting):

$$\begin{aligned} \phi_{\text{M}}(f) &= \phi_{\text{M,0}} = \frac{\pi}{2} \\ \phi_{\text{A1}}(f) &= \phi_{\text{A1,0}} = 0 \\ \phi_{\text{A2}}(f) &= \phi_{\text{A2,0}} = \frac{\pi}{2} \end{aligned} \tag{5.2}$$

5.2 Model with ideal transistors

5.2.1 Model

Reconducting the structure to the generic topology developed:

- the Main branch is made by a single transmission line, so $T_{\mathrm{M}} = T_{\mathrm{TL1}}$;
- the A1 branch is made by a single transmission line, so $T_{\mathrm{A1}} = T_{\mathrm{TL3}}$;
- on A2 branch there are no passive elements, so $T_{\mathrm{A2}} = I$;
- T_1 is made only by a transmission line, so $T_1 = T_{\mathrm{TL2}}$;
- T_2 is made only by a short-circuit, so $T_2 = I$.

The initial simulation assumed that the output stage of each active component is a current generator dependent on the input, as depicted in Figure 5.2. After fixing R_{L}, $P_{\mathrm{DPA,sat}}$, and OBO thresholds, impedance matching of every quarter-wave TL in Figure 5.2 can be estimated using the following method:

$$\begin{aligned} Z_1 &= \frac{V_{\mathrm{MAX,M}}}{I_{\mathrm{x}}(1)} = \frac{V_{\mathrm{MAX,M}}}{\alpha_1}\sqrt{\frac{R_{\mathrm{L}}}{2P_{\mathrm{DPA,sat}}}} \\ Z_2 &= \frac{V_{\mathrm{MAX,A2}}}{I_{\mathrm{z}}(1)} = \frac{V_{\mathrm{MAX,A2}}}{1-\alpha_1}\sqrt{\frac{R_{\mathrm{L}}}{2P_{\mathrm{DPA,sat}}}} \\ Z_3 &= \frac{V_{\mathrm{MAX,A2}}}{I_{\mathrm{y}}(x_2)} = \frac{V_{\mathrm{MAX,A1}}V_{\mathrm{MAX,A2}}}{2\alpha_2(1-\alpha_1)P_{\mathrm{DPA,sat}}} \end{aligned} \tag{5.3}$$

Active device parameters can be derived using Kirchoff laws and exploiting the properties of quarter-wave TLs.

$$\begin{aligned} I_{\mathrm{fund,M}} &= \frac{V_{\mathrm{L}}(1)}{Z_1} = \alpha_1\frac{2P_{\mathrm{DPA,sat}}}{V_{\mathrm{Max,M}}} \\ I_{\mathrm{fund,A1}} &= \frac{V_{\mathrm{Max,A2}}}{Z_3} = \alpha_2(1-\alpha_1)\frac{2P_{\mathrm{DPA,sat}}}{V_{\mathrm{Max,A1}}} \\ I_{\mathrm{fund,A2}} &= (1-\alpha_1-\alpha_2+\alpha_1\alpha_2)\cdot\frac{2P_{\mathrm{DPA,sat}}}{V_{\mathrm{Max,A2}}} \end{aligned} \tag{5.4}$$

$P_{\mathrm{DPA,sat}}, \mathrm{W}$	R_{L}, Ω	$\alpha_1(OBO1)$	$\alpha_2(OBO2)$
3.5	11.3	0.2512 (12dB)	0.5012 (6dB)
$V_{\mathrm{DD,sub}}, \mathrm{V}$	$V_{\mathrm{k,sub}}, \mathrm{V}$	Z_1, Ω	Z_2, Ω
20	4	81	27
Z_3, Ω	$I_{\mathrm{fund,M}}, \mathrm{mA}$	$I_{\mathrm{fund,A1}}, \mathrm{mA}$	$I_{\mathrm{fund,A2}}, \mathrm{mA}$
97	110	164	164

Table 5.1: Sizing of each element.

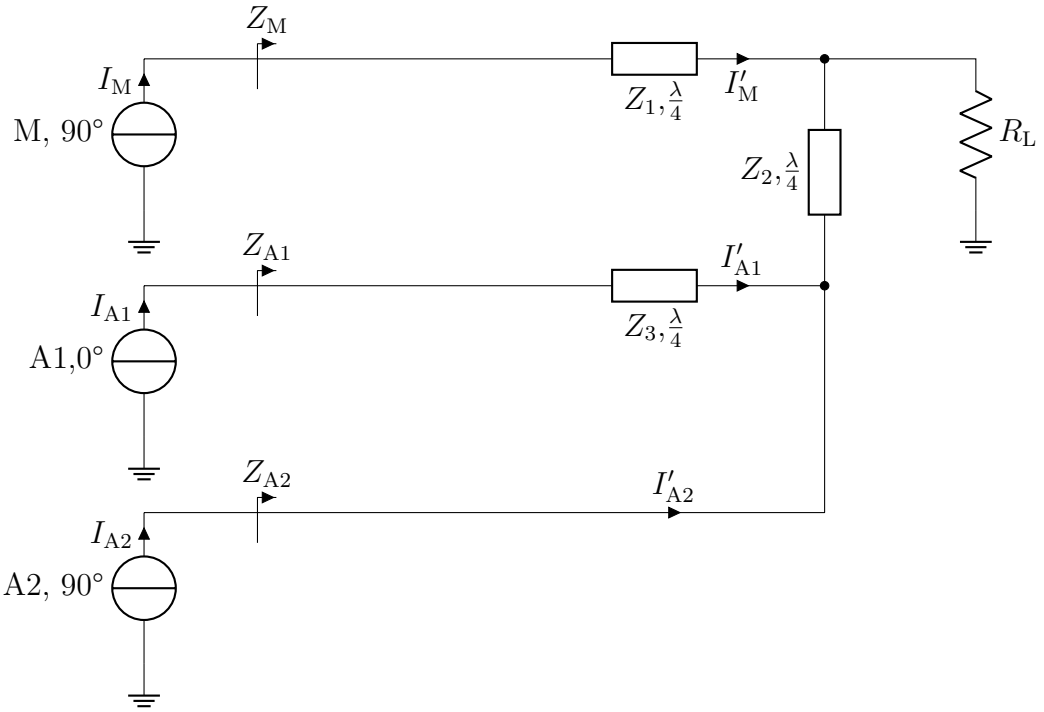

Figure 5.2: Simulation model for the ideal case, without parasitic elements in the output stage of each active device.

5.2.2 Simulations and results comparison

To verify if the code is working as expected, impedances simulated by the script with those simulated by ADS have been compared. As explained in section 5.1, the combiner behaves similarly whether it is supplied by a stimulus that responds to the physics of the system or by a mathematical signal that responds to electrotechnical laws but is incompatible with the dynamics of the DPA. Figures 5.3-5.4-5.5 and Figures 5.6-5.7-5.8 show the impedance seen by the internal section in OBO1, OBO2, and saturation. The script developed in this work produces the same simulation results as those from ADS. There are no reactive elements in the schematic, so the frequency behaviour depends solely on the transmission lines in the combiner. The internal section corresponds to the combiner input stage. It is interesting to note that the impedance levels seen by each internal section correspond to the ideal load for each active element, confirming that the combiner is well-designed for the purpose. All imaginary parts are null at f_0. Reactance is present only due to the presence of transmission lines in the combiner that are appropriately dimensioned. Furthermore, there is symmetry around f_0 for both real and imaginary parts, thanks to the absence of reactive elements. The system is completely balanced around the central frequency. The electrical quantity profiles in the system are designed for the central frequency, which means there is no clipping and the current profile is as expected. Figure 5.9 compares the profiles produced by the script and ADS. It is clear that each transistor is switched on at the back-off level corresponding to $\alpha_1 = 0.25$ and $\alpha_2 = 0.50$. The same results apply to the voltage profile estimated with the different simulation methods shown in Figure 5.10a and 5.10b. At f_0, the voltage profiles are the same. However, Figure 5.11b shows the limitation of ADS. Changing the frequency has a direct effect on the voltage profile, but for some frequencies, the voltages exceed the saturation limit of 16V. This is because the model cannot be implemented on ADS while respecting the limits imposed by the supply. Therefore, the simulation performed in ADS does not have a physical meaning. This means that, for certain frequencies, the voltage and current will be clipped by the MATLAB code. Unmeaningful simulations have a significant impact on the power delivered to the load. This can result in the power delivered exceeding the maximum previously designed power of 3.5W for a specific frequency set. At the fundamental simulation level, the output power and DC absorption remain the same (see Figures 5.12 and 5.14). However, when analyzing the simulations produced by ADS, it becomes clear that the limit is exceeded most strongly in the highest part of the dynamic range. This means that clipping is likely to occur more frequently in the near-saturation power region. The previous considerations have an impact on the efficiency diagrams shown in Figure 5.16. When it comes to f_0, the simulation performed with MATLAB agrees with the one performed with ADS. However, the frequency behaviour of the system produces no physical

meaning in Figure 5.16b. Here, for $OBO > -2$dB, efficiency exceeds the maximum value possible for this configuration, while for $OBO < -2$dB, MATLAB results are the same as those provided by ADS. All these considerations confirm that while ADS produces unphysical results for low back-off, the script developed allows the user to describe the correct behaviour from the system's point of view. In Figures 5.17-5.18-5.19, the effect of MATLAB's clipping implementation can be seen. On the left side, the clipping matrix coefficient is plotted for saturation, OBO2, and OBO1 conditions. It is possible to observe that the clipping parameters are less than 1 when the voltage is greater than $V_{\text{sub,MAX}}$. When it comes to saturation, the I/V profiles are scaled according to the clipping parameter corresponding to $C(f, n)$. The scaling at saturation is enough for OBO1 and OBO2, where the clipping factor is still 1. This means that, according to the clipping algorithm developed, once scaling is done for the saturation condition, the profiles remain in the acceptable range automatically for each frequency in the range. On the right side, the clipping effect on voltages is highlighted. It is crucial that each Power Amplifier (PA) that should be ON works near $V_{\text{sub,MAX}}$, which means an efficient design has been performed. In Figure 5.21, the load modulation effect is shown in detail. At frequency f_0, the results produced by the ADS simulation are the same as those simulated by the script. Figure 5.22 and 5.23 compares the energetic consideration estimated by the script with the one estimated for different back-off levels (-12dB, -6dB, and saturation). The MATLAB result provides curves that are compatible with the device's working principle, while the simulation performed with ADS gives inaccurate results as the frequency moves from f_0. As the back-off increases, the power delivered to the load decreases, and there is a frequency band where this effect is noticeable:

- power delivered to load does not decrease under a certain threshold;
- efficiency remains approximately constant.

On ADS, results are wrong because efficiency and P_{out} overcome the maximum allowed values, corresponding to the one at f_0. Smith charts shown in Figures 5.24 and 5.25 display the estimated reflection coefficients for each combiner input. These calculations were done using the optimal load for each stage and the standard 50Ω as a reference. The results generated by the script match those obtained through simulation in ADS. The diagram in Figure 5.27 shows the core of the mathematical model developed for the simulation, that is the Z-matrix describing the combiner.

5.2.3 Plot section

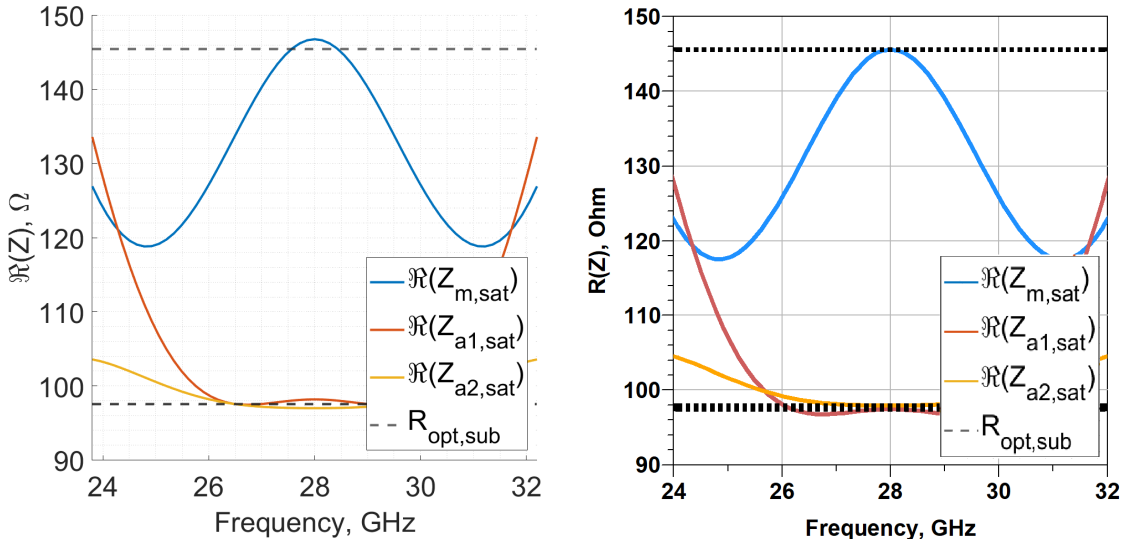

Figure 5.3: Real part of impedances seen by each internal section in saturation. (a): simulation performed by MATLAB, (b): simulation performed by ADS.

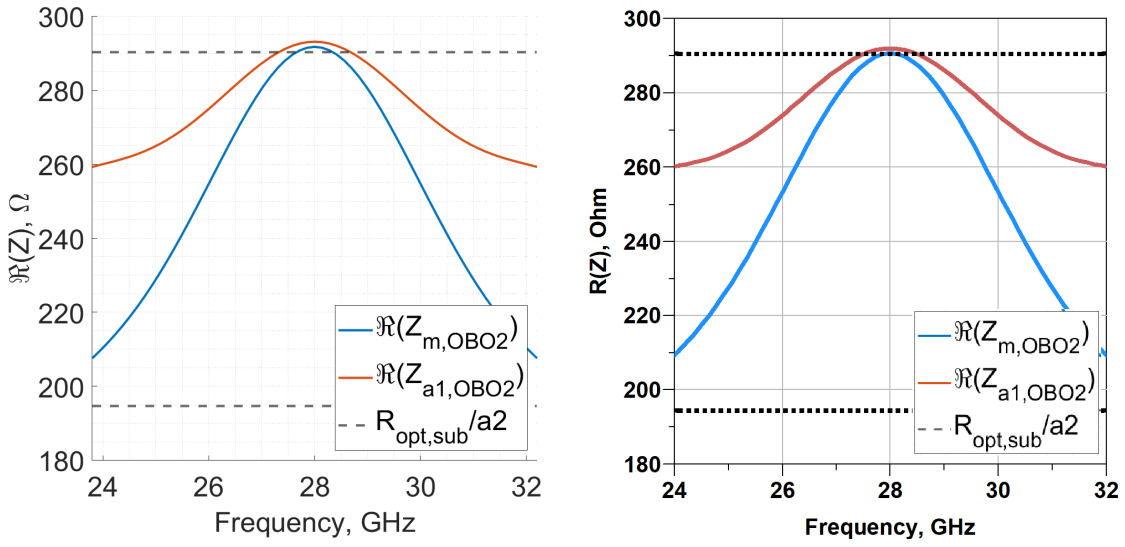

Figure 5.4: Real part of impedances seen by each internal section in OBO2. (a): simulation performed by MATLAB, (b): simulation performed by ADS.

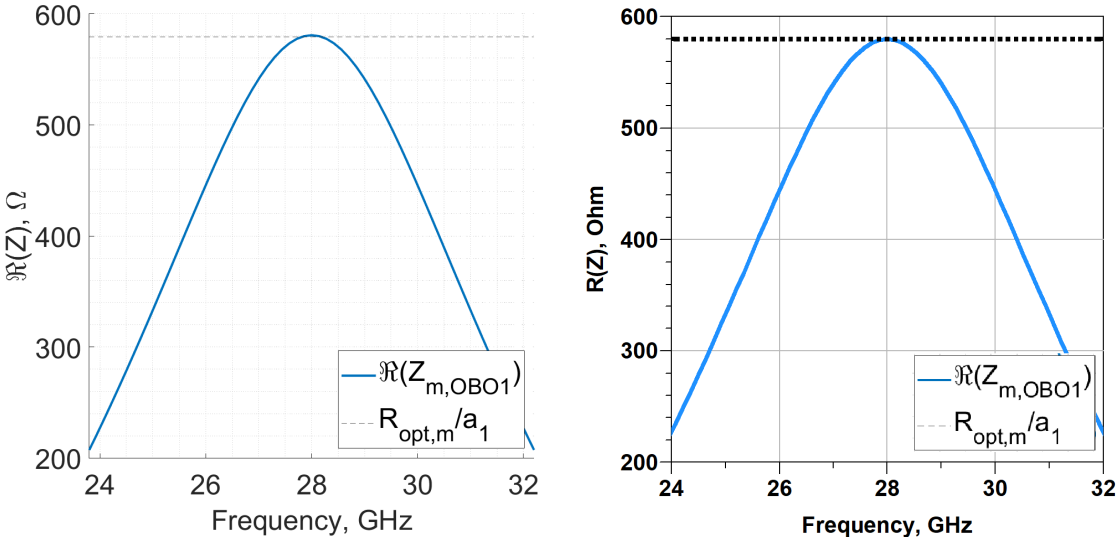

Figure 5.5: Real part of impedances seen by each internal section in OBO1. (a): simulation performed by MATLAB, (b): simulation performed by ADS.

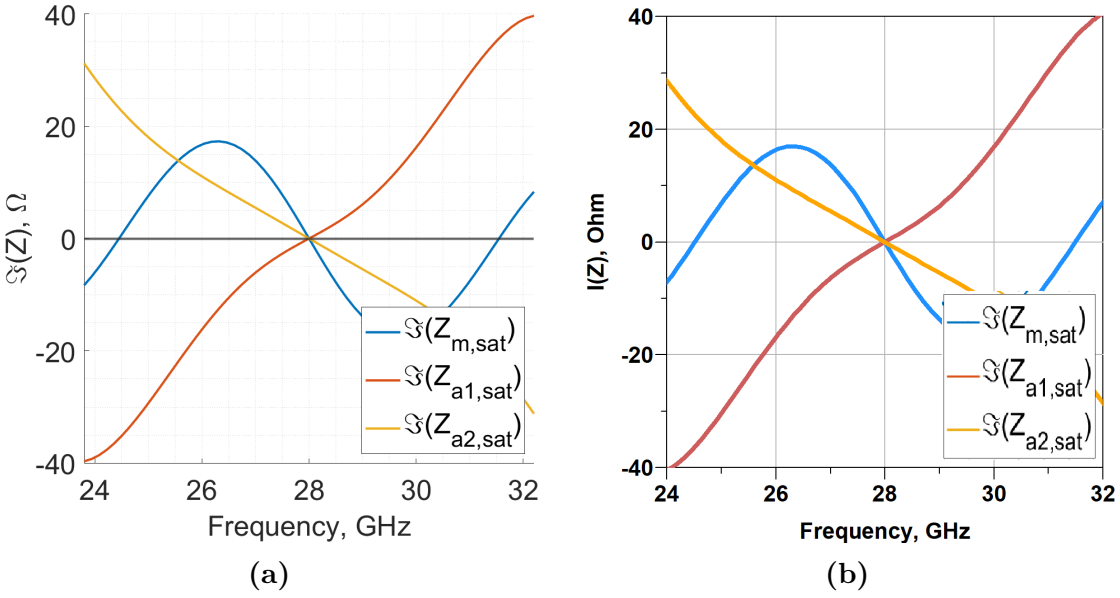

Figure 5.6: Imaginary part of impedances seen by each internal section in saturation. (a): simulation performed by MATLAB, (b): simulation performed by ADS.

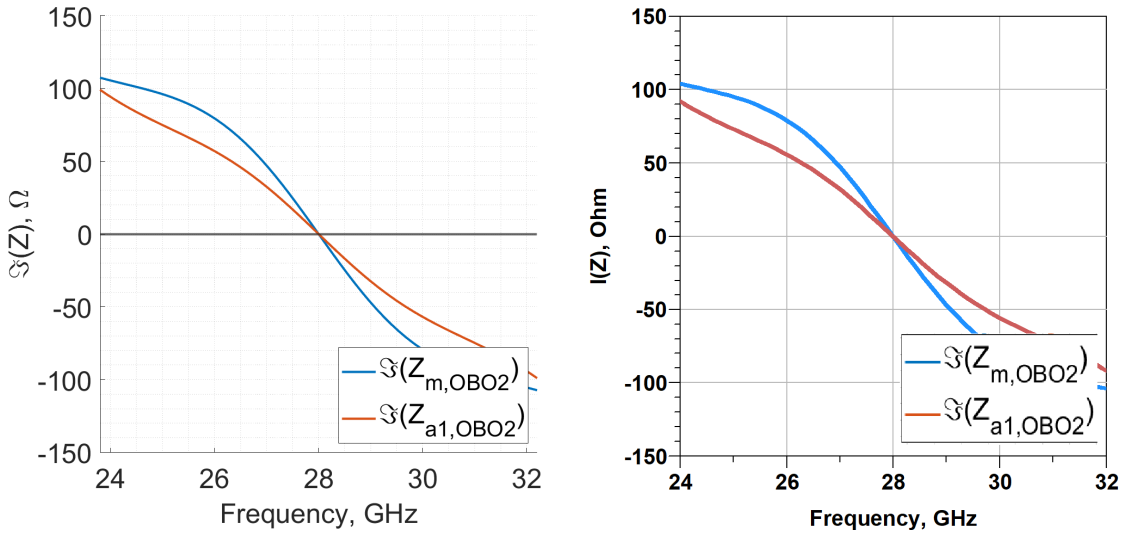

(a) **(b)**

Figure 5.7: Imaginary part of impedances seen by each internal section in OBO2. (a): simulation performed by MATLAB, (b): simulation performed by ADS.

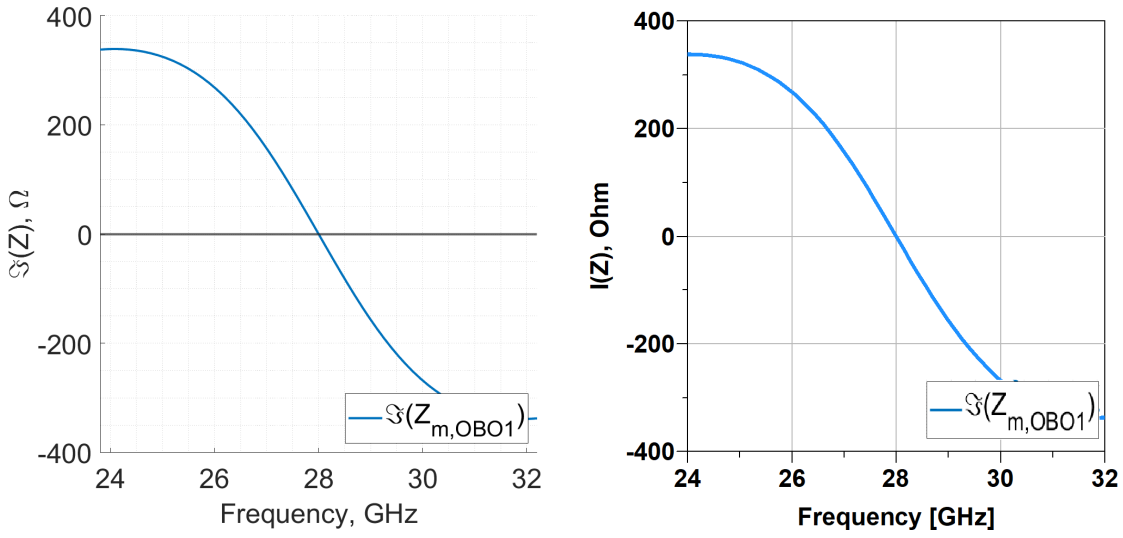

(a) **(b)**

Figure 5.8: Imaginary part of impedances seen by each internal section in OBO1. (a): simulation performed by MATLAB, (b): simulation performed by ADS.

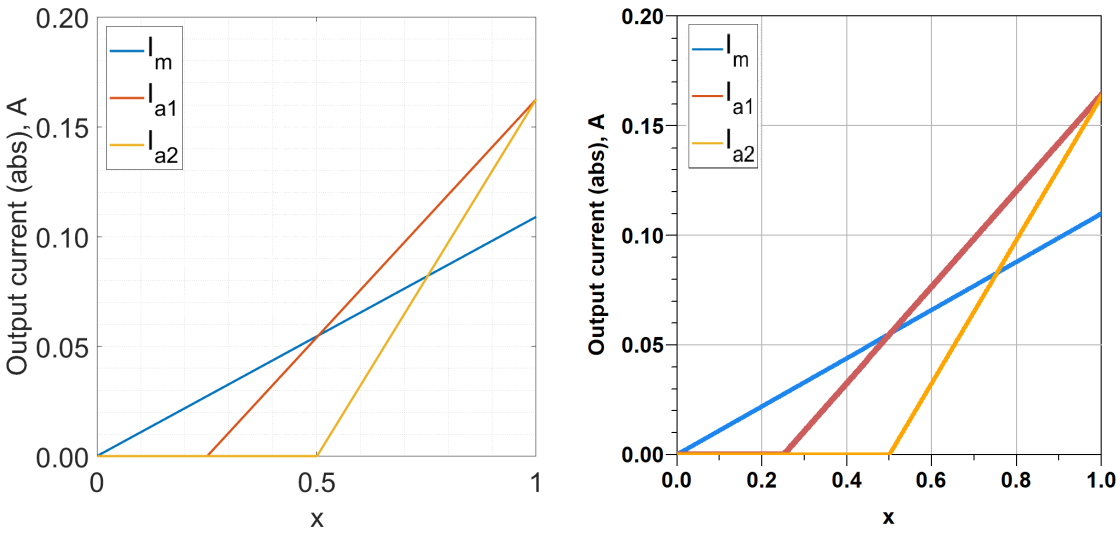

Figure 5.9: Current profile at central frequency. (a): simulation by MATLAB, (b): simulation by ADS.

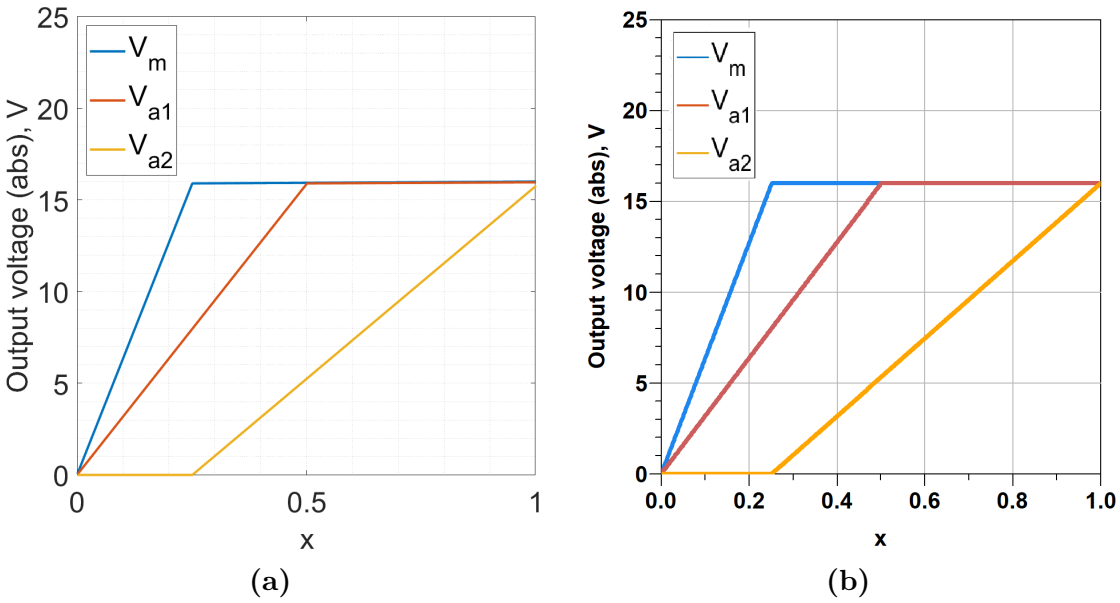

Figure 5.10: Voltage profile at the central frequency. (a): simulation by MATLAB, (b): simulation by ADS.

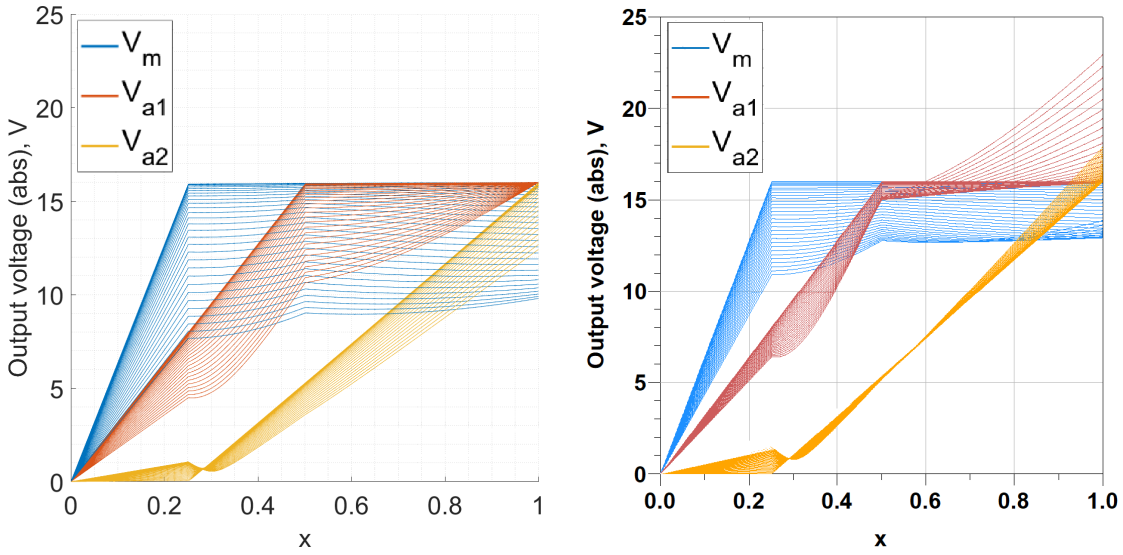

Figure 5.11: Voltage profiles in band. (a): simulation by MATLAB, (b): simulation by ADS.

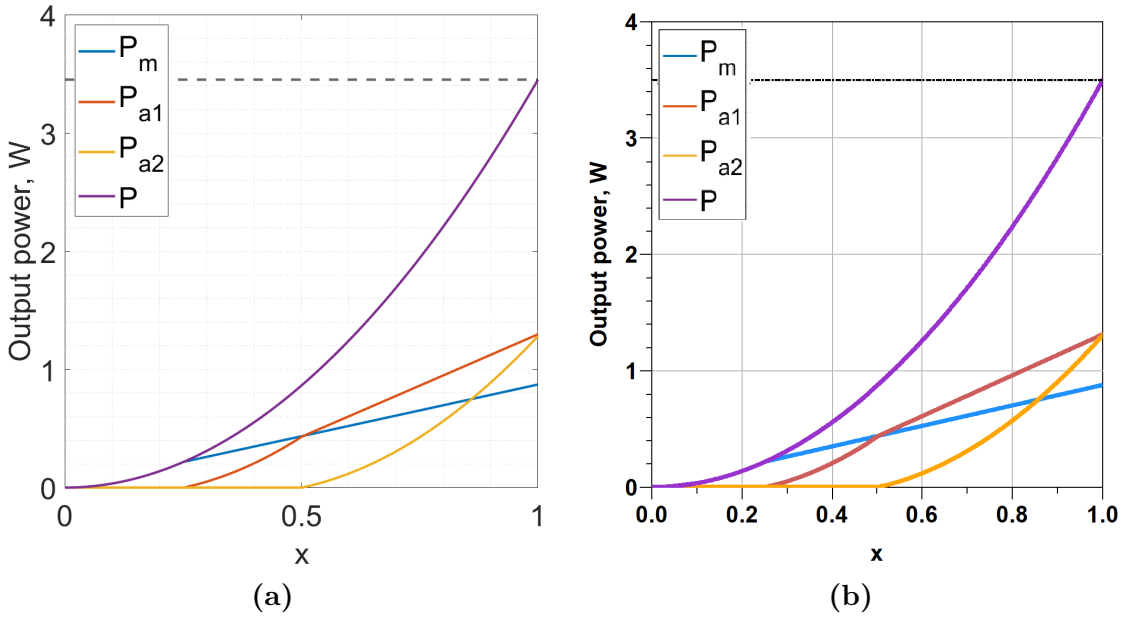

Figure 5.12: Output power delivered to the load at central frequency. (a): simulation by MATLAB, (b): simulation by ADS.

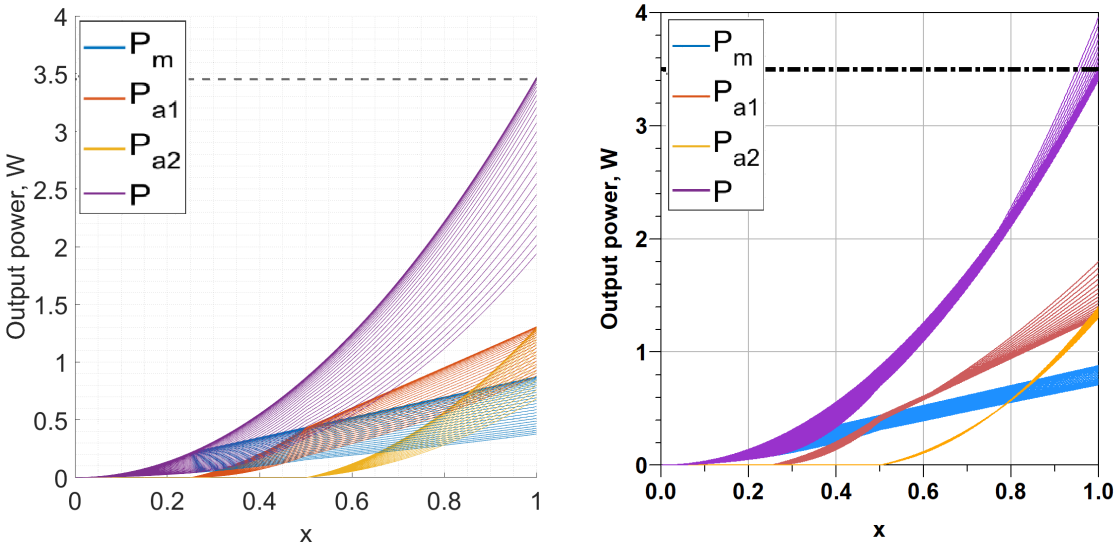

Figure 5.13: Output power delivered to the load in band. (a): simulation by MATLAB, (b): simulation by ADS.

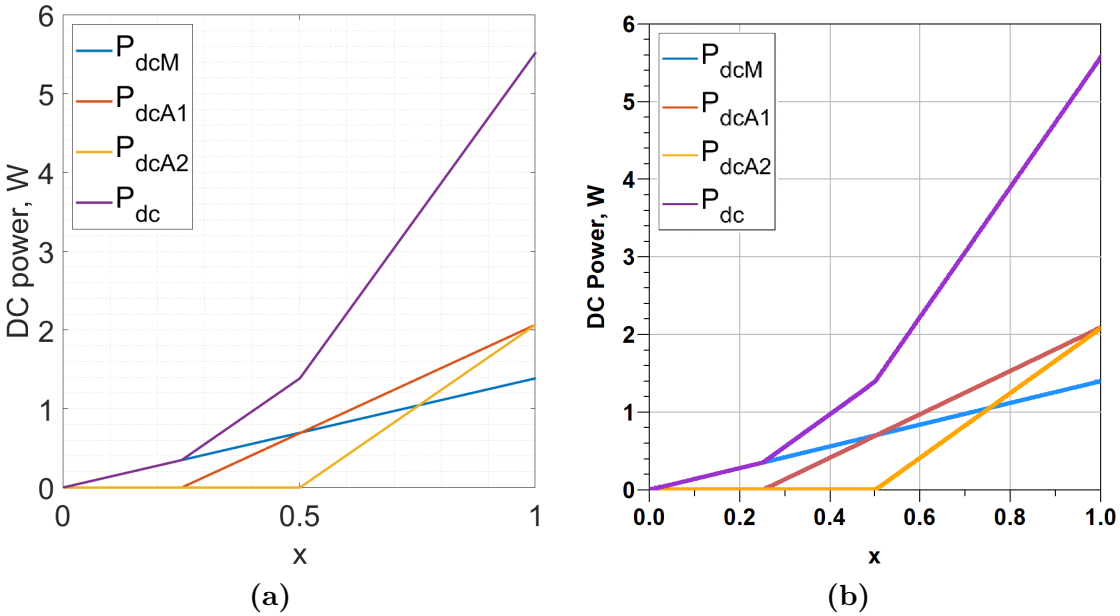

Figure 5.14: DC power. (a): simulation by MATLAB, (b): simulation by ADS.

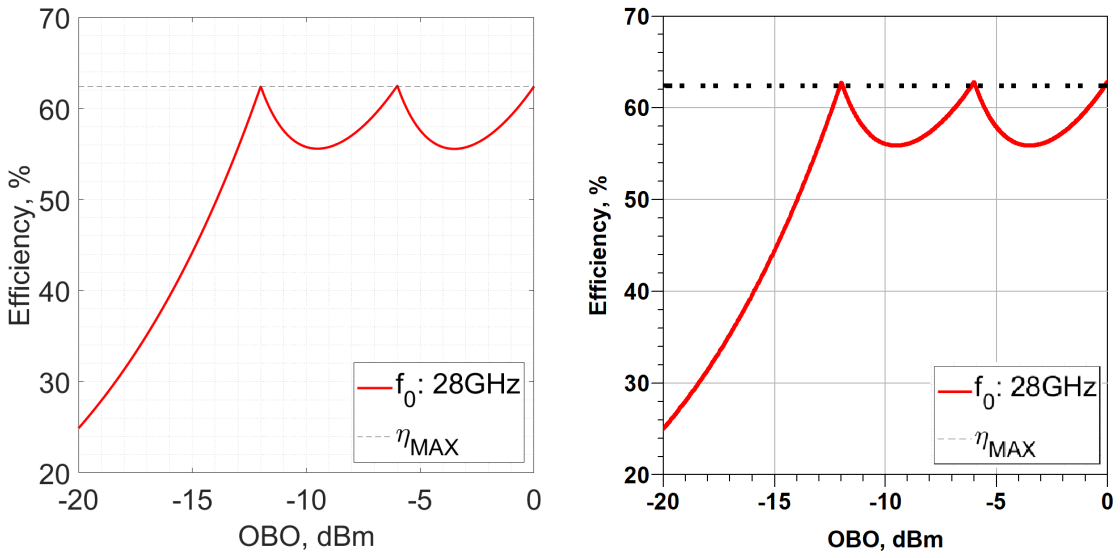

Figure 5.15: Efficiency curves at central frequency. (a): simulation by MATLAB, (b): simulation by ADS.

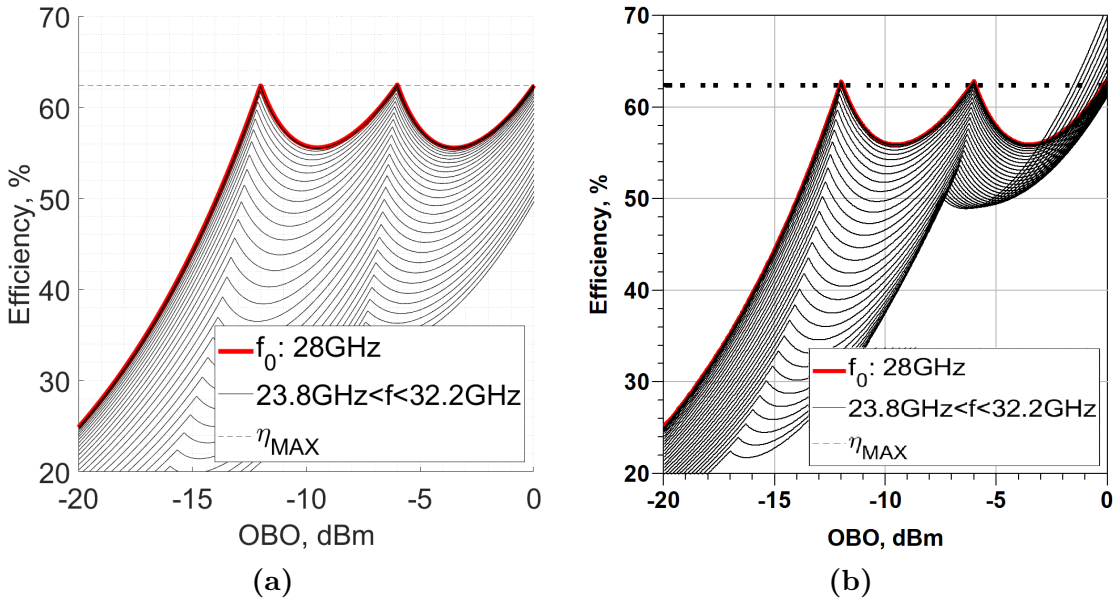

Figure 5.16: Efficiency curves in band. (a): simulation by MATLAB, (b): simulation by ADS.

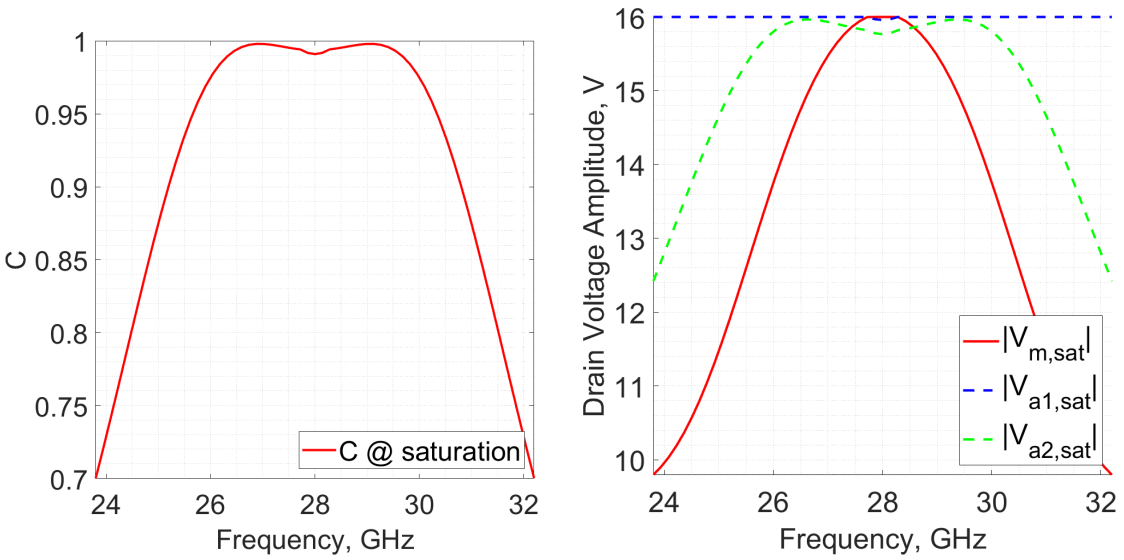

(a) (b)

Figure 5.17: Clipping effect implemented in the MATLAB script at saturation. (a): clipping coefficient, (b): effect of clipping on each drain voltage.

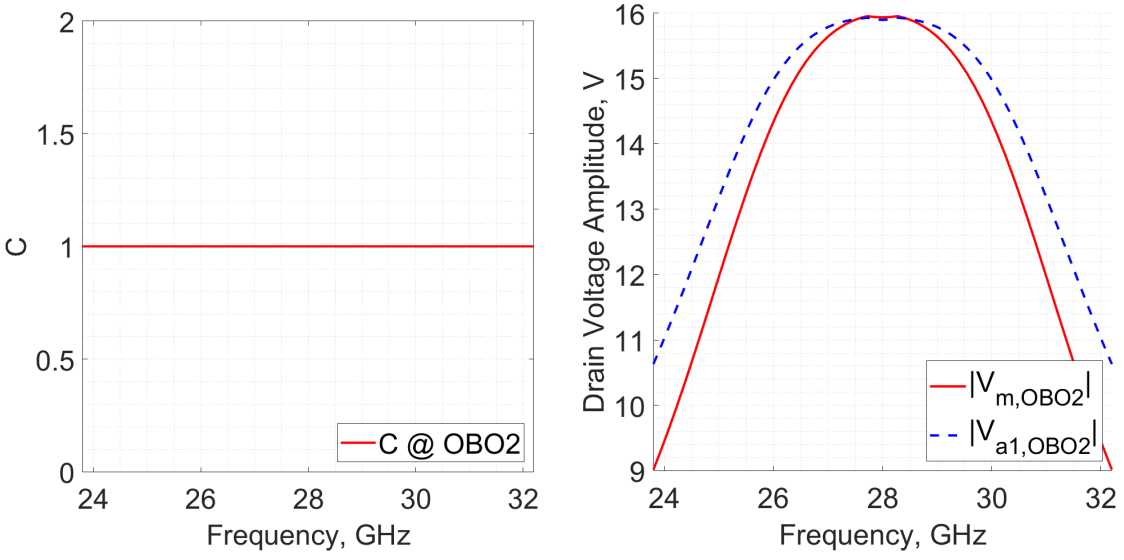

(a) (b)

Figure 5.18: Clipping effect implemented in the MATLAB script in OBO2. (a): clipping coefficient, (b): effect of clipping on each drain voltage.

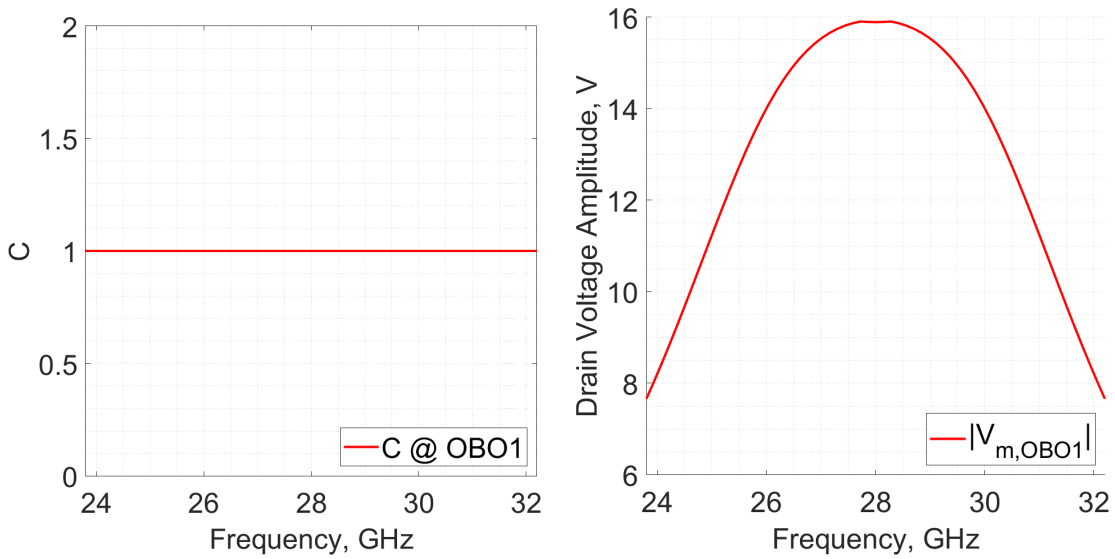

(a) **(b)**

Figure 5.19: Clipping effect implemented in the MATLAB script in OBO1. (a): clipping coefficient, (b): effect of clipping on each drain voltage.

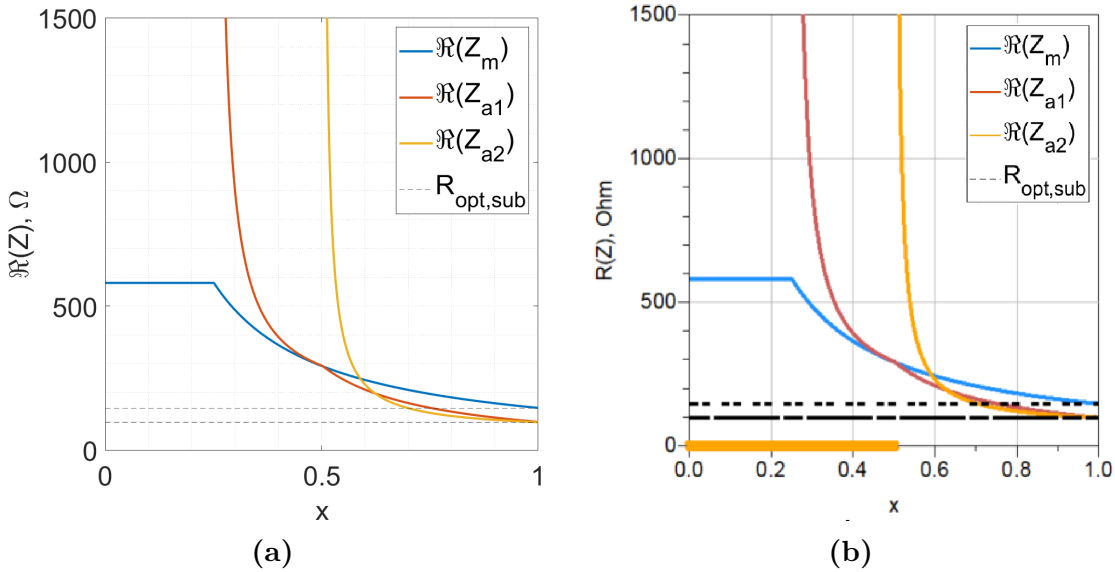

(a) **(b)**

Figure 5.20: Effect of the load modulation at central frequency. (a): simulation by MATLAB, (b): simulation by ADS.

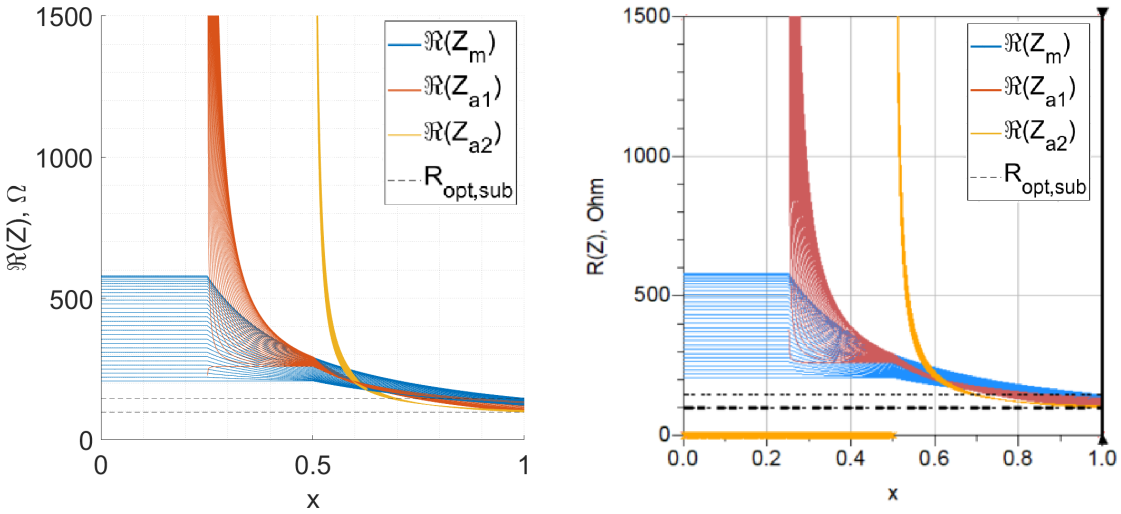

(a) (b)

Figure 5.21: Effect of the load modulation in band. (a): simulation by MATLAB, (b): simulation by ADS.

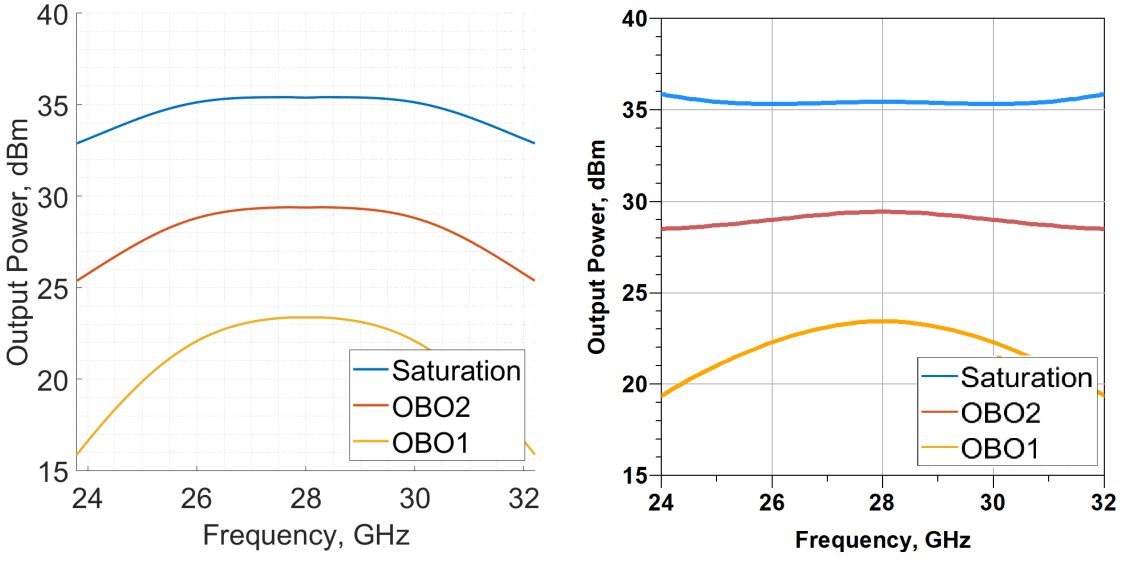

(a) (b)

Figure 5.22: Output power in different back-off condition. (a): simulation by MATLAB, (b): simulation by ADS.

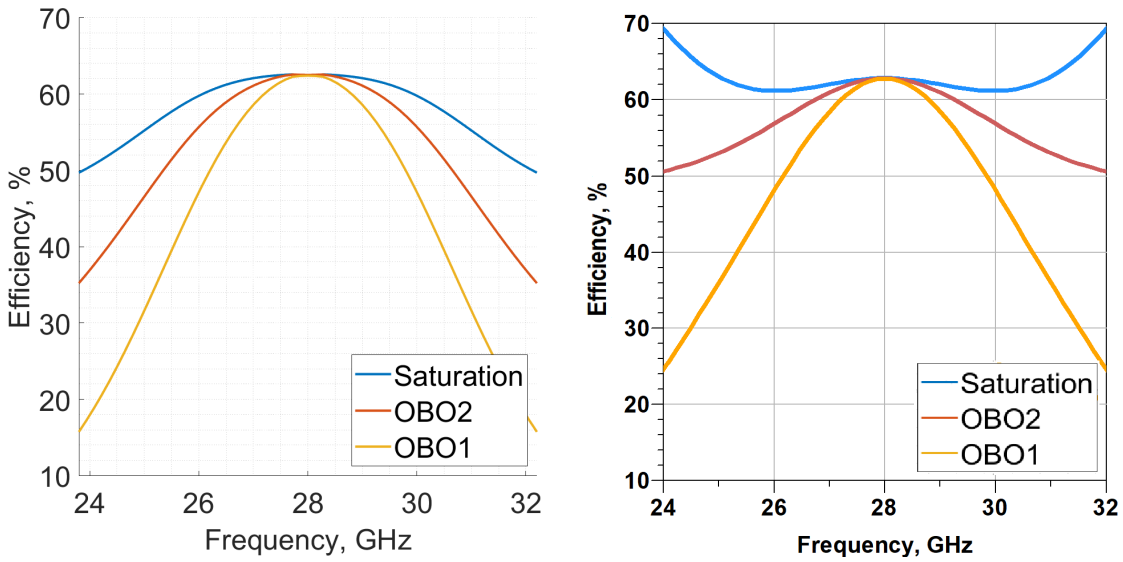

(a) **(b)**

Figure 5.23: Efficiency in different back-off condition. (a): simulation by MATLAB, (b): simulation by ADS.

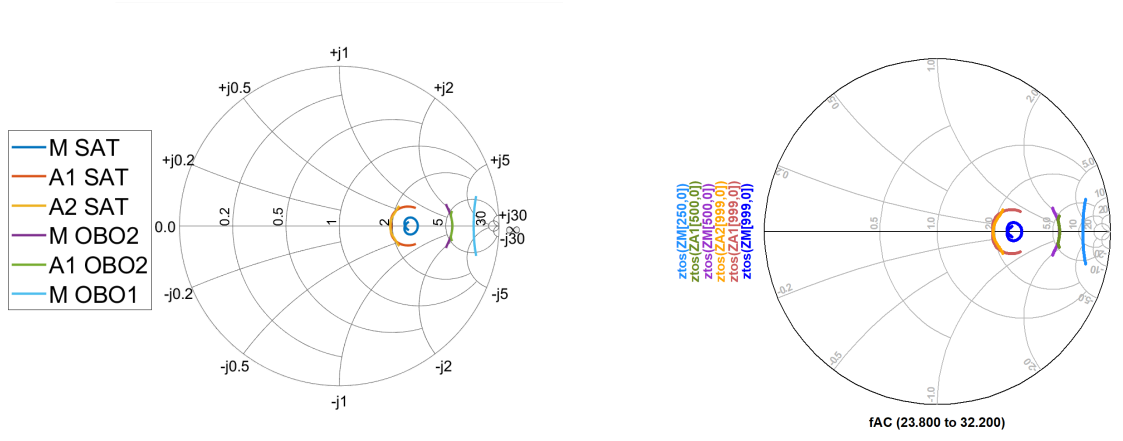

(a) **(b)**

Figure 5.24: Reflection coefficient referred to 50Ω. (a): simulation by MATLAB, (b): simulation by ADS.

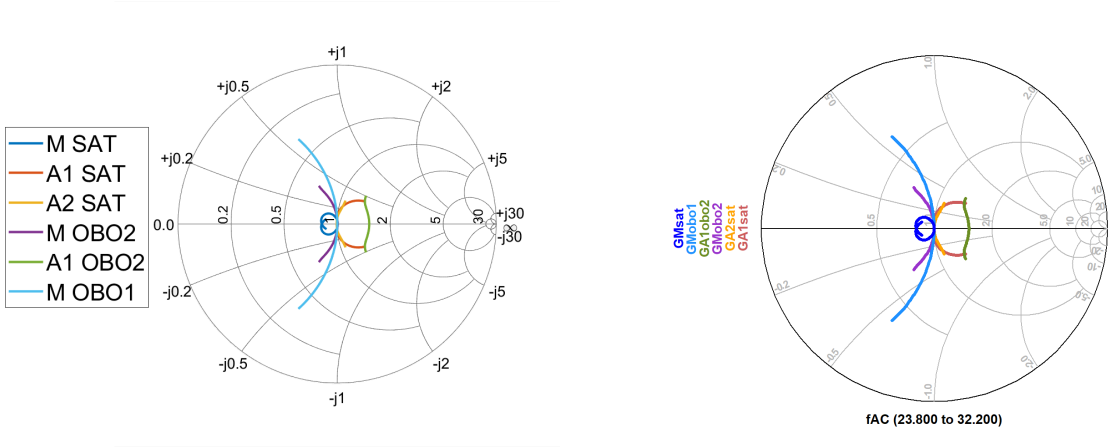

(a) **(b)**

Figure 5.25: Reflection coefficient referred to $R_{\text{opt,sub}}$. (a): simulation by MATLAB, (b): simulation by ADS.

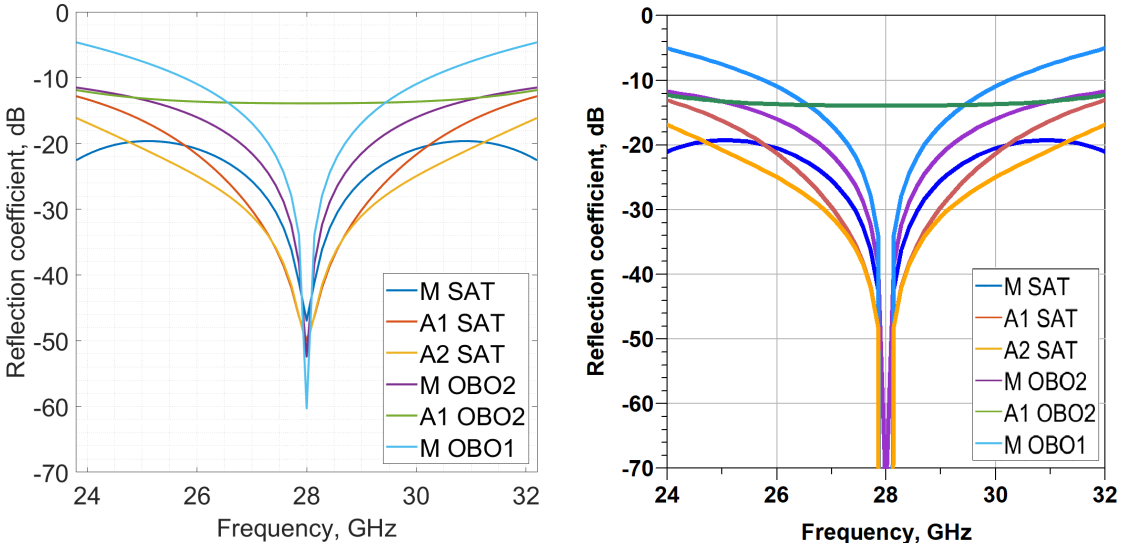

(a) **(b)**

Figure 5.26: Reflection coefficient magnitude referred to $R_{\text{opt,sub}}$. (a): simulation by MATLAB, (b): simulation by ADS.

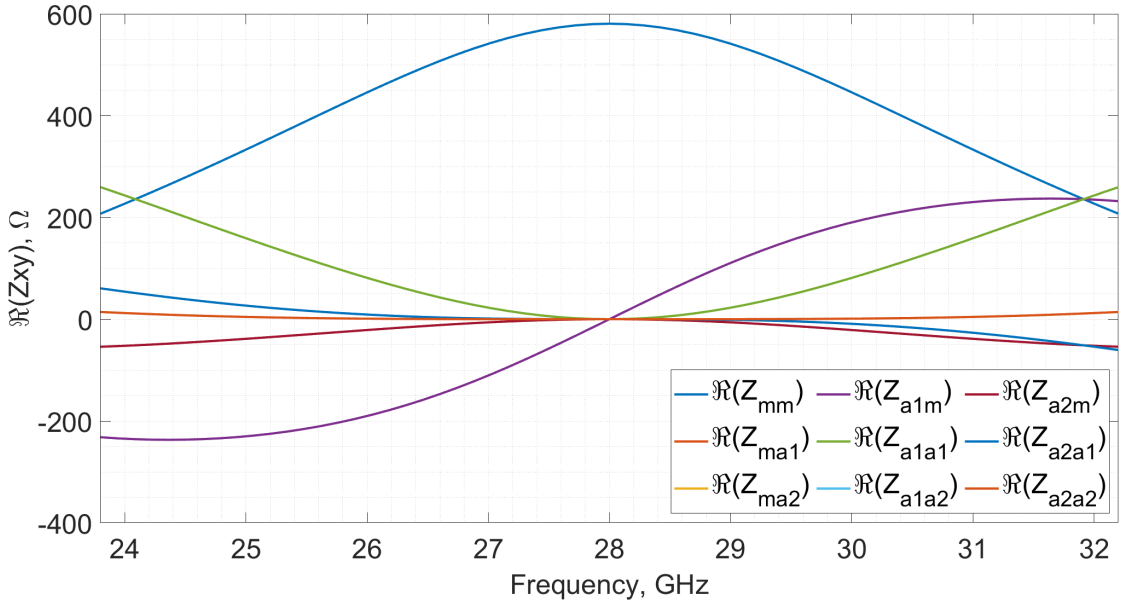

(a)

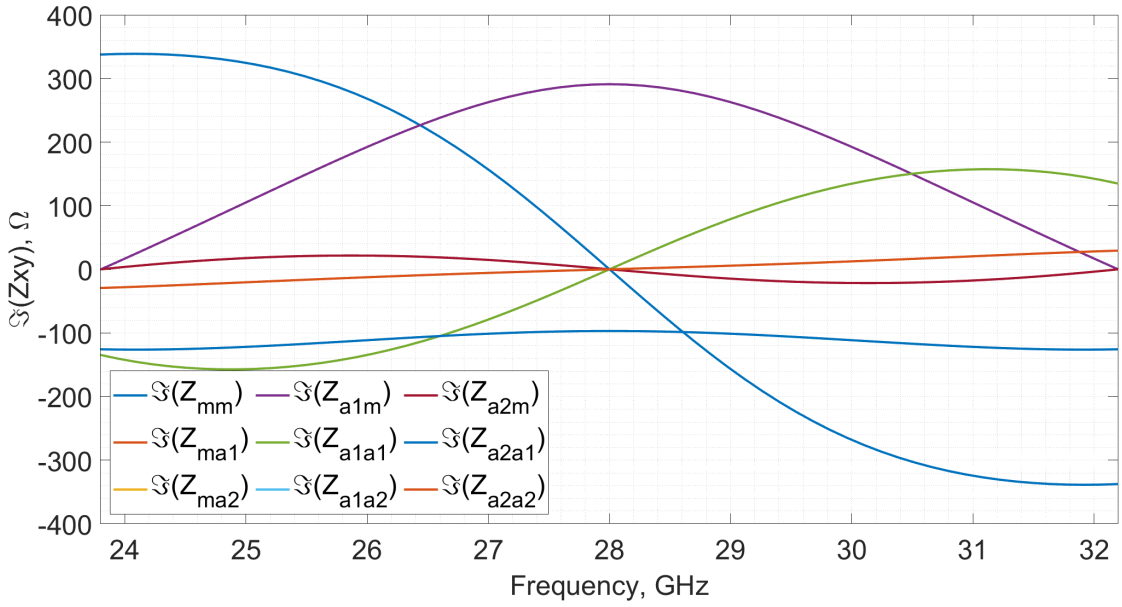

(b)

Figure 5.27: Z-matrix of the combiner estimated by MATLAB. (a): real part, (a): imaginary part.

5.3 Simplified parasitic model for transistors

5.3.1 Model

To make the model more realistic, a parasitic element represented by a shunt capacitor $C_{\mathrm{O,sub}}$ is introduced in the output mode. One way to design this is to include a shunt inductance $L_{\mathrm{C,sub}}$ in parallel in every output combiner branch. This inductance should be calculated to resonate with the equivalent parasitic capacitance model. It is worth noting that a resonant parallel circuit behaves like an open circuit at the resonant frequency.

$$L_{\mathrm{C,sub}} = \frac{1}{\omega_0^2 C_{\mathrm{O,sub}}} \tag{5.5}$$

One benefit of this compensation technique is that impedance levels remain constant from the internal section of each transistor to the combiner plane, as shown in the next section. The output parasitic capacitor values and their corresponding compensation elements are as follows:

$$\begin{cases} C_{\mathrm{O,M}} = 125\mathrm{fF} \\ C_{\mathrm{O,A1/2}} = 230\mathrm{fF} \end{cases} \Longrightarrow \begin{cases} L_{\mathrm{C,M}} = 258\mathrm{pH} \\ L_{\mathrm{C,A1/2}} = 140\mathrm{pH} \end{cases} \tag{5.6}$$

Reconducting the structure to the generic topology developed:

- the Main branch is made by a cascade of the parasitic shunt capacitor followed by the resonant inductor and a transmission line, so $T_{\mathrm{M}} = T_{\mathrm{C_{0,M}},sh} T_{\mathrm{L_{C,M}},sh} T_{\mathrm{TL1}}$;
- the A1 branch is made by a cascade of the parasitic shunt capacitor followed by the resonant inductor and a transmission line, so $T_{\mathrm{A1}} = T_{\mathrm{TL3}} T_{\mathrm{L_{C,A1}},sh} T_{\mathrm{C_{0,A1}},sh}$;
- on A2 branch there are only parasitic and compensation elements, so $T_{\mathrm{A2}} = T_{\mathrm{L_{C,A2}},sh} T_{\mathrm{C_{0,A2}},sh}$;
- T_1 is made only by a transmission line, so $T_1 = T_{\mathrm{TL2}}$;
- T_2 is made only by a short-circuit, so $T_2 = I$.

Note that transmission matrixes have been estimated with conventional directions assumed in the mathematical model.

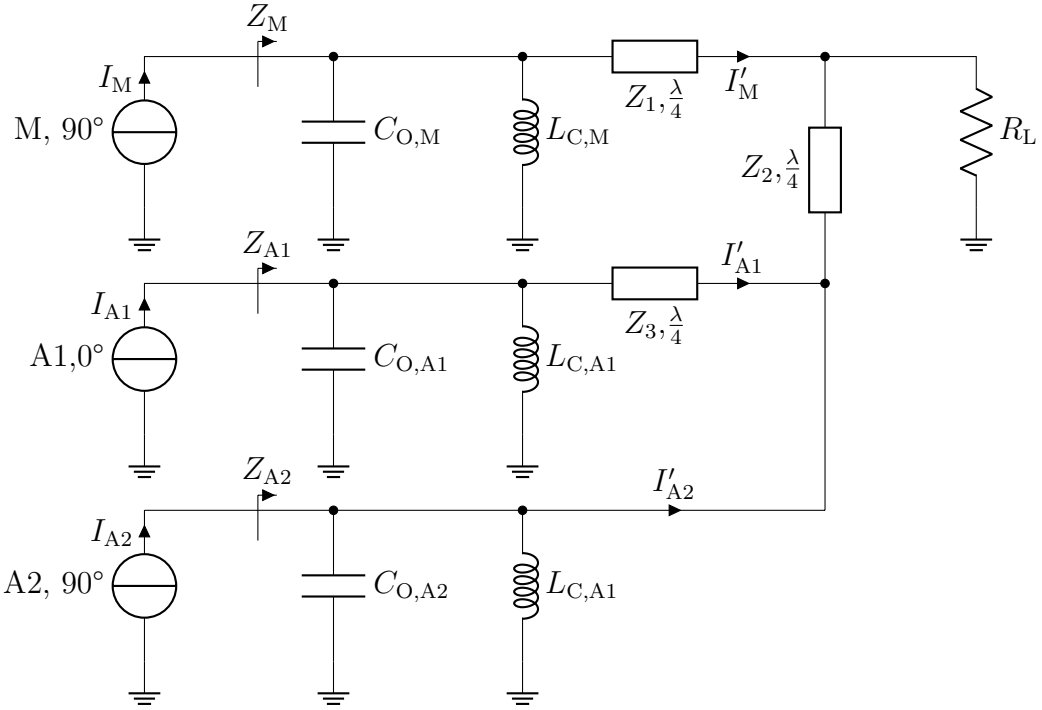

Figure 5.28: Simulation model collecting parasitic effects in a shunt capacitor, compensated by a shunt inductor in resonance.

5.3.2 Simulations and results comparison

In the second simulation, the developed model produced simulation results that were compatible with those obtained by ADS through impedance comparison. The impedance levels in the frequency range under analysis were shown to be the same in Figures 5.29-5.30-5.30 and Figures 5.32-5.33-5.34. Despite the presence of reactances in the parasitic model and compensation, a certain symmetry around f_0 was still maintained due to the resonance effect. This allowed for a real impedance at the fundamental. Although the symmetry was not achieved perfectly due to numerical approximation in the $L_{\mathrm{C,sub}}$ calculation, the compensation method used was quite simple and allowed for perfect compensation at f_0. Load modulation was used to achieve optimal real impedance at the fundamental, even though the overall bandwidth of the system was narrower than the previous ideal situation. The I/V profiles (Figures 5.35 and 5.36) are still valid even in the current simulation. The designed profile is achieved by both simulation methods at the fundamental frequency. However, as the frequency changes, ADS cannot provide reliable results, as shown in Figure 5.37b. This figure indicates that the output voltage does not respect the maximum achievable value for some frequencies. Due to the voltage

overestimation, the power estimated by ADS is impacted, leading to an error that is more evident near the 0dB back-off region. The maximum power threshold is not respected in this region, leading to an overestimation of the power curves. At f_0, both simulations produce the same results. However, as the frequency moves from the fundamental, power curves are shifted, and near the 0dB back-off region, they exceed the upper threshold imposed by the design. This problem gives wrong simulation results in the ADS environment, but it does not affect the MATLAB simulation, thanks to the clipping function implemented in the code. For the DC power, nothing changes in frequency, and both simulations provide the same result, as shown in Figure 5.40. It has been observed that the simulation of voltage and current on ADS can be unphysical, leading to erroneous efficiency estimation, as shown in Figure 5.42b. Although both methods produce similar efficiency curves at fundamental, peaks greater than the limit can be achieved at certain frequency values. This is due to the presence of reactance in the combiner topology, caused by parasitics and compensation network. As a result, the entire system's efficiency curves are drastically shaped, with degradation occurring as the frequency moves away from the resonant value f_0. MATLAB's clipping model restores physical meaning, as seen in Figure 5.43-5.44-5.45. Saturation scaling is performed using $C(f, n)$, which seems sufficient for lower back-off, with $C(f, n/\alpha_2)$ assuming values lower than 1 at some frequency points, even in OBO2. The clipping effect at OBO2 is completely negligible, possibly due to an unaccounted numerical error in the MATLAB implementation. Furthermore, each PA that's switched on in 0dB, OBO1 and OBO2 works at its proper $V_{\text{sub,MAX}}$ thanks to a well-dimensioned combiner, which allows the right load modulation in back-off and saturation. Figure 5.47 shows how the system exploits load modulation from the internal section, corresponding to the section before the parasitic capacitance. The simulation script produces results that match those provided by ADS. Figures 5.48 and 5.49 shows that the presence of reactive elements significantly reduces the bandwidth of the DPA in terms of power delivered to the load and efficiency. Moving further away from f_0, the efficiency decreases even more. This result is important because it highlights the negative effect of output parasitics and suggests that the compensation method used is narrowband. In addition, any previous simulation errors in ADS are propagated, resulting in incorrect results in the band. However, the reflection coefficient estimation is correct for both methods, as shown in Figures 5.50, 5.51 and 5.52. In Figure 5.53 it is possible to observe Z-parameters of the combiner topology adopted, including parasitics and compensations.

5.3.3 Plot section

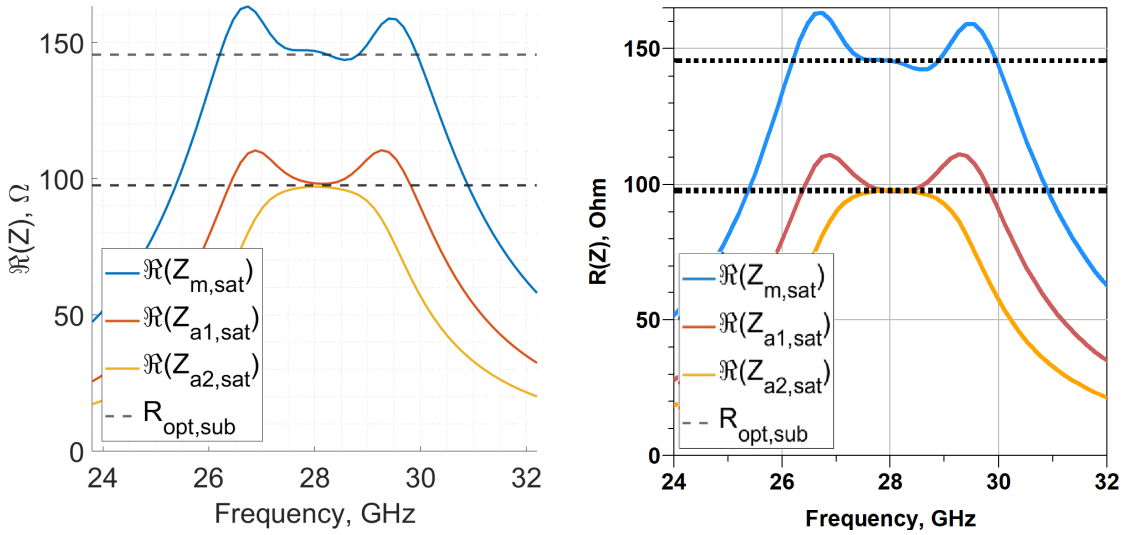

Figure 5.29: Real part of impedances seen by each internal section in saturation. (a): simulation performed by MATLAB, (b): simulation performed by ADS.

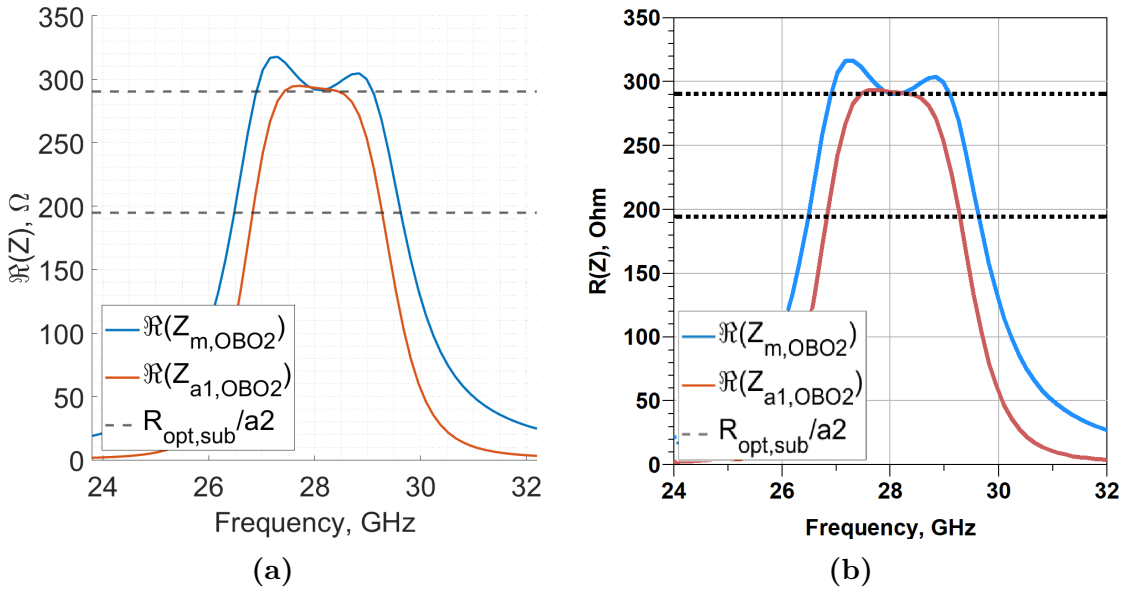

Figure 5.30: Real part of impedances seen by each internal section in OBO2. (a): simulation performed by MATLAB, (b): simulation performed by ADS.

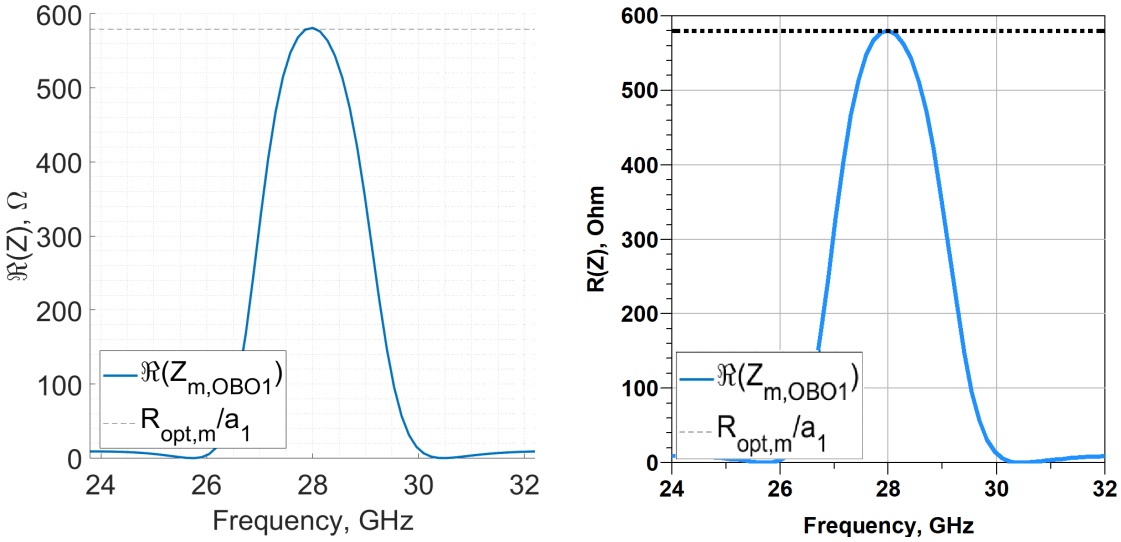

Figure 5.31: Real part of impedances seen by each internal section in OBO1. (a): simulation performed by MATLAB, (b): simulation performed by ADS.

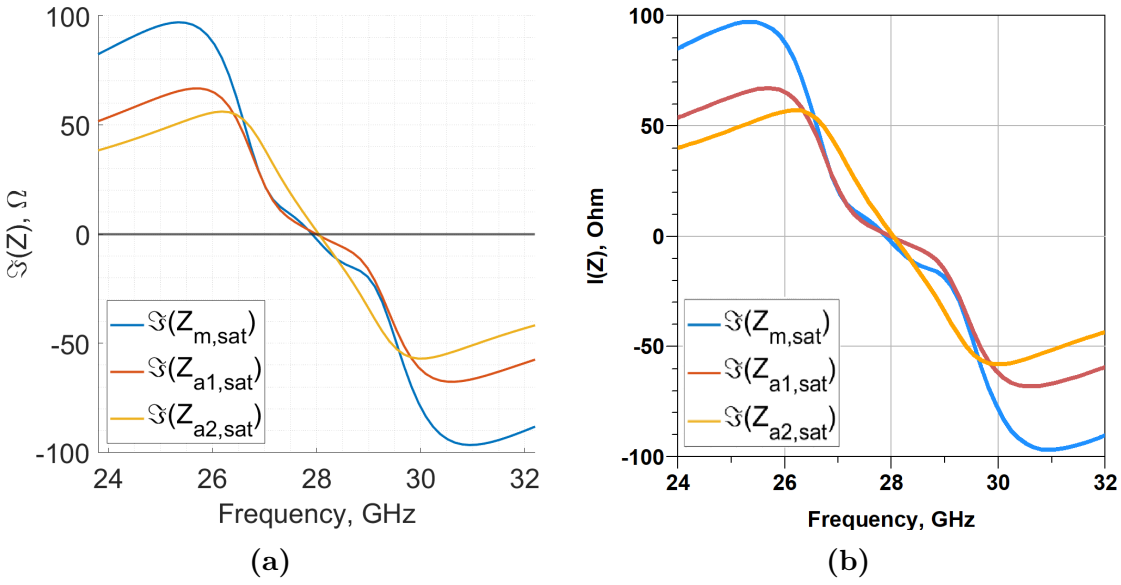

Figure 5.32: Imaginary part of impedances seen by each internal section in saturation. (a): simulation performed by MATLAB, (b): simulation performed by ADS.

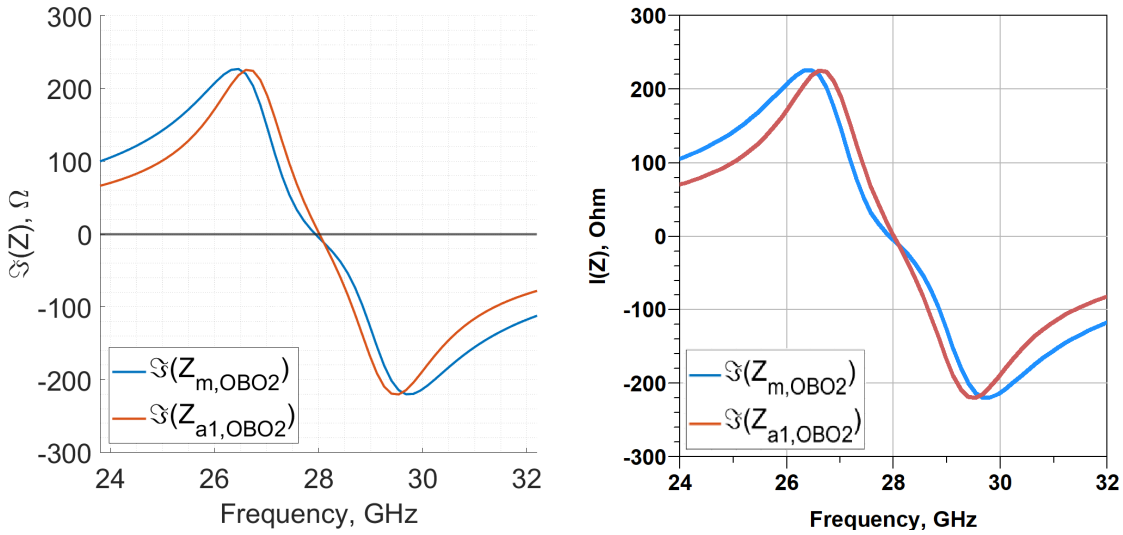

(a) **(b)**

Figure 5.33: Imaginary part of impedances seen by each internal section in OBO2. (a): simulation performed by MATLAB, (b): simulation performed by ADS.

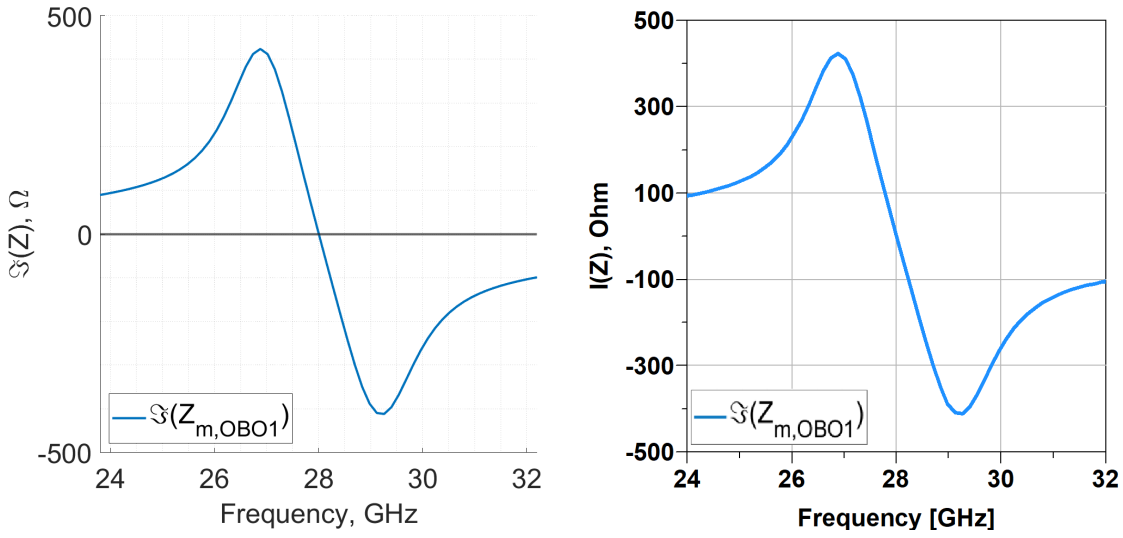

(a) **(b)**

Figure 5.34: Imaginary part of impedances seen by each internal section in OBO1. (a): simulation performed by MATLAB, (b): simulation performed by ADS.

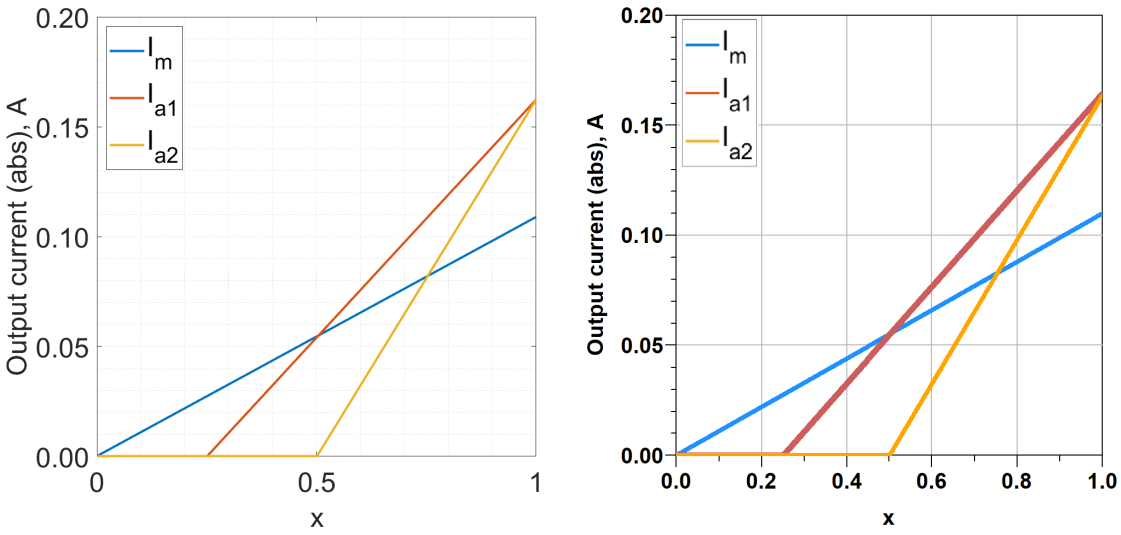

Figure 5.35: Current profile at central frequency. (a): simulation by MATLAB, (b): simulation by ADS.

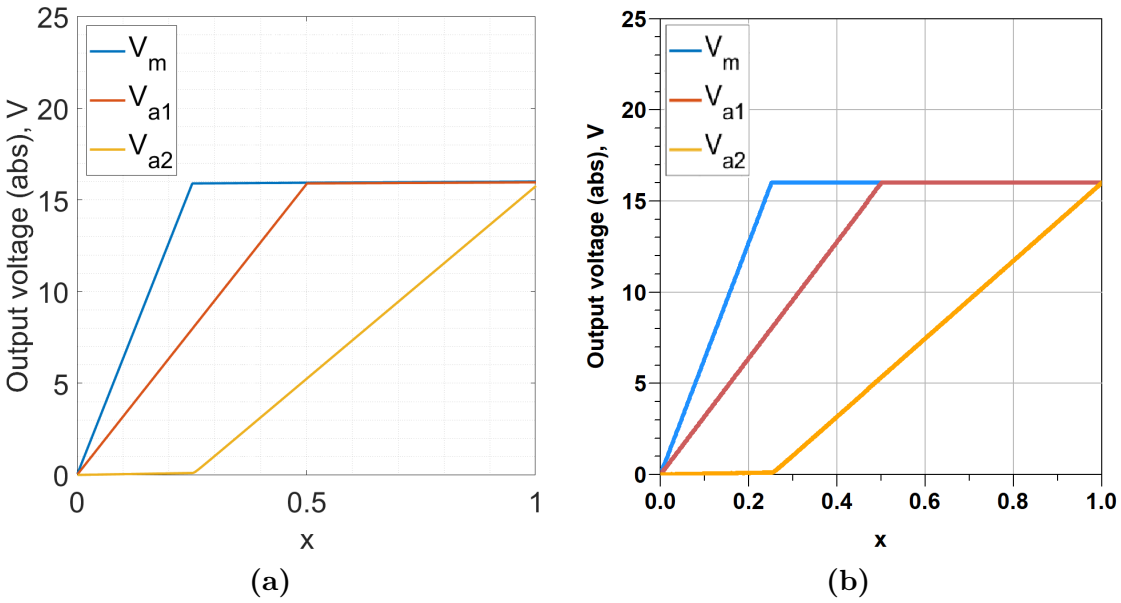

Figure 5.36: Voltage profile at the central frequency. (a): simulation by MATLAB, (b): simulation by ADS.

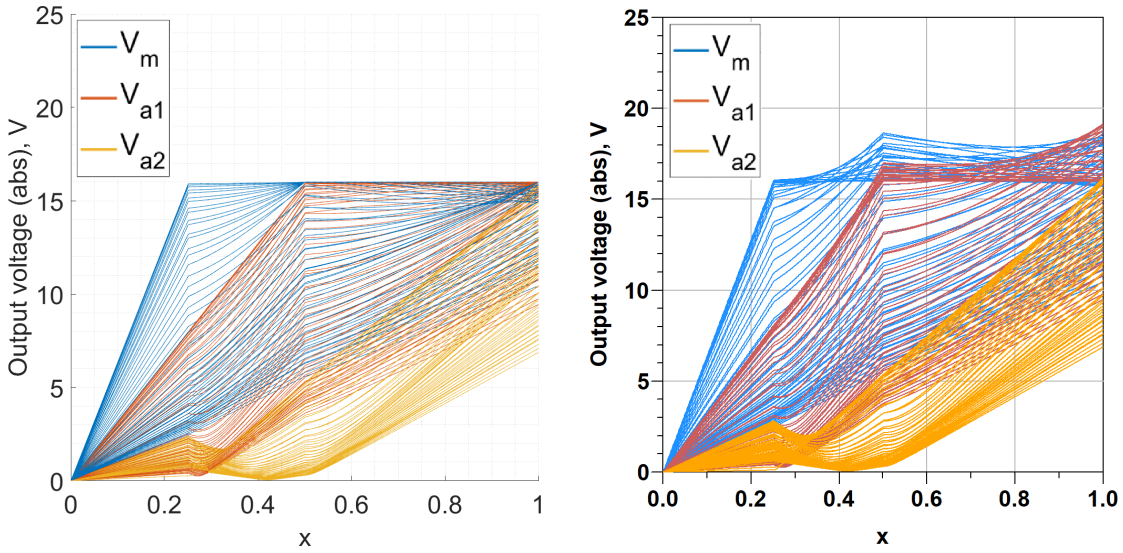

Figure 5.37: Voltage profiles in band. (a): simulation by MATLAB, (b): simulation by ADS.

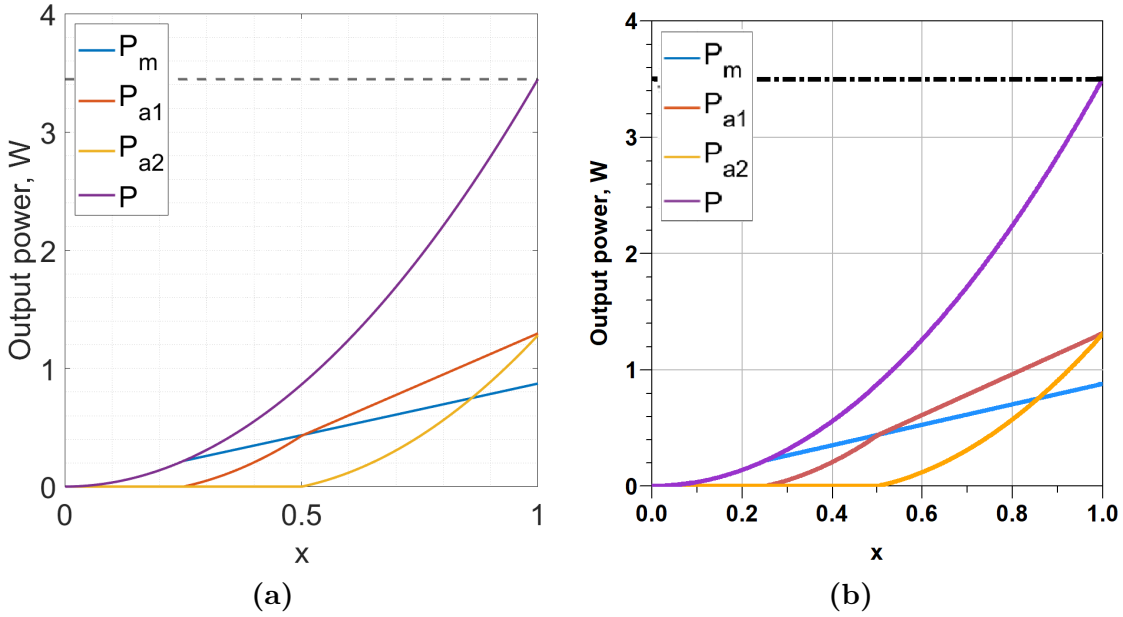

Figure 5.38: Output power delivered to the load at central frequency. (a): simulation by MATLAB, (b): simulation by ADS.

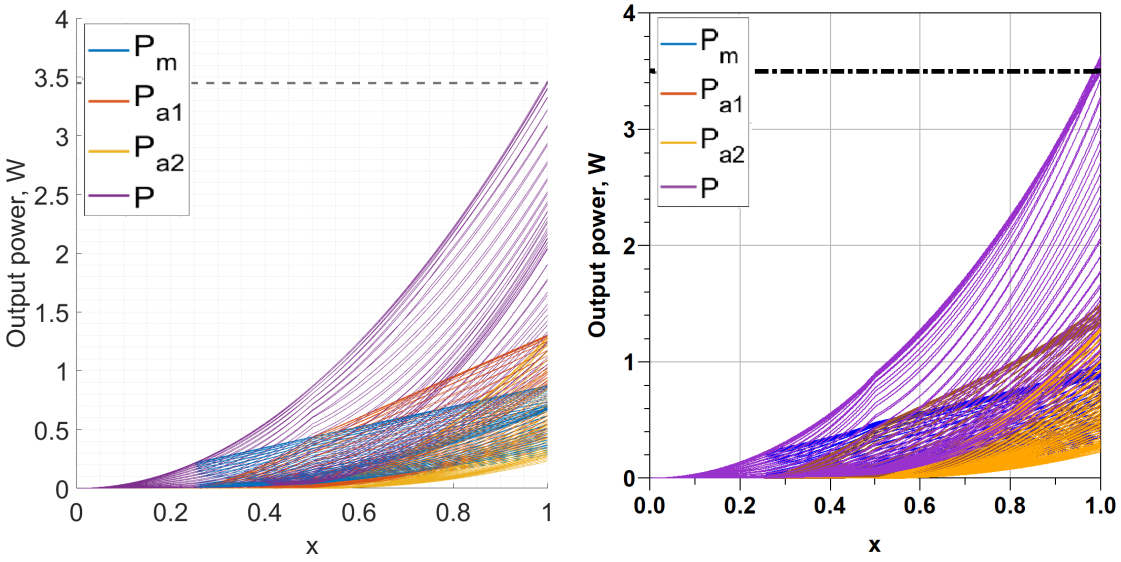

Figure 5.39: Output power delivered to the load in band. (a): simulation by MATLAB, (b): simulation by ADS.

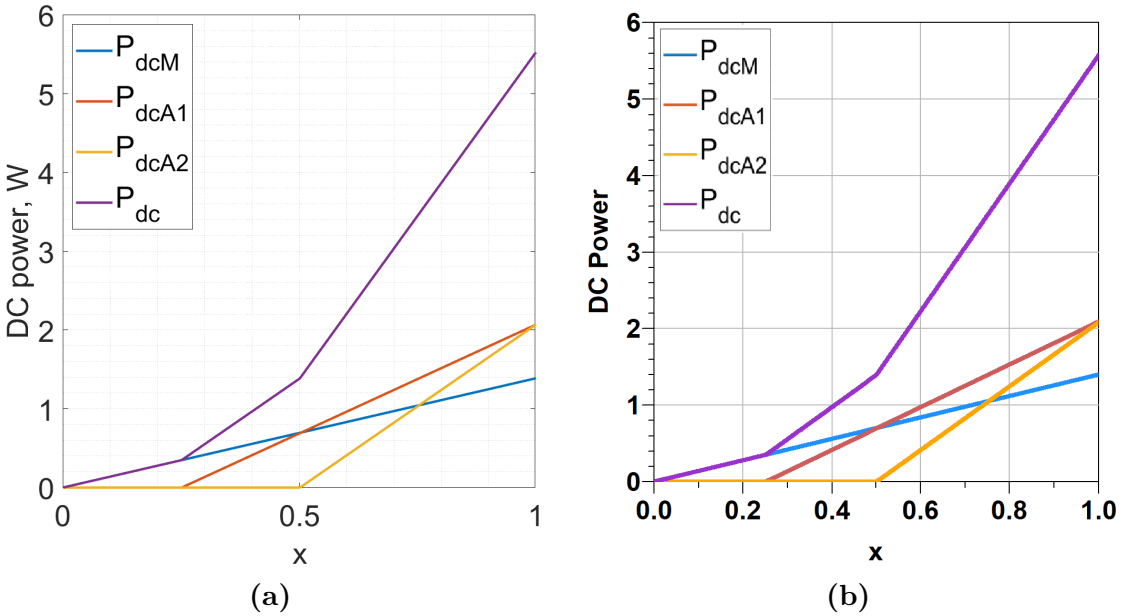

Figure 5.40: DC power. (a): simulation by MATLAB, (b): simulation by ADS.

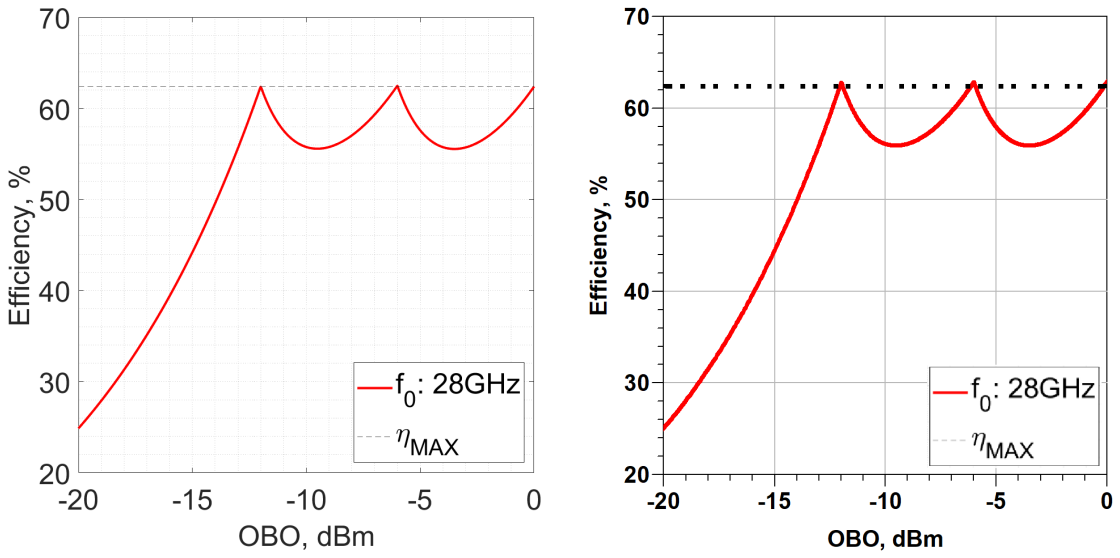

Figure 5.41: Efficiency curves at central frequency. (a): simulation by MATLAB, (b): simulation by ADS.

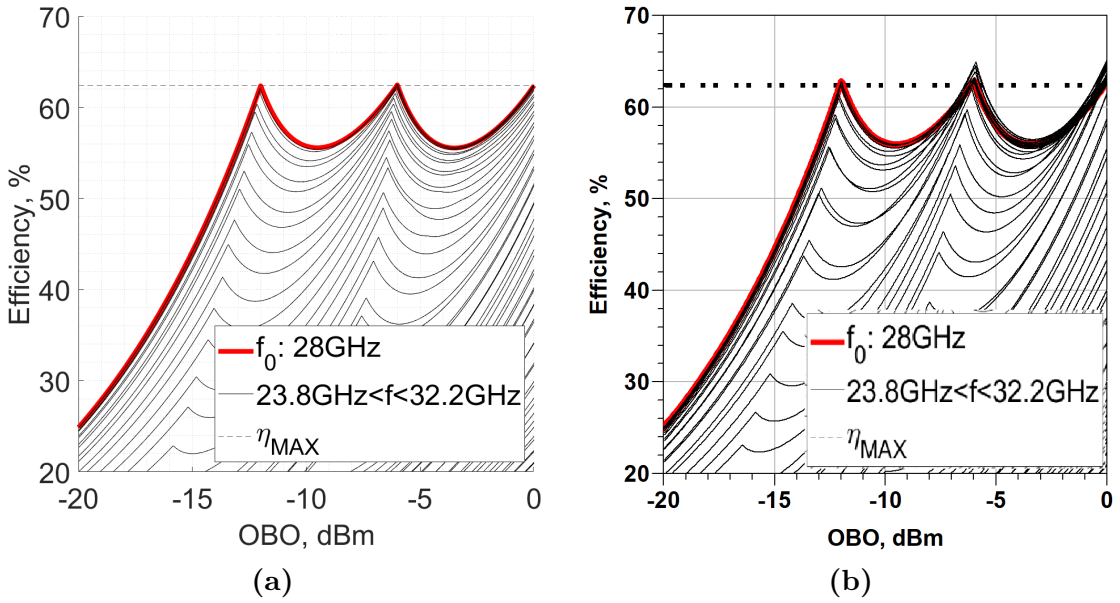

Figure 5.42: Efficiency curves in band. (a): simulation by MATLAB, (b): simulation by ADS.

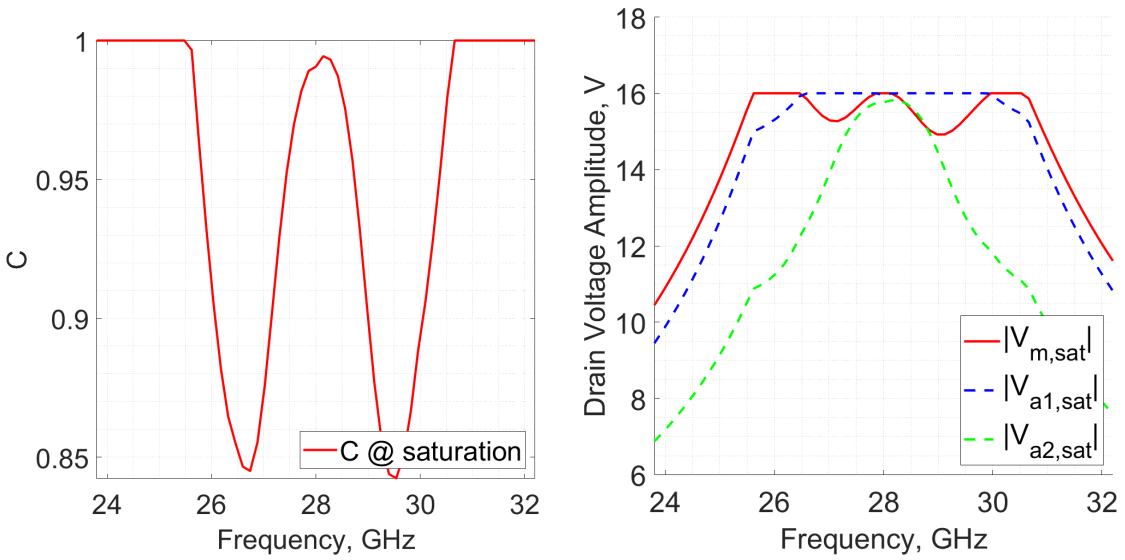

(a) (b)

Figure 5.43: Clipping effect implemented in the MATLAB script at saturation. (a): clipping coefficient, (b): effect of clipping on each drain voltage.

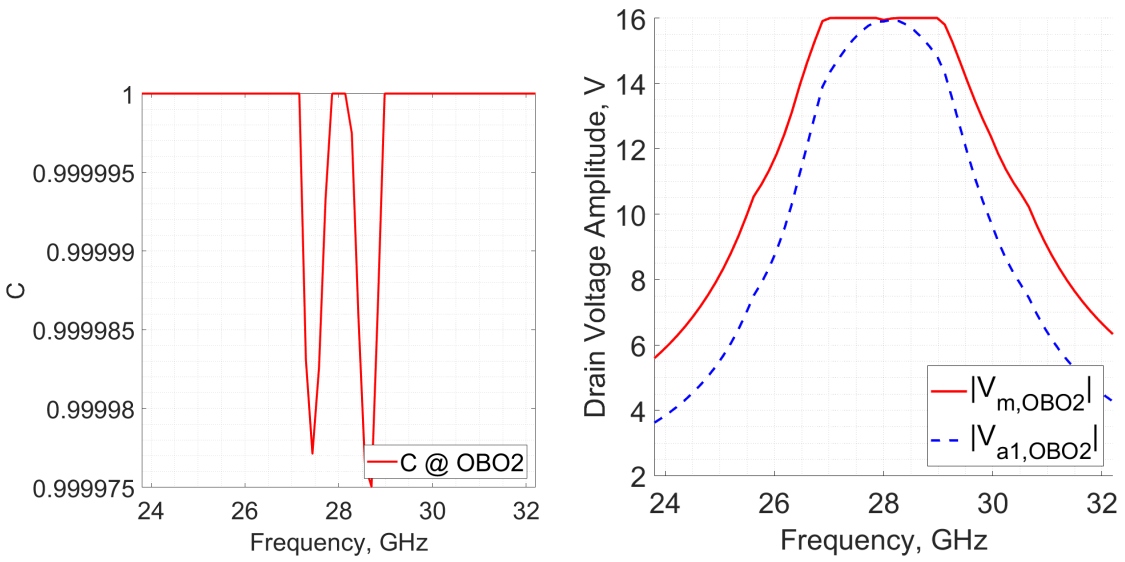

(a) (b)

Figure 5.44: Clipping effect implemented in the MATLAB script in OBO2. (a): clipping coefficient, (b): effect of clipping on each drain voltage.

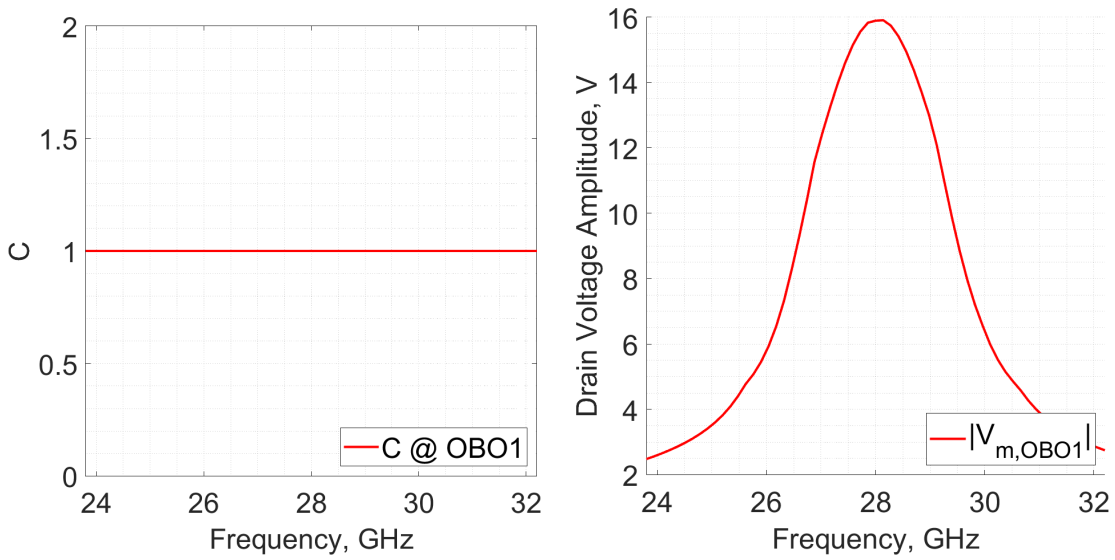

(a) **(b)**

Figure 5.45: Clipping effect implemented in the MATLAB script in OBO1. (a): clipping coefficient, (b): effect of clipping on each drain voltage.

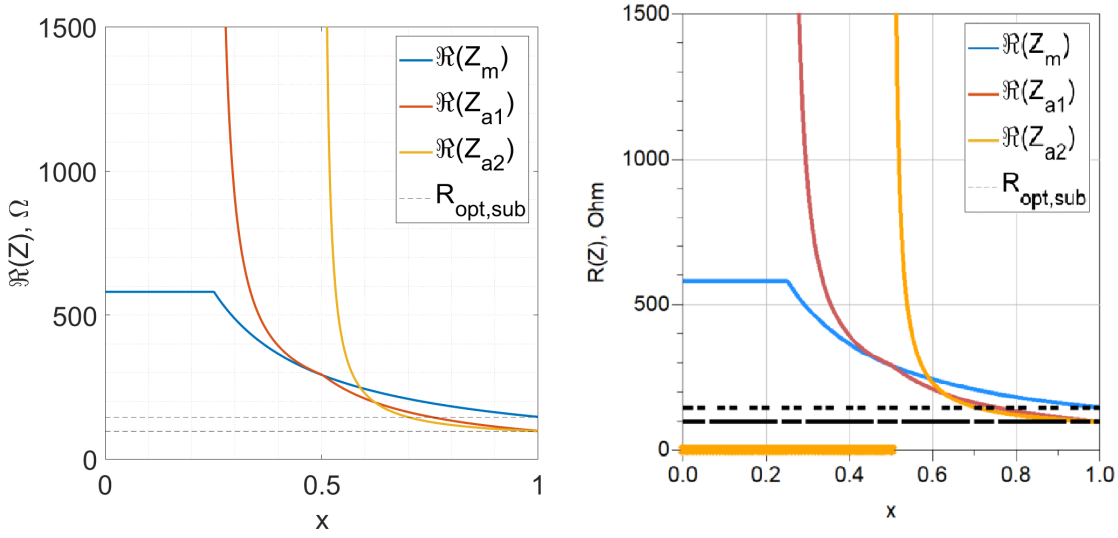

(a) **(b)**

Figure 5.46: Effect of the load modulation at central frequency. (a): simulation by MATLAB, (b): simulation by ADS.

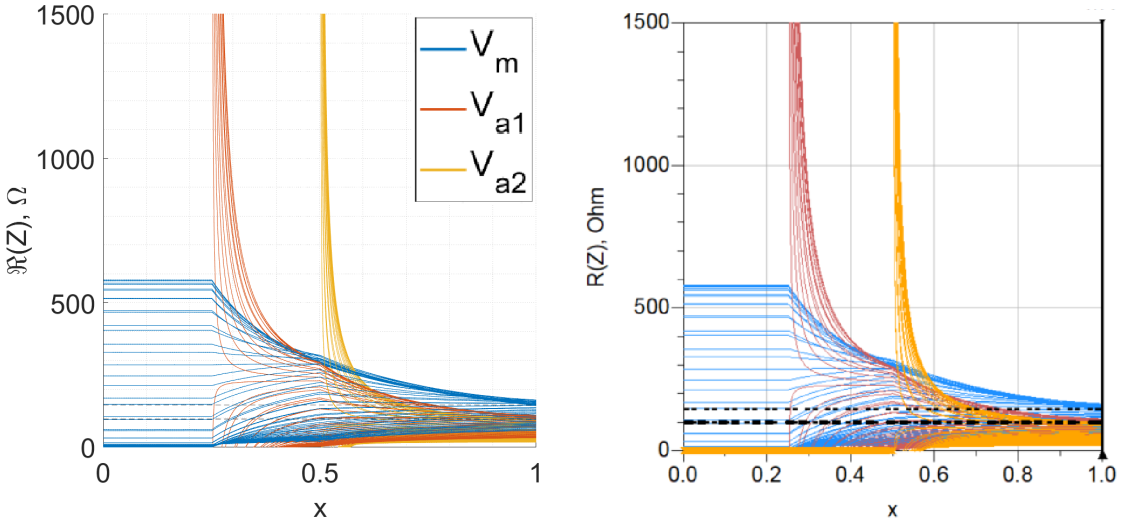

(a) (b)

Figure 5.47: Effect of the load modulation in band. (a): simulation by MATLAB, (b): simulation by ADS.

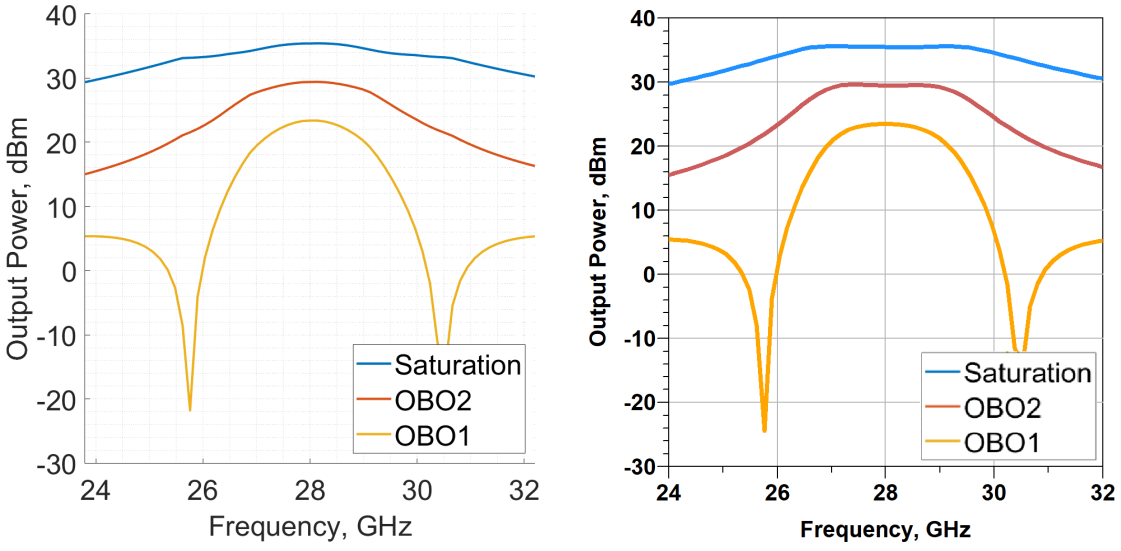

(a) (b)

Figure 5.48: Output power in different back-off condition. (a): simulation by MATLAB, (b): simulation by ADS.

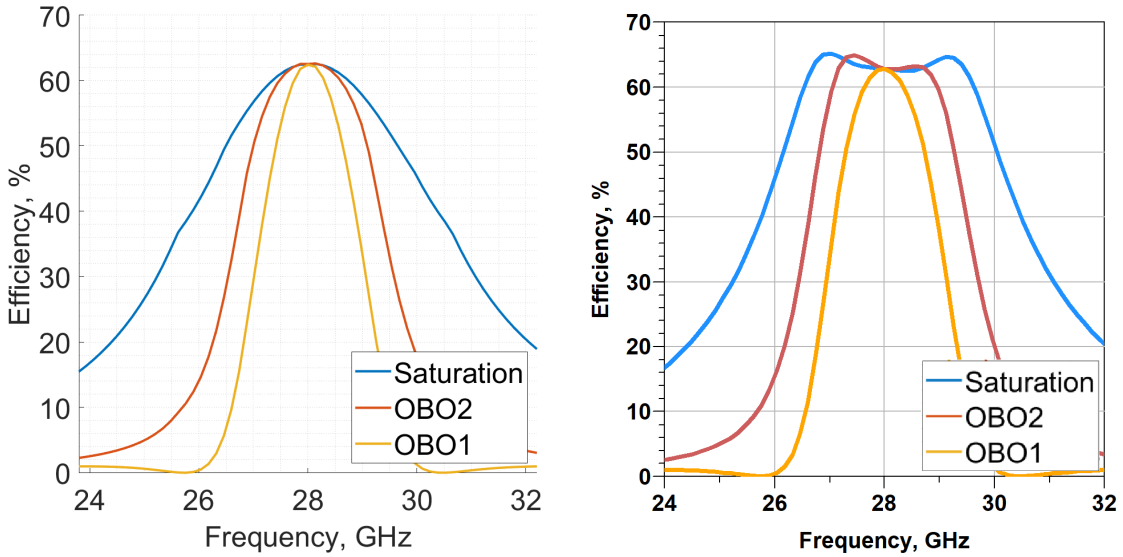

(a) **(b)**

Figure 5.49: Efficiency in different back-off condition. (a): simulation by MATLAB, (b): simulation by ADS.

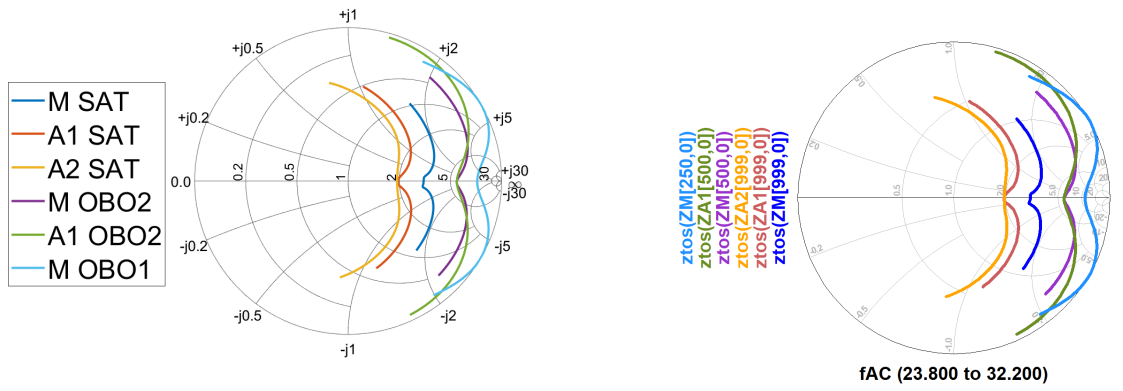

(a) **(b)**

Figure 5.50: Reflection coefficient referred to 50Ω. (a): simulation by MATLAB, (b): simulation by ADS.

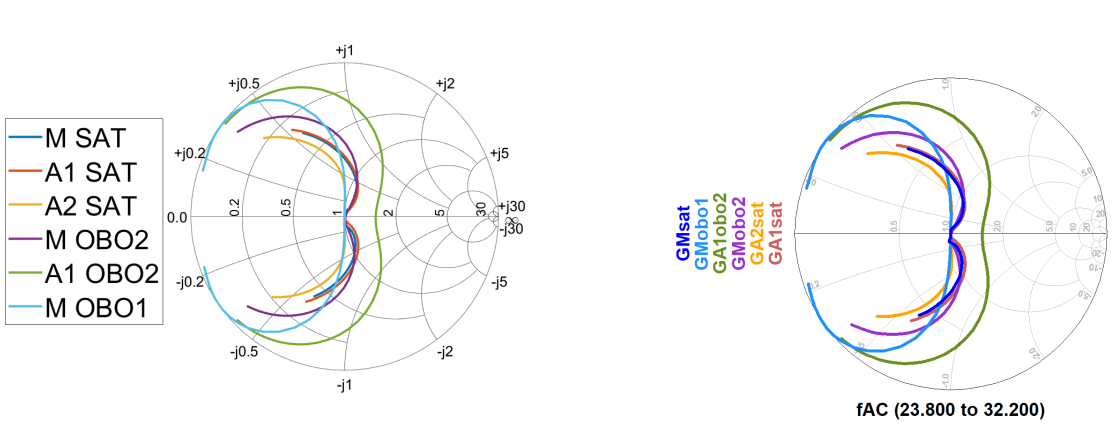

(a) **(b)**

Figure 5.51: Reflection coefficient referred to $R_{\text{opt,sub}}$. (a): simulation by MATLAB, (b): simulation by ADS.

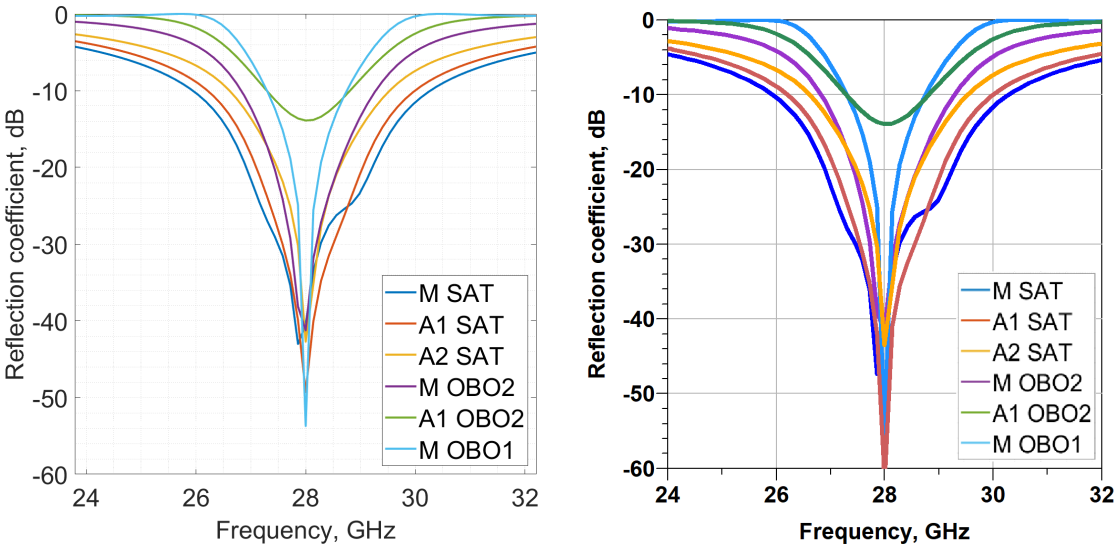

(a) **(b)**

Figure 5.52: Reflection coefficient magnitude referred to $R_{\text{opt,sub}}$. (a): simulation by MATLAB, (b): simulation by ADS.

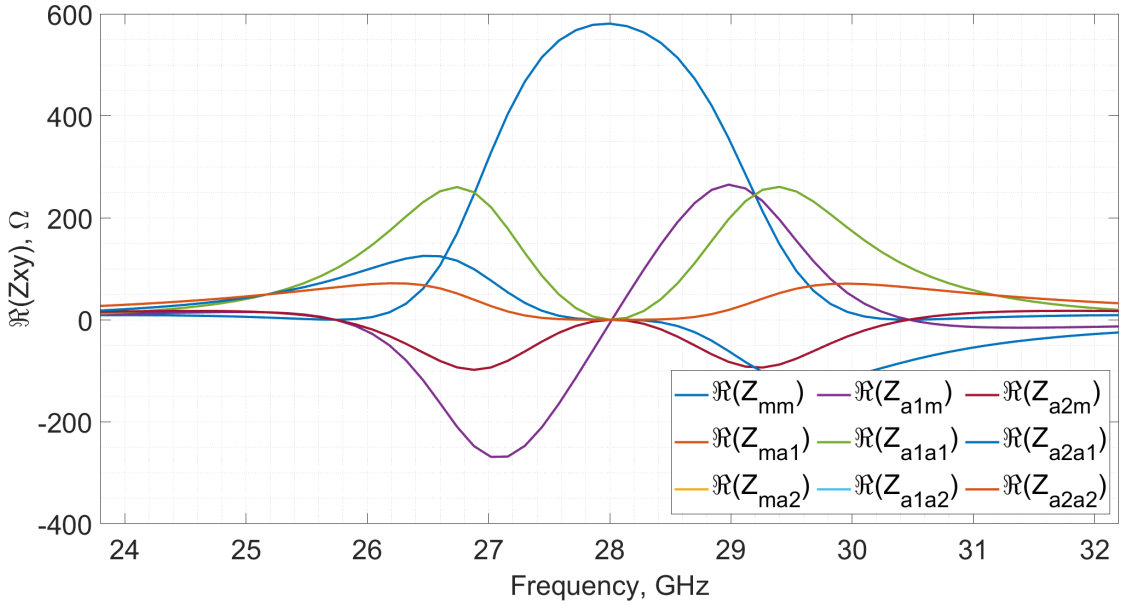

(a)

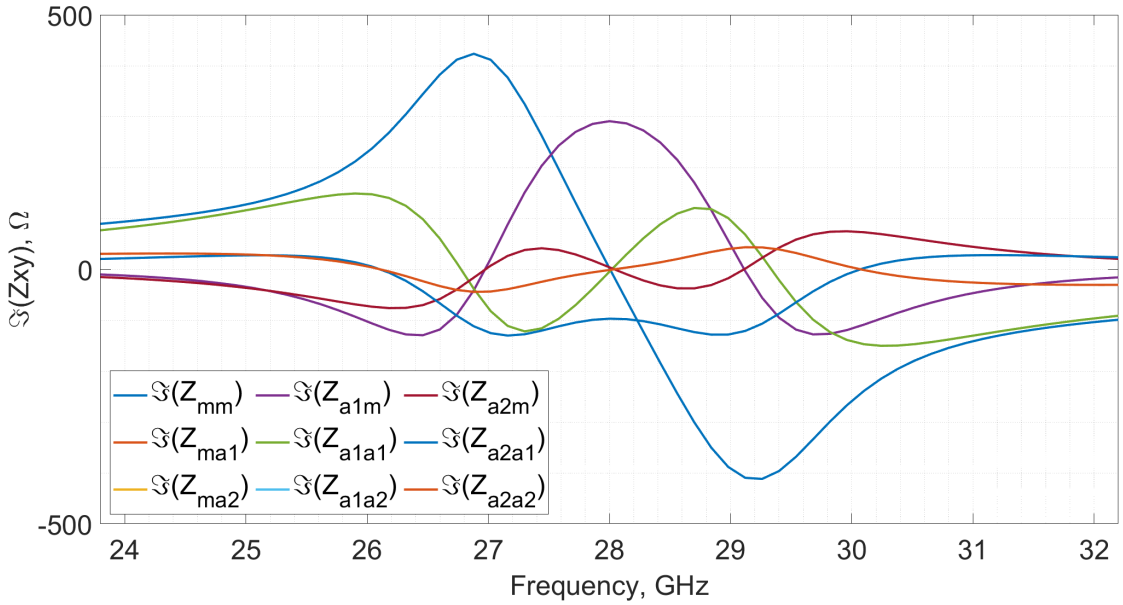

(b)

Figure 5.53: Z-matrix of the combiner estimated by MATLAB. (a): real part, (a): imaginary part.

5.4 Complete parasitic model for transistors

5.4.1 Model

This model is capable of representing output parasitic at high frequencies, while also accounting for a lumped inductor in series of each active component. You can see the complete network in figure 5.54. The lumped model is constructed as follows:

- A shunt capacitor $C_{\mathrm{O,sub}}$;
- A series inductor $L_{\mathrm{O,sub}}$.

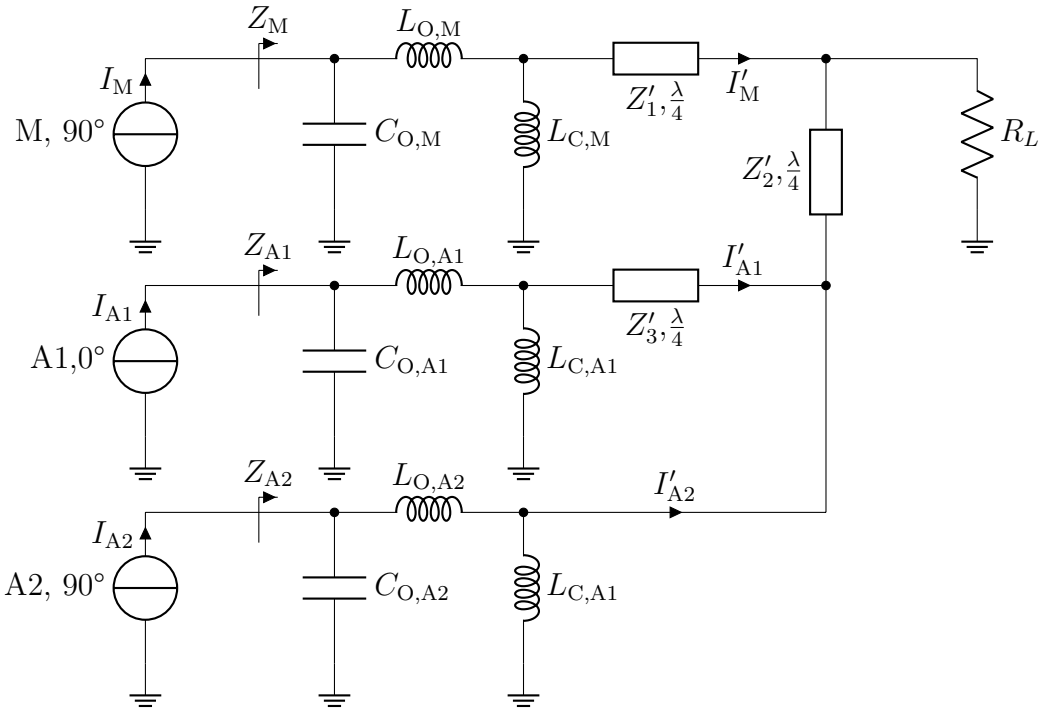

Figure 5.54: Simulation model collecting parasitic effects in a shunt capacitor and a series inductor, compensated by a shunt element.

To simplify the compensation network, a shunt reactive element B_0 is used to nullify the reactance of the parasitic network at the central frequency, similar to the previous example. In this case, a shunt inductor $L_{\mathrm{C,\,sub}}$ is used. However, it is not possible to maintain the real part of the impedance from the external section from the internal one due to the series inductor. This needs to be taken into account when designing TLs, which should be resized to achieve the correct load

modulation effect. By using admittance, the calculation process can be simplified (see Figure 5.55).

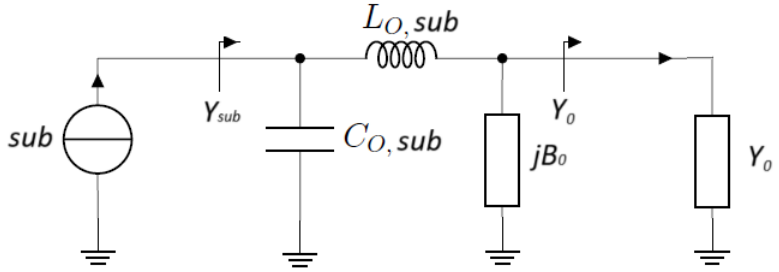

Figure 5.55: Model used for compensation design.

To simplify the method, it is assumed that the optimal load seen at the input of each combiner branch is $Y_0 = R_{\text{opt,sub}}^{-1}$. By placing a shunt element in parallel, the new admittance Y_{sub} seen by the internal section is the result of the cascade between the parasitic network and the parallel between Y_0 and B_0.

$$\begin{aligned} Y_{\text{sub}} &= j\omega C_{\text{O,sub}} + \frac{\frac{1}{j\omega L_{\text{O,sub}}} \cdot Y_0}{\frac{1}{j\omega L_{\text{O,sub}}} + Y_0} = j\omega C_{\text{O,sub}} + \frac{Y_0}{1 - j\omega L_{\text{O,sub}} Y_0}\Big|_{Y_0 = G_0 - jB_0} = \\ &= j\omega C_{\text{O,sub}} + \frac{G_0 - jB_0}{1 - j\omega L_{\text{O,sub}} G_0 - jB_0}\Big|_{Y_0 = G_0 - jB_0} \end{aligned} \tag{5.7}$$

The previous equation can be rewritten to explicitly show the real and imaginary parts of Y_{sub}.

$$Y_{\text{sub}} = \frac{G_0}{(1 - \omega L_{\text{O,sub}} B_0)^2 - (\omega L_{\text{O,sub}} G_0)^2} + j\left[\omega C_{\text{O,sub}} + \frac{B_0(1 - B_0 \omega L_{\text{O,sub}}) - \omega L G_0^2}{(1 - \omega L_{\text{O,sub}} B_0)^2 - (\omega L_{\text{O,sub}} G_0)^2}\right] \tag{5.8}$$

It is important to note that when $L_{\text{O,sub}}$ is zero, the compensation method can be carried out using the same approach as the previous simulation.

$$L_{\text{O,sub}} = 0 \Longrightarrow Y_{\text{sub}} = G_0 + j[\omega C_{\text{O,sub}} + B_0] \tag{5.9}$$

$$\begin{cases} B_0 = -\omega C_{\text{O,sub}} \\ Z_{\text{L}_{\text{C,sub}}} = j\omega L_{\text{C,sub}} \end{cases} \Longrightarrow L_{\text{C,sub}} = \frac{1}{\omega_0^2 C_{\text{O,sub}}} \tag{5.10}$$

However, in the general case, $L_{\text{C,sub}}$ is not zero (as in this simulation) and, assuming no compensation, the natural system admittance seen by the internal section is:

$$\begin{cases} L_{\text{O,sub}} \neq 0 \\ B_0 = 0 \end{cases} \Longrightarrow Y_{\text{sub}} = \frac{G_0}{1 - (\omega L_{\text{O,sub}} G_0)^2} + j\left[\omega C_{\text{O,sub}} - \frac{\omega L G_0^2}{1 - (\omega L_{\text{O,sub}} G_0)^2}\right] \tag{5.11}$$

At the moment, the admittance in the absence of a compensation network is represented by (5.11), while the admittance with compensation is represented by (5.8). By comparing these two equations, It is possible to observe that compensation not only impacts $\Im\{Y_{\text{sub}}\}$ but also $\Re\{Y_{\text{sub}}\}$. This demonstrates that the compensation can neutralize the reactive effect of parasitics, but the system must be redimensioned to achieve the desired impedance levels for the internal section. Additionally, the voltage drop on the parasitic and compensation network must be taken into account. (5.3) can be used to estimate new parameters.

$$\begin{cases} C_{\text{O,M}} = 125\text{fF} \\ L_{\text{O,M}} = 36\text{pH} \\ C_{\text{O,A1/2}} = 230\text{fF} \\ L_{\text{O,A1/2}} = 30\text{pH} \end{cases} \implies \begin{cases} L_{\text{C,M}} = 225\text{pH} \\ L_{\text{C,A1/2}} = 111\text{pH} \\ Z'_1 = 70\Omega \\ Z'_2 = 21\Omega \\ Z'_1 = 61\Omega \end{cases} \tag{5.12}$$

Reconducting the structure to the generic topology developed:

- the Main branch is made by a cascade of the parasitic shunt capacitor and the series parasitic inductor, followed by the resonant inductor and a transmission line, so $T_{\text{M}} = T_{\text{C}_{0,\text{M}},sh} T_{\text{L}_{0,\text{M}},ser} T_{\text{L}_{\text{C,M}},sh} T_{\text{TL1}}$;
- the A1 branch is made by a cascade of the parasitic shunt capacitor and the series parasitic inductor, follower by the resonant inductor and a transmission line, so $T_{\text{A1}} = T_{\text{TL3}} T_{\text{L}_{\text{C,A1}},sh} T_{\text{L}_{0,\text{A1}},ser} T_{\text{C}_{0,\text{A1}},sh}$;
- on A2 branch there are only parasitic and compensation elements, so $T_{\text{A2}} = T_{\text{L}_{\text{C,A2}},sh} T_{\text{L}_{0,\text{A2}},ser} T_{\text{C}_{0,\text{A2}},sh}$;
- T_1 is made only by a transmission line, so $T_1 = T_{\text{TL2}}$;
- T_2 is made only by a short-circuit, so $T_2 = I$.

5.4.2 Simulations and results comparison

Although the MATLAB script generated correct simulation results compared to the impedance data obtained by ADS, it did not produce the expected behavioural results. Specifically, the compensation adopted was meant to neutralize the reactive effect of the parasitic element in the output stage for each device. However, this did not happen, and at f_0, the imaginary part of the impedance seen by each internal section was not zero (as shown in Figures 5.59-5.60-5.61), and the real parts did not fit well with the optimal load expected (as shown in Figures 5.56-5.57-5.58). This indicates that the method itself fails to consider some behavioural issues. It is important to observe that the use of a non-rigorous compensation method has a strong impact on the I and V profiles at the fundamental frequency (f_0). The combiner topology fails to maintain the saturation condition for each amplifier as desired, which may be due to non-ideal load modulation. The adopted compensation method does not take into account some phenomena highlighted in the simulation, which makes the ADS estimation unphysical when the frequency is varied (as shown in Figure 5.64b). This suggests that the topology is not well-dimensioned, and the approximation results in the entire DPA working improperly compared to the desired behaviour. Note that an inaccurate combiner design can result in the entire DPA delivering lower power to the load than expected. Even if the results obtained by different methods are identical at f_0 (as shown in Figure 5.67), ADS simulations may not be reliable in such cases. The same curves were obtained for DC power absorption, and the same considerations apply as with the other simulations. In this simulation, it is observed that although the fundamental efficiency curves for both ADS and MATLAB are the same, the efficiency peaks exceed the maximum limit at each OBO peak. To counter the effect of PAs saturation, the script uses the clipping function, which in this case performs a strong compensation as shown in Figures 5.70, 5.71 and 5.72. The main compensation occurs at 0dB OBO, but the combiner topology does not allow each PA to operate at saturation in OBO1 and OBO2 as desired for a typical DPA at f_0. This is due to the incorrect voltage profile, which does not allow for optimal load modulation. Regarding other simulated quantities, the considerations made in the previous simulation still hold true. From Figures 5.75 and 5.76, it is noticeable that this compensation provides an in-band behaviour similar to the one obtained in the second simulation.

5.4.3 Plot section

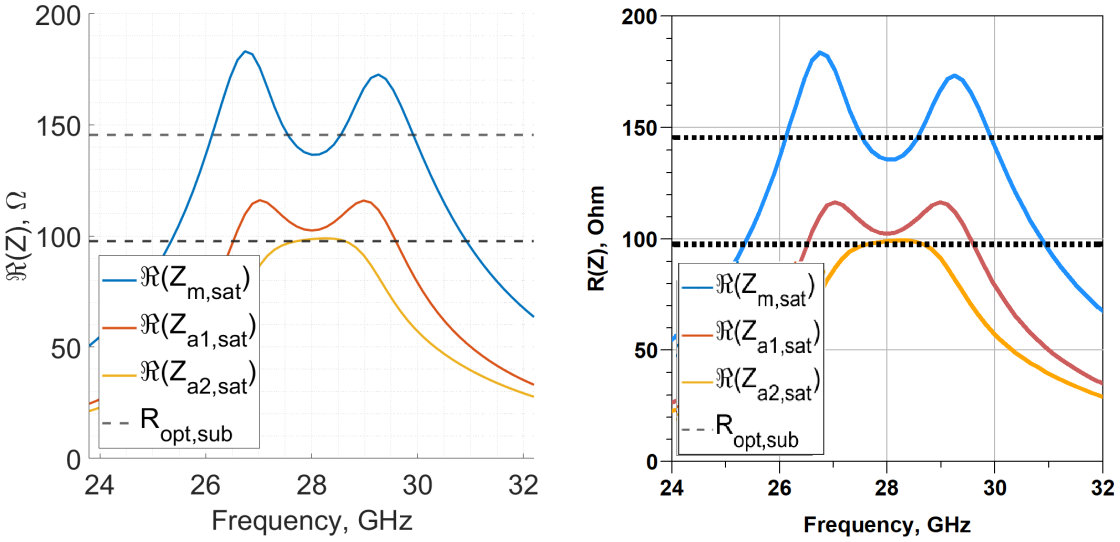

Figure 5.56: Real part of impedances seen by each internal section in saturation. (a): simulation performed by MATLAB, (b): simulation performed by ADS.

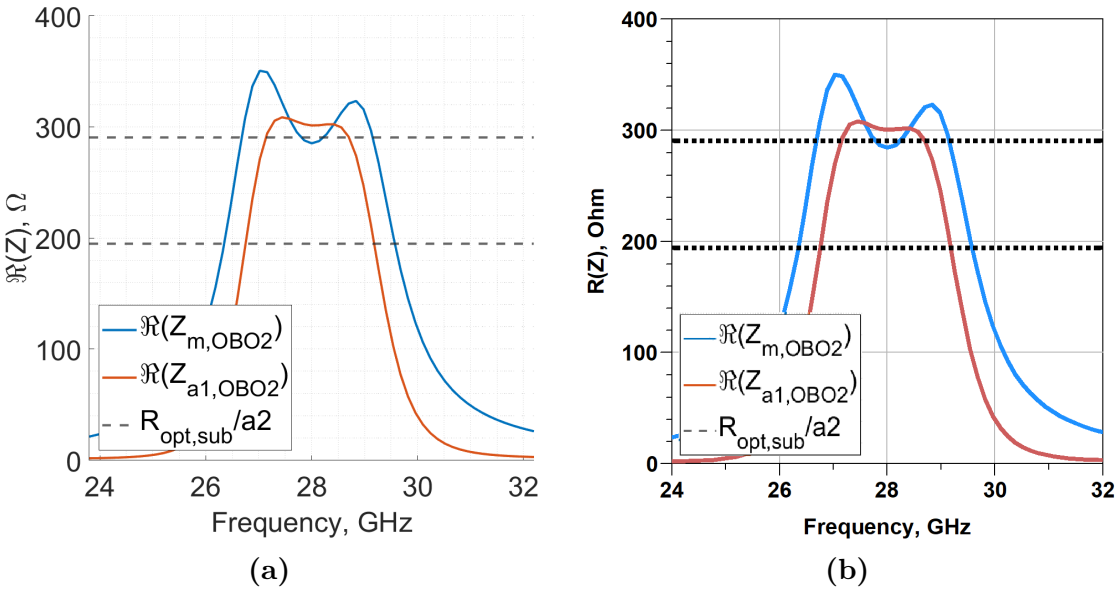

Figure 5.57: Real part of impedances seen by each internal section in OBO2. (a): simulation performed by MATLAB, (b): simulation performed by ADS.

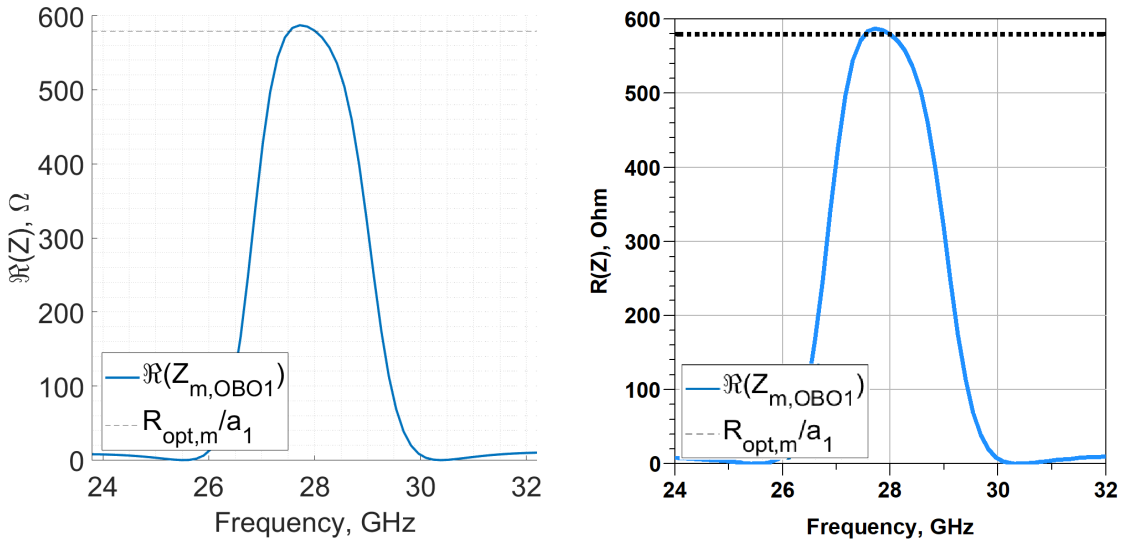

Figure 5.58: Real part of impedances seen by each internal section in OBO1. (a): simulation performed by MATLAB, (b): simulation performed by ADS.

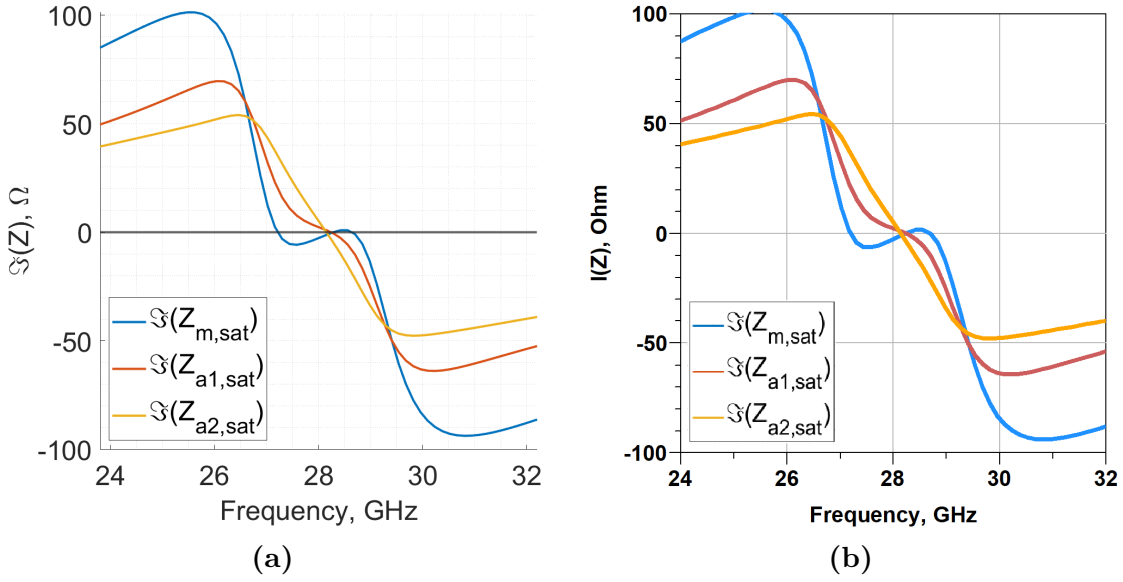

Figure 5.59: Imaginary part of impedances seen by each internal section in saturation. (a): simulation performed by MATLAB, (b): simulation performed by ADS.

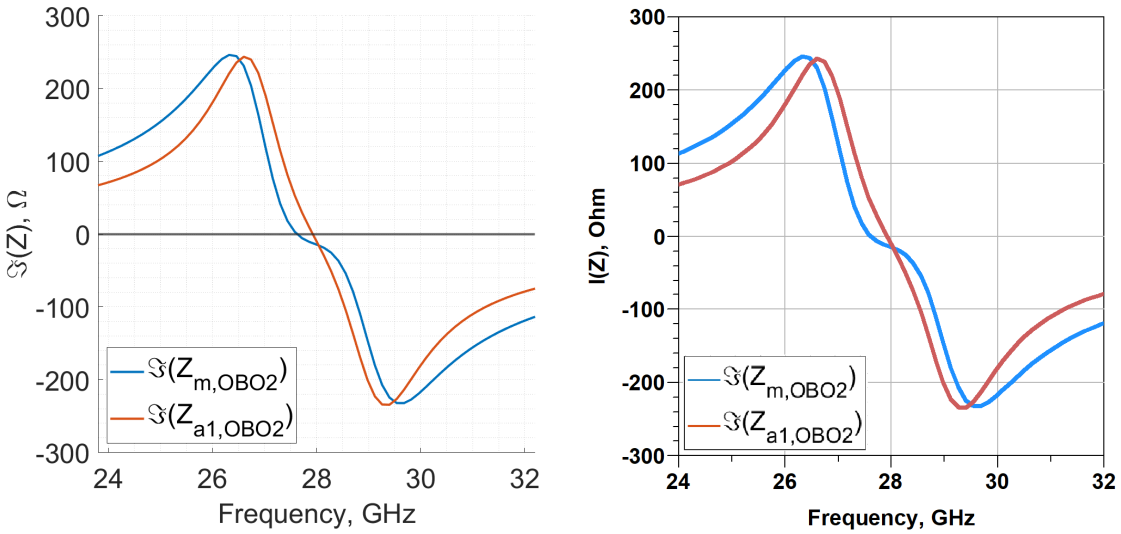

(a) (b)

Figure 5.60: Imaginary part of impedances seen by each internal section in OBO2. (a): simulation performed by MATLAB, (b): simulation performed by ADS.

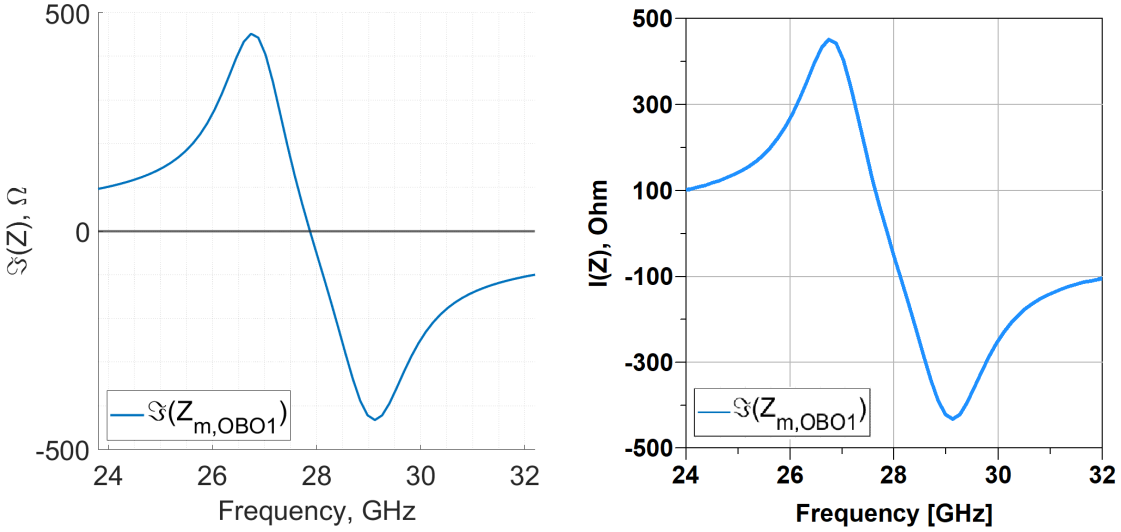

(a) (b)

Figure 5.61: Imaginary part of impedances seen by each internal section in OBO1. (a): simulation performed by MATLAB, (b): simulation performed by ADS.

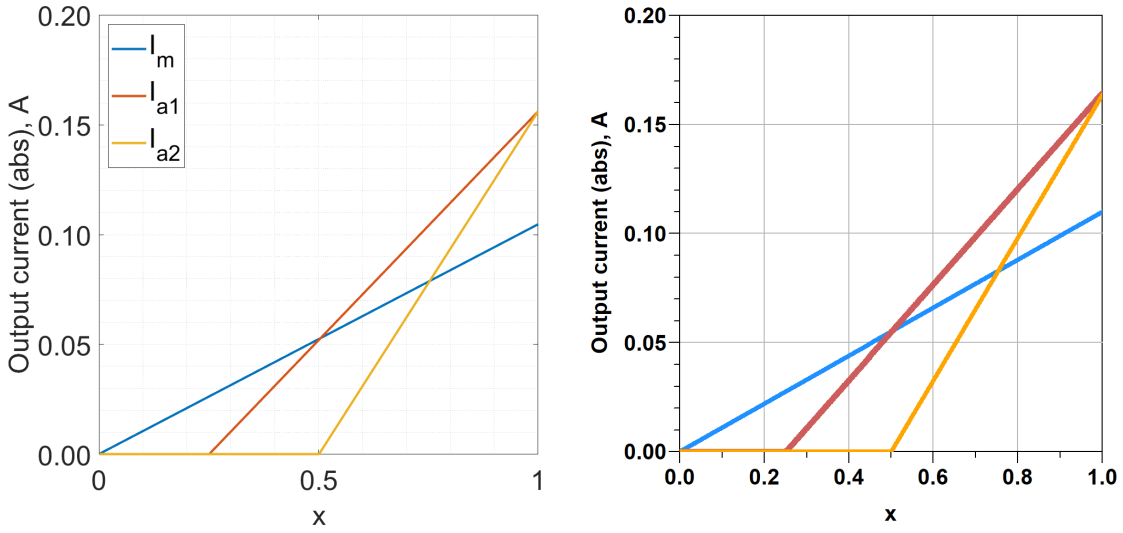

Figure 5.62: Current profile at central frequency. (a): simulation by MATLAB, (b): simulation by ADS.

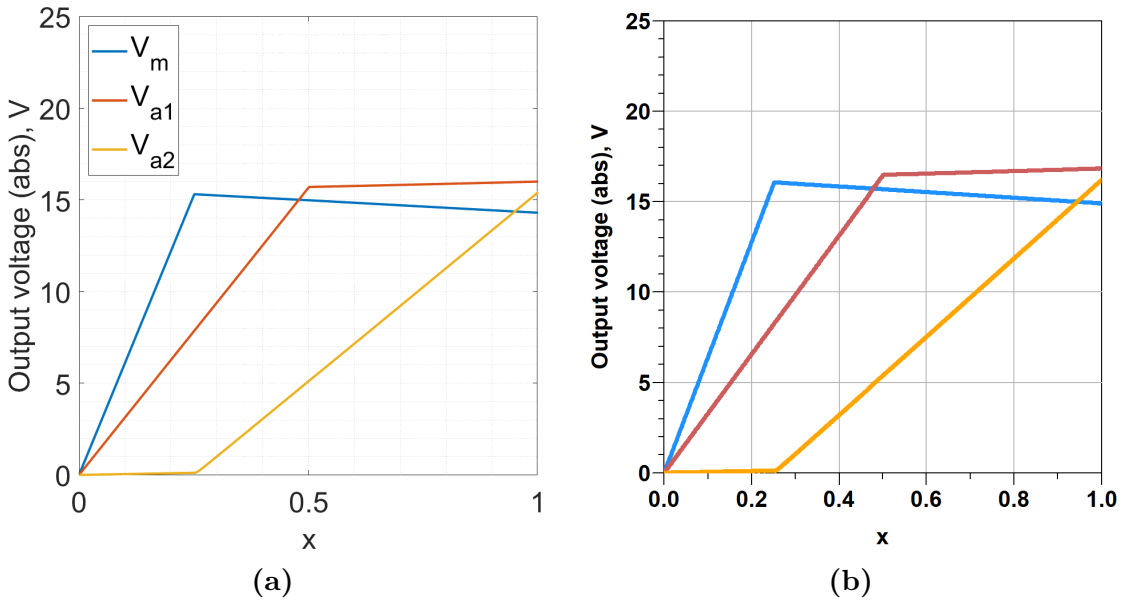

Figure 5.63: Voltage profile at the central frequency. (a): simulation by MATLAB, (b): simulation by ADS.

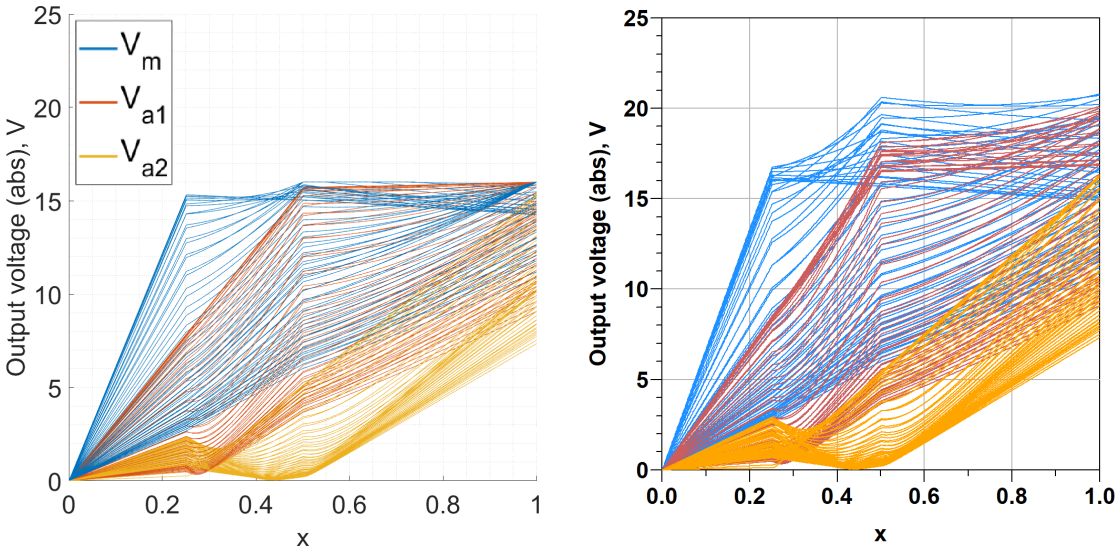

Figure 5.64: Voltage profiles in band. (a): simulation by MATLAB, (b): simulation by ADS.

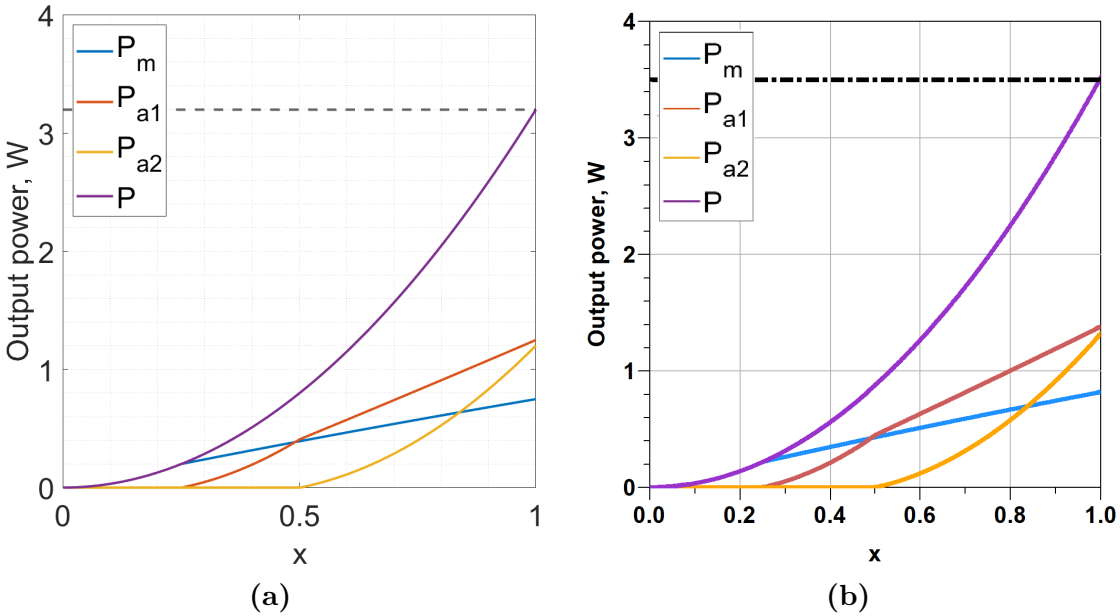

Figure 5.65: Output power delivered to the load at central frequency. (a): simulation by MATLAB, (b): simulation by ADS.

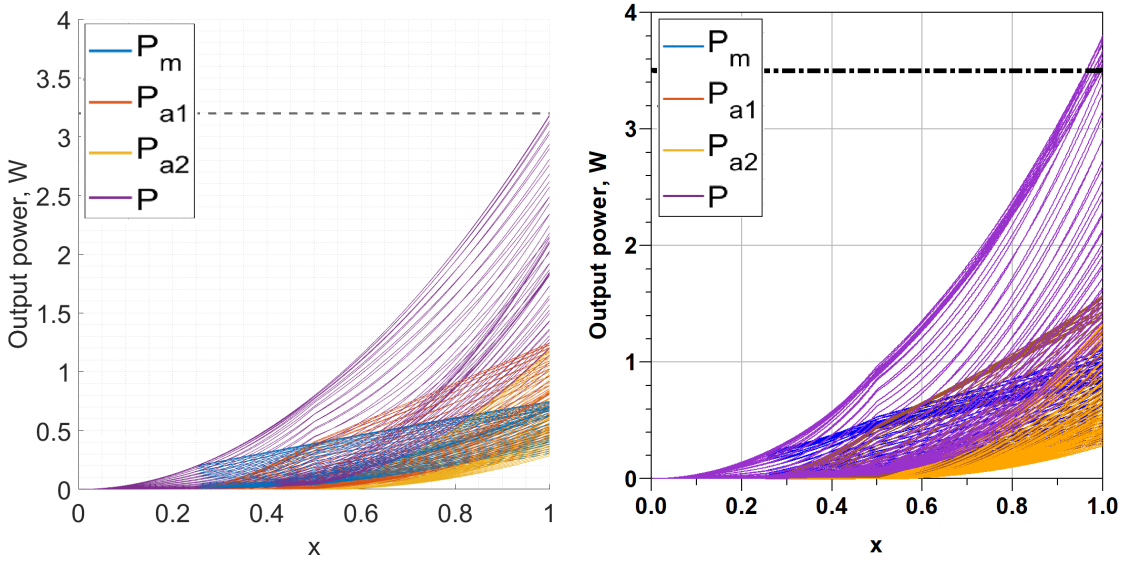

Figure 5.66: Output power delivered to the load in band. (a): simulation by MATLAB, (b): simulation by ADS.

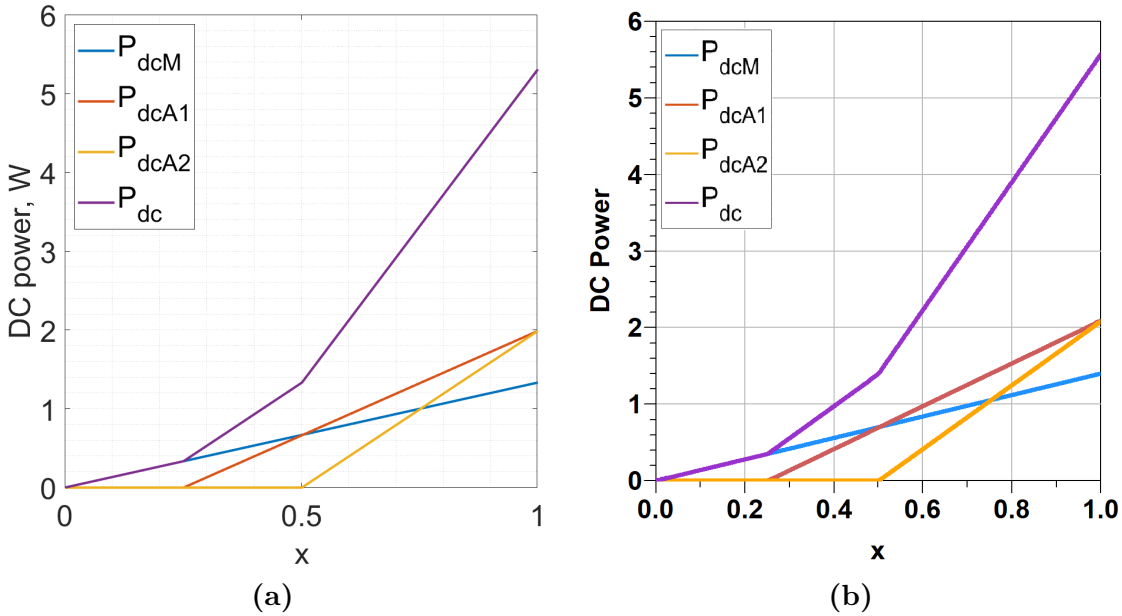

Figure 5.67: DC power. (a): simulation by MATLAB, (b): simulation by ADS.

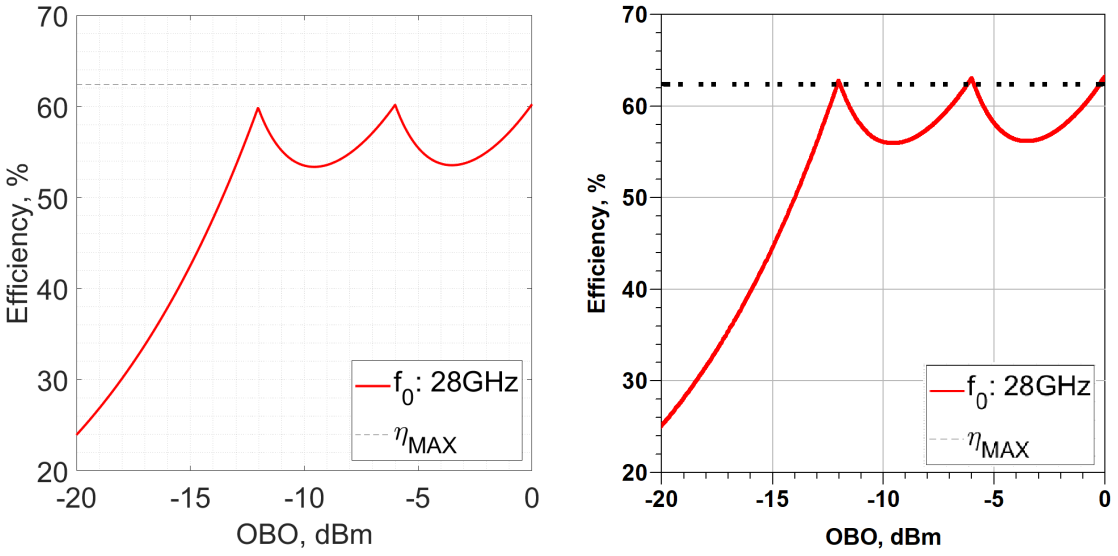

Figure 5.68: Efficiency curves at central frequency. (a): simulation by MATLAB, (b): simulation by ADS.

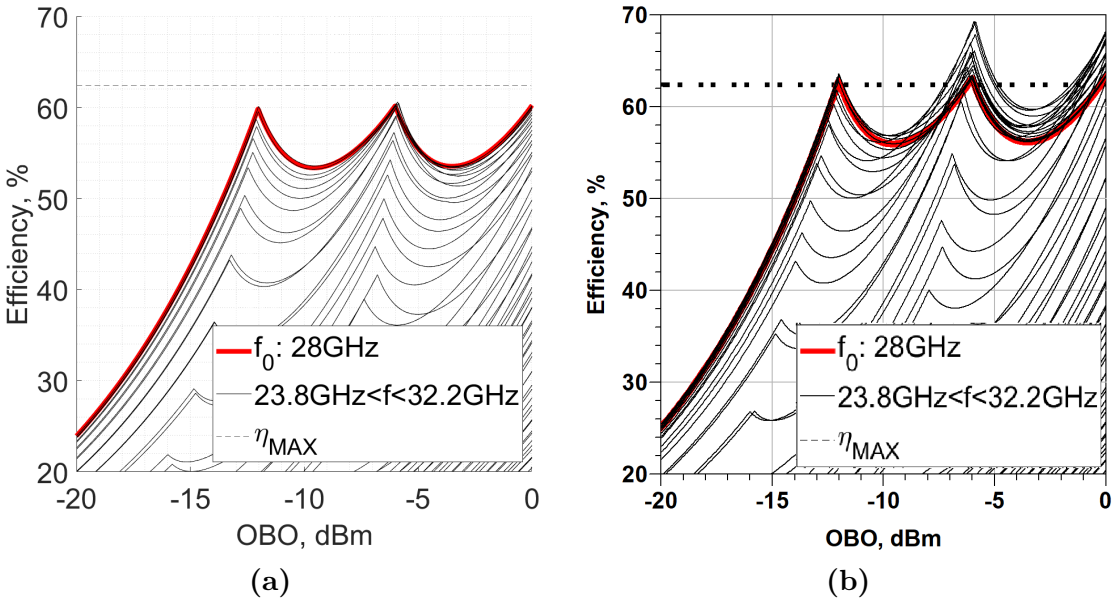

Figure 5.69: Efficiency curves in band. (a): simulation by MATLAB, (b): simulation by ADS.

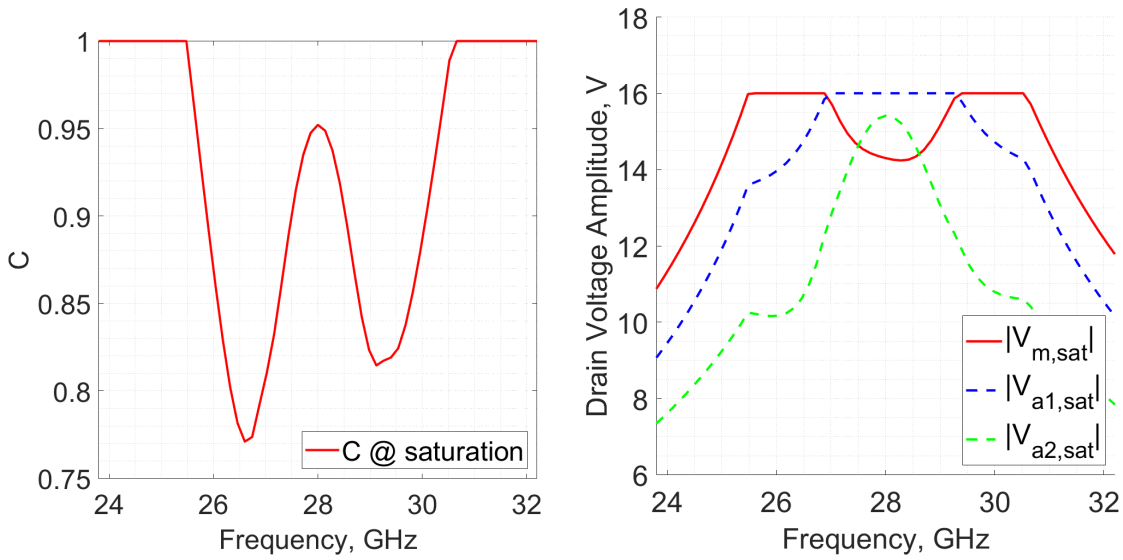

(a) **(b)**

Figure 5.70: Clipping effect implemented in the MATLAB script at saturation. (a): clipping coefficient, (b): effect of clipping on each drain voltage.

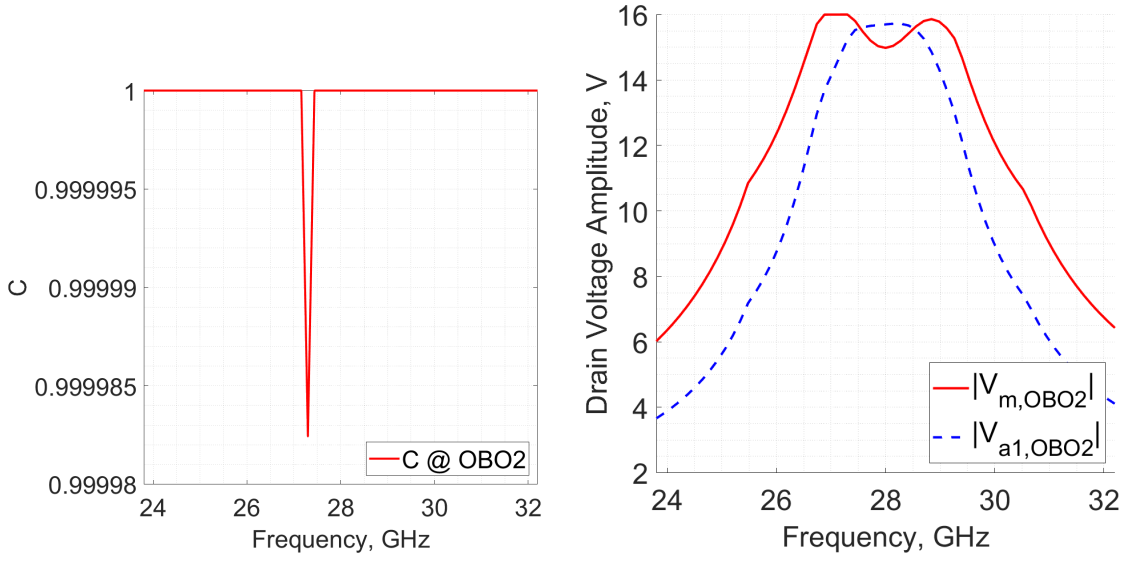

(a) **(b)**

Figure 5.71: Clipping effect implemented in the MATLAB script in OBO2. (a): clipping coefficient, (b): effect of clipping on each drain voltage.

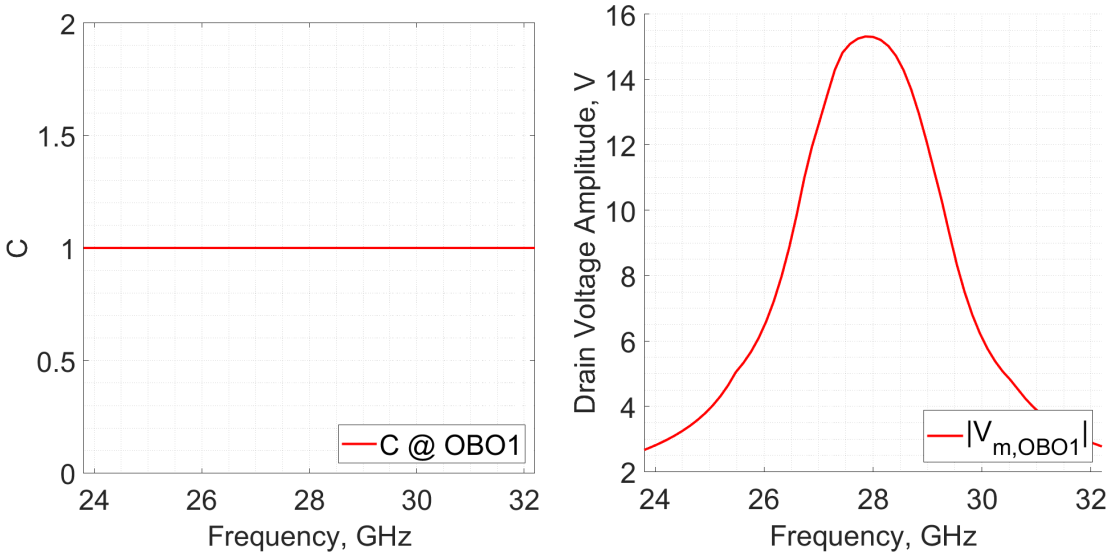

(a) (b)

Figure 5.72: Clipping effect implemented in the MATLAB script in OBO1. (a): clipping coefficient, (b): effect of clipping on each drain voltage.

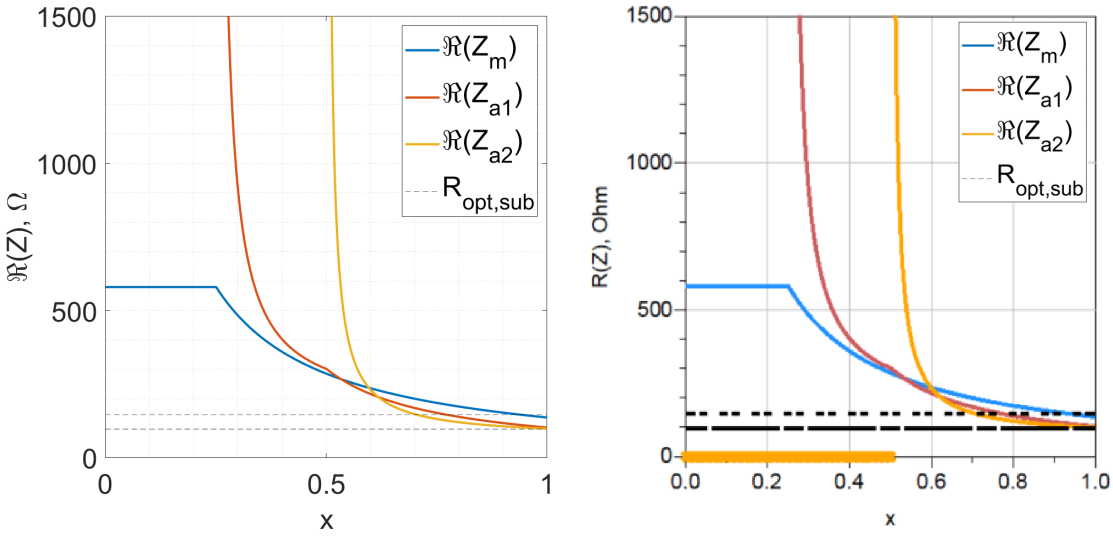

(a) (b)

Figure 5.73: Effect of the load modulation at central frequency. (a): simulation by MATLAB, (b): simulation by ADS.

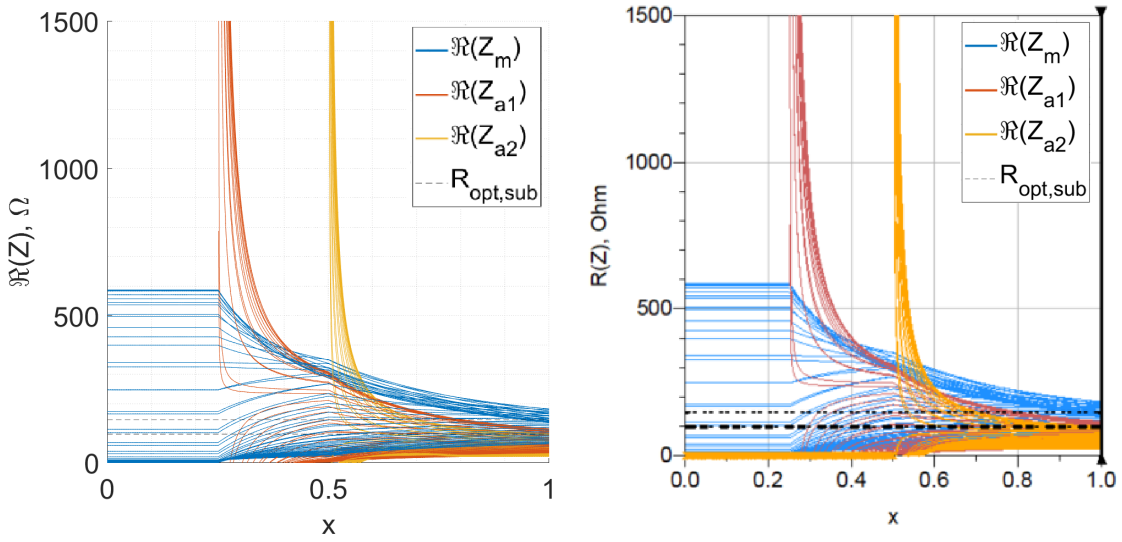

(a) **(b)**

Figure 5.74: Effect of the load modulation in band. (a): simulation by MATLAB, (b): simulation by ADS.

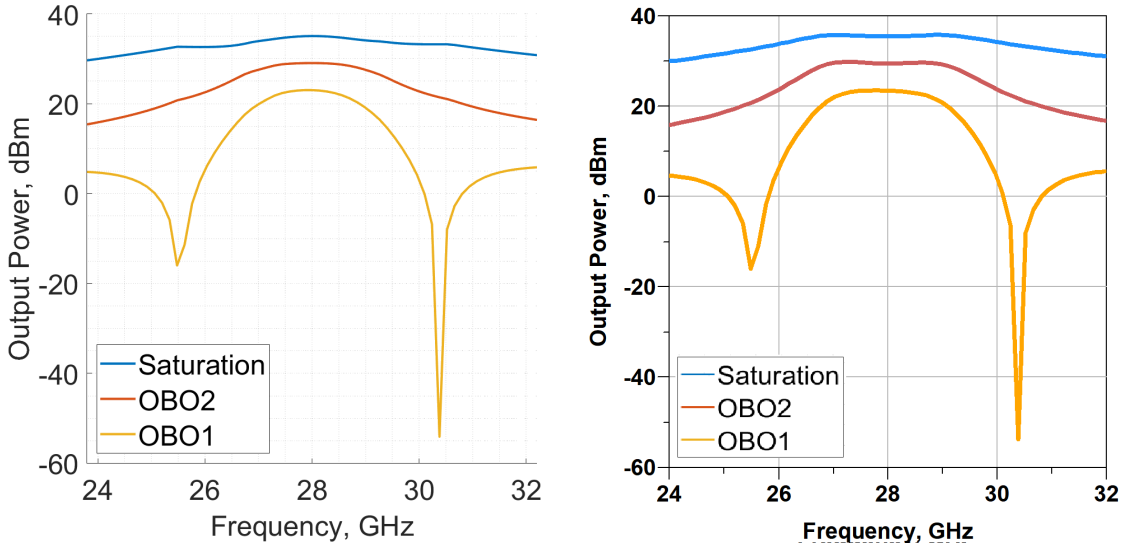

(a) **(b)**

Figure 5.75: Output power in different back-off condition. (a): simulation by MATLAB, (b): simulation by ADS.

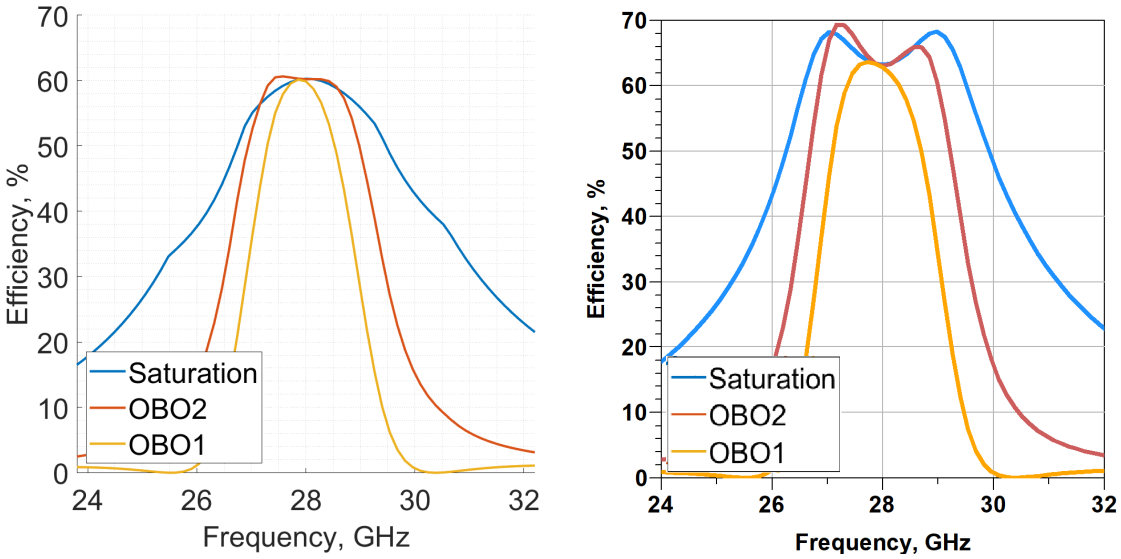

(a) (b)

Figure 5.76: Efficiency in different back-off condition. (a): simulation by MATLAB, (b): simulation by ADS.

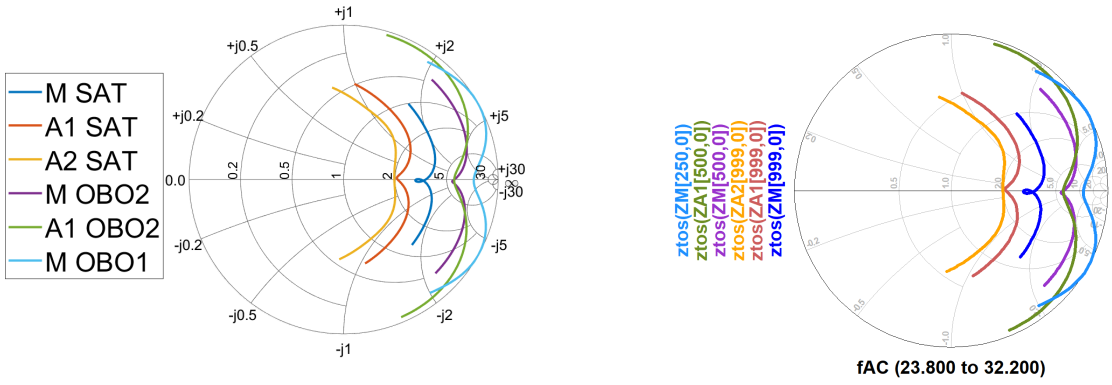

(a) (b)

Figure 5.77: Reflection coefficient referred to 50Ω. (a): simulation by MATLAB, (b): simulation by ADS.

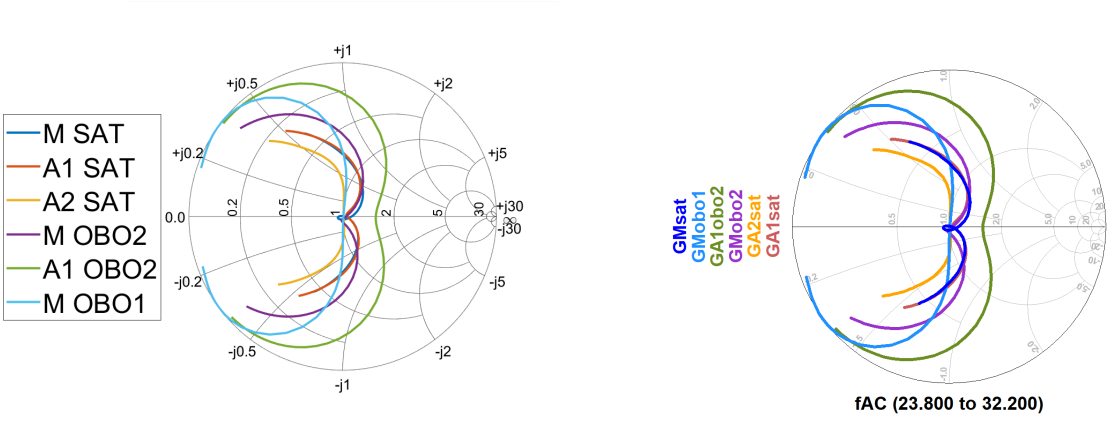

(a) **(b)**

Figure 5.78: Reflection coefficient referred to $R_{\text{opt,sub}}$. (a): simulation by MATLAB, (b): simulation by ADS.

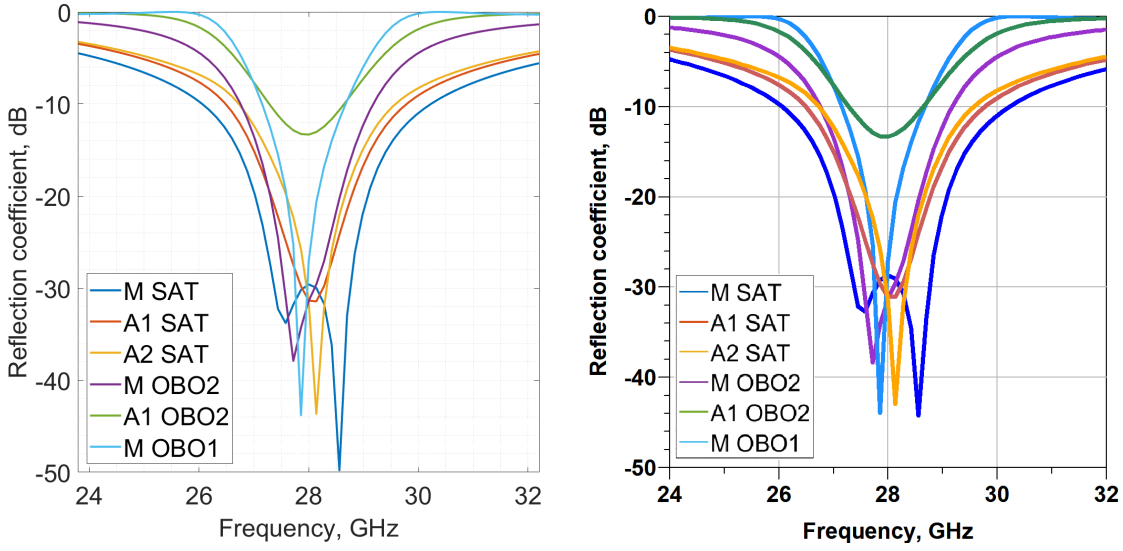

(a) **(b)**

Figure 5.79: Reflection coefficient magnitude referred to $R_{\text{opt,sub}}$. (a): simulation by MATLAB, (b): simulation by ADS.

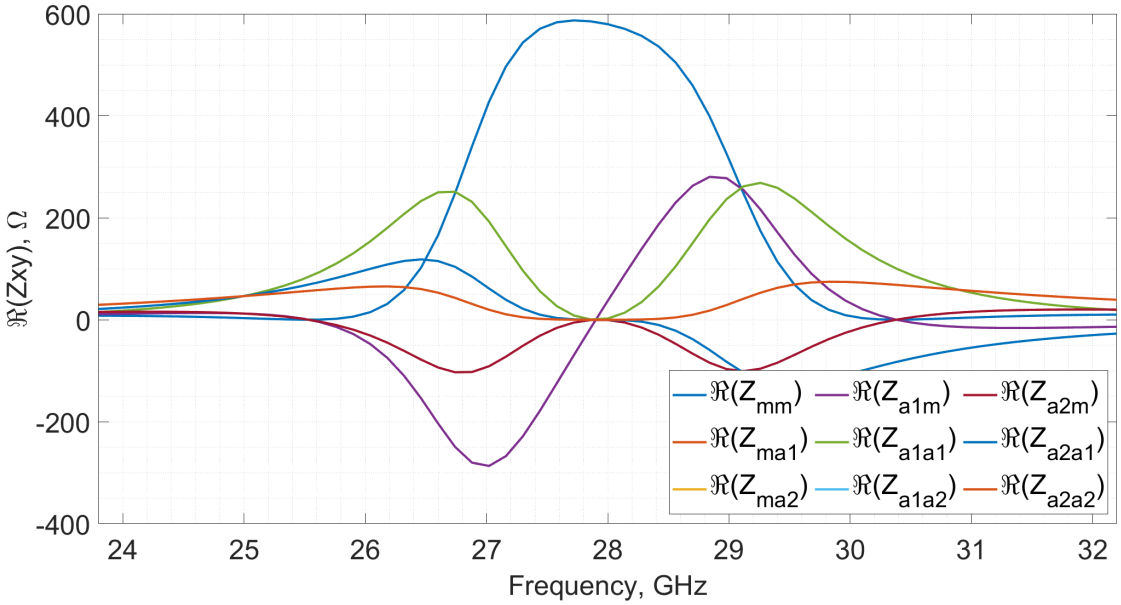

(a)

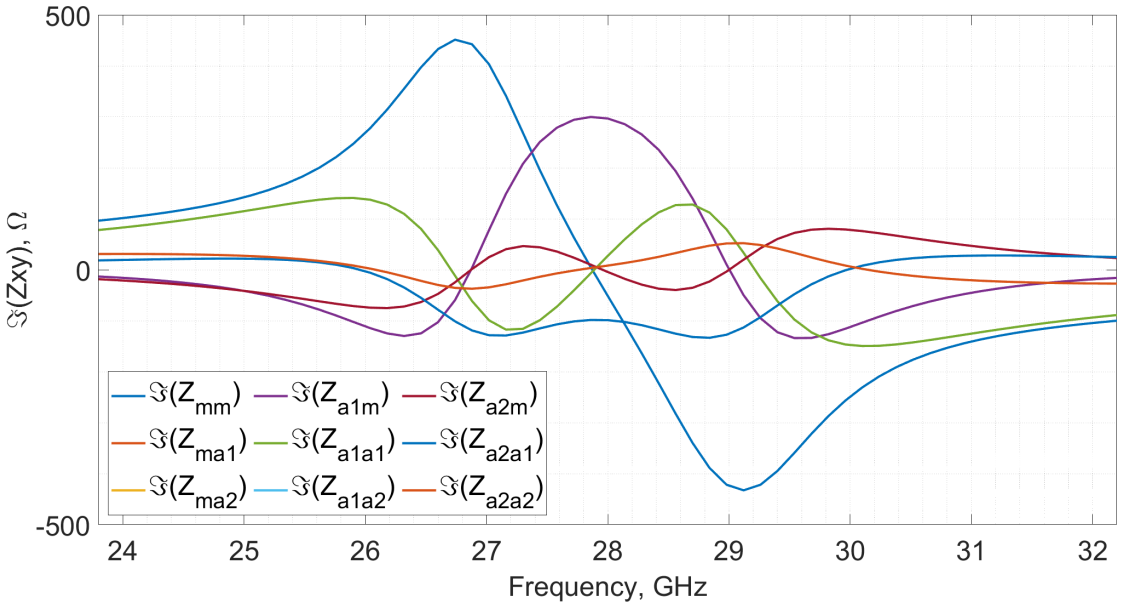

(b)

Figure 5.80: Z-matrix of the combiner estimated by MATLAB. (a): real part, (b): imaginary part.

Chapter 6

Conclusion

6.1 Considerations about the effectiveness of the novel method

The effectiveness of the Doherty topology becomes significant when all amplifiers work in saturation and deliver maximum power to the load. In this saturation, CAD is not able to represent the reality. In such cases, it becomes crucial to have an instrument that can perform physically consistent simulations immediately, even with a linear approximation of a strongly non-linear system. The aim of this project is to develop a simplified linear method that can model the output section of a 3-stage DPA according to the topology used. The method starts with the mathematical model of the combiner, which is described using Z-parameters grouped in a 3x3 matrix. This approach allows designers to avoid non-linear simulation with Spice models and CADs that are available on the market. Although CADs like ADS used in this work can simulate a wide range of phenomena associated with the configuration adopted, non-linear device models require non-linear simulation, which is computationally complex and time-consuming. Therefore, it is more convenient to use a simplified linear model that is suitable for linear simulation with a simple approach. This approach can also be performed with ADS, but the model's limitation does not allow the CAD to consider the dynamic range limited by the supply. This aspect is important because it is the differentiating factor between a mathematical approach and a physical model that describes a real system. For linear simulation, this aspect must be considered because it has an impact on the system level and does not depend on component non-linearity, which is not considered in this work. The developed model simplifies topology description by considering active device saturation. The tool is simple, approximate, and speedy, allowing users to perform linear simulations while considering saturation phenomena. The previous chapter's simulation demonstrated the effectiveness of

the developed script. A comparison of the ADS and MATLAB simulations validated the model. Since the combiner's mathematical description does not depend on the supply, all simulations performed on the intrinsic combiner characterization in terms of impedance are the same for both methods. The effectiveness of the methods is highlighted when the system is analyzed in its DPA working. In ADS, due to the unlimited supply considered, the simulated electrical quantities lead to physically incompatible results with the adopted configuration. However, the developed script provides a reliable dataset in frequency. This means that the simplified approach is sufficient to provide designers with a way to understand the behaviour of the adopted configuration. Additionally, the model's simplicity significantly reduces computational complexity, resulting in simulations that are performed in a fraction of the time required by ADS. Table 6.1 highlights the time consumption for both simulation methods.

Simulation	**ADS**	**MATLAB script**
No parasitic model	22.39s	2.52s
C parasitic model	31.74s	2.82s
LC parasitic model	31.08s	2.55s

Table 6.1: Simulation time (without considering plotting section).

About validating the method's simulations, it is interesting to analyze the combiner's behaviour under different parasitic assumptions. Assuming that the output stage of each active component is ideal, the entire DPA behaves ideally, and the maximum bandwidth estimated in terms of output power is achieved. The combiner design perfectly matches the device specifications assumed at first, and the frequency behaviour is only limited by the transmission line in the combiner structure. In the second simulation, only the parasitic capacitance was considered. The compensation method used a shunt inductor that effectively compensated for the capacitance at f_0. However, the introduction of reactive elements had a strong impact on the frequency behaviour, reducing the bandwidth considerably. Despite this, the parasitic model was simple and the compensation network resonance was easy to achieve, even though the band was not amplified. In the latest simulation, a more complex parasitic method was considered where a shunt capacitor and a series inductor were used. The same resonance approach was used for compensation, under some hypothetical assumption. However, upon analyzing the simulation results, it was found that the compensation was not achieved as expected. One possible reason for this is that in the admittance estimation at the internal section, each branch has been considered as an isolated system, which is not true because each branch interacts with the others. It should be remembered that the combiner is made up of passive elements. This problem may be insignificant compared to

the design tolerance and non-ideality of each active device. However, achieving the desired I and V profiles in DPA, taking into account PAs bias and non-linearities, can be a difficult task.

6.2 Possible improvement and ideas for future project

The strength point of the model developed and its script implementation can be resumed in the following statements:

- The model is linear and quite simple to implement through non-linear simulation, reducing the computational complexity and using a defined number of iterations;
- The simulator developed allows designers to estimate, with approximation, performance in bandwidth taking into account some physical effects that cannot be taken into account when implementing the same model in CADs;
- The simplicity of the model allows fast simulation.

Starting from this release, future work could improve performance and reliability. The following ideas could be taken into account for improving the work:

- It would be beneficial to expand the library of combiner topologies with mathematical models to enhance the tool's versatility.
- more simulation features could be implemented, such as electrical quantities in arbitrary points into the scheme;
- It would be beneficial to have a graphical interface for setting the simulation environment, instead of directly modifying the script.;
- the mathematical model can be studied from a numerical point of view in order to avoid eventual bad-conditioned systems in calculations;
- The original approach could be rewritten in an object-oriented programming language, allowing for more precise definition of each building block.

The tool developed in this work provides designers with a simple method to obtain simulation results that have physical meaning. Even though non-linear phenomena are not considered, the tool is effective in designing future systems. Thus, designers can use this straightforward instrument to design future systems.

Appendix A

MATLAB scripts

A.1 Main.m

```
%% DEVELOPMENT OF GENERALIZED BANDWIDTH ESTIMATION AND OPTIMIZATION
%% TECHNIQUES FOR LOAD MODULATED POWER AMPLIFIERS.
% Relatore: Prof. Vittorio CAMARCHIA
% Correlatori: Dott.ssa Anna Piacibello, Daniele FERRANTE
% Autore: Stefano FIORITONI

clear all
close all
clc

%% DATA SET DEFINITION

dataset_noparasitic;
% dataset_Cparasitic;
% dataset_LCparasitic;

%% INITIALIZATION

simulation_init;

%% FREQUENCY SIMULATION

% Z-parameters estimation

for findex = 1:length(f)

    Z = NoParasiticCombiner(f0,f(findex,1),Z1,theta01,Z2,theta02,Z3,...
        theta03,RL);

    % Z = CCompensationCombiner(Co_m,Co_a1,Co_a2,Lc_m,Lc_a1,Lc_a2,...
    % f0,f(findex),Z1,theta01,Z2,theta02,Z3,theta03,RL);

    % Z = LCCompensationCombiner(Co_m,Co_a1,Co_a2,Lo_m,Lo_a1,Lo_a2,Lc_m,...
    % Lc_a1,Lc_a2,f0,f(findex),Z1,theta01,Z2,theta02,Z3,theta03,RL);
```

```
35
36      Zmm(findex,1)   = Z(1,1);
37      Zma1(findex,1)  = Z(1,2);
38      Zma2(findex,1)  = Z(1,3);
39      Za1m(findex,1)  = Z(2,1);
40      Za1a1(findex,1) = Z(2,2);
41      Za1a2(findex,1) = Z(2,3);
42      Za2m(findex,1)  = Z(3,1);
43      Za2a1(findex,1) = Z(3,2);
44      Za2a2(findex,1) = Z(3,3);
45
46  end
47
48  % Voltages and currents simulation
49
50  x = [1:1000];
51
52  for x_index = 1000:-1:1
53      for findex = 1:length(f)
54
55          Im(findex,x_index) = IfundM.*x_index./1000.*exp(1i.*phiM(findex));
56          if x_index/1000 < a1
57              Ia1(findex,x_index) = 0;
58          else
59              Ia1(findex,x_index) = IfundA1/(1-a1)*(x_index/1000-a1).*...
60                  exp(1i.*phiA1(findex));
61          end
62          if x_index/1000 < a2
63              Ia2(findex,x_index) = 0;
64          else
65              Ia2(findex,x_index) = IfundA2/(1-a2)*(x_index/1000-a2).*.....
66                  exp(1i.*phiA2(findex));
67          end
68
69      end
70
71      Vm(:,x_index)  = Zmm(:).*Im(:,x_index)  + Zma1(:).*Ia1(:,x_index)  +...
72          Zma2(:).*Ia2(:,x_index);
73      Va1(:,x_index) = Za1m(:).*Im(:,x_index) + Za1a1(:).*Ia1(:,x_index) +...
74          Za1a2(:).*Ia2(:,x_index);
75      Va2(:,x_index) = Za2m(:).*Im(:,x_index) + Za2a1(:).*Ia1(:,x_index) +...
76          Za2a2(:).*Ia2(:,x_index);
77
78  end
79
80  clipping;
81
82  %DC currents
83
84  IOm = 2*abs(Im)./pi;
85  IOa1 = 2*abs(Ia1)./pi;
86  IOa2 = 2*abs(Ia2)./pi;
87
88  %Impedances
89
90  Zm = Vm./Im; Ym = 1./Zm;
```

```
91  GAMm = (Zm-50)./(Zm+50);
92  GAMm_opt = (Zm-RoptM./(x./1000))./(Zm+RoptM./(x./1000));
93
94  Za1 = Va1./Ia1; Ya1 = 1./Za1;
95  GAMa1 = (Za1-50)./(Za1+50);
96  GAMa1_opt = (Za1-RoptA1./(x./1000))./(Za1+RoptA1./(x./1000));
97
98  Za2 = Va2./Ia2; Ya2 = 1./Za2;
99  GAMa2 = (Za2-50)./(Za2+50);
100 GAMa2_opt = (Za2-RoptA2./(x./1000))./(Za2+RoptA2./(x./1000));
101
102 %Power and efficiency
103
104 PdcM = VDD.*IOm;
105 PdcA1 = VDD.*IOa1;
106 PdcA2 = VDD.*IOa2;
107 Pdc = PdcM+PdcA1+PdcA2;
108 Pm = 0.5*real(Vm.*conj(Im));
109 Pm_dBm = 30+10*log10(Pm);
110 Pa1 = 0.5*real(Va1.*conj(Ia1));
111 Pa1_dBm = 30+10*log10(Pa1);
112 Pa2 = 0.5*real(Va2.*conj(Ia2));
113 Pa2_dBm = 30+10*log10(Pa2);
114 P = Pm+Pa1+Pa2;
115 P_dBm = 30+10*log10(P);
116 Pmax = (max(P'))';
117 Pmax_dBm = 30+10*log10(Pmax);
118 OBO = P_dBm-Pmax_dBm;
119 eta = P./Pdc;
120
121 % Saturation, OBO2 and OBO1 parameters extraction
122
123 % @saturation
124 Imsat  = Im(:,1000);
125 Ia1sat = Ia1(:,1000);
126 Ia2sat = Ia2(:,1000);
127
128 IOmsat = IOm(:,1000);
129 IOa1sat = IOa1(:,1000);
130 IOa2sat = IOa2(:,1000);
131
132 Vmsat  = Vm(:,1000);
133 Va1sat = Va1(:,1000);
134 Va2sat = Va2(:,1000);
135
136 Zmsat = Zm(:,1000); Ymsat = 1./Zmsat;
137 GAMmsat = GAMm(:,1000);
138 GAMmsat_opt = GAMm_opt(:,1000);
139
140 Za1sat = Za1(:,1000); Ya1sat = 1./Za1sat;
141 GAMa1sat = GAMa1(:,1000);
142 GAMa1sat_opt = GAMa1_opt(:,1000);
143
144 Za2sat = Za2(:,1000); Ya2sat = 1./Za2sat;
145 GAMa2sat = GAMa2(:,1000);
146 GAMa2sat_opt = GAMa2_opt(:,1000);
```

```
147
148 PdcMsat = PdcM(:,1000);
149 PdcA1sat = PdcA1(:,1000);
150 PdcA2sat = PdcA2(:,1000);
151 Pdcsat = Pdc(:,1000);
152 Pmsat = Pm(:,1000);
153 Pa1sat = Pa1(:,1000);
154 Pa2sat = Pa2(:,1000);
155 Psat = P(:,1000);
156 eta_sat = eta(:,1000);
157
158 % @OBO2
159
160 Imobo2  = Im(:,round(1000*a2));
161 Ia1obo2 = Ia1(:,round(1000*a2));
162 Ia2obo2 = Ia2(:,round(1000*a2));
163
164 IOmobo2 = IOm(:,round(1000*a2));
165 IOa1obo2 = IOa1(:,round(1000*a2));
166 IOa2obo2 = IOa2(:,round(1000*a2));
167
168 Vmobo2  = Vm(:,round(1000*a2));
169 Va1obo2 = Va1(:,round(1000*a2));
170
171 Zmobo2 = Zm(:,round(1000*a2)); Ymobo2 = 1./Zmobo2;
172 GAMmobo2 = GAMm(:,round(1000*a2));
173 GAMmobo2_opt = GAMm_opt(:,round(1000*a2));
174
175 Za1obo2 = Za1(:,round(1000*a2)); Ya1obo2 = 1./Za1obo2;
176 GAMa1obo2 = GAMa1(:,round(1000*a2));
177 GAMa1obo2_opt = GAMa1_opt(:,round(1000*a2));
178
179 PdcMobo2 = PdcM(:,round(1000*a2));
180 PdcA1obo2 = PdcA1(:,round(1000*a2));
181 PdcA2obo2 = PdcA2(:,round(1000*a2));
182 Pdcobo2 = Pdc(:,round(1000*a2));
183 Pmobo2 = Pm(:,round(1000*a2));
184 Pa1obo2 = Pa1(:,round(1000*a2));
185 Pa2obo2 = Pa2(:,round(1000*a2));
186 Pobo2 = P(:,round(1000*a2));
187 eta_obo2 = eta(:,round(1000*a2));
188
189 % @OBO1
190
191 Imobo1  = Im(:,round(1000*a1));
192 Ia1obo1 = Ia1(:,round(1000*a1));
193 Ia2obo1 = Ia2(:,round(1000*a1));
194
195 IOmobo1 = IOm(:,round(1000*a1));
196 IOa1obo1 = IOa1(:,round(1000*a1));
197 IOa2obo1 = IOa2(:,round(1000*a1));
198
199 Vmobo1  = Vm(:,round(1000*a1));
200
201 Zmobo1 = Zm(:,round(1000*a1)); Ymobo1 = 1./Zmobo1;
202 GAMmobo1 = GAMm(:,round(1000*a1));
```

```
203 GAMmobo1_opt = GAMm_opt(:,round(1000*a1));
204
205 PdcMobo1 = PdcM(:,round(1000*a1));
206 PdcA1obo1 = PdcA1(:,round(1000*a1));
207 PdcA2obo1 = PdcA2(:,round(1000*a1));
208 Pdcobo1 = Pdc(:,round(1000*a1));
209 Pmobo1 = Pm(:,round(1000*a1));
210 Pa1obo1 = Pa1(:,round(1000*a1));
211 Pa2obo1 = Pa2(:,round(1000*a1));
212 Pobo1 = P(:,round(1000*a1));
213 eta_obo1 = eta(:,round(1000*a1));
214
215 OBO1 = 10*log10(Psat./Pobo1);
216 OBO2 = 10*log10(Psat./Pobo2);
217
218 %% Plot section @f0
219
220 f0_plots;
221
222 %% Plot section in-band
223
224 frequency_range_plots;
```

A.2 simulation_init.m

```
1  %parameters estimation
2  f = [fmin:f_res:fmax].';
3  w0 = 2*pi*f0;
4  phiM = phiM.*ones(length(f),1);
5  phiA1 = phiA1.*ones(length(f),1);
6  phiA2 = phiA2.*ones(length(f),1);
7
8  % %efficiency init
9  ETAMAX = max([VMAX_m VMAX_a2 VMAX_a1])/VDD*78;
10
11
12 %Electrical quantities init
13 Vm = zeros(length(f),1000);
14 Va1 = zeros(length(f),1000);
15 Va2 = zeros(length(f),1000);
16 Im = zeros(length(f),1000);
17 Ia1 = zeros(length(f),1000);
18 Ia2 = zeros(length(f),1000);
19
20 %Clipping init
21 C = ones(length(f),1000);
22 C_M = C;
23 C_A1 = C;
24 C_A2 = C;
```

A.3 dataset_noparasitic.m

```
% Frequency range

f0 = 28e9;
fmin = f0*0.85;
fmax = f0*1.15;
f_res = f0/200;

% Transistor parastitic model

Lo_m = 0;
Lo_a1 = 0;
Lo_a2 = 0;
Co_m = 0;
Co_a1 = 0;
Co_a2 = 0;

%Compensation network


% Supply and treshold
VDD = +20;
VKm = 4;
VKa1 = 4;
VKa2 = 4;
VMAX_m = VDD-VKm;
VMAX_a1 = VDD-VKa1;
VMAX_a2 = VDD-VKa2;
OBO1 = 12;
OBO2 = 6;
a1 = 10.^(-OBO1./20);
a2 = 10.^(-OBO2./20);
b1 = 1;
b2 = 1;

%output currents
% IMAX = 2*VMAX/Ropt;
IfundM = 0.110;     phiM = -pi/2;
IfundA1 = 0.164;    phiA1 = 0;
IfundA2 = 0.164;    phiA2 = -pi/2;
IMaxM = 2.*IfundM;
IMaxA1 = 2.*IfundA1;
IMaxA2 = 2.*IfundA2;

%impedance definitions
RL = 11.3;
RoptM = 2.*VMAX_m./IMaxM;
RoptA1 = 2.*VMAX_a1./IMaxA1;
RoptA2 = 2.*VMAX_a2./IMaxA2;
Z1 = 81; theta01 = pi/2;
Z2 = 27; theta02 = pi/2;
Z3 = 97;   theta03 = pi/2;
```

A.4 dataset_Cparasitic.m

```
% Frequency range

f0 = 28e9;
fmin = 0.85*f0;
fmax = 1.15*f0;
f_res = f0/200;

% Transistor parastitic model

Lo_m = 0;
Lo_a1 = 0;
Lo_a2 = 0;
Co_m = 125e-15;
Co_a1 = 230e-15;
Co_a2 = 230e-15;

%Compensation network

% Lc_m = 1/((2*pi*f0)^2*Co_m)*1;
% Lc_a1 = 1/((2*pi*f0)^2*Co_a1)*1;
% Lc_a2 = 1/((2*pi*f0)^2*Co_a2)*1;
Lc_m = 258e-12;
Lc_a1 = 140e-12;
Lc_a2 = 140e-12;

% Supply and treshold
VDD = +20;
VKm = 4;
VKa1 = 4;
VKa2 = 4;
VMAX_m = VDD-VKm;
VMAX_a1 = VDD-VKa1;
VMAX_a2 = VDD-VKa2;
OBO1 = 12;
OBO2 = 6;
a1 = 10.^(-OBO1./20);
a2 = 10.^(-OBO2./20);
b1 = 1;
b2 = 1;

%output currents
% IMAX = 2*VMAX/Ropt;
IfundM = 0.110;     phiM = -pi/2;
IfundA1 = 0.164;    phiA1 = 0;
IfundA2 = 0.164;    phiA2 = -pi/2;
IMaxM = 2.*IfundM;
IMaxA1 = 2.*IfundA1;
IMaxA2 = 2.*IfundA2;

%impedance definitions
RL = 11.3;
RoptM = 2.*VMAX_m./IMaxM;
```

```
RoptA1 = 2.*VMAX_a1./IMaxA1;
RoptA2 = 2.*VMAX_a2./IMaxA2;
Z1 = 81; theta01 = pi/2;
Z2 = 27; theta02 = pi/2;
Z3 = 97;   theta03 = pi/2;
```

A.5 dataset_LCparasitic.m

```
% Frequency range

f0 = 28e9;
fmin = 0.85*f0;
fmax = 1.15*f0;
f_res = f0/200;

% Transistor parastitic model

Lo_m = 36e-12;
Lo_a1 = 30e-12;
Lo_a2 = 30e-12;
Co_m = 125e-15;
Co_a1 = 230e-15;
Co_a2 = 230e-15;

%Compensation network

Lc_m = 225e-12;
Lc_a1 = 111e-12;
Lc_a2 = 111e-12;

% Supply and treshold
VDD = +20;
VKm = 4;
VKa1 = 4;
VKa2 = 4;
VMAX_m = VDD-VKm;
VMAX_a1 = VDD-VKa1;
VMAX_a2 = VDD-VKa2;
OBO1 = 12;
OBO2 = 6;
a1 = 10.^(-OBO1./20);
a2 = 10.^(-OBO2./20);
% a1 = 0.250;
% a2 = 0.500;
% OBO1 = -20*log(a1);
% OBO2 = -20*log(a2);
b1 = 1;
b2 = 1;

%output currents
% IMAX = 2*VMAX/Ropt;
IfundM = 0.110;     phiM = -pi/2;
```

```
IfundA1 = 0.164;    phiA1 = 0;
IfundA2 = 0.164;    phiA2 = -pi/2;
IMaxM = 2.*IfundM;
IMaxA1 = 2.*IfundA1;
IMaxA2 = 2.*IfundA2;

%impedance definitions
RL = 11.3;
RoptM = 2.*VMAX_m./IMaxM;
RoptA1 = 2.*VMAX_a1./IMaxA1;
RoptA2 = 2.*VMAX_a2./IMaxA2;
Z1 = 70; theta01 = pi/2;
Z2 = 21; theta02 = pi/2;
Z3 = 61;   theta03 = pi/2;
```

A.6 NoParasiticCombiner.m

```
function Z = NoParasiticCombiner(f0,f,Z1,theta01,Z2,theta02,Z3,theta03,RL)

w = 2*pi*f;
w0 = 2*pi*f0;

%main

ABCD_TLs_m = ABCD_SeriesTxLine(w0,w,Z1,theta01);
Tm = ABCD_TLs_m;

%load
ABCD_RL = ABCD_ShuntAdmittance(1/RL);
Tl = ABCD_RL;

%impedance inverter 1

ABCD_inv1 = ABCD_SeriesTxLine(w0,w,Z2,theta02);
T1 = ABCD_inv1;

%auxiliary 1

ABCD_TLs_a1 = ABCD_SeriesTxLine(w0,w,Z3,theta03);
Ta1 = ABCD_TLs_a1;

%impedance inverter 2

T2 = [1,0;0,1];

%auxiliary 2

Ta2 = [1,0;0,1];

%transformation of a 2-ports ABCD-matrix cascate into a 3-port Z-matrix

M = Tm*Tl*T1;
```

```
36  T2tot = T2*Ta2;
37  A2 = Tm*Tl*T1*T2*Ta2;
38  Am = Tm*Tl*T1;
39
40  OMEGA = [1, -Am(1,2).*Ta1(2,1), -A2(1,1);...
41      0, -Am(2,2).*Ta1(2,1), -A2(2,1);...
42      0,     Ta1(1,1),       -T2tot(1,1)];
43  S = [0, -Am(1,2).*Ta1(2,2), -A2(1,2);...
44      -1, -Am(2,2).*Ta1(2,2),  -A2(2,2);...
45      0,      +Ta1(1,2),      -T2tot(1,2)];
46  Z = OMEGA\S;
47
48
49  end
```

A.7 CCompensationCombiner.m

```
1   function Z = CCompensationCombiner(Co_m,Co_a1,Co_a2,Lc_m,Lc_a1,Lc_a2,f0,...
2       f,Z1,theta01,Z2,theta02,Z3,theta03,RL)
3
4   w = 2*pi*f;
5   w0 = 2*pi*f0;
6
7   %main
8   ABCD_Cout_m = ABCD_ShuntCapacitor(Co_m,w);
9   ABCD_Lres_m = ABCD_ShuntInductor(Lc_m,w);
10
11  ABCD_TLs_m = ABCD_SeriesTxLine(w0,w,Z1,theta01);
12
13  ABCD_m = ABCD_Cout_m*ABCD_Lres_m*ABCD_TLs_m;
14  Tm = ABCD_m;
15
16  %load
17  ABCD_RL = ABCD_ShuntAdmittance(1/RL);
18  Tl = ABCD_RL;
19
20  %impedance inverter 1
21  ABCD_inv1 = ABCD_SeriesTxLine(w0,w,Z2,theta02);
22  T1 = ABCD_inv1;
23
24  %auxiliary 1
25  ABCD_Cout_a1 = ABCD_ShuntCapacitor(Co_a1,w);
26  ABCD_Lres_a1 = ABCD_ShuntInductor(Lc_a1,w);
27
28  ABCD_TLs_a1 = ABCD_SeriesTxLine(w0,w,Z3,theta03);
29
30  ABCD_a1 = ABCD_TLs_a1*ABCD_Lres_a1*ABCD_Cout_a1;
31  Ta1 = ABCD_a1;
32
33  %impedance inverter 2
34
35  T2 = [1,0;0,1];
```

```
36
37  %auxiliary 2
38  ABCD_Cout_a2 = ABCD_ShuntCapacitor(Co_a2,w);
39  ABCD_Lres_a2 = ABCD_ShuntInductor(Lc_a2,w);
40
41  ABCD_TLs_a2 =[1,0;0,1];
42
43  ABCD_a2 = ABCD_TLs_a2*ABCD_Lres_a2*ABCD_Cout_a2;
44  Ta2 = ABCD_a2;
45
46  %transformation of a 2-ports ABCD-matrix cascate into a 3-port Z-matrix
47
48  M = Tm*Tl*T1;
49  T2tot = T2*Ta2;
50  A2 = Tm*Tl*T1*T2*Ta2;
51  Am = Tm*Tl*T1;
52
53  OMEGA = [1, -Am(1,2).*Ta1(2,1), -A2(1,1);...
54      0, -Am(2,2).*Ta1(2,1), -A2(2,1);...
55      0,     Ta1(1,1),       -T2tot(1,1)];
56  S = [0, -Am(1,2).*Ta1(2,2), -A2(1,2);...
57      -1, -Am(2,2).*Ta1(2,2),  -A2(2,2);...
58      0,      +Ta1(1,2),      -T2tot(1,2)];
59  Z = OMEGA\S;
60
61  end
```

A.8 LCCompensationCombiner.m

```
1   function Z = LCCompensationCombiner(Co_m,Co_a1,Co_a2,Lo_m,Lo_a1,Lo_a2,...
2       Lc_m,Lc_a1,Lc_a2,f0,f,Z1,theta01,Z2,theta02,Z3,theta03,RL)
3
4   w = 2*pi*f;
5   w0 = 2*pi*f0;
6
7   %main
8   ABCD_Cout_m = ABCD_ShuntCapacitor(Co_m,w);
9   ABCD_Lout_m = ABCD_SeriesInductor(Lo_m,w);
10  ABCD_Lc_m = ABCD_ShuntInductor(Lc_m,w);
11
12  ABCD_TLs_m = ABCD_SeriesTxLine(w0,w,Z1,theta01);
13
14  ABCD_m = ABCD_Cout_m*ABCD_Lout_m*ABCD_Lc_m*ABCD_TLs_m;
15  Tm = ABCD_m;
16
17  %load
18  ABCD_RL = ABCD_ShuntAdmittance(1/RL);
19  Tl = ABCD_RL;
20
21  %impedance inverter 1
22  ABCD_inv1 = ABCD_SeriesTxLine(w0,w,Z2,theta02);
23  T1 = ABCD_inv1;
```

```
24
25  %auxiliary 1
26  ABCD_Cout_a1 = ABCD_ShuntCapacitor(Co_a1,w);
27  ABCD_Lout_a1 = ABCD_SeriesInductor(Lo_a1,w);
28  ABCD_Lc_a1 = ABCD_ShuntInductor(Lc_a1,w);
29
30  ABCD_TLs_a1 = ABCD_SeriesTxLine(w0,w,Z3,theta03);
31
32  ABCD_a1 = ABCD_TLs_a1*ABCD_Lc_a1*ABCD_Lout_a1*ABCD_Cout_a1;
33  Ta1 = ABCD_a1;
34
35  %impedance inverter 2
36
37  T2 = [1,0;0,1];
38
39  %auxiliary 2
40  ABCD_Cout_a2 = ABCD_ShuntCapacitor(Co_a2,w);
41  ABCD_Lout_a2 = ABCD_SeriesInductor(Lo_a2,w);
42  ABCD_Lc_a2 = ABCD_ShuntInductor(Lc_a2,w);
43
44  ABCD_TLs_a2 =[1,0;0,1];
45
46  ABCD_a2 = ABCD_TLs_a2*ABCD_Lc_a2*ABCD_Lout_a2*ABCD_Cout_a2;
47  Ta2 = ABCD_a2;
48
49  %transformation of a 2-ports ABCD-matrix cascate into a 3-port Z-matrix
50
51  M = Tm*Tl*T1;
52  T2tot = T2*Ta2;
53  A2 = Tm*Tl*T1*T2*Ta2;
54  Am = Tm*Tl*T1;
55
56  OMEGA = [1, -Am(1,2).*Ta1(2,1), -A2(1,1);...
57      0, -Am(2,2).*Ta1(2,1), -A2(2,1);...
58      0,     Ta1(1,1),       -T2tot(1,1)];
59  S = [0, -Am(1,2).*Ta1(2,2), -A2(1,2);...
60      -1, -Am(2,2).*Ta1(2,2),  -A2(2,2);...
61      0,      +Ta1(1,2),      -T2tot(1,2)];
62  Z = OMEGA\S;
63
64  end
65
```

A.9 clipping.m

```
1  for x_index = 1000:-1:1
2      iiM = find(abs(Vm(:,x_index)) > VMAX_m);
3      iiA1 = find(abs(Va1(:,x_index)) > VMAX_a1);
4      iiA2 = find(abs(Va2(:,x_index)) > VMAX_a2);
5      C_M(iiM,x_index) = VMAX_m./abs(Vm(iiM,x_index));
6      C_A1(iiA1,x_index) = VMAX_a1./abs(Va1(iiA1,x_index));
7      C_A2(iiA2,x_index) = VMAX_a2./abs(Va2(iiA2,x_index));
```

```
    C(:,x_index) = min([C_M(:,x_index).'; C_A1(:,x_index).'; ...
        C_A2(:,x_index).']).';
    Im(:,1:x_index) = Im(:,1:x_index).*C(:,x_index);
    Ia1(:,1:x_index) = Ia1(:,1:x_index).*C(:,x_index);
    Ia2(:,1:x_index) = Ia2(:,1:x_index).*C(:,x_index);
    Vm(:,1:x_index)  = Zmm(:).*Im(:,1:x_index)  + Zma1(:).*...
        Ia1(:,1:x_index)  + Zma2(:).*Ia2(:,1:x_index);
    Va1(:,1:x_index) = Za1m(:).*Im(:,1:x_index) + Za1a1(:).*...
        Ia1(:,1:x_index) + Za1a2(:).*Ia2(:,1:x_index);
    Va2(:,1:x_index) = Za2m(:).*Im(:,1:x_index) + Za2a1(:).*...
        Ia1(:,1:x_index) + Za2a2(:).*Ia2(:,1:x_index);
end
```

A.10 f0_plots.m

```
f0index = find(f==f0)
Pmax(f0index)

% Currents and voltages

hf = figure;
ha = axes;
subplot(1,2,1)
plot(x/1000,abs(Im(f0index,:)),'DisplayName',['I_m'],'LineWidth',2);
hold on;
plot(x/1000,abs(Ia1(f0index,:)),'DisplayName',['I_{a1}'],'LineWidth',2);
plot(x/1000,abs(Ia2(f0index,:)),'DisplayName',['I_{a2}'],'LineWidth',2);
grid minor;
xlabel('x');
ylim([0 0.20])
ylabel('Output current (abs), A');
legend();
fontsize(24,"points")
% title(['Currents curves @ f_0:' num2str(f(f0index)/1e9) 'GHz'],...
%     'FontSize',12)
ytickformat('%.2f')
axis square;


subplot(1,2,2)
plot(x/1000,abs(Vm(f0index,:)),'DisplayName',['V_m'],'LineWidth',2);
hold on;
plot(x/1000,abs(Va1(f0index,:)),'DisplayName',['V_{a1}'],'LineWidth',2);
plot(x/1000,abs(Va2(f0index,:)),'DisplayName',['V_{a2}'],'LineWidth',2);
grid minor;
ylim([0 25])
xlabel('x');
ylabel('Output voltage (abs), V');
legend();
fontsize(24,"points")
% title(['Voltage curves @ f_0:' num2str(f(f0index)/1e9) 'GHz'],...
%     'FontSize',12)
```

```
38  axis square;
39
40  hf = figure;
41  ha = axes;
42  hold on;
43  for i = 1:1:length(f)
44      if i ~= f0index
45          plot(x/1000,abs(Vm(i,:)),'Color' , '#0072BD','LineWidth',0.5)
46          plot(x/1000,abs(Va1(i,:)),'Color' , '#D95319','LineWidth',0.5)
47          plot(x/1000,abs(Va2(i,:)),'Color' , '#EDB120','LineWidth',0.5)
48      end
49  end
50  grid minor;
51  ylim([0 25])
52  xlabel('x');
53  ylabel('Output voltage (abs), V');
54  fontsize(24,"points")
55  % title(['Voltage curves @ f_0:' num2str(f(f0index)/1e9) 'GHz'],...
56  %     'FontSize',12)
57  axis square;
58
59  %power curves
60
61  hf = figure;
62  ha = axes;
63  subplot(1,2,1);
64  plot(x/1000,Pm(f0index,:),'DisplayName',['P_m'],'LineWidth',2);
65  hold on;
66  plot(x/1000,Pa1(f0index,:),'DisplayName',['P_{a1}'],'LineWidth',2);
67  plot(x/1000,Pa2(f0index,:),'DisplayName',['P_{a2}'],'LineWidth',2);
68  plot(x/1000,P(f0index,:),'DisplayName',['P'],'LineWidth',2);
69  grid minor;
70  yline(Pmax(f0index),'--','HandleVisibility','off','LineWidth',2);
71  ylim([0 4])
72  xlabel('x');
73  ylabel('Output power, W');
74  legend();
75  fontsize(24,"points")
76  % title(['Power curve @ f_0:' num2str(f(f0index)/1e9) 'GHz'],'FontSize',12);
77  axis square;
78
79  subplot(1,2,2);
80  plot(x/1000,PdcM(f0index,:),'LineWidth',2);
81  hold on;
82  plot(x/1000,PdcA1(f0index,:),'LineWidth',2);
83  plot(x/1000,PdcA2(f0index,:),'LineWidth',2);
84  plot(x/1000,Pdc(f0index,:),'LineWidth',2);
85  grid minor;
86  xlabel('x');
87  ylabel('DC power, W');
88  legend('P_{dcM}', 'P_{dcA1}', 'P_{dcA2}', 'P_{dc}');
89  fontsize(24,"points")
90  % title(['Power curve DC @ f_0:' num2str(f(f0index)/1e9) 'GHz'],...
91  %     'FontSize',12);
92  axis square;
93
```

```
hf = figure;
ha = axes;
hold on;
for i = 1:1:length(f)
    if i ~= f0index
        plot(x/1000,Pm(i,:),'Color' , '#0072BD','LineWidth',0.5)
        plot(x/1000,Pa1(i,:),'Color' , '#D95319','LineWidth',0.5)
        plot(x/1000,Pa2(i,:),'Color' , '#EDB120','LineWidth',0.5)
        plot(x/1000,P(i,:),'Color' , '#7E2F8E','LineWidth',0.5)
    end
end
grid minor;
yline(Pmax(f0index),'--','HandleVisibility','off','LineWidth',2);
ylim([0 4])
xlabel('x');
ylabel('Output power, W');
%legend();
fontsize(24,"points")
%title(['Power curve @ f_0:' num2str(f(f0index)/1e9) 'GHz'],'FontSize',12);
axis square;

% Efficiency curves

hf = figure;
ha = axes;
subplot(1,2,1);
plot(x/1000,eta(f0index,:)*100,'r','DisplayName',['f_0: ' ...
    num2str(f(f0index)/1e9) 'GHz'],'LineWidth',2);
hold on;
grid minor;
yline(ETAMAX,'--','DisplayName',['\eta_{MAX}']);
xlabel('x');
ylabel('Efficiency, %');
xlim([0 1])
ylim([20 70])
legend();
fontsize(24,"points")
% title('Efficiency curves','FontSize',12)
axis square;
subplot(1,2,2);
hold on;
p=plot(x/1000,eta(f0index,:)*100,'r','DisplayName',['f_0: ' ...
    num2str(f(f0index)/1e9) 'GHz'],'LineWidth',4);
pf=plot(x/1000,eta(1,:)*100,'k','DisplayName',[num2str(f(1)/1e9)...
    'GHz<f<' num2str(f(length(f))/1e9) 'GHz'],'LineWidth',0.5);
for i = 1:1:length(f)
    if i ~= f0index
        plot(x/1000,eta(i,:)*100,'k','LineWidth',0.5)
    end
end
grid minor;
max=yline(ETAMAX,'--','DisplayName',['\eta_{MAX}']);
xlabel('x');
ylabel('Efficiency, %');
xlim([0 1])
ylim([20 70])
```

```
150 legend([p pf max]);
151 fontsize(24,"points")
152 % title('Efficiency curves','FontSize',12)
153 axis square;
154
155
156 hf = figure;
157 ha = axes;
158 subplot(1,2,1);
159 plot(OBO(f0index,:),eta(f0index,:)*100,'r','DisplayName',['f_0: ' ...
160     num2str(f(f0index)/1e9) 'GHz'],'LineWidth',2);
161 hold on;
162 grid minor;
163 yline(ETAMAX,'--','DisplayName',['\eta_{MAX}']);
164 xlabel('OBO, dBm');
165 ylabel('Efficiency, %');
166 xlim([-20 0])
167 ylim([20 70])
168 legend();
169 fontsize(24,"points")
170 % title('Efficiency curves','FontSize',12)
171 axis square;
172 subplot(1,2,2);
173 hold on;
174 plot(OBO(f0index,:),eta(f0index,:)*100,'DisplayName',['f_0: ' ...
175     num2str(f(f0index)/1e9) 'GHz'],'LineWidth',2);
176 plot(x/1000,eta(1,:)*100,'--','DisplayName',['f: ' num2str(f(1)/1e9)...
177     'GHz'],'LineWidth',2)
178 for i = 1:1:5
179     plot(OBO(round(length(f)/5*i),:),eta(round(length(f)/5*i),:)*100,...
180         '--','LineWidth',1);
181 end
182 grid minor;
183 yline(ETAMAX,'--','DisplayName',['\eta_{MAX}']);
184 xlabel('OBO [dBm]');
185 ylabel('\eta [%]');
186 xlim([-20 0])
187 legend();
188 fontsize(24,"points")
189 % title('Efficiency curves','FontSize',12)
190 axis square;
191 subplot(1,2,2);
192 hold on;
193 p=plot(OBO(f0index,:),eta(f0index,:)*100,'r','DisplayName',['f_0: ' ...
194     num2str(f(f0index)/1e9) 'GHz'],'LineWidth',4);
195 pf=plot(OBO(1,:),eta(1,:)*100,'k','DisplayName',[num2str(f(1)/1e9)...
196     'GHz<f<' num2str(f(length(f))/1e9) 'GHz'],'LineWidth',0.5);
197 for i = 1:1:length(f)
198     if i ~= f0index
199         plot(OBO(i,:),eta(i,:)*100,'k','LineWidth',0.5);
200     end
201 end
202 grid minor;
203 max=yline(ETAMAX,'--','DisplayName',['\eta_{MAX}']);
204 xlabel('OBO, dBm');
205 ylabel('Efficiency, %');
```

```
206 xlim([-20 0])
207 ylim([20 70])
208 legend([p pf max]);
209 fontsize(24,"points")
210 % title('Efficiency curves','FontSize',12)
211 axis square;
212
213 % Impedances
214
215 hf = figure;
216 ha = axes;
217 subplot(1,2,1);
218 plot(OBO(f0index,:),real(Zm(f0index,:)),'DisplayName',['\Re(Z_{m})'],...
219     'LineWidth',2);
220 hold on;
221 plot(OBO(f0index,:),real(Za1(f0index,:)),'DisplayName',['\Re(Z_{a1})'],...
222     'LineWidth',2);
223 plot(OBO(f0index,:),real(Za2(f0index,:)),'DisplayName',['\Re(Z_{a2})'],...
224     'LineWidth',2);
225 grid minor;
226 xlabel('OBO, dBm');
227 ylabel('\Re(Z), \Omega');
228 axis([-20 0 0 1500])
229 legend();
230 yline(RoptM,'--','DisplayName',['R_{opt,sub}'])
231 yline(RoptA1,'--','HandleVisibility','off')
232 yline(RoptA2,'--','HandleVisibility','off')
233 fontsize(24,"points")
234 % title(['Impedances (real parts) @ f_0:' num2str(f(f0index)/1e9) 'GHz'],...
235 %     'FontSize',12)
236 axis square;
237
238 subplot(1,2,2);
239 plot(OBO(f0index,:),imag(Zm(f0index,:)),'DisplayName',['\Im(Z_{m})'],...
240     'LineWidth',2);
241 hold on;
242 plot(OBO(f0index,:),imag(Za1(f0index,:)),'DisplayName',['\Im(Z_{a1})'],...
243     'LineWidth',2);
244 plot(OBO(f0index,:),imag(Za2(f0index,:)),'DisplayName',['\Im(Z_{a2})'],...
245     'LineWidth',2);
246 grid minor;
247 xlabel('OBO, dBm');
248 ylabel('\Im(Z), \Omega');
249 xlim([-20 0])
250 legend();
251 fontsize(24,"points")
252 % title(['Impedances (imaginary parts) @ f_0:' num2str(f(f0index)/1e9)...
253 %     'GHz'],'FontSize',12)
254 axis square;
255
256 hf = figure;
257 ha = axes;
258 subplot(1,2,1);
259 plot(x/1000,real(Zm(f0index,:)),'DisplayName',['\Re(Z_{m})'],...
260     'LineWidth',2);
261 hold on;
```

```
plot(x/1000,real(Za1(f0index,:)),'DisplayName',['\Re(Z_{a1})'],...
    'LineWidth',2);
plot(x/1000,real(Za2(f0index,:)),'DisplayName',['\Re(Z_{a2})'],...
    'LineWidth',2);
grid minor;
xlabel('x');
ylabel('\Re(Z), \Omega');
axis([0 1 0 1500])
yline(RoptM,'--','DisplayName',['R_{opt,sub}'])
yline(RoptA1,'--','HandleVisibility','off')
yline(RoptA2,'--','HandleVisibility','off')
legend();
fontsize(24,"points")
% title(['Impedances (real parts) @ f_0:' num2str(f(f0index)/1e9)...
%     'GHz'],'FontSize',12)
axis square;

subplot(1,2,2);
plot(x/1000,imag(Zm(f0index,:)),'DisplayName',['\Im(Z_{m})'],...
    'LineWidth',2);
hold on;
plot(x/1000,imag(Za1(f0index,:)),'DisplayName',['\Im(Z_{a1})'],...
    'LineWidth',2);
plot(x/1000,imag(Za2(f0index,:)),'DisplayName',['\Im(Z_{a2})'],...
    'LineWidth',2);
grid minor;
xlabel('x');
ylabel('\Im(Z), \Omega');
legend();
fontsize(24,"points")
% title(['Impedances (imaginary parts) @ f_0:' num2str(f(f0index)/1e9)...
%     'GHz'],'FontSize',12);
axis square;

hf = figure;
ha = axes;
subplot(1,2,1);
hold on;
for i = 1:1:length(f)
    if i ~= f0index
        plot(x/1000,real(Zm(i,:)),'Color' , '#0072BD','LineWidth',0.5)
        plot(x/1000,real(Za1(i,:)),'Color' , '#D95319','LineWidth',0.5)
        plot(x/1000,real(Za2(i,:)),'Color' , '#EDB120','LineWidth',0.5)
    end
end
grid minor;
xlabel('x');
ylabel('\Re(Z), \Omega');
axis([0 1 0 1500])
yline(RoptM,'--','DisplayName',['R_{opt,sub}'])
yline(RoptA1,'--','HandleVisibility','off')
yline(RoptA2,'--','HandleVisibility','off')
%legend();
fontsize(24,"points")
% title(['Impedances (real parts) @ f_0:' num2str(f(f0index)/1e9)...
%     'GHz'],'FontSize',12)
```

```
318 axis square;
319
320 subplot(1,2,2);
321 hold on;
322 for i = 1:1:length(f)
323     if i ~= f0index
324         plot(x/1000,imag(Zm(i,:)),'Color' , '#0072BD','LineWidth',0.5)
325         plot(x/1000,imag(Za1(i,:)),'Color' , '#D95319','LineWidth',0.5)
326         plot(x/1000,imag(Za2(i,:)),'Color' , '#EDB120','LineWidth',0.5)
327     end
328 end
329 grid minor;
330 xlabel('x');
331 ylabel('\Im(Z), \Omega');
332 %legend();
333 fontsize(24,"points")
334 % title(['Impedances (imaginary parts) @ f_0:' num2str(f(f0index)/1e9)...
335 %     'GHz'],'FontSize',12);
336 axis square;
```

A.11 frequency_range_plots.m

```
1  %effects of clipping
2
3  hf = figure;
4  ha = axes;
5  subplot(1,2,1);
6  plot(f*1e-9,C(:,1000),'r','DisplayName',['C @ saturation'],...
7      'LineWidth',2);
8  grid minor
9  xlabel('Frequency, GHz');
10 ylabel('C');
11 xlim([fmin*1e-9 fmax*1e-9])
12 % title('C(f) - parameter @ saturation','FontSize',12)
13 axis square;
14 legend();
15 fontsize(24,"points")
16
17 subplot(1,2,2);
18 hold on;
19 grid minor
20 plot(f*1e-9,abs(Vmsat),'r','DisplayName',['|V_{m,sat}|'],'LineWidth',2);
21 plot(f*1e-9,abs(Va1sat),'--b','DisplayName',['|V_{a1,sat}|'],...
22     'LineWidth',2);
23 plot(f*1e-9,abs(Va2sat),'--g','DisplayName',['|V_{a2,sat}|'],...
24     'LineWidth',2);
25 xlabel('Frequency, GHz');
26 ylabel('Drain Voltage Amplitude, V');
27 xlim([fmin*1e-9 fmax*1e-9]);
28 % title('Clipping effect @ saturation','FontSize',12)
29 axis square;
30 legend();
```

```
fontsize(24,"points")

hf = figure;
ha = axes;
subplot(1,2,1);
plot(f*1e-9,C(:,round(1000*a2)),'r','DisplayName',['C @ OBO2'],...
    'LineWidth',2)
grid minor
xlabel('Frequency, GHz')
ylabel('C')
xlim([fmin*1e-9 fmax*1e-9])
% title('C(f) - parameter @ OBO2','FontSize',12)
fontsize(24,"points")
axis square;
legend();

subplot(1,2,2);
hold on
grid minor
plot(f*1e-9,abs(Vmobo2),'r','DisplayName',['|V_{m,OBO2}|'],'LineWidth',...
    2)
plot(f*1e-9,abs(Va1obo2),'--b','DisplayName',['|V_{a1,OBO2}|'],...
    'LineWidth',2);
xlabel('Frequency, GHz')
ylabel('Drain Voltage Amplitude, V');
xlim([fmin*1e-9 fmax*1e-9])
legend();
fontsize(24,"points")
% title('Clipping effect @ OBO2','FontSize',12)
axis square;
legend();

hf = figure;
ha = axes;
subplot(1,2,1);
plot(f*1e-9,C(:,round(1000*a1)),'r','DisplayName',['C @ OBO1'],...
    'LineWidth',2)
grid minor
xlabel('Frequency, GHz')
ylabel('C')
xlim([fmin*1e-9 fmax*1e-9])
% title('C(f) - parameter @ OBO1','FontSize',12)
fontsize(24,"points")
axis square;
legend();

subplot(1,2,2);
grid minor;
hold on;
plot(f*1e-9,abs(Vmobo1),'r','DisplayName',['|V_{m,OBO1}|'],'LineWidth',2)
xlabel('Frequency, GHz')
ylabel('Drain Voltage Amplitude, V');
xlim([fmin*1e-9 fmax*1e-9])
legend();
fontsize(24,"points")
% title('Clipping effect @ OBO1','FontSize',12)
```

```
87  axis square;
88  legend();
89
90  %Power and efficiency
91
92  hf = figure;
93  ha = axes;
94  subplot(1,2,1);
95  hold on
96  grid minor
97  plot(f*1e-9,30+10*log10(Psat),'DisplayName',['Saturation'],'LineWidth',2)
98  plot(f*1e-9,30+10*log10(Pobo2),'DisplayName',['OBO2'],'LineWidth',2)
99  plot(f*1e-9,30+10*log10(Pobo1)','DisplayName',['OBO1'],'LineWidth',2)
100 %set(ha,'YLim',[34 44],'YTick',[34:1:44])
101 xlabel('Frequency, GHz')
102 ylabel('Output Power, dBm')
103 xlim([fmin*1e-9 fmax*1e-9])
104 % title('Output power','FontSize',12)
105 axis square;
106 legend();
107 fontsize(24,"points")
108
109 subplot(1,2,2);
110 hold on
111 grid minor
112 plot(f*1e-9,100*eta_sat,'DisplayName',['Saturation'],'LineWidth',2)
113 plot(f*1e-9,100*eta_obo2,'DisplayName',['OBO2'],'LineWidth',2)
114 plot(f*1e-9,100*eta_obo1,'DisplayName',['OBO1'],'LineWidth',2)
115 xlabel('Frequency, GHz')
116 ylabel('Efficiency, %')
117 xlim([fmin*1e-9 fmax*1e-9])
118 % title('Efficiency','FontSize',12)
119 axis square;
120 legend()
121 fontsize(24,"points")
122
123 %Z-matrix
124
125 hf = figure;
126 ha = axes;
127 plot(f*1e-9,real(Zmm),'DisplayName',['\Re(Z_{mm})'],'LineWidth',2)
128 hold on
129 grid minor
130 plot(f*1e-9,real(Zma1),'DisplayName',['\Re(Z_{ma1})'],'LineWidth',2)
131 plot(f*1e-9,real(Zma2),'DisplayName',['\Re(Z_{ma2})'],'LineWidth',2)
132 plot(f*1e-9,real(Za1m),'DisplayName',['\Re(Z_{a1m})'],'LineWidth',2)
133 plot(f*1e-9,real(Za1a1),'DisplayName',['\Re(Z_{a1a1})'],'LineWidth',2)
134 plot(f*1e-9,real(Za1a2),'DisplayName',['\Re(Z_{a1a2})'],'LineWidth',2)
135 plot(f*1e-9,real(Za2m),'DisplayName',['\Re(Z_{a2m})'],'LineWidth',2)
136 plot(f*1e-9,real(Za2a1),'DisplayName',['\Re(Z_{a2a1})'],'LineWidth',2)
137 plot(f*1e-9,real(Za2a2),'DisplayName',['\Re(Z_{a2a2})'],'LineWidth',2)
138 % set(ha,'YLim',[-2 2],'YTick',[-2:0.5:2])
139 xlabel('Frequency, GHz')
140 ylabel('\Re(Zxy), \Omega')
141 xlim([fmin*1e-9 fmax*1e-9])
142 % title('Z-parameters (real part)','FontSize',12)
```

```
%axis square;
legend()
fontsize(24,"points")

hf = figure;
ha = axes;
plot(f*1e-9,imag(Zmm),'DisplayName',['\Im(Z_{mm})'],'LineWidth',2)
hold on
grid minor
plot(f*1e-9,imag(Zma1),'DisplayName',['\Im(Z_{ma1})'],'LineWidth',2)
plot(f*1e-9,imag(Zma2),'DisplayName',['\Im(Z_{ma2})'],'LineWidth',2)
plot(f*1e-9,imag(Za1m),'DisplayName',['\Im(Z_{a1m})'],'LineWidth',2)
plot(f*1e-9,imag(Za1a1),'DisplayName',['\Im(Z_{a1a1})'],'LineWidth',2)
plot(f*1e-9,imag(Za1a2),'DisplayName',['\Im(Z_{a1a2})'],'LineWidth',2)
plot(f*1e-9,imag(Za2m),'DisplayName',['\Im(Z_{a2m})'],'LineWidth',2)
plot(f*1e-9,imag(Za2a1),'DisplayName',['\Im(Z_{a2a1})'],'LineWidth',2)
plot(f*1e-9,imag(Za2a2),'DisplayName',['\Im(Z_{a2a2})'],'LineWidth',2)
% set(ha,'YLim',[-2 2],'YTick',[-2:0.5:2])
xlabel('Frequency, GHz')
ylabel('\Im(Zxy), \Omega')
xlim([fmin*1e-9 fmax*1e-9])
% title('Z-parameters (Imaginal part)','FontSize',12)
%axis square;
legend()
fontsize(24,"points")

%Input impedances

hf = figure;
ha = axes;
subplot(1,2,1)
hold on
grid minor
plot(f*1e-9,real(Zmsat),'DisplayName',['\Re(Z_{m,sat})'],'LineWidth',2)
plot(f*1e-9,real(Za1sat),'DisplayName',['\Re(Z_{a1,sat})'],'LineWidth',2)
plot(f*1e-9,real(Za2sat),'DisplayName',['\Re(Z_{a2,sat})'],'LineWidth',2)
xlabel('Frequency, GHz')
ylabel('\Re(Z), \Omega')
yline(RoptM,'--','DisplayName',['R_{opt,sub}'],'LineWidth',2)
yline(RoptA1,'--','HandleVisibility','off','LineWidth',2)
yline(RoptA2,'--','HandleVisibility','off','LineWidth',2)
xlim([fmin*1e-9 fmax*1e-9])
axis square;
legend()
fontsize(24,"points")

subplot(1,2,2)
hold on
grid minor
plot(f*1e-9,imag(Zmsat),'DisplayName',['\Im(Z_{m,sat})'],'LineWidth',2)
plot(f*1e-9,imag(Za1sat),'DisplayName',['\Im(Z_{a1,sat})'],'LineWidth',2)
plot(f*1e-9,imag(Za2sat),'DisplayName',['\Im(Z_{a2,sat})'],'LineWidth',2)
xlabel('Frequency, GHz')
ylabel('\Im(Z), \Omega')
yline(0,'HandleVisibility','off','LineWidth',2)
xlim([fmin*1e-9 fmax*1e-9])
```

```
199 axis square;
200 legend()
201 fontsize(24,"points")
202 
203 hf = figure;
204 ha = axes;
205 subplot(1,2,1)
206 hold on
207 grid minor
208 plot(f*1e-9,real(Zmobo2),'DisplayName',['\Re(Z_{m,OBO2})'],'LineWidth',2)
209 plot(f*1e-9,real(Za1obo2),'DisplayName',['\Re(Z_{a1,OBO2})'],'LineWidth',2)
210 xlabel('Frequency, GHz')
211 ylabel('\Re(Z), \Omega')
212 yline(RoptM/a2,'--','DisplayName',['R_{opt,sub}/a2'],'LineWidth',2)
213 yline(RoptA1/a2,'--','HandleVisibility','off','LineWidth',2)
214 xlim([fmin*1e-9 fmax*1e-9])
215 axis square;
216 legend()
217 fontsize(24,"points")
218 
219 subplot(1,2,2)
220 hold on
221 grid minor
222 plot(f*1e-9,imag(Zmobo2),'DisplayName',['\Im(Z_{m,OBO2})'],'LineWidth',2)
223 plot(f*1e-9,imag(Za1obo2),'DisplayName',['\Im(Z_{a1,OBO2})'],'LineWidth',2)
224 xlabel('Frequency, GHz')
225 ylabel('\Im(Z), \Omega')
226 yline(0,'HandleVisibility','off','LineWidth',2)
227 xlim([fmin*1e-9 fmax*1e-9])
228 axis square;
229 legend()
230 fontsize(24,"points")
231 
232 hf = figure;
233 ha = axes;
234 subplot(1,2,1)
235 hold on
236 grid minor
237 plot(f*1e-9,real(Zmobo1),'DisplayName',['\Re(Z_{m,OBO1})'],'LineWidth',2)
238 xlabel('Frequency, GHz')
239 ylabel('\Re(Z), \Omega')
240 yline(RoptM/a1,'--','DisplayName',['R_{opt,m}/a_1'])
241 xlim([fmin*1e-9 fmax*1e-9])
242 axis square;
243 legend()
244 fontsize(24,"points")
245 
246 subplot(1,2,2)
247 hold on
248 grid minor
249 plot(f*1e-9,imag(Zmobo1),'DisplayName',['\Im(Z_{m,OBO1})'],'LineWidth',2)
250 xlabel('Frequency, GHz')
251 ylabel('\Im(Z), \Omega')
252 yline(0,'HandleVisibility','off','LineWidth',2)
253 xlim([fmin*1e-9 fmax*1e-9])
254 axis square;
```

```
255 legend()
256 fontsize(24,"points")
257
258
259 %Refection 50ohm and opt
260
261 hf = figure;
262 ha = axes;
263 subplot(1,2,1)
264
265 smithplot(f*1e-9, GAMmsat,'LineWidth',2)
266 hold on
267 grid minor
268 smithplot(f*1e-9, GAMa1sat,'LineWidth',2)
269 smithplot(f*1e-9, GAMa2sat,'LineWidth',2)
270 smithplot(f*1e-9, GAMmobo2,'LineWidth',2)
271 smithplot(f*1e-9, GAMa1obo2,'LineWidth',2)
272 smithplot(f*1e-9, GAMmobo1,'LineWidth',2)
273 axis square;
274 legend('M SAT','A1 SAT','A2 SAT','M OBO2','A1 OBO2','M OBO1')
275 fontsize(24,"points")
276
277 subplot(1,2,2)
278 smithplot(f*1e-9, GAMmsat_opt,'LineWidth',2)
279 hold on
280 grid minor
281 smithplot(f*1e-9, GAMa1sat_opt,'LineWidth',2)
282 smithplot(f*1e-9, GAMa2sat_opt,'LineWidth',2)
283 smithplot(f*1e-9, GAMmobo2_opt,'LineWidth',2)
284 smithplot(f*1e-9, GAMa1obo2_opt,'LineWidth',2)
285 smithplot(f*1e-9, GAMmobo1_opt,'LineWidth',2)
286 axis square;
287 legend('M SAT','A1 SAT','A2 SAT','M OBO2','A1 OBO2','M OBO1')
288 fontsize(24,"points")
289
290
291 %reflection db (opt)
292
293 hf = figure;
294 ha = axes;
295 plot(f*1e-9,20*log10(abs(GAMmsat_opt)),'DisplayName',['M SAT'],'LineWidth',2)
296 hold on
297 grid minor
298 plot(f*1e-9,20*log10(abs(GAMa1sat_opt)),'DisplayName',['A1 SAT'],'LineWidth',2)
299 plot(f*1e-9,20*log10(abs(GAMa2sat_opt)),'DisplayName',['A2 SAT'],'LineWidth',2)
300 plot(f*1e-9,20*log10(abs(GAMmobo2_opt)),'DisplayName',['M OBO2'],'LineWidth',2)
301 plot(f*1e-9,20*log10(abs(GAMa1obo2_opt)),'DisplayName',['A1 OBO2'],'LineWidth',2)
302 plot(f*1e-9,20*log10(abs(GAMmobo1_opt)),'DisplayName',['M OBO1'],'LineWidth',2)
303 % plot(f*1e-9,imag(Zam),'g')
304 % set(ha,'YLim',[-2 2],'YTick',[-2:0.5:2])
305 %axis([14 24 -40 0])
306 xlabel('Frequency, GHz')
307 ylabel('Reflection coefficient, dB')
308 xlim([fmin*1e-9 fmax*1e-9])
309 axis square;
310 legend()
```

```
311 fontsize(24,"points")
312
313 %others
314
315 hf = figure;
316 ha = axes;
317 subplot(1,2,1);
318 hold on
319 grid minor
320 plot(f*1e-9,real(Ymsat),'DisplayName',['M SAT'],'LineWidth',2)
321 plot(f*1e-9,real(Ya1sat),'DisplayName',['A1 SAT'],'LineWidth',2)
322 plot(f*1e-9,real(Ya2sat),'DisplayName',['A2 SAT'],'LineWidth',2)
323 plot(f*1e-9,real(Ymobo2),'DisplayName',['M OBO2'],'LineWidth',2)
324 plot(f*1e-9,real(Ya1obo2),'DisplayName',['A1 OBO2'],'LineWidth',2)
325 plot(f*1e-9,real(Ymobo1),'DisplayName',['M OBO1'])
326 % plot(f*1e-9,imag(Zam),'g')
327 % set(ha,'YLim',[-2 2],'YTick',[-2:0.5:2])
328 %axis([14 24 0 2])
329 xlabel('Frequency, GHz')
330 ylabel('\Re(Y M,A), S')
331 xlim([fmin*1e-9 fmax*1e-9])
332 axis square;
333 legend()
334 fontsize(24,"points")
335
336 subplot(1,2,2);
337 hold on
338 grid minor
339 plot(f*1e-9, 1./real(Ymsat),'DisplayName',['M SAT'],'LineWidth',2)
340 plot(f*1e-9, 1./real(Ya1sat),'DisplayName',['A1 SAT'],'LineWidth',2)
341 plot(f*1e-9, 1./real(Ya2sat),'DisplayName',['A2 SAT'],'LineWidth',2)
342 plot(f*1e-9, 1./real(Ymobo2),'DisplayName',['M OBO2'])
343 plot(f*1e-9, 1./real(Ya1obo2),'DisplayName',['A1 OBO2'],'LineWidth',2)
344 plot(f*1e-9, 1./real(Ymobo1),'DisplayName',['M OBO1'])
345 % plot(f*1e-9,imag(Zam),'g')
346 %set(ha,'YLim',[0 150],'YTick',[0:10:150])
347 axis([fmin*1e-9 fmax*1e-9 0 2000])
348 xlabel('Frequency, GHz')
349 ylabel('1/{\Re(Y M,A)}, \Omega')
350 xlim([fmin*1e-9 fmax*1e-9])
351 axis square;
352 legend()
353 fontsize(24,"points")
```

A.12 ABCD_ShuntInductor.m

```
1 function ABCD = ABCD_ShuntInductor(L,w)
2 ABCD = [1,0; 1/(1i*w*L),1];
3 end
```

A.13 ABCD_ShuntCapacitor.m

```
function ABCD = ABCD_ShuntCapacitor(C,w)
ABCD = [1,0;1i*w*C,1];
end
```

A.14 ABCD_ShuntAdmittance.m

```
function ABCD = ABCD_ShuntAdmittance(Y)
ABCD = [1,0;Y,1];
end
```

A.15 ABCD_SeriesTxLine.m

```
function ABCD = ABCD_SeriesTxLine(w0,w,Zch,theta)
ABCD = [cos(theta*w/w0),1i*Zch*sin(theta*w/w0); 1i/Zch*sin(theta*w/w0),cos(theta*w/w0)];
end
```

A.16 ABCD_SeriesTxLine.m

```
function ABCD = ABCD_SeriesInductor(L,w)
ABCD = [1,1i*w*L;0,1];
end
```

A.17 ABCD_SeriesImpedance.m

```
function ABCD = ABCD_SeriesImpedance(Z)
ABCD = [1,Z;0,1];
end
```

A.18 ABCD_SeriesCapacitor.m

```
function ABCD = ABCD_SeriesCapacitor(C,w)
ABCD = [1,1/(1i*w*C);0,1];
end
```

Appendix B

ADS simulation environment

B.1 Simulation schemes

B.1.1 Simulation 1: model with ideal transistors

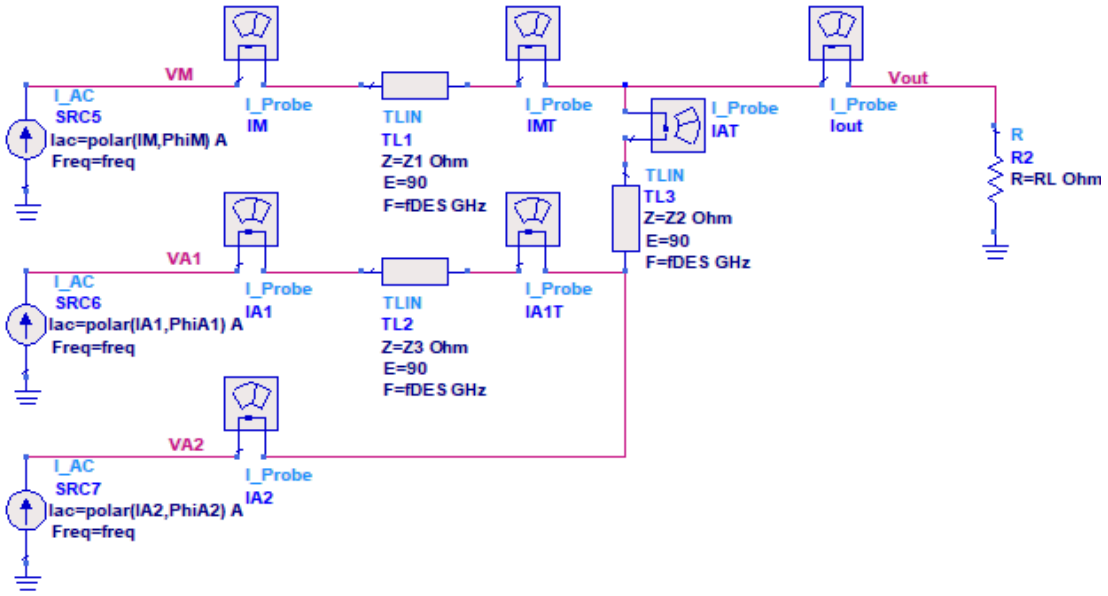

Figure B.1: Scheme used in simulation.

B.1.2 Simulation 2: simplified parasitic model

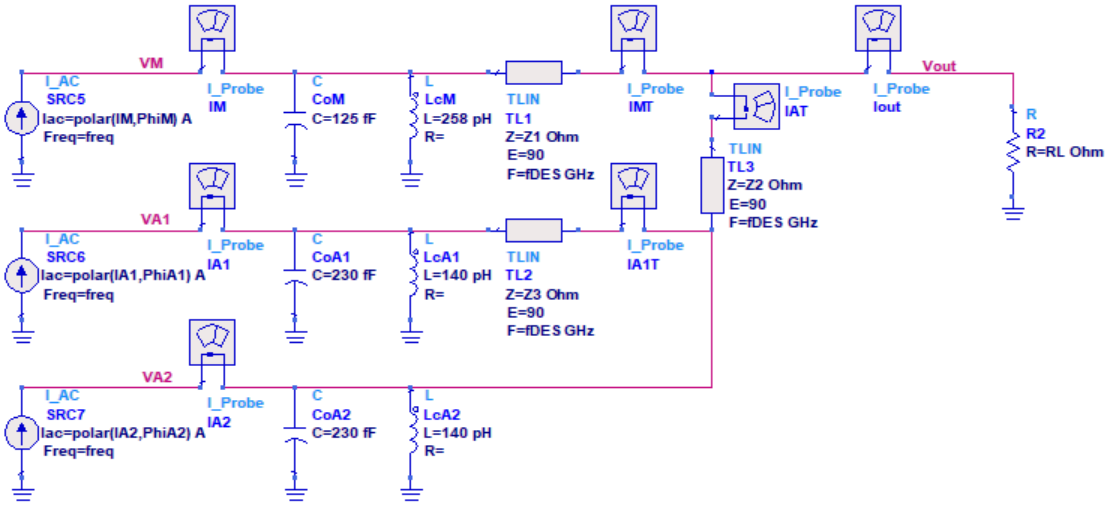

Figure B.2: Scheme used in simulation.

B.1.3 Simulation 3: complete parasitic model

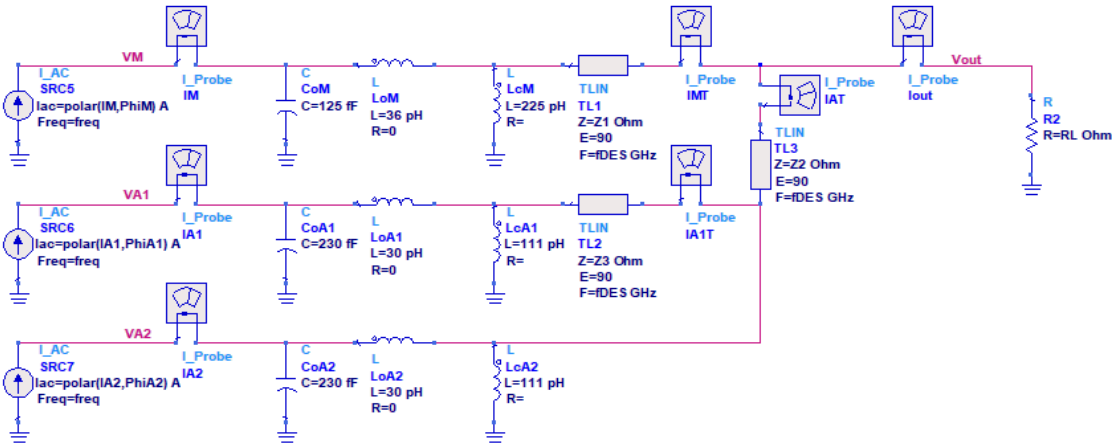

Figure B.3: Scheme used in simulation.

B.2 Simulation commands

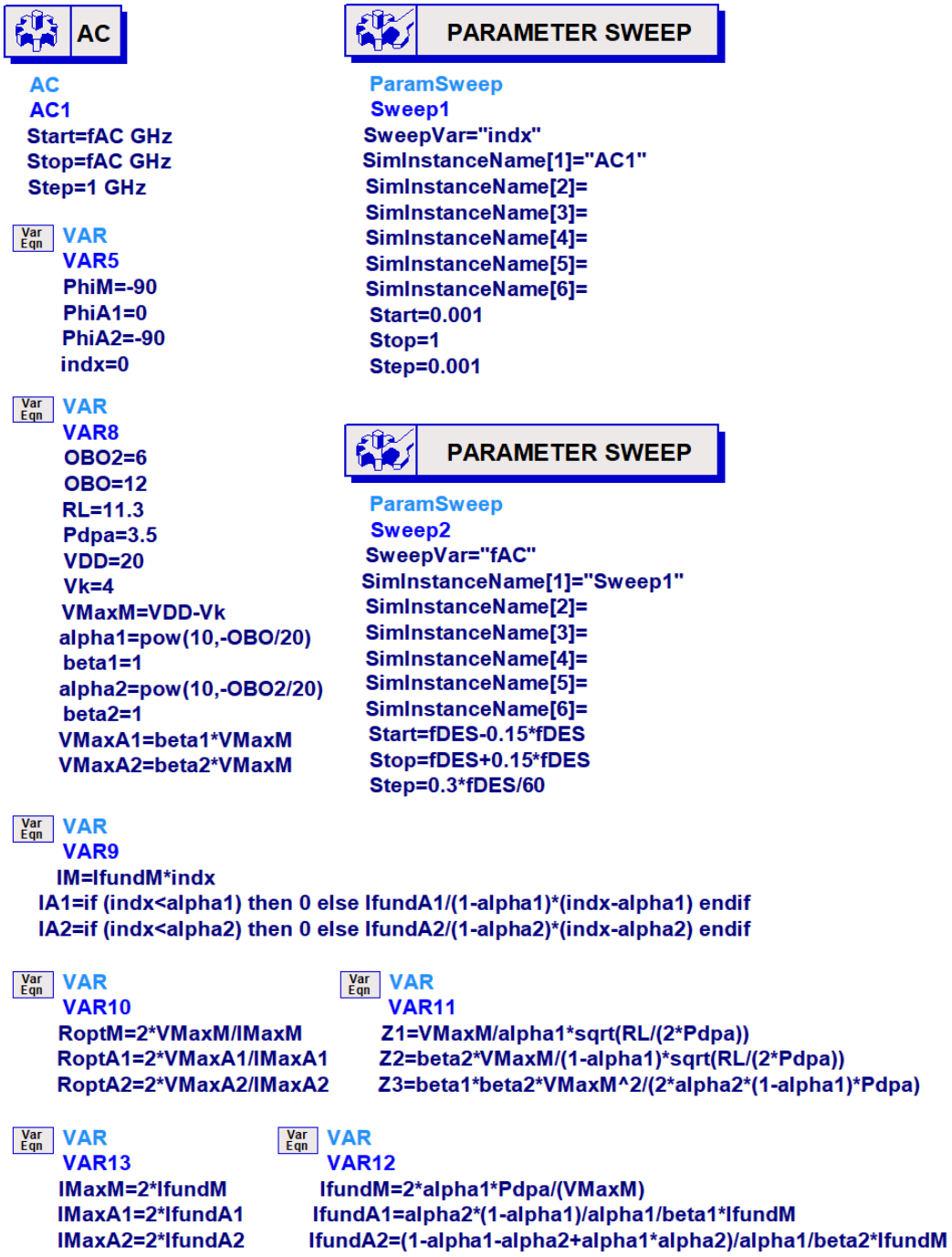

Figure B.4: Simulation command.

Bibliography

[1] D. Del Corso, V. Camarchia, R.Quaglia, and P. Bardella. *Telecommunication Electronics*. Artech House, 2020 (cit. on pp. 2, 3, 6–9, 11, 14, 15, 17, 20–22, 24, 28–30, 32–34, 36).

[2] Steve C. Crips. *RF Power Amplifiers for Wireless Communications, Second Edition*. 2006 (cit. on pp. 26, 36–38, 43, 46, 47).

[3] D.A. Frickey. «Conversions between S, Z, Y, H, ABCD, and T parameters which are valid for complex source and load impedances». In: *IEEE Transactions on Microwave Theory and Techniques* 42.2 (1994), pp. 205–211. DOI: 10.1109/22.275248 (cit. on pp. 27, 56).

[4] Wikipedia. *Two-port network*. URL: https://en.wikipedia.org/wiki/Two-port_network# (cit. on p. 27).

[5] Steve C. Crips. *Advanced Techniques in RF Power Amplifier Design*. Artech House, 2002 (cit. on p. 35).

[6] Robert Paulo, David Ihle, Christoph Tzschoppe, Robert Wolf, Paolo Valerio Testa, and Frank Ellinger. «Input transmission line adjustment for efficiency enhancement in Doherty amplifiers». In: *2015 SBMO/IEEE MTT-S International Microwave and Optoelectronics Conference (IMOC)*. 2015, pp. 1–4. DOI: 10.1109/IMOC.2015.7369112 (cit. on p. 39).

[7] C. Tongchoi, M. Chongcheawchamnan, and A. Worapishet. «Lumped element based Doherty power amplifier topology in CMOS process». In: *Proceedings of the 2003 International Symposium on Circuits and Systems, 2003. ISCAS '03.* Vol. 1. 2003, pp. I–I. DOI: 10.1109/ISCAS.2003.1205596 (cit. on p. 44).

[8] P. Colantonio, F. Giannini, and E. Limiti. *High Efficiency RF and Microwave Solid State Power Amplifiers*. Wiley, Tor Vergata, 2002 (cit. on pp. 45, 47, 51–53).

[9] Bumman Kim, Jangheon Kim, Ildu Kim, and Jeonghyeon Cha. «The Doherty power amplifier». In: *IEEE Microwave Magazine* 7.5 (2006), pp. 42–50. DOI: 10.1109/MW-M.2006.247914 (cit. on p. 47).

[10] Gholamreza Nikandish, Robert Bogdan Staszewski, and Anding Zhu. «Breaking the Bandwidth Limit: A Review of Broadband Doherty Power Amplifier Design for 5G». In: *IEEE Microwave Magazine* 21.4 (2020), pp. 57–75. DOI: 10.1109/MMM.2019.2963607 (cit. on pp. 47–49).

[11] Jorge Julian Moreno Rubio, Vittorio Camarchia, Marco Pirola, and Roberto Quaglia. «Design of an 87% Fractional Bandwidth Doherty Power Amplifier Supported by a Simplified Bandwidth Estimation Method». In: *IEEE Transactions on Microwave Theory and Techniques* 66.3 (2018), pp. 1319–1327. DOI: 10.1109/TMTT.2017.2767586 (cit. on pp. 49, 57).

[12] Vittorio Camarchia, Marco Pirola, Roberto Quaglia, Seunghoon Jee, Yunsung Cho, and Bumman Kim. «The Doherty Power Amplifier: Review of Recent Solutions and Trends». In: *IEEE Transactions on Microwave Theory and Techniques* 63.2 (2015), pp. 559–571. DOI: 10.1109/TMTT.2014.2387061 (cit. on pp. 50, 53).

[13] Anna Piacibello, Vittorio Camarchia, Paolo Colantonio, and Rocco Giofrè. «3-Way Doherty Power Amplifiers: Design Guidelines and MMIC Implementation at 28 GHz». In: *IEEE Transactions on Microwave Theory and Techniques* 71.5 (2023), pp. 2016–2028. DOI: 10.1109/TMTT.2022.3225316 (cit. on pp. 52, 66, 80).

[14] T. Reveyrand. «Multiport conversions between S, Z, Y, h, ABCD, and T parameters». In: *2018 International Workshop on Integrated Nonlinear Microwave and Millimetre-wave Circuits (INMMIC)*. 2018, pp. 1–3. DOI: 10.1109/INMMIC.2018.8430023 (cit. on p. 56).

[15] Y. C. Lin and T. H. Chu. «Reconstructing scattering matrix of a three-port nonreciprocal network from One-Port measurements». In: *2015 Asia-Pacific Microwave Conference (APMC)*. Vol. 2. 2015, pp. 1–3. DOI: 10.1109/APMC.2015.7413079 (cit. on p. 56).

[16] N. Srirattana, A. Raghavan, D. Heo, P.E. Allen, and J. Laskar. «Analysis and design of a high-efficiency multistage Doherty power amplifier for wireless communications». In: *IEEE Transactions on Microwave Theory and Techniques* 53.3 (2005), pp. 852–860. DOI: 10.1109/TMTT.2004.842505 (cit. on p. 67).